Copyright

by

Changyoung Kim

2012

The Dissertation Committee for Changyoung Kim Certifies that this is the approved version of the following dissertation:

Development of the Spectral-Analysis-of-Body-Waves (SABW) Method for Downhole Seismic Testing with Boreholes or Penetrometers

Committee:

Kenneth H. Stokoe II, Supervisor

Robert B. Gilbert

Clark R. Wilson

Loukas F. Kallivokas

Jinying Zhu

Development of the Spectral-Analysis-of-Body-Waves (SABW) Method for Downhole Seismic Testing with Boreholes or Penetrometers

by

Changyoung Kim, B.S.; M.S.

Dissertation

Presented to the Faculty of the Graduate School of

The University of Texas at Austin

in Partial Fulfillment

of the Requirements

for the Degree of

Doctor of Philosophy

The University of Texas at Austin

August 2012

Dedication

To My Parents and Wife

Acknowledgements

I would like to express my sincere gratitude to the following individuals who made this research possible.

I would like to thank my supervising professor, Kenneth H. Stokoe, II, for his guidance, support and unlimited enthusiasm throughout my doctoral study. His patience and understanding during the study have been a great comfort to me who is an international student. The field trips with him have been a great time to learn his knowledge and experience. Besides the learning experience, I will not forget the fun times during the trips with him.

I am also sincerely grateful to the remaining members of my dissertation committee, Professors Robert B. Gilbert, Clark R. Wilson, Loukas F. Kallivokas and Jinying Zhu, for reviewing this manuscript and for their concern in this study. I do not think I could finish my doctoral study without taking their classes, their guidance and advices.

I would like to thank my fellow geotechnical graduate students for conversations and discussions, especially Minjae Jung, Jiabei Yuan, Boo Nam, Jisuk Yoon, Wing Shun Kwan, Matthew Thad LeBlanc, Yin-Cheng Lin, Greg Dellinger, Trevor Walker, Thomas Sully, Jung Su Lee, Boonam Shin, Sungmoon Hwang. Bohyoung Lee, Wei Rui, Onur Kacar, Julio Ferreira, Michael Plaisted, David Umberg, Julia Roberts, Ching-Hsiang Chen and others.

I also appreciate Dr. Farn-yuh Menq for expanding my knowledge in field data acquisition. Thanks are also extended to Cecil Hoffpauir, Curtis Mullins and Robert Kent who performed many field tests with me for my doctoral study.

I would like to thank Teresa Tice-Boggs, Melinda Jakobovits, Chris Trevino and Shannon Wilkerson for their administrative assistance that facilitated my research process.

During my doctoral studies at the University of Texas at Austin I have been working on projects sponsored by the George E. Brown, Jr. Network for Earthquake Engineering Simulation (NEES) funded by National Science Foundation (NSF). Thanks are extended to these organizations for their financial support.

Finally, and most of all, I want to thank my wife Jisunmi, my parents and family for their endless love, patience, help, support and prayers.

Austin, 9 August 2012

Development of the Spectral-Analysis-of-Body-Waves (SABW) Method for Downhole Seismic Testing with Boreholes or Penetrometers

Changyoung Kim, Ph.D.

The University of Texas at Austin, 2012

Supervisor: Kenneth H. Stokoe II

Downhole seismic testing and seismic cone penetration testing (SCPT) have shown little change since the 1990's, with essentially the same sensors, sources, test procedures and analytical methods being used. In these tests, the time differences of first-arrivals or other reference points early in the time-domain signals have been used to calculate shear and compression wave velocities in soil and rock layers. This time-domain method requires an operator to pick the first arrival or other reference point of each seismic wave in the time record. Picking these reference points correctly is critical in calculating wave velocities. However, picking these points in time records is time consuming and is not always easy because of low signal-to-noise ratios, especially in the case of shear waves which arrive later in the time record. To avoid picking reference points, a cross-correlation method is sometimes applied to determine travel times of the seismic waves, especially in traditional downhole testing. One benefit of the cross-correlation method is that it can be automated. The cross-correlation method is not, however, appropriate for evaluation other body wave characteristics such as wave dispersion and material damping.

An alternate approach is to use frequency-domain analysis methods which are well suited for evaluating time changes between all types of waveforms measured at

spatially different points. In addition, frequency-domain methods can be automated and attenuation measurements can also be performed. Examples of such testing procedures with Rayleigh-type surface waves in geotechnical earthquake engineering are the Spectral-Analysis-of-Surface-Waves (SASW) and Multi-Channel-Analysis-of-Surface-Waves (MASW) methods. In this research, an automated procedure for calculating body wave velocities that is based on frequency-domain analysis is presented. The basis for and an automated procedure to calculated body wave dispersion is also presented. Example results showing shear wave velocity and material damping measurements in the SCPT are presented.

The objective of this study is to improve downhole seismic tests with boreholes, cone penetrometers or flat-plate dilatometers by developing a frequency-domain analysis method which overcomes many of the disadvantages of time-domain analyses. The frequency-domain method is called the Spectral-Analysis-of-Body-Waves (SABW) method. The SABW method does not require an operator to pick the first-arrival or other reference times. As a result, the shear wave velocities and wave dispersion can be calculated in real time using the interpretation method with an automatic calculation procedure, thus reducing human subjectivity. Also, the SABW method can be used to determine additional information from the dispersion curves such as the material damping ratio and an estimate of soil type based on the dispersion relationship.

In this research, field SCPT measurements are presented as an example to illustrate the potential of the SABW method. Measurements with shear waves are highlighted because these measurements are most often required in geotechnical earthquake engineering studies.

Table of Contents

List of Tables xiii

List of Figures xiv

Chapter 1: Introduction 1

1.1 Seismic Tests with Boreholes or Penetrometers 1

1.2 Background of Downhole Seismic Testing 3

1.3 Objectives of Research 4

1.4 Organization of Dissertation 5

Chapter 2: Literature Review of In-Situ Seismic Testing Related to This Research 8

2.1 Introduction 8

2.2 Dynamic Soil Properties 8

2.3 Motions of Body Waves 15

2.4 Downhole Test 18

2.5 Crosshole Test 19

2.6 SCPT and SDMT Tests 23

2.7 SASW Test 28

2.8 Summary 32

Chapter 3: Instrumentation for Downhole and SCPT Tests 37

3.1 Introduction 37

3.2 Downhole Sensor 37

3.3 Seismic Cone Portion of SCPT 45

3.3.1 Sensors (28-Hz Geophone vs. 24-Hz Geophone) 45

3.3.2 Sensor Housing 48

3.4 Trigger System 54

3.4.1 Electrical Trigger 54

3.4.2 3-D Reference Sensors 58

3.5 Data Acquisition System 62

3.6 Summary 65

Chapter 4: Field Test Procedures for Downhole and SCPT Testing 68
4.1 Introduction.....68
4.2 Testing Setup 68
4.3 Installation of 3-D Reference Sensor.....72
4.4 Seismic Sensor Installation.....74
4.4.1 Downhole Borehole and Sensor Installation.....76
4.4.2 Seismic Cone Installation 82
4.5 Generation of Body Waves.....86
4.6 Extraction of Sensors 90
4.6.1 Extraction of Downhole Sensors 90
4.6.2 Seismic Cone Extraction.....90
4.6.3 Extraction of 3-D Reference sensors 92
4.7 Summary.....92

Chapter 5: V_S and V_P Profiling in the SCPT Test with Conventional and Advanced Testing and Analysis Procedures.....93
5.1 Introduction.....93
5.2 SCPT Testing Set-up.....94
5.3 SCPT Testing at Hornsby Bend.....95
5.4 V_S Measurements Using Time-Domain Methods from Seismic Cone Testing 98
5.4.1 V_S measurements based on first arrivals.....99
5.4.2 Advanced time-domain V_S measurements based on interval travel times and various time-domain reference points 103
5.4.3 Advanced V_S measurements based on interval travel times and cross correlation 106
5.5 V_P Measurements Using Time-Domain Method from Seismic Cone Testing 107
5.5.1 V_P measurements based on first arrivals.....107
5.5.2 Advanced V_P measurements based on interval travel times and various time-domain reference points.....117
5.5.3 Advanced V_P measurements based on interval travel times and cross correlation 117

5.6 Summary 118

Chapter 6: Development of the Spectral-Analysis-of-Body-Waves (SABW) Method 124

6.1 Introduction 124

6.2 Testing Set-up for SABW Testing with Impact Sources 124

6.3 Analysis Procedures for S-Wave Phase Velocity, Material Damping and Dispersion 127

6.3.1 Analysis procedure for S-wave phase velocity measurements 127

6.3.2 Analysis procedure for S-wave material damping measurements 139

6.3.3 S-wave dispersion measurements 146

6.4 Analysis Procedure for P-Waves 150

6.5 Summary 151

Chapter 7: Application of the SABW Method Using a Sinusoidal Source 153

7.1 Introduction 153

7.2 Testing Set-up for SCPT with Sinusoidal and Impulsive Sources 153

7.3 V_S Profiling with Sinusoidal Source 154

7.4 Summary 156

Chapter 8: Summary, Conclusions and Recommendations for Future Work 162

8.1 Summary 162

8.2 Conclusion 165

8.2.1 Improvement of SCPT sensor 165

8.2.2 Estimation of Sensor Rotation in SCPT Testing 165

8.2.3 Comparison of SASW and SCPT test results 166

8.2.4 V_S and V_P measurements using time-domain methods in SCPT testing 167

8.2.5 V_S and material damping measurements, and soil type characterizations using the SABW method 168

8.2.6 Characterization of soil profile using in-situ seismic tests 169

8.3 Recommendations for Future Work 169

Appendix A: V_S Profiling following Conventional SCPT Testing and Analysis Procedures.....171

Appendix B: In-Situ Seismic Test Results 208

References.....237

Vita 242

List of Tables

Table 3.1: Characteristics of the Individual Geophones in a 3-D Receiver and of the Completed 3-D Receiver (from Stokoe et al., 2009a) 40

Table 3.2: Example Calibration Records of the Data Physics Dynamic Signal Analyzer for Channels 1 through 16; 10-kHz Square Wave Input...65

List of Figures

Figure 1.1: Illustration of Borehole Seismic Methods (after Hoar, 1982).....2

Figure 1.2: Illustration of Seismic Cone Penetration Test (SCPT) using the Downhole Configuration (from Campanella et al., 1986).....3

Figure 2.1: Distribution of Body and Surface Waves from a Vibrating Circular Footing on a Homogeneous, Isotropic, Elastic Half-space (from Woods, 1968).....10

Figure 2.2: Typical Shear Modulus Variation with Shearing Strain Amplitude as Determined by In Situ and Laboratory Tests (from Stokoe et al., 1978).....12

Figure 2.3: The Effect of Confining Pressure on (a) Normalized Modulus Reduction and (b) Material Damping Curves of Silty Sands Evaluated as Part of the ROSRINE Study (From Darendeli, 2001).....13

Figure 2.4: Comparison of Estimated G-log γ and τ-γ Curves with Similar Curves Evaluated in The Laboratory (from Stokoe and Santamarina, 2000)14

Figure 2.5: Illustration of Propagation of Body Waves within a Homogeneous, Isotropic, Linear, Infinite Medium (after Bolt, 1976).....16

Figure 2.6: Illustration of Downhole Test Using One, 3-D Receiver (from Mok, 1987).....20

Figure 2.7: Illustration of Downhole Test Using Two, 3-D Receivers (from Mok, 1987).....21

Figure 2.8: Illustration of Crosshole Test (after Mok, 1987).....22

Figure 2.9: Illustration of Orientation of a Three-Component Receiver in Typical Crosshole and Downhole Tests (after Mok, 1987).....24

Figure 2.10: Illustration of the Equipment and Procedure of Seismic Cone Penetration Test (from http://www.fes.co.uk/downloads/CPT-general.pdf) 26
Figure 2.11: Illustration of Seismic Dilatometer: (a) Seismic DMT (b) Seismic Dilatometer Test using True Interval Method (c) Seismic Dilatometer Equipment (from Marchetti et al., 2008) 27
Figure 2.12: Illustration of Rayleigh Waves with Different Wavelengths Sampling Materials in a Multi-Layered Material (after Stokoe et al., 1994)....29
Figure 2.13: Illustration of the Equipment Arrangement Using One Receiver Pair in the SASW Testing (after Stokoe et al., 1994).....30
Figure 2.14: Phase of the Transfer Function Measured with the Bulldozer as the Seismic Source and a 100-ft Receiver Spacing (from Stokoe et al., 2009b) 33
Figure 2.15: Individual Experimental Dispersion Curves Created from the Unwrapped Phase Records Measured with a 100-ft Receiver Spacing (Shown in Figure 13b) and a 150-ft Receiver Spacing using a Bulldozer Source (from Stokoe et al., 2009b) 34
Figure 2.16: Composite Experimental Dispersion Curve Created from Phase Measurements Performed at all (8) Receiver Spacings using Geological and Sledge Hammers and a Bulldozer as the Seismic Sources (from Stokoe et al., 2009b). 34
Figure 2.17: Theoretical Dispersion Curve Matched to the Composite Experimental Dispersion Curve (from Stokoe et al., 2009b) 35
Figure 2.18: Shear Velocity Profile Determined from the Iterative Forward Modeling shown in Figure 2.16 (from Stokoe et al., 2009b) 35

Figure 3.1: Three-Dimensional Receiver (one, 3-D Sensor) Used in Typical Downhole Testing....39
Figure 3.2: Conventional Geophone and the Dissembled Geophone Components (from Barzilai, 2000) 40
Figure 3.3: Two, 3-Dimensional Receivers Connected by an Adopter Rod Ready for Use in the Downhole Test....43
Figure 3.4: Examples of 1-D Geophones with Different Natural Frequencies Used for SASW (1 and 4.5 Hz), Downhole (4.5 and 14 Hz) and SCPT (24 and 28 Hz) Tests....44
Figure 3.5: Experimental Set-up Used to Calibrate 28- and 24-Hz Geophones: Reference Accelerometer and Proximitor Used to Measuring Motion Created by a Shaking Table....47
Figure 3.6: Frequency Response Curves of 28- and 24-Hz Geophones Calibrated from 0.5 to 300 Hz Using an Accelerometer as a Reference....48
Figure 3.7: Three-Component, 24-Hz Geophone Securely Assembled in a Teflon Housing with Marine Epoxy....50
Figure 3.8: The Metal Housing and Installation Tool....51
Figure 3.9: Dimensions and Shape of the Cone Tip Used in the Seismic Cone in this Research; Dimensions follow the Ideal Dimension of ASTM D5778-07 52
Figure 3.10: Geophones in Seismic Cone Calibrated Using an Accelerometer and Proximitor as references on an Electromagnetic Shaker 53
Figure 3.11: Response Curves of the Vertical Geophone at the Top of the Teflon Housing; Calibrations over the Frequency Range of 5 to 300 Hz 55

Figure 3.12: Response Curves of the Horizontal (H1) Geophone at the Middle of the Teflon Housing; Calibrations over the Frequency Range of 5 to 300 Hz 56
Figure 3.13: Response Curves of the Horizontal (H2) Geophone at the Bottom of the Teflon Housing; Calibrations over the Frequency Range of 5 to 300 Hz 57
Figure 3.14: Electrical Trigger System with a 9-V Battery and a 2-KΩ Resistor Connected to a Sledge Hammer and then connected to an Aluminum S-Wave Plank and to a Steel P-Wave Plate with Electric Wires 59
Figure 3.15: 3-D Reference Sensor Consisting of Three, 24-Hz Geophones 60
Figure 3.16: 3-D Reference Sensor Calibrated with an Accelerometer and Proximitor on an Electromagnetic Shaker 61
Figure 3.17: Phase Differences and Amplitude between the Seismic Cone and a 3-D Reference Sensor Evaluated with an Accelerometer in the High Frequency Range (40-600 Hz) and a Proximitor in the Low Frequency Range (5-50 Hz).....63
Figure 3.18: Data Acquisition System for Downhole or SCPT Testing 64
Figure 4.1: Photographs of the Testing Setups Used in Downhole Testing with Impulsive Seismic Sources 69
Figure 4.2: Photographs of the Testing Setups Used in Downhole Testing with a Vibroseis Truck.....70
Figure 4.3: Photograph and Profile View of the Testing Setup Used in SCPT Testing 71
Figure 4.4: Preparation of a Borehole for a 3-D Reference sensor 74
Figure 4.5: Illustration of Procedure Used to Install 3-D Reference sensor 75

Figure 4.6: Preparation of a Borehole for Downhole Testing 77
Figure 4.7: Two, 3-Dimensional Sensors Connected by an Adopter Rod Ready for Use in the Downhole Test 79
Figure 4.8: Procedure Used to Install Downhole Sensor (s) 80
Figure 4.9: Photograph Showing a Cable Holder with Two, 3-D Sensors in the PVC-Cased Borehole 81
Figure 4.10: Photograph Showing Rope Attached to One, 3-D Sensor with a Short Rod 82
Figure 4.11: Photographs Showing a Seismic Cone with Three, 24-Hz Geophones 84
Figure 4.12: Installation of a Seismic Cone using the Hydraulic Cylinder on the Rear Bumper of T-Rex connected to a Push Rod 85
Figure 4.13: Photograph of the Pushing and Pulling Adaptors that Connect the Hydraulic Cylinder on the Rear Bumper of T-Rex to the Push Rods (from Cox, 2006) 86
Figure 4.14: Setup of Impulsive Sources Used to Generate Shear and Compression Waves 88
Figure 4.15: Thumper Used to Generate Shear and Compression Waves (from http://nees.utexas.edu/Equipment-Thumper.shtml) 89
Figure 4.16: Theoretical Force Output of Thumper (from http://nees.utexas.edu/Equipment-Thumper.shtml) 89
Figure 4.17: Extraction of a Seismic Cone using the Pulling Adapter Coupled to the Hydraulic Cylinder on the Rear Bumper of T-Rex 91
Figure 5.1: Setup for SCPT Testing Performed in This Research Using a 3-D Receiver and Measuring P and S waves. 96
Figure 5.2: Platt 4 at Hornsby Bend 97

Figure 5.3: Typical CPT Profile at Platt 4 of the Hornsby Bend Site 98

Figure 5.4: Waterfall Plot of Polarized S-Wave Signals Recorded by a Horizontal (H2) geophone in the 3-D Receiver of the Seismic Cone Obtained 15 ft away from the CPT Profile Shown in Figure 5.3.....100

Figure 5.5: S-Wave Travel Time Corrected to the S-wave Travel Time in the Vertical Path versus Depth Obtained 15 ft away from the CPT Profile Shown in Figure 5.3 101

Figure 5.6: V_S Profile Calculated from the Slopes of the Three Best-Fit Lines Shown in Figure 5.5 102

Figure 5.7: Reference Points Identified on Two Signals Generated with Impacts in the Forward-Direction (1: First Arrival; 2: First Trough; 3: First Cross-Over Point; and 4: First Peak).....104

Figure 5.8: Comparison of the V_S Profiles Calculated with 4 Reference Points of Signals for Entire Depth and V_S Profile Calculated by the Time-Depth Plot Shown in Figure 5.6 105

Figure 5.9: Cross Correlation of the Two, S_{vh} Signals Shown in Figure 5.7 107

Figure 5.10: Comparison of the V_S Profile Calculated by the Time vs. Depth Plot and V_S Profile Calculated by Cross Correlation of Signals.....108

Figure 5.11: Comparison of the V_S Profiles Calculated with (1) the Time vs. Depth Plot, (2) Cross Correlation of Signals and (3) the Average Interval Velocity of all 4 Reference Points 109

Figure 5.12: Waterfall Plot of Signals Recorded by the Vertical (V) Geophone in the 3-D Receiver of the Seismic Cone Obtained 15 ft away from the CPT Profile Shown in Figure 5.3 111

Figure 5.13: Waterfall Plot of Signals Recorded by the Horizontal (H1) Geophone in the 3-D Receiver of the Seismic Cone Obtained 15 ft away from the CPT Profile Shown in Figure 5.3.....112

Figure 5.14: The First Arrivals, First Peaks and Second Peaks of Two Waveforms Recorded by the Vertical Geophone at Depths of 39.1 ft and 42.4 ft (1: First Arrival, 2: First Peak, and 3: Second Peak).....113

Figure 5.15: P-wave Travel Time Corrected to the P-wave Travel Time in the Vertical Path versus Depth Calculated from First Arrivals Show on the Waterfall Plot in Figure 5.13 114

Figure 5.16: V_P Profile Calculated from the Slopes of the Three Best-Fit Lines Shown in Figure 5.15.....115

Figure 5.17: The Profile of Possion's Ratios Calculated from the Relationship between V_S and V_P Values Shown in the Profiles Shown in Figures 5.6 and 5.16.....116

Figure 5.18: Waterfall Plot of Signals Recorded by the Vertical (V) Geophone in the 3-D Receiver of the Seismic Cone in Figure 5.12 and P Waves Windowed by a Rectangular Window with the Time Period of 0.01 Seconds 119

Figure 5.19: Waterfall Plot of Signals Recorded by the Horizontal (H1) Geophone in the 3-D Receiver of the Seismic Cone in Figure 5.13 and P Waves Windowed by a Rectangular Window with the Time Period of 0.01 Seconds 120

Figure 5.20: Comparison of the V_P Profiles Calculated by Cross Correlation of Signals and Windowed Signals Recorded to the Vertical (V) Geophone, and the V_P Profile Calculated by the Averaged 1st Arrivals 121

Figure 5.21: Comparison of the V_P Profiles Calculated by Cross Correlation of Signals and Windowed Signals Recorded to the Horizontal (H1) Geophone, the V_P Profile Calculated by the 1st Arrivals, and the V_P Profile Calculated by the Time-Depth Plot.....122
Figure 6.1: CPT Profiles Showing Clay and Sand Layers at SCPT Test Site at Hornsby Bend 125
Figure 6.2: Setup for SCPT Testing Using Impulsive Sources.....126
Figure 6.3: Cross Correlation of Signals: (a) Two Signals from Depths of 16.2 ft and 26.0 ft that were Generated by a S-wave Plank Struck by a Sledge Hammer in the Forward Direction and (b) Cross Correlation of the Two Signals.....128
Figure 6.4: S-Wave Phase Velocity from Analysis of the Transfer Function between the Embedded Reference H-2 Receiver at a Depth of 3.3 ft and the Seismic Cone H-2 Receiver at a Depth of 16.2 ft.....131
Figure 6.5: S-Wave Phase Velocity from Analysis of the Transfer Function between the Embedded Reference H-2 Receiver at a Depth of 3.3 ft and the Seismic Cone H-2 Receiver at a Depth of 26.0 ft.....132
Figure 6.6: S-Wave Phase Velocity from Analysis of the Transfer Function between the H-2 Geophone in the Seismic Cone at a Depth of 16.2 ft and the Same H-2 Geophone in the Seismic Cone at a Depth of 26.0 ft.....135
Figure 6.7: Comparison of V_S Profiles of Average Interval Phase Velocity for Frequency Ranges of Analysis Ranging 20 to 280 Hz, 50 to 250 Hz and 100 to 250 Hz.....137
Figure 6.8: Comparison of V_S Profiles from Three Analysis Methods.....138

Figure 6.9: Variation in H-2 Geophone Output in the Seismic Cone with (a) Frequency and (b) Interval Distance/ Wavelength over the Useable Frequency Range for S-Wave Material Damping Ratio Measurements 144

Figure 6.10: Best-Fit Straight Line through the Unwrapped Phase versus Frequency Relationship 145

Figure 6.11: Attenuation Coefficient, α, Calculated from the Spectral Amplitudes of S-Waves Propagating through the Clay Layer in the Depth Range of 16.2 to 22.7 ft; Relationship Exhibits Dispersion 145

Figure 6.12: Plots Showing Dispersive Damping Ratio and Average Damping Ratio Calculated from the Spectral Amplitudes of S-Waves Propagating through the Clay Layer Ranging from 16.2 to 22.7 ft 146

Figure 6.13: General Effect of Excitation Frequency on Small-Strain Shear Modulus, G_{max}, and Small-Strain Material Damping Ratio in Shear, $D_{S\ min}$ (from Stokoe and Santamarina, 2000) 147

Figure 6.14: V_S Dispersion Curves Showing Two Different Soil Types 149

Figure 6.15: V_S Dispersion Curves Showing Different Soil Types at Two Soil Layers of the Same V_S 150

Figure 7.1: CPT Profiles for Seismic Cone Tests Using Two Different Sources at Platt 4 of the Hornsby Bend.....154

Figure 7.2: Testing Setup Used in SCPT testing with an Impulsive Source and Sinusoidal Source.....155

Figure 7.3: Analysis of the Transfer Function of Two Waves Recorded from Embedded Reference Sensor at Depth of 3.3 ft and Seismic Cone at Depth of 30.4 ft at the Same Time (Source: Thumper): (a) Wrapped Phase, (b) Unwrapped Phase, and (c) Phase Velocity 157

Figure 7.4: Analysis of the Transfer Function of Two Waves Recorded from Embedded Reference Sensor at Depth of 3.3 ft and Seismic Cone at Depth of 36.9 ft at the Same Time (Source: Thumper): (a) Wrapped Phase, (b) Unwrapped Phase, and (c) Phase Velocity 158

Figure 7.5: Analysis of the Transfer Function of Two Waves Recorded from Seismic Cone at Depth of 30.4 ft and Seismic Cone at Depth of 36.9 ft in Different Time (Source: Thumper): (a) Wrapped Phase, (b) Unwrapped Phase, and (c) Phase Velocity.....159

Figure 7.6: Comparison of V_S Profile Comparison for Shear Waves Generated by Thumper and an S-Wave Plank Struck a Sledge Hammer at Platt 4160

Figure 7.7: Comparison of Output Voltages of H2 Geophone Excited by S-Waves Generated with Thumper and a Sledge Hammer at 47.9 ft Depth..161

Chapter 1: Introduction

1.1 Seismic Tests with Boreholes or Penetrometers

The linear and nonlinear dynamic properties of the ground are important information parameters in many types of civil engineering problems. Small-strain (linear) dynamic properties, in the form of compression (P) and shear (S) wave velocities, are directly measured by in-situ seismic tests with boreholes or penetrometers. The measurements are initiated by generating body waves in the ground. Various types of man-made sources are used to generate P and S waves. The times for the waves to travel from the source to receivers are determined. The receivers are generally used to record first-arrival times of these body (P and S) waves. Knowing the arrival times and the distances between the source and receivers, one is able to calculate the wave velocities from which shear moduli and constrained moduli are determined. .

The borehole methods used to perform seismic measurements are typically grouped according to the geometrical configuration of the sources and receivers. Various borehole methods that have been used in civil engineering applications are illustrated in Figure 1.1. One of the most popular borehole methods, the downhole method that is conceptually illustrated in Figure 1.1b, is studied in this research. The generalized downhole method has also been adopted for use with penetrometers (generally cone and dilatometer types) instead of a borehole as shown in Figure 1.2 for the Seismic Cone Penetration Test (SCPT).

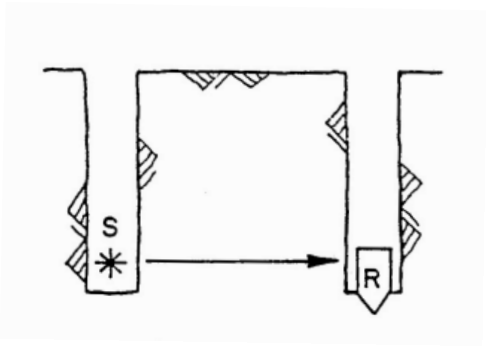

a. Crosshole

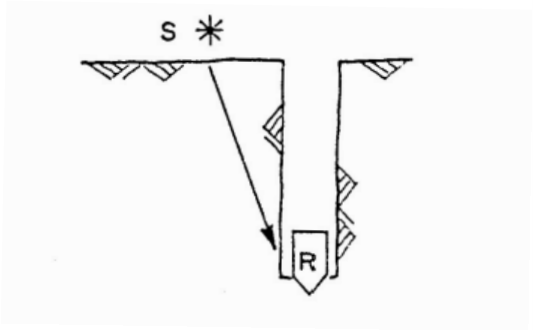

b. Downhole

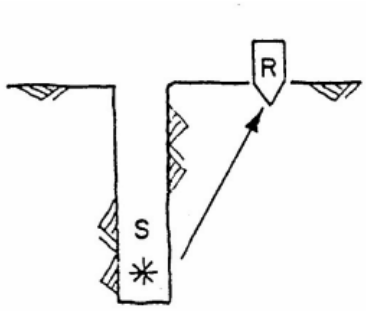

c. Uphole

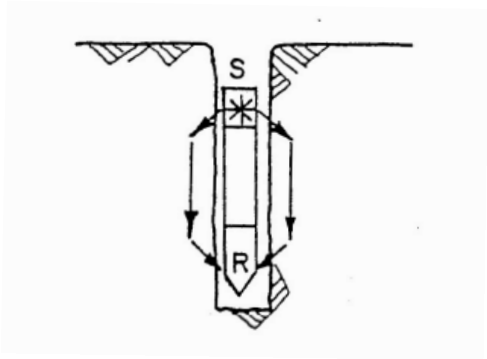

d. In-hole

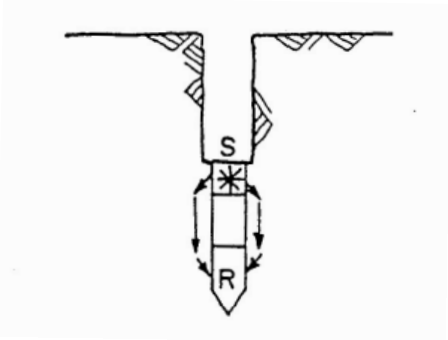

e. Bottom-hole

Figure 1.1: Illustration of Borehole Seismic Methods (after Hoar, 1982)

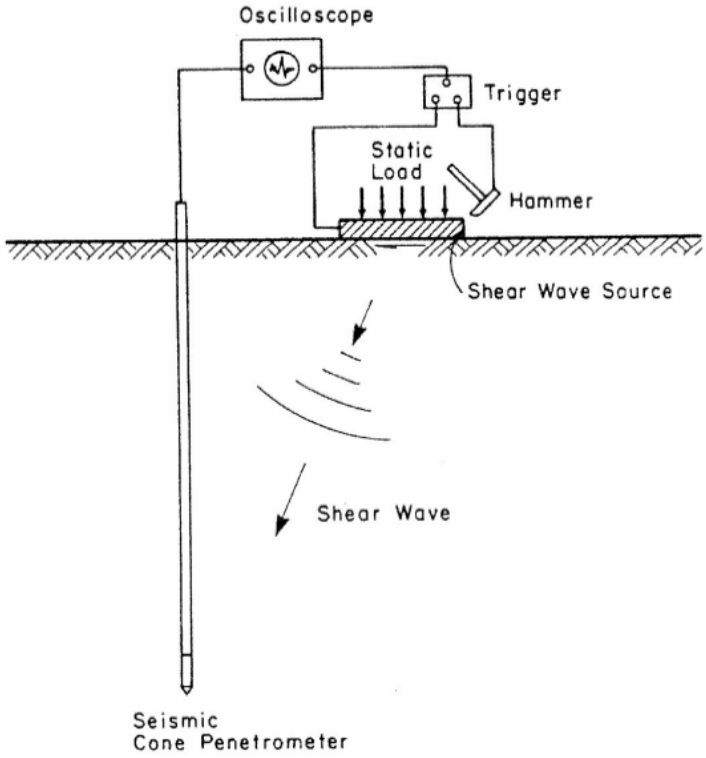

Figure 1.2: Illustration of Seismic Cone Penetration Test (SCPT) using the Downhole Configuration (from Campanella et al., 1986)

1.2 BACKGROUND OF DOWNHOLE SEISMIC TESTING

Downhole seismic tests with boreholes or penetrometers have shown little improvement since the 1980's. They continue to employ essentially the same sensors, sources, test procedures and analytical methods. In these tests, the travel times of first arrivals in time-domain records are used to calculate the velocities of shear and compression waves that propagate through soil and rock layers. The time-domain analytical method generally requires an operator to pick first arrivals of P and S waves in the time domain. Picking first arrivals correctly is critical in calculating the correct wave velocities. However, picking first arrivals correctly in the time domain is not always easy

because of low signal-to-noise records, especially in the case of shear waves and longer travel paths (i.e., say 150 ft (45.7 m) or more). To avoid picking first arrivals, the cross-correlation method has been popularly applied in geophysics to calculate shear and compression wave velocities in downhole tests. The cross-correlation method is automated for determining the time shift between two similarly shaped shear or compression waveforms passing different depths. Even though cross correlation is automated, it is still only used in the calculation of body wave velocities. The reason is that cross correlation is also a time-domain analysis method.

1.3 OBJECTIVES OF RESEARCH

The objectives of this research are to: (1) improve the understanding of conventional downhole seismic testing with boreholes or penetrometers and show how 3-D receivers in the SCPT can improve the test, and (2) by developing a frequency-domain method that overcomes many of the shortcomings of time-domain analysis methods. The frequency-domain method is called the Spectral-Analysis-of-Body-Waves (SABW) method. The SABW method does not require picking first-arrival times. As a result, shear wave velocities can be calculated in the real time using the interpretation method with an automatic calculation procedure, reducing human subjectivity. In addition, the SABW method can be used to evaluate dispersion in body waves from which general soil types can be estimated and calculations of material damping ratio can be performed.

In this dissertation, the first-generation research towards developing the Spectral-Analysis-of-Body-Waves (SABW) method is presented. The frequency-domain analysis method is based on the Spectral-Analysis-of-Surface-Waves (SASW) method which has been developed at the University of Texas at Austin. Calculation procedures for phase

velocities and material damping ratios have been adopted from the SASW method and applied to the basic downhole seismic arrangement with a borehole or a penetrometer.

As a part of the research, improved seismic cone penetrometer downhole sensors have been developed. Two different source triggers were also developed and applied in borehole and penetrometer set-ups. Transient (hammer) and sinusoidal (vibroseis) sources were applied in the SCPT set-up. Downhole tests with a borehole or a penetrometer were performed with the new sensors, triggers and source types at several locations at the Hornsby Bend site about 10 miles from the main campus of the University of Texas. This site exhibits a range in soil profiles. SASW tests were also performed at the site so that V_S profiles could be compared with the results from SCPT and downhole tests. The soil profiles estimated from cone resistances and friction ratios were compared with the V_S profiles and help differentiate differences in the profiles.

1.4 ORGANIZATION OF DISSERTATION

This dissertation is organized into eight chapters. In Chapter 2, the theory of motions of body waves in the ground is introduced. Borehole tests such as the downhole and crosshole tests and seismic tests with penetrometers, such as the seismic cone penetration test (SCPT) and seismic flat-plate dilatometer test (SDMT) are introduced in this chapter. The basic concepts and calculation procedures used in the SASW method are also presented in Chapter 2 because they form the basis for developing the SABW method. In addition, SASW measurements were performed for comparison with the V_S profiles determined with the downhole and SCPT tests.

In Chapter 3, equipment designed and constructed for this research is presented. Downhole sensors were developed by designing and constructing an adaptor connecting two, 3-D geophones. The 3-D geophones contained 24- and 28-Hz geophones. These

geophones were calibrated and the calibration factors were compared to find an appropriate sensor for the seismic cone penetrometer. The overall sensor housing for the SCPT consisted of an outer, stainless-steel housing and an inner Teflon housing. The outer housing was designed to penetrate soil layers and deliver the 3-D sensor safely into the ground. Electrical triggers and a reference tri-axial sensor were developed and calibrated for use in conducting conventional and advanced SCPT testing as well as the new SABW test. The data acquisition system is also briefly introduced in Chapter 3.

The field test procedures used in downhole and SCPT testing are described in Chapter 4. A borehole was prepared for downhole tests at the Hornsby Bend site. A borehole and CPT rods were used to position the seismic sensors in the ground for the downhole and SCPT tests, respectively. Different sensor delivery systems for the installation and extraction of the sensors are a key difference in the downhole and SCPT tests. On the other hand, the same impulsive hammer sources and the same vibroseis, called Thumper, were used in both test procedures to generate shear and compression waves.

Preliminary testing was performed at the Hornsby Bend site to evaluate the functionality of the 3-D sensor in the SCPT test. The preliminary work is presented in Appendix A. S-wave velocities based on first arrivals were calculated with the conventional, time-depth SCPT data analysis procedure. V_S profiles from SCPT and SASW tests are plotted and compared. The possible rotation of the seismic cone is discussed and verified with laboratory calibration tests using the two, orthogonal, horizontal receivers in the 3-D receiver. All of this preliminary testing is contained in Appendix A because it only represents “back-up” material and not the thrust of this work.

Several types of conventional and advanced testing and analysis procedures used in SCPT tests are introduced in Chapter 5. All of this work is time-domain based. The

resulting V_S profiles are compared. S- and P-wave velocities were calculated using time differences based on first arrivals and other reference points and with the cross correlation of signals. P-wave arrivals were identified by using waveforms on both the vertical and radial horizontal geophones.

The Spectral-Analysis-of-Body-Waves (SABW) method is introduced in Chapter 6. The analysis procedures for velocity and damping measurements for S- and P-waves are developed and discussed. The field measurements are concentrated on S waves because the analysis of P-waves needs additional study for using the SABW method. The dispersive characteristic of S-wave velocities and damping ratios in shear is introduced and it is shown how additional information related to soil types is determined.

In Chapter 7, use of the SABW test with a sinusoidal source (the vibroseis called Thumper) is presented. Comparisons are made with impact sources to show V_S profiles and the voltage amplitudes generated from the transverse horizontal (H-2) geophone in the seismic cone. The comparisons prove that (1) Thumper generating S- and P-waves with various waveforms in the interesting frequency range is more controllable and (2) Thumper is more energetic to perform the test in deeper depths.

In-situ downhole and SCPT tests according to the field test procedures presented in Chapter 4 were performed at the Hornsby Bend site. The results of downhole and seismic cone tests are compared as well as are profiles from the results of CPT and SASW tests in Appendix B. It is discussed how the differences of location and time influence on V_S profiles.

Summary, conclusions, recommendations and future work are presented in Chapter 8.

Chapter 2: Literature Review of In-Situ Seismic Testing Related to This Research

2.1 INTRODUCTION

In this chapter, dynamic soil properties such as shear and constrained moduli and material damping are briefly discussed in the context of how they are evaluated by in situ seismic tests. Dynamic moduli are calculated using stress wave velocities and material densities. Material damping, which is caused by geometrical spreading, back-scattering and frictional energy loss in soil, is evaluated from attenuation measurements. Stress wave velocity and material damping are calculated and described by equations modeling wave propagation and motions. Velocities of body waves such as shear and constrained waves are measured by in situ seismic tests. Shear wave velocity profiles are obtained by performing in situ seismic tests with proper testing and analytical procedures. These testing and data analysis procedures are introduced and discussed in this chapter for the following in situ seismic tests: (1) downhole, (2) crosshole, (3) SCPT, (4) SDMT and (5) SASW.

2.2 DYNAMIC SOIL PROPERTIES

Stress waves are not dispersive in a homogeneous, isotropic, elastic material. In other words, the wave velocity in the material is independent of frequency or wavelength. Generally, dynamic soil behavior depends on the stiffness and damping of the material. The stiffness and mass density of the material affect the velocities of elastic stress wave as:

$$V_s = \sqrt{\frac{G}{\rho}} \tag{2.1}$$

$$V_p = \sqrt{\frac{M}{\rho}} = \sqrt{\frac{\lambda + 2G}{\rho}} = \sqrt{\frac{E(1-\nu)}{\rho(1+\nu)(1-2\nu)}} \tag{2.2}$$

Where: V_s and V_p are shear and compression wave velocities respectively,

G, M and E are shear, constrained and Young's moduli respectively,

ρ is mass density,

λ is Lame's constant, and

ν is Poisson's ratio.

Compression and shear wave velocities are related through Poisson's ratio by:

$$V_p = V_s \sqrt{\frac{2(1-\nu)}{1-2\nu}} \tag{2.3}$$

Material particle motion decreases as stress waves propagate away from a source. The stress wave attenuation is called damping. Damping is caused by geometrical spreading, frictional energy loss and back-scattering. In this study, the back-scattering will not be discussed because the diameters of soil particles over wavelengths are relatively small. In Figure 2.1, the component of damping caused by geometrical spreading is described. Body waves propagating radially outward from a vibrating circular footing on the surface of a homogeneous, isotropic, elastic half-space are shown. Body waves (compression (P) and shear (S)) propagate along hemispherical wave fronts. The body waves generated by the source spread radially into increasingly larger volumes as the waves propagate away. The energy of body waves attenuates with increasing distance from the source as r^{-1} within the mass and r^{-2} along the surface. Rayleigh (R) waves are also shown in Figure 2.1. R waves are surface waves and mainly propagate within 1.5 wavelengths of the half-space surface. As noted in Figure 2.1, R waves

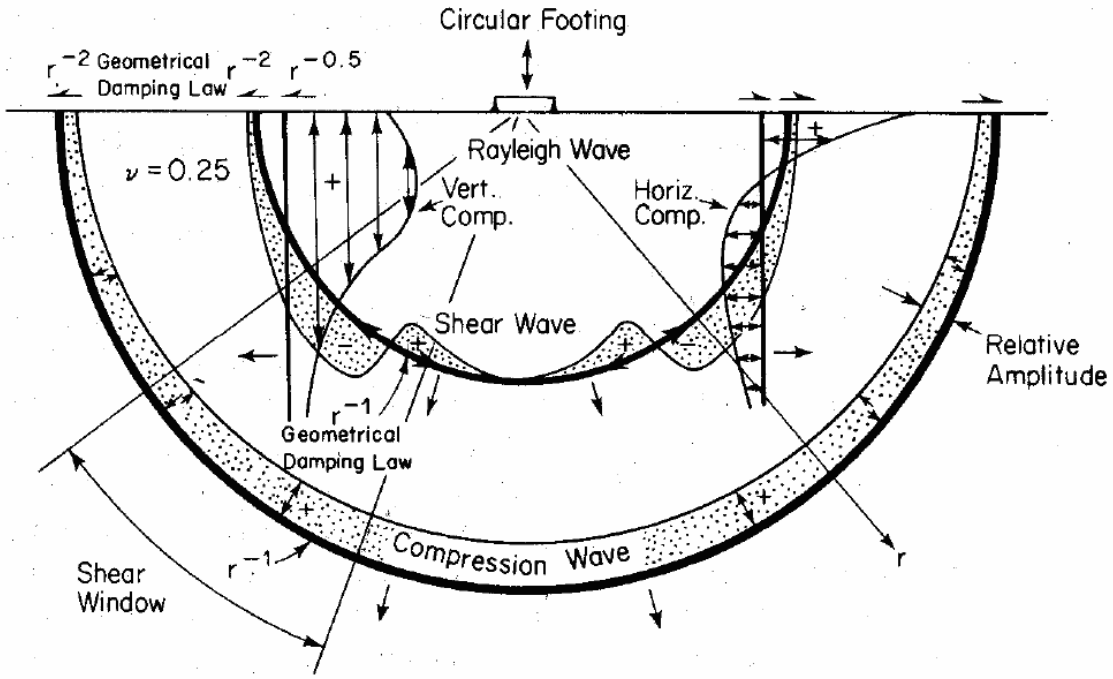

Figure 2.1: Distribution of Body and Surface Waves from a Vibrating Circular Footing on a Homogeneous, Isotropic, Elastic Half-space (from Woods, 1968)

attenuate according to $1/\sqrt{r}$ in a homogeneous, isotropic, elastic half-space.

In geotechnical engineering, the frictional energy loss per cycle of loading is called material damping. Material damping in this linear system is quantified by using the quality factor, Q or the damping ratio, D, as:

$$D = \frac{1}{2Q} = \frac{\Delta E}{4\pi E} = \frac{\alpha V}{2\pi f} = \frac{\alpha \lambda}{2\pi} = \frac{\delta}{2\pi} = \frac{\Delta f}{2 f_r} \tag{2.4}$$

where $D =$ damping ratio, $Q =$ quality factor, $\Delta E =$ the amount of energy dissipated per cycle of harmonic excitation in a certain volume, $E =$ the peak elastic energy stored in the same volume, $\alpha =$ attenuation coefficient, $V =$ propagation velocity, $f =$ frequency,

$\lambda =$ wavelength, $\delta =$ logarithmic decrement from the free vibration decay, $\Delta f =$ resonance width, and $f_r =$ resonant frequency.

Parameters influencing shear modulus and damping are the effective confining pressure, confining time, stress history, void ratio, number of cycles, and, in a nonlinear system, the amplitude of loading. The influence of these parameters has been studied by numerous investigators such as Seed and Idriss (1970), Richart, Hall and Woods (1970), Hardin and Drnevich (1972a and 1972b), Hardin (1978), Drnevich et al. (1978), Seed et al. (1984), Ishihara (1996), Santamarina et al. (2001) and Darendeli et al. (2001) in the laboratory. Laboratory methods have allowed studies of the effects of various soil and state parameters to be conducted that are not possible in the field. Important examples of these studies are studies of the impact of shearing strain on shear modulus and material damping. However, the shear modulus (G_{max}) and material damping ($D_{s,min}$) at small strains can be evaluated through in situ tests. The relation of modulus and damping in shear, collected by laboratory and field methods, has been studied and discussed by Stokoe et al. (1978), Idriss (1991) and Stokoe and Santamarina (2000).

Stokoe et al. (1978) showed the generalized relationship between G-log γ measured in the laboratory and the in-situ maximum shear modulus. This generalized relationship is presented in Figure 2.2. The shear modulus difference from the laboratory and field methods is largely because of disturbance and stress relief during and after sampling the soil, the long-term time effect and the intrinsic differences between the native environment and laboratory conditions.

Darendeli et al. (2001) studied the effects of parameters that control nonlinear soil behavior and their relative importance in terms of affecting normalized modulus reduction and material damping curves. The parameters are strain amplitude, mean effective confining pressure, soil type and plasticity, number of loading cycles, frequency

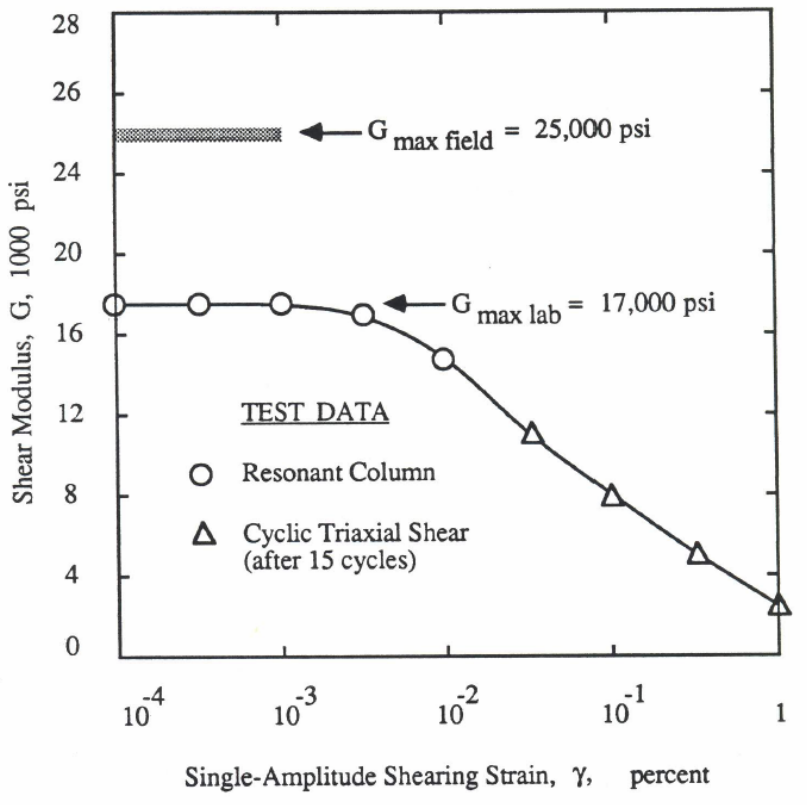

Figure 2.2: Typical Shear Modulus Variation with Shearing Strain Amplitude as Determined by In Situ and Laboratory Tests (from Stokoe et al., 1978)

of loading, overconsolidation ratio, void ratio, degree of saturation, and the characteristics, size, shape, gradation and mineralogy of grain. The effect of confining pressure on normalized modulus reduction and material damping curves of silty sands are shown in Figure 2.3.

Stokoe and Santamarina (2000) emphasized the importance of in situ tests because $G_{\max,field}$ collected by in situ seismic tests for various soil types are often quite different from $G_{\max,lab}$ evaluated by laboratory tests for the same materials. As a result, $G_{\max,field}$ has been used to scale laboratory shear modulus reduction curves to estimate field shear modulus reduction curves as illustrated in Figure 2.4. The in situ shear

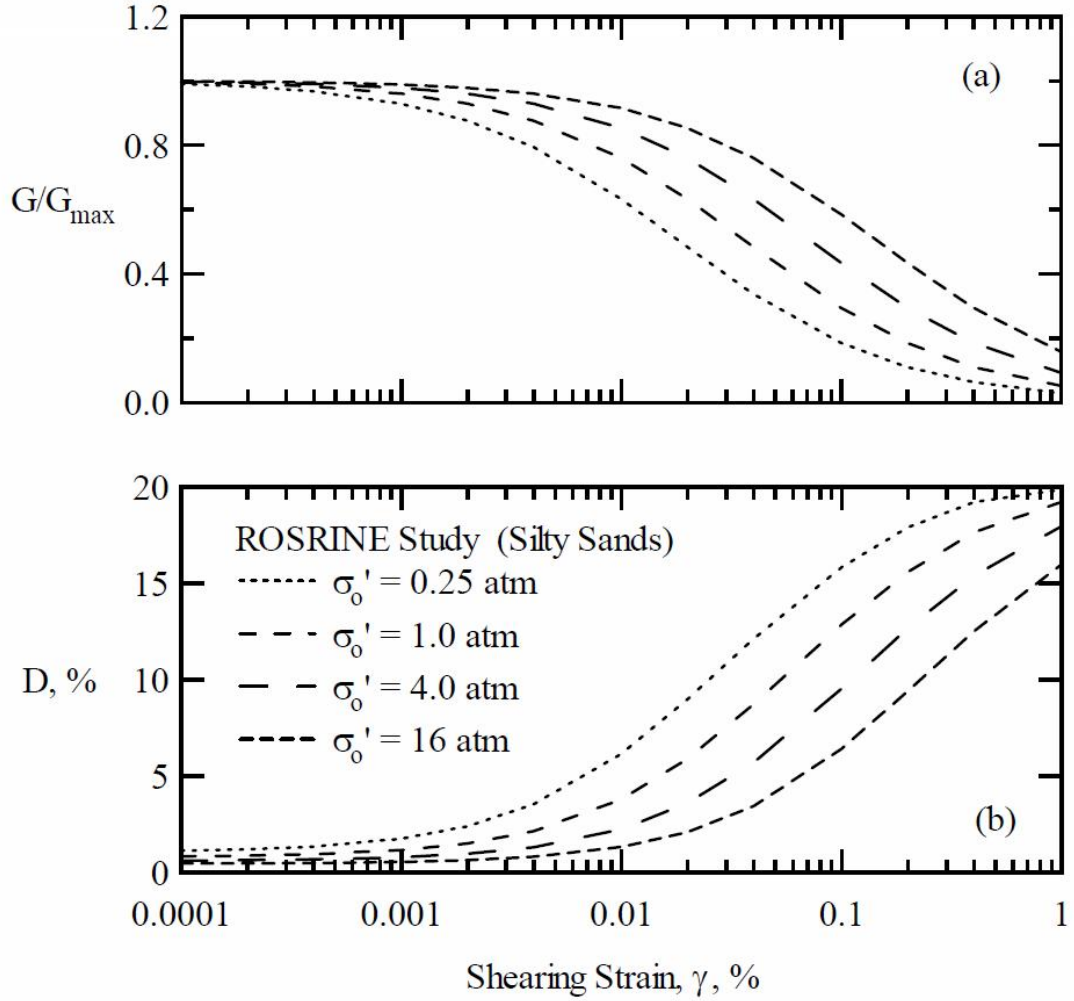

Figure 2.3: The Effect of Confining Pressure on (a) Normalized Modulus Reduction and (b) Material Damping Curves of Silty Sands Evaluated as Part of the ROSRINE Study (From Darendeli, 2001)

modulus reduction curves are estimated from:

$$G_{\gamma,field} = \left(\frac{G_{\gamma,lab}}{G_{\max,lab}} \right) \cdot G_{\max,field} \tag{2.5}$$

where $G_{\gamma,field}$ = estimated in situ shear modulus at a shearing strain of γ, $G_{\gamma,lab}$ = shear modulus evaluated by laboratory tests with an intact specimen at a shearing strain of γ,

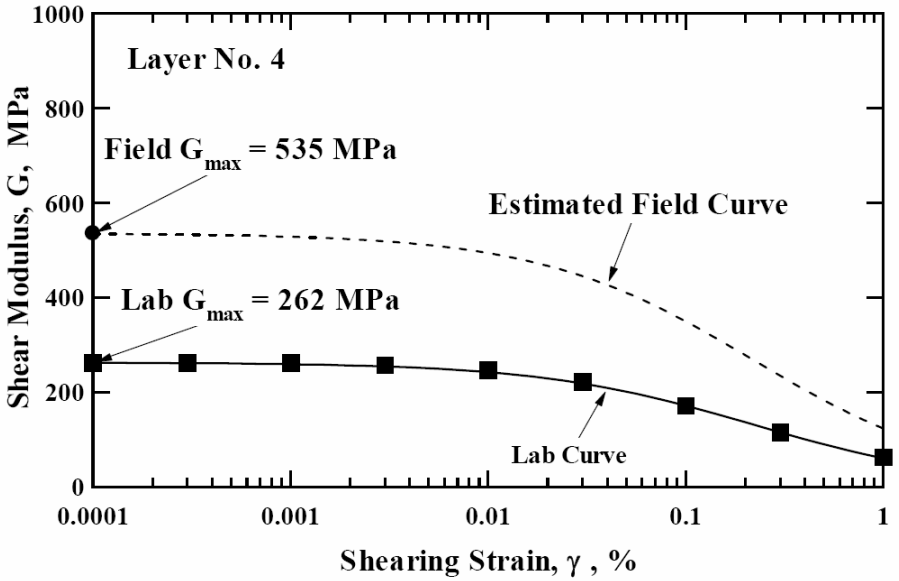

a. Estimated Laboratory and Field Modulus

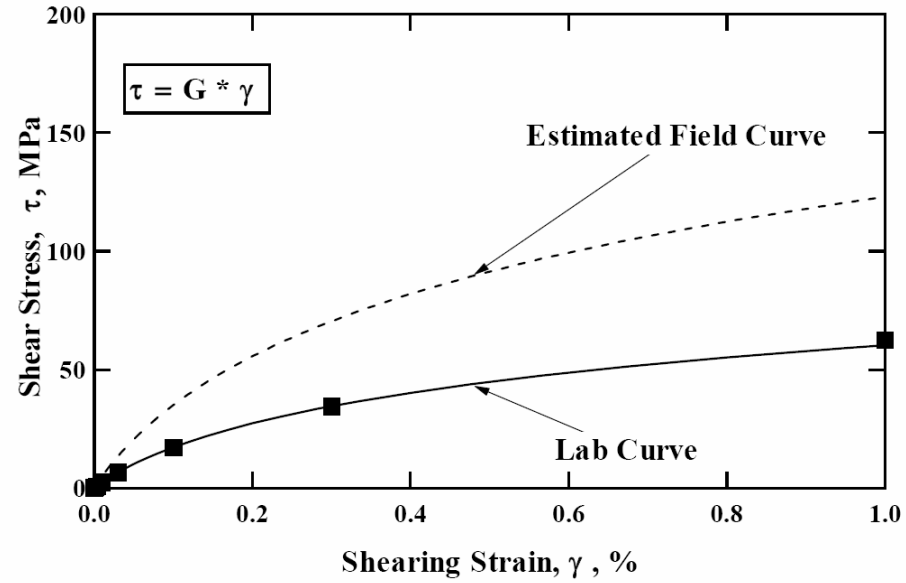

b. Estimated Laboratory and Field Stress-Strain Curves

Figure 2.4: Comparison of Estimated G-log γ and τ-γ Curves with Similar Curves Evaluated in The Laboratory (from Stokoe and Santamarina, 2000)

$G_{\max,lab}$ = small-strain shear modulus evaluated by the laboratory tests and $G_{\max,field}$ = shear modulus determined by in situ seismic tests.

In terms of this research, the shear stiffness and material damping of soil are mostly discussed at small strains (less than 0.001 percent) because this research focuses on in-situ seismic tests. The shear modulus and material damping in shear determined with vertically propagating and horizontally polarized shear waves (S_{vh}-waves) are the focus of this research. The method of testing is the downhole method and the seismic source is either a shear plank with a sledge hammer or a vibroseis ("Thumper") with horizontal shaking using the stepped-sine mode. The S_{vh}-waves are generally assumed to be vertically propagating so that they are not converted into compression waves by horizontal soil layers of different impedances.

2.3 MOTIONS OF BODY WAVES

Disturbances created by an impulsive source in a homogeneous, isotropic, linear, elastic continuum propagate as stress waves. The stress waves are compression and shear waves. Motions created by the stress waves near the impulsive source are quite complex because the propagating waves include near- and far-field terms (Sanchez-Salinero et al., 1986). In this study, only the far-field terms are considered because the near-field terms decay rapidly, generally within a propagating distance of two wavelengths or less. The far-field motions of horizontally propagating compression waves and horizontally propagating and vertically polarized shear waves are shown in Figure 2.5. The stress waves are called body waves because they propagate within the body of the half-space.

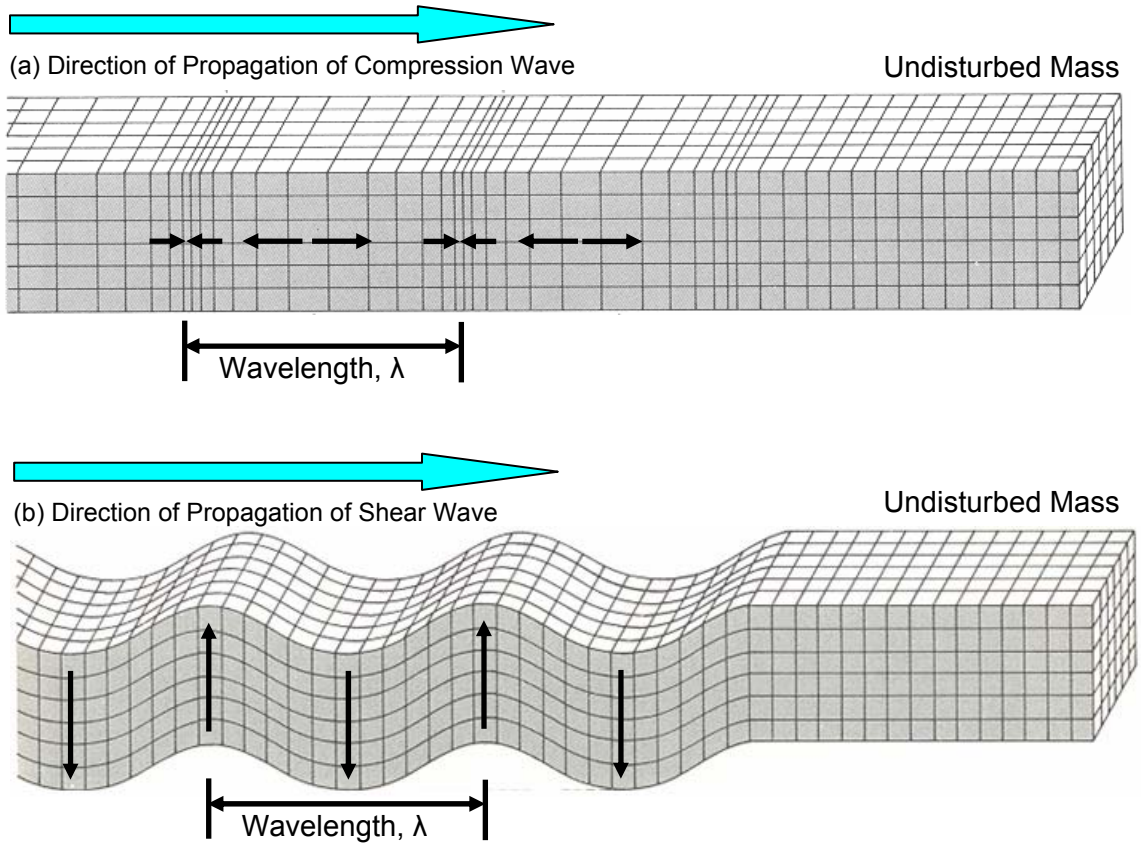

Figure 2.5: Illustration of Propagation of Body Waves within a Homogeneous, Isotropic, Linear, Infinite Medium (after Bolt, 1976)

The motion of a sinusoidal wave propagating within a uniform soil can be described by:

$$A(x,t) = A_0 e^{i\frac{2\pi}{\lambda}\cdot(x-Vt)} \tag{2.6}$$

Where: A_0 is the initial amplitude of the wave for the initial condition ($x = 0$, $t = 0$), λ is wavelength, x is the distance from source, V is the wave velocity and t is the time. Equation 2.6 describes a sinusoidal wave propagating along the positive x-axis at velocity, V without attenuation.

To simplify Equation 2.6, $k = \frac{2\pi}{\lambda}$, $\omega = 2\pi f = \frac{2\pi}{T}$ and $T = \frac{\lambda}{V}$ are introduced and Equation 2.6 is simplified to:

$$A(x,t) = A_0 e^{i(kx-\omega t)} \tag{2.7}$$

where k is the wave number, ω is the circular frequency and T is period. Equation 2.7 is for the waves propagating along one axis.

When considering propagation of waves in a 3-dimensional soil mass, and in particular the propagation of S_{vh} waves, the displacement can be expressed as:

$$A(r,t) = \frac{A_0}{r} e^{i(kr-\omega t)} \tag{2.8}$$

where r here denotes the radial distance from a source of S_{vh} waves to the receiver where the motion $A(r,t)$ is recorded. $\frac{A_0}{r}$ is the amplitude of the S_{vh} waves decreased by geometrical spreading. The expression is valid for a homogeneous, isotropic soil medium.

The soil mass must be considered a visco-elastic material with frictional losses in the soil itself. A simplistic way of accounting for material attenuation is to modify the wave number in Equation 2.8 by introducing an imaginary part, i.e., by setting as:

$$k = k_r + i\alpha \tag{2.9}$$

where k_r is the real part of the wave number and α is the attenuation coefficient. With Equation 2.9, Equation 2.8 can be written as:

$$A(r,t) = \frac{A_0}{r} \cdot e^{i(k_r r-\omega t)} \cdot e^{-\alpha r} \tag{2.10}$$

where now the factor $e^{-\alpha r}$ accounts for material attenuation along the radial direction.

2.4 DOWNHOLE TEST

In the downhole test, vertically propagating and horizontally polarized shear waves (S_{vh} waves) and vertically propagating compression waves (P_v waves) travel from an S-wave source and a P-wave source on the ground surface to receivers at a known depth in a borehole or in a probe, respectively. Vertically traveling S_{vh} and P_v waves are not converted to other waves by a horizontal boundary. As shown in Figure 2.6, the horizontal distance between a source and a borehole is known and the distance between a source and a receiver is calculated. The first arrival times of S_{vh} or P_v waves are measured in each depth. The time difference of the first arrival times of S_{vh} or P_v waves, and the distance difference in each depth are used to calculate wave velocities.

A simple plank which is heavily loaded is located about 2 to 3 m from the borehole. The plank is struck horizontally by a sledge hammer to generate S_{vh} waves. The plank source and testing technique are described in detail by Patel (1981). The S_{vh} waves generated by the source are recorded using a waveform analyzer. A triggering device that is connected to the sledge hammer is used to trigger the analyzer. Various triggering devices were introduced by Stokoe and Hoar (1978b). The importance of a good triggering device was emphasized by Stokoe and Hoar (1978b). A waveform analyzer should have high resolution for timing, and frequency measurements.

Two or more receivers with known distances between them can be used in downhole test as shown in Figure 2.7. The first arrival times of two or more receivers are recorded at different depths. This measurement is called a “true interval” travel time because the waves are produced by the same impulse. On the other hand, pseudo-interval

measurements, that involve waves that are produced by different impulses associated with the same receiver at different depths, are illustrated in Figure 2.6. True-interval measurements show less scatter for the wave velocity profiles than pseudo-interval measurements (Mok, 1987).

Determination of correct wave velocities requires correctly determining the wave travel distance and associated wave arrival times at two or more locations. Mok (1987) measured the inclination of the borehole in downhole and crosshole tests to get the correct distance between a source and a receiver or between a source and two receivers. Batsila (1995) and Kim et al. (2004) used an analytical method considering the effect of refraction in the ray paths of body waves, such as Snell's Law, to get a correct distance. Patel (1981) and Rice (1984) suggested closely locating the source to reduce the refraction of body waves.

2.5 CROSSHOLE TEST

In the crosshole test, the time of body waves propagating horizontally from a source in one borehole to one or more receivers in other boreholes at the same depth as the source is measured as illustrated in Figure 2.8. A mechanical source was developed at the University of Texas by Mok (1987) for the crosshole testing. The moveable hammer in the source strikes a wedging block in the borehole. Frictional forces holding the mechanical source in place increase for an instant and simultaneously apply transient shearing and compressional forces to the source borehole in which the mechanical source is wedged. This compressional and shearing forces cause the borehole casing and surrounding grout or rock around the source borehole to strain and generate horizontally propagating compression waves (P_h waves) as well as horizontally propagating and

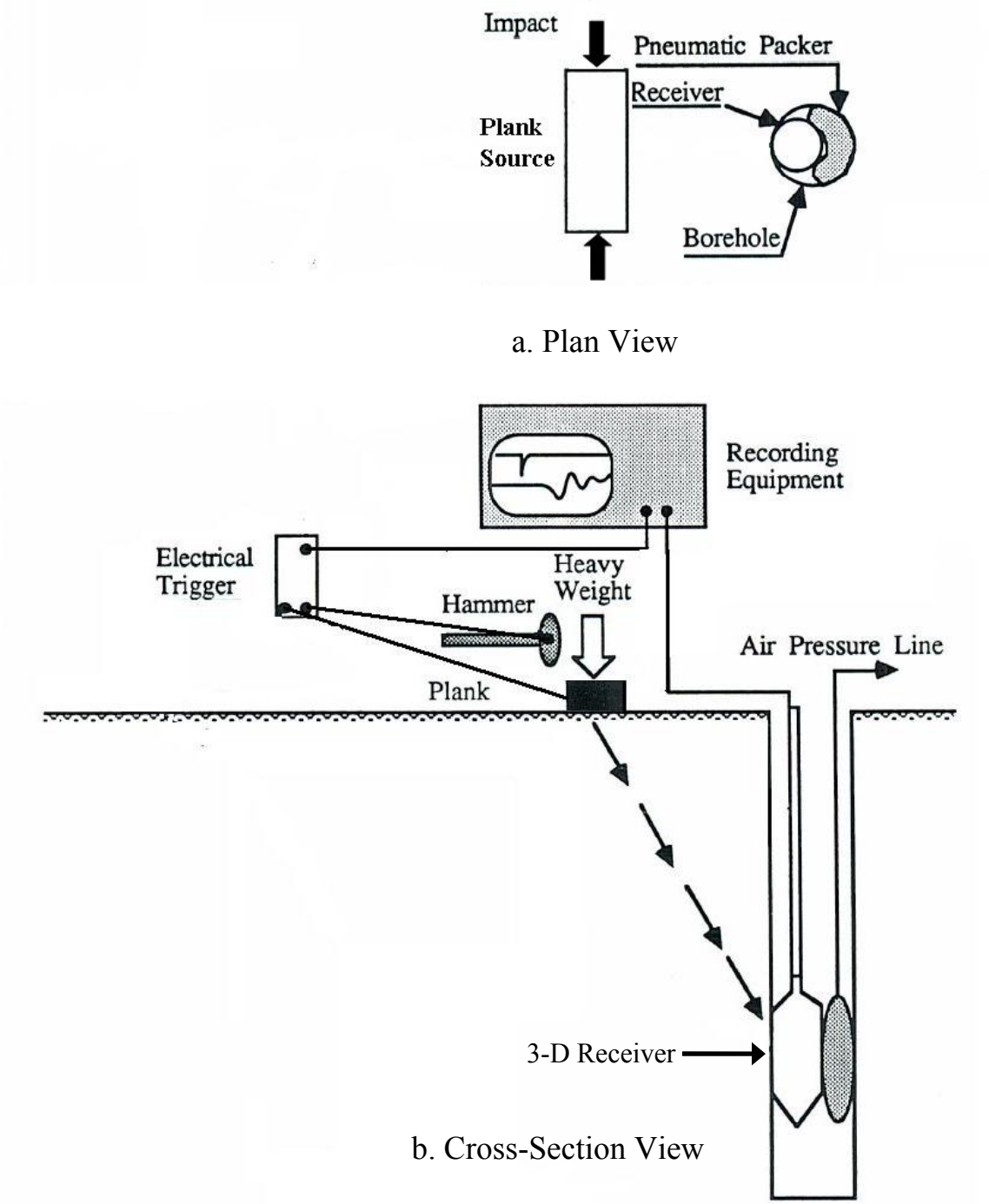

Figure 2.6: Illustration of Downhole Test Using One, 3-D Receiver (from Mok, 1987)

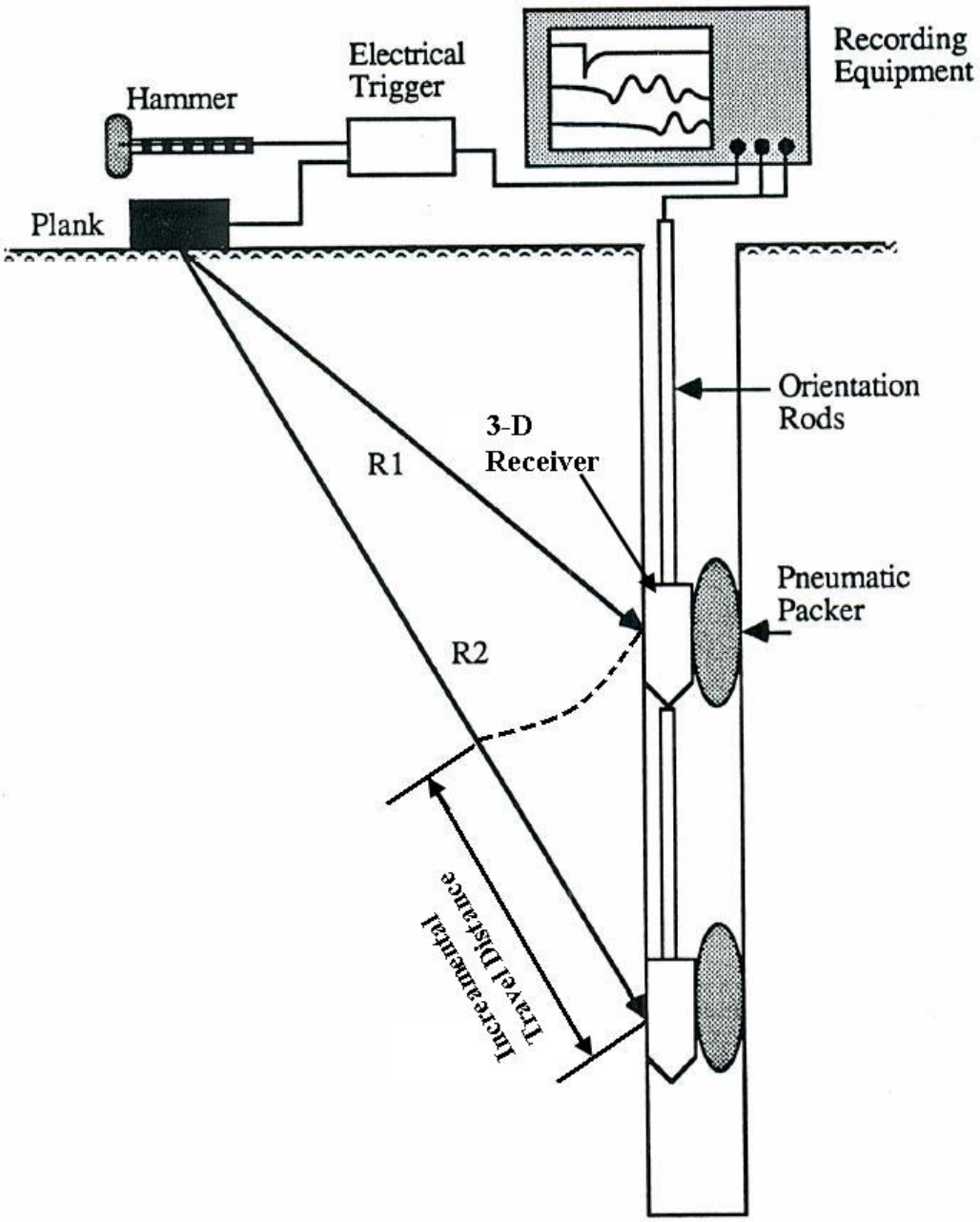

Figure 2.7: Illustration of Downhole Test Using Two, 3-D Receivers (from Mok, 1987)

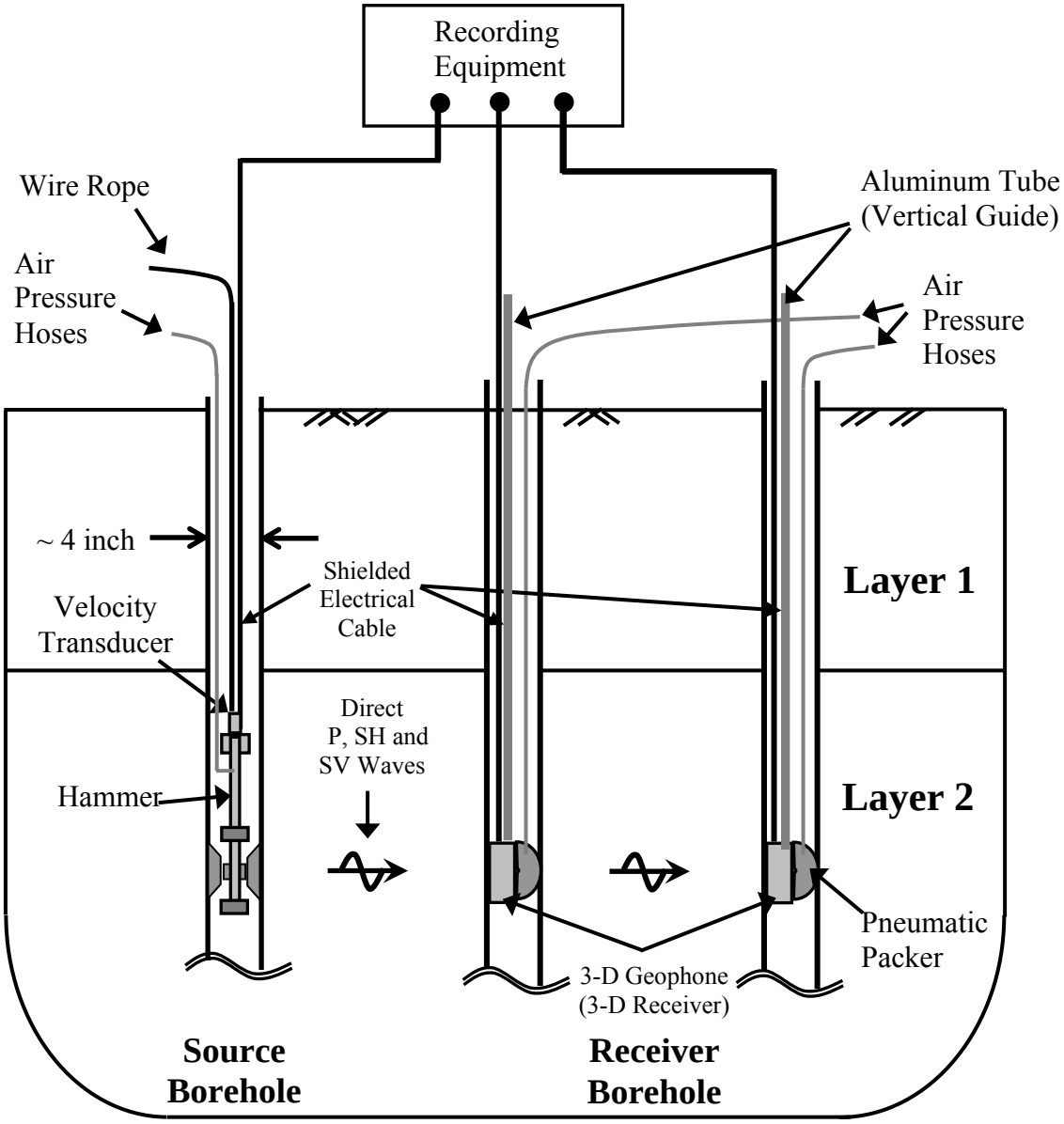

Figure 2.8: Illustration of Crosshole Test (after Mok, 1987)

vertically polarized shear waves (S_{hv} waves) as shown in Figure 2.9a. The mechanical source is reversible so that two sets of S_{hv} waves are generated, one with downward impacts and one with upward impacts. The reversibility makes the initial arrival of the polarized shear wave to be more easily identified.

A vertical velocity transducer is mounted on top of the mechanical source as a trigger. The impact generated by the mechanical source excites the trigger and a three component receiver that is held in wall by a pneumatic packer for each borehole. The motions of P_h and S_{hv} waves are measured using radial horizontal and vertical geophones in each three-component receiver as in Figure 2.9.

The procedure for generating and recording waves is repeated at given depth intervals, generally ranging from 2.5 ft to 10 ft (Mok, 1987). Accurate wave velocities are calculated using the correct distances determined from inclination surveys of the boreholes measured by some type of slope indicator.

Various discussions of test procedures and data analysis methods are found in Stokoe and Woods (1972), Woods (1978), Stokoe and Hoar (1978a), Hoar (1982) and Mok (1987).

2.6 SCPT AND SDMT TESTS

The downhole test that uses the Cone Penetration Test (CPT) was developed by Campanella et al. (1986). It is called the Seismic Cone Penetration Test (SCPT). By combining the CPT and seismic sensors, engineers and geophysicists are able to perform the CPT and downhole test at the same time, as illustrated in Figure 2.10. By using push rods of the CPT as the tool delivering the seismic sensors, the need for and the additional cost of a borehole are eliminated. The vertical thrust applied at the surface in the CPT rig

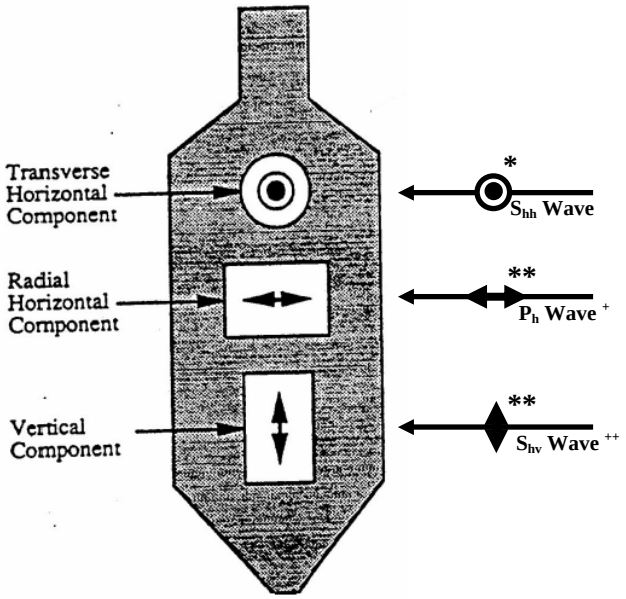

Note: P_h^+ and S_{hv}^{++} waves are generated in typical crosshole testing with a vertically excited source.

a. Crosshole

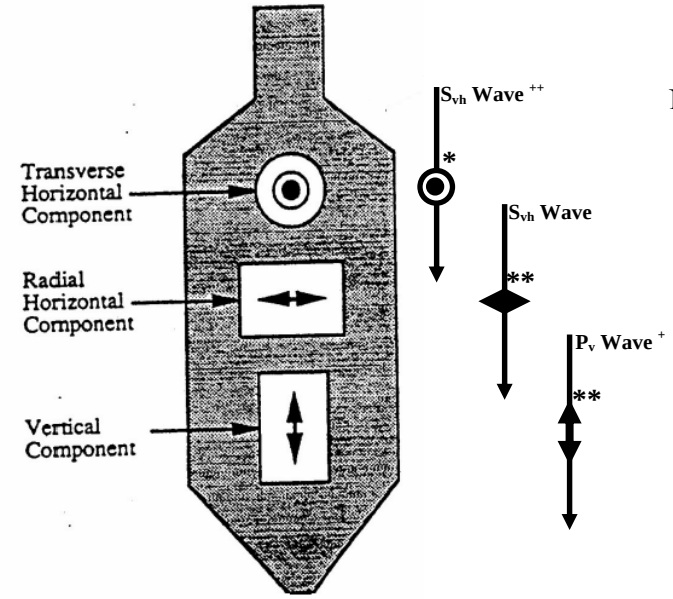

Note: A P_v^+ wave and one S_{vh}^{++} wave are generated in typical downhole testing. Vertical impacts are used to generate P_v waves while horizontal impacts are used to S_{vh} waves.

b. Downhole

* indicates particle motion perpendicular to the plane of the figure.
** indicates particle motion in the plane of the figure.

Figure 2.9: Illustration of Orientation of a Three-Component Receiver in Typical Crosshole and Downhole Tests (after Mok, 1987)

forces the push rods downward or upward. Furthermore, pushing the seismic sensor into the ground creates excellent coupling between the receivers and surrounding soil.

Campanella et al. (1986) used a horizontal 28-Hz geophone for the SCPT. Campanella and Stewart (1991) suggested the use of the cross-over method which involves comparing polarized shear wave signals that are reversed by applying opposite impacts to the source plate struck by a sledge hammer. This method was suggested because the first arrival times of shear waves were not always clear. Campanella and Stewart (1992) also used the cross-correlation method for two shear wave signals at different depths in the SCPT. The cross-correlation method uses the time shift between peak points of two similar wave signals to calculate a wave velocity. The use of cross-correlation enabled one to eliminate picking the first arrival time in the time domain. Butcher et al. (2005) introduced a guide line for seismic cone downhole testing and analysis procedures to measure shear wave velocity. Areias and Van Impe (2006) showed that, generally, variations between true and assumed direct travel paths were small and could be ignored in Seismic Cone Penetration Testing (SCPT) calculations.

Kates (1996) and Martin and Mayne (1997 and 1998) combined the conventional flat-plate dilatometer and seismic downhole testing by placing a velocity transducer in a rod connecting the dilatometer blade. It is called the seismic flat-plate dilatometer test (SDMT). The SDMT enables one to perform both the conventional dilatometer testing and downhole testing at the same time just like the SCPT combines two testing techniques. Steel rods instead of a borehole are used to deliver the seismic sensor into the ground, creating good coupling between the seismic sensor and the surrounding soil Mayne, Schneider and Martin (1999) utilized the shear wave velocity and inflation pressures obtained from SDMT and a modified hyperbola in order to connect the small-strain seismic region to large-strain strength. Marchetti et al. (2008) measured the interval

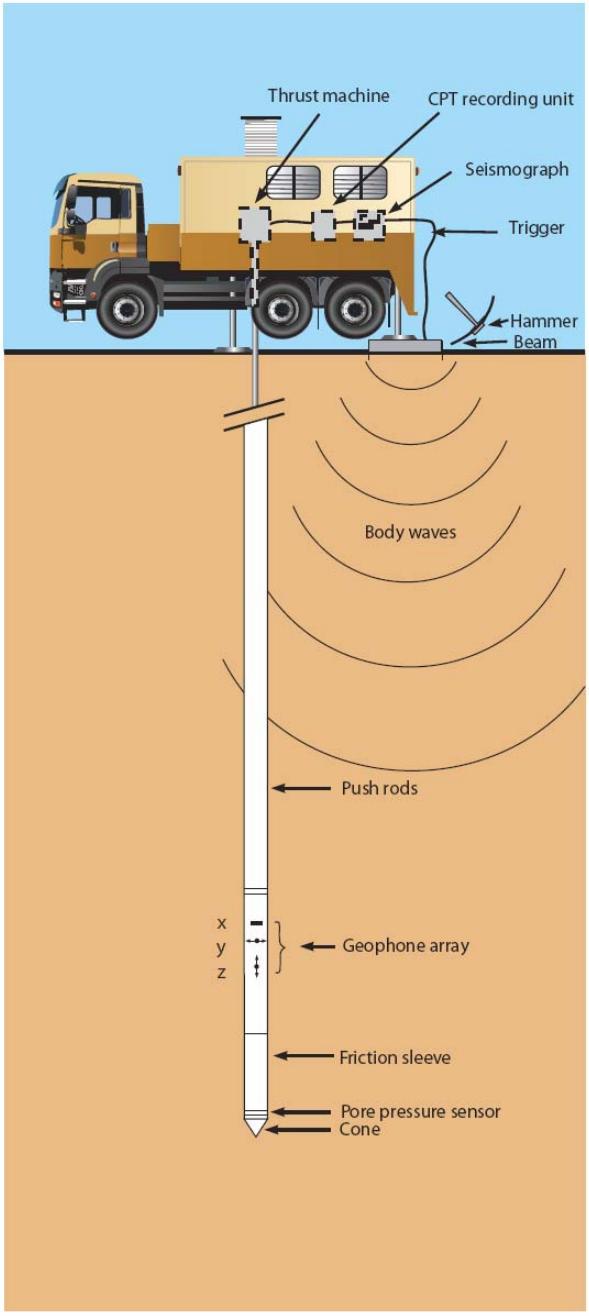

Figure 2.10: Illustration of the Equipment and Procedure of Seismic Cone Penetration Test (from http://www.fes.co.uk/downloads/CPT-general.pdf)

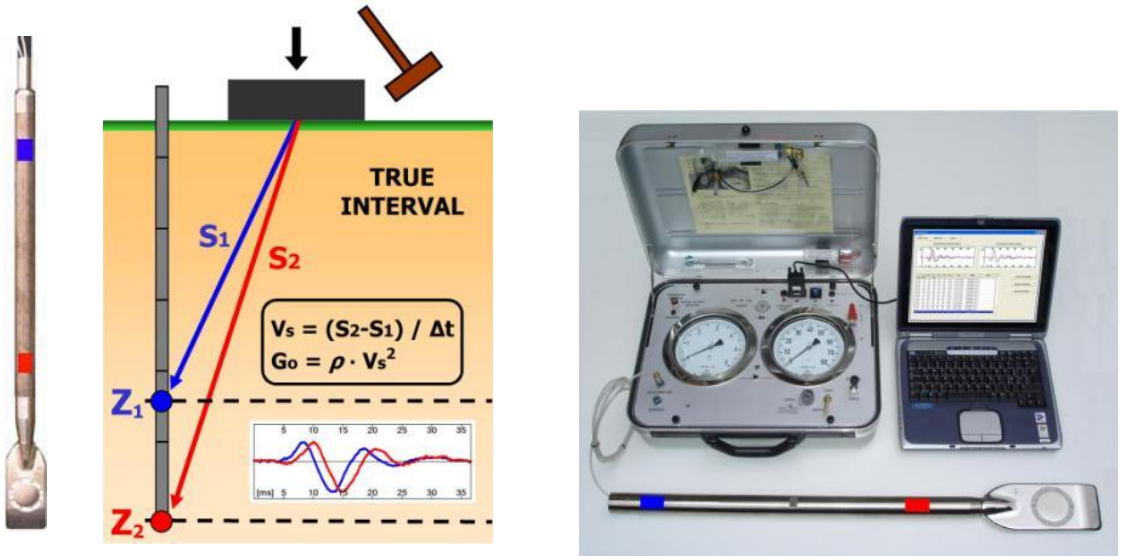

(a) (b) (c)

Figure 2.11: Illustration of Seismic Dilatometer: (a) Seismic DMT (b) Seismic Dilatometer Test using True Interval Method (c) Seismic Dilatometer Equipment (from Marchetti et al., 2008)

velocities by placing two sensors in the SDMT and using the time shift of the two signals collected from two sensors (Figure 2.11). They summarized and discussed the experience obtained from the SDMT tests performed at 34 sites. They constructed diagrams showing interrelationships between experimental maximum shear modulus (G_0), dilatometer modulus (E_D), constrained modulus (M_{DMT}). Totani et al. (2009) used the SDMT to obtain shear wave velocities in a backfilled borehole in non-penetrable soils including gravel or dense sand.

The SCPT and SDMT tests are the same as the seismic downhole test except that a thrust machine and steel rods are used for installation and extraction of the seismic sensor instead of a borehole. Even though the SCPT and SDMT tests eliminate the additional expense of a borehole and guarantee excellent coupling, the use of push rods is

not possible in stiff soil, gravelly soils with cobbles or rock. As a result, the SCPT and SDMT have been primarily used in softer ground.

2.7 SASW TEST

Nazarian and Stokoe (1984) began the initial developments of the Spectral-Analysis-of-Surface-Waves (SASW) method to measure in-situ Vs profiles. This method is discussed herein because the data processing forms the basic of the Spectral-Anlaysis-of-Body-Waves (SABW) method developed in this research. The SASW method uses the characteristic that Rayleigh (R) waves propagating in layered material are dispersive. The SASW method has been used as a robust seismic surface wave method since the late 1980's because the development of signal analyzers performing filtering and Discrete Fourier Transform (DFT) simultaneously for the data collected combined with multi-channels has increased the productivity and efficiency of the SASW method. The procedure of V_S measurements with the SASW method consists of: (1) recoding the field R-wave dispersion data, (2) extracting experimental dispersion curve and (3) performing forward modeling to theoretically match the field dispersion curve. The resulting match permits a V_S profile for the site to be determined as discussed below.

The Rayleigh wave velocity changes with frequency or wavelength in a layered material of different stiffnesses. This change in velocity with wavelength or frequency is called dispersion. Figure 2.12 illustrates the dispersion characteristic of Rayleigh waves propagating through a multi-layered material. As discussed by Stokoe et al. (1994), "a high frequency Rayleigh wave with a short wavelength stresses material near the exposed surface and thus samples the properties of the near-surface material (Figure 2.12b). A lower-frequency Rayleigh wave with a longer wavelength stresses material to a greater

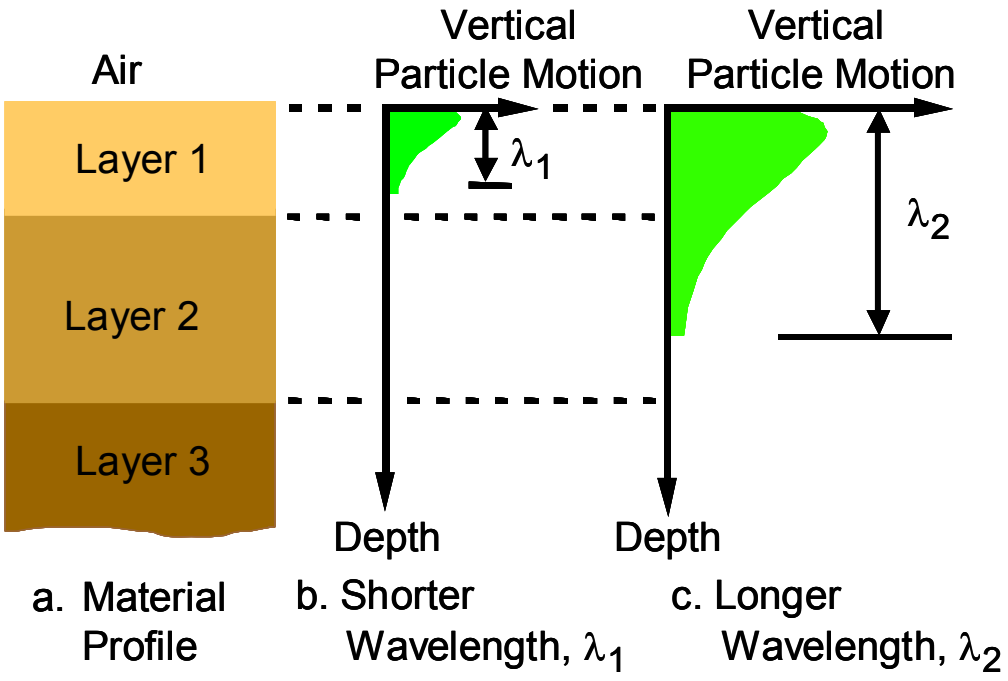

Figure 2.12: Illustration of Rayleigh Waves with Different Wavelengths Sampling Materials in a Multi-Layered Material (after Stokoe et al., 1994)

depth and thus samples the properties of the near-surface and deeper materials (Figure 2.12c)". As discussed by Joh (1996), "the dispersive waves are separated by frequency and wavelength to determine the experimental dispersion curve using spectral analysis. A theoretical dispersion curve matching the experimental dispersion curve is calculated and plotted by using forward modeling analysis and thus the closely matched shear wave velocities and thicknesses are obtained for the one-dimensional, multi-layered soil".

One spot on the ground surface is loaded with an impulsive, random, or sinusoidal source and Rayleigh waves propagating along the ground surface are created. The vertical motions of the waves are measured at two or three locations along a single radial path from the source by vertically oriented transducers as shown Figure 2.13. Successively increasing spacings between the source and first receiver and between the first and second receivers is used to measure progressively longer and longer

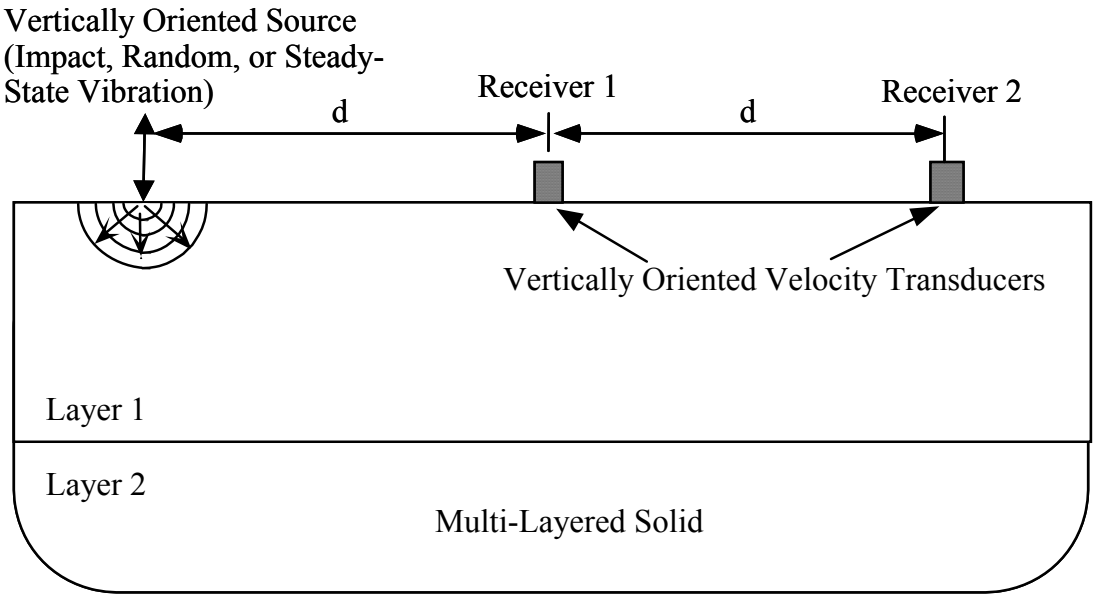

Figure 2.13: Illustration of the Equipment Arrangement Using One Receiver Pair in the SASW Testing (after Stokoe et al., 1994)

wavelengths. Testing is typically performed using six or more sets of source-receivers locations when depths from 50 to 150 ft are profiled.

The time-domain records (x(t) and y(t)) collected from the two receivers in each receiver pair at each receiver spacing are transformed into the Laplace form (X(s) and Y(s)) by the dynamic signal analyzer. Then the transfer function H(s) of the two frequency domain signals (X(s) and Y(s)) is calculated and displayed by the dynamic signal analyzer in real time. The internal calculation procedure of the dynamic signal analyzer is outlined as:

$$X(s) = L\{x(t)\} = \int_0^\infty x(t)e^{-st}dt \tag{2.11}$$

$$Y(s) = L\{y(t)\} = \int_0^\infty y(t)e^{-st}dt \tag{2.12}$$

$$H(s) = \frac{Y(s)}{X(s)} \tag{2.13}$$

$$G(\omega) = \frac{|Y|}{|X|} = |H(j\omega)| \tag{2.14}$$

$$\phi(\omega) = \arg(Y) - \arg(X) = \arg(H(j\omega)) \tag{2.15}$$

Where: $G(\omega)$ is the amplitude spectrum, $H(j\omega)$ is the frequency response, and $\phi(\omega)$ is the phase difference. The changes of the sinusoid signals for every frequency, ω, are described by the frequency response, $H(j\omega)$. The phase shift of the frequency response measured between each pair of receivers is used to calculate the wave velocity by:

$$V_R = f \cdot \lambda = f \cdot \frac{360}{\phi} \cdot d \tag{2.16}$$

Where: V_R is the phase velocity of Rayleigh wave, f is the frequency, λ is the wavelength, ϕ is the unwrapped phase angle in degrees at frequency f, and d is the distance between the two receivers.

The analysis procedure for the SASW method is described by Stokoe et al. (2009b) with the following example. A bulldozer was used as the seismic source. The results from two receiver spacings, 100 ft and 150 ft are shown with a site in California. The wrapped phase shift determined between two receivers is shown in Figure 2.14a. The wrapped phase spectrum is manually masked to eliminate the near-field and any poor-signal zones in the laboratory as shown in Figure 2.14b. Then, the masked wrapped-phase spectrum is unwrapped. Equation 2.16 (with the unwrapped phase) is used to calculate the wave velocities. The resulting individual experimental dispersion curve is plotted in Figure 2.15 using open circles and stars for the 100-ft receiver spacing. The wave velocities determined with a 150-ft receiver spacing using the bulldozer source are also

shown in Figure 2.15. The experimental dispersion curves are plotted and combined for all source-receiver spacings at the site as shown in Figure 2.16. The combined experimental dispersion curve is called the composite experimental dispersion curve. Using an iterative forward modeling procedure in WinSASW written by Joh (1992), a theoretical dispersion curve is generated and progressively matched to the composite experimental dispersion curve. The final by eye match is shown in Figure 2.17 and the resulting shear wave velocity profile is plotted in Figure 2.18.

2.8 SUMMARY

Dynamic soil properties, including the wave velocity and material damping, can be determined by performing in situ seismic tests or laboratory tests. The dynamic soil properties of the in-place soil can be only obtained by in situ seismic tests. The in situ seismic tests were reviewed in this chapter. The bulk of the comments were directed towards in-situ measurements of compression and shear wave velocities, since these are well-developed measurements. However, some comments on in-situ measurements of material damping, which are rarely performed in geotechnical earthquake engineering, were added because a limited amount of this work is also conducted in this research effort.

Downhole testing with a borehole or a penetrometer (CPT or dilatometer) and crosshole testing have been developed and used by Civil Engineers since the 1960's. These tests are the most commonly used in-situ seismic tests today. In the downhole and crosshole tests, the distance between a source and a receiver or between a source and two receivers is determined. Times that the body waves travel from the source to one or more receivers are measured at each depth by a digital recording system. The distances and

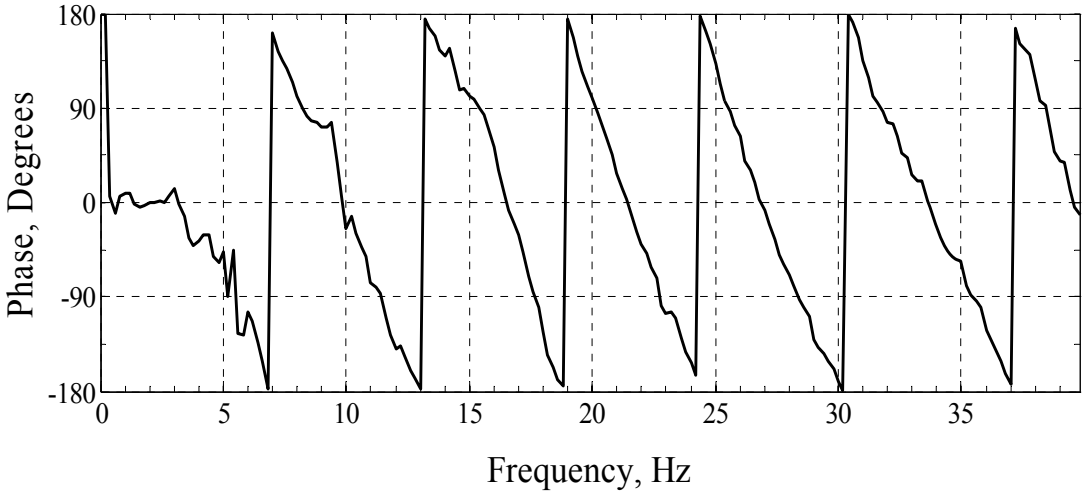

a. Wrapped Phase Calculated from Transfer Function

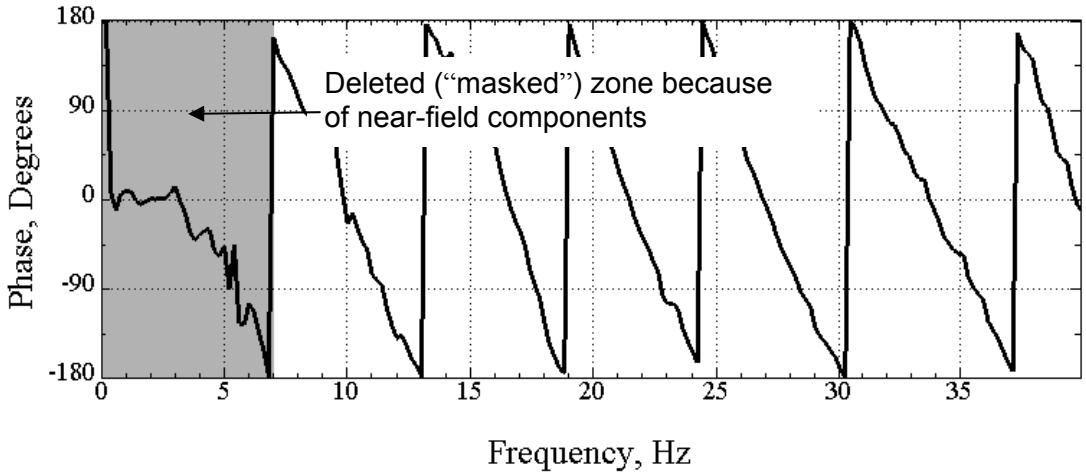

b. Masked Wrapped Phase to Minimize Near-Field Components

Figure 2.14: Phase of the Transfer Function Measured with the Bulldozer as the Seismic Source and a 100-ft Receiver Spacing (from Stokoe et al., 2009b)

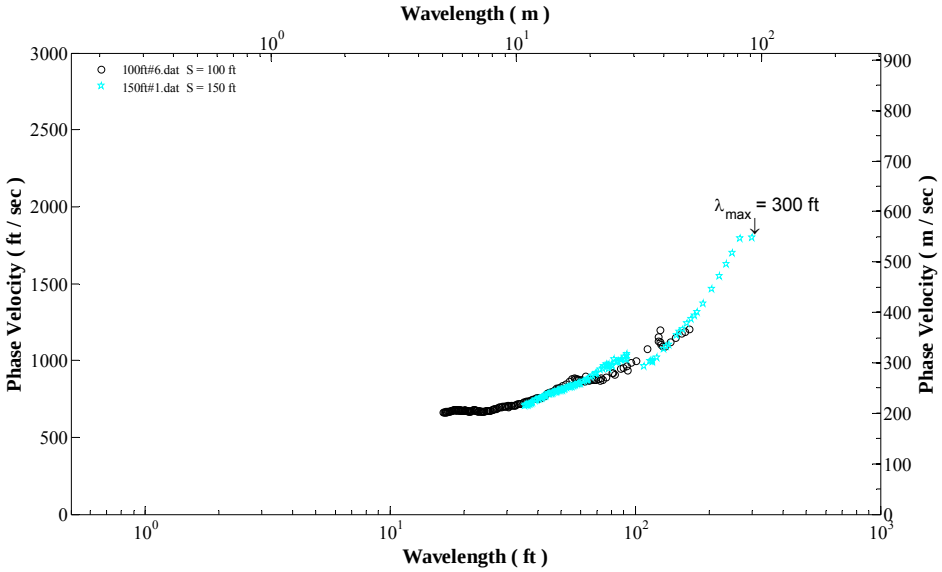

Figure 2.15: Individual Experimental Dispersion Curves Created from the Unwrapped Phase Records Measured with a 100-ft Receiver Spacing (Shown in Figure 13b) and a 150-ft Receiver Spacing using a Bulldozer Source (from Stokoe et al., 2009b)

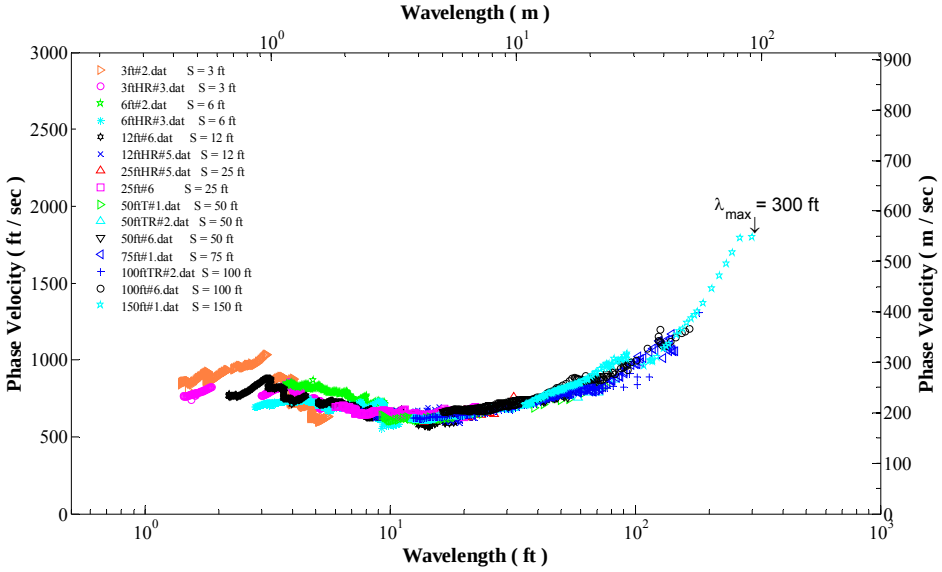

Figure 2.16: Composite Experimental Dispersion Curve Created from Phase Measurements Performed at all (8) Receiver Spacings using Geological and Sledge Hammers and a Bulldozer as the Seismic Sources (from Stokoe et al., 2009b).

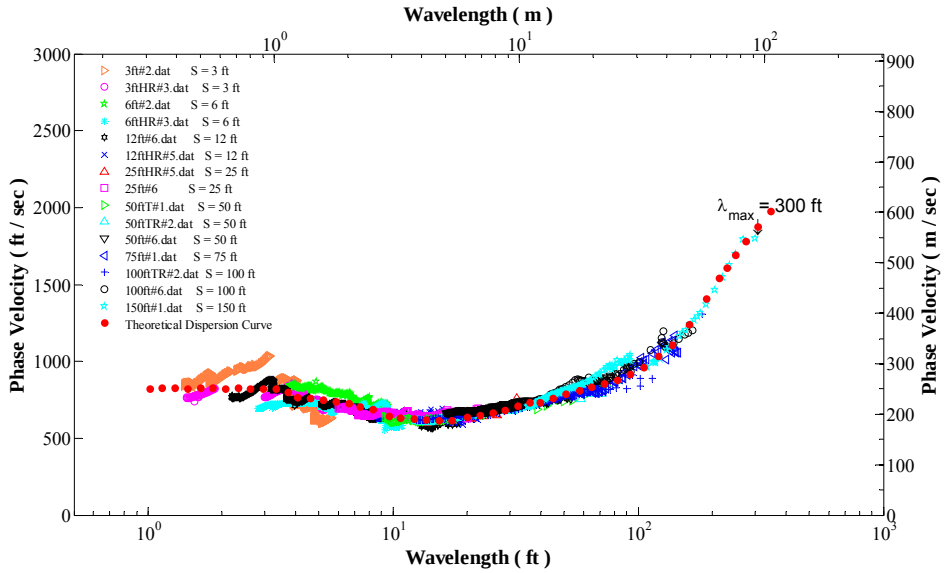

Figure 2.17: Theoretical Dispersion Curve Matched to the Composite Experimental Dispersion Curve (from Stokoe et al., 2009b)

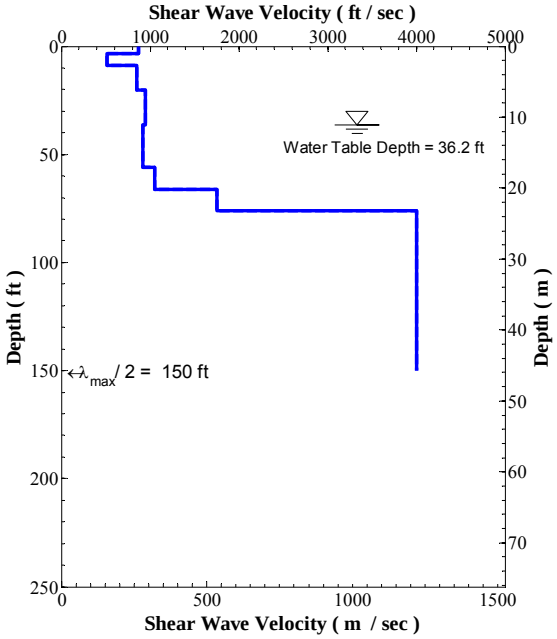

Figure 2.18: Shear Velocity Profile Determined from the Iterative Forward Modeling shown in Figure 2.16 (from Stokoe et al., 2009b)

times are used to calculate profiles of the wave velocities of the natural material.

The SASW method was also described in detail including the theoretical background, testing procedure and analytical procedure. This description was presented because the basic concept is used to develop the Spectral-Analysis-of-Body-Waves (SABW) method applied to the crosshole and downhole methods.

The conventional downhole tests, SCPT and SASW described in this chapter were performed at the Hornsby Bend site for this research and wave velocities and other results obtained by conventional testing procedures and the analytical methods presented herein are compared to verify the applicability of the SABW method in Chapters 5 and 6.

Chapter 3: Instrumentation for Downhole and SCPT Tests

3.1 INTRODUCTION

The major components of the instrumentation required to perform downhole and SCPT tests can be subdivided into the following three categories: (1) seismic P- and S-wave sensors, (2) triggering systems and (3) data acquisition systems to record the output signals. The sensors used in downhole testing are either one, 3-D sensor used in measuring pseudo-interval velocities or in developing travel time vs. depth plots and two, 3-D sensors used in measuring true-interval velocities. The sensors for SCPT testing are a cone penetrometer for CPT testing and usually one, 3-D sensor positioned above the cone portion of the device. In this research, SCPT testing was actually performed in two steps. The first step is simply a CPT test. The second step involved a dummy cone in which a 3-D sensor was installed. This second step is called the "seismic cone" herein and the combination of the first and second steps is called an SCPT. The CPT, seismic cone and downhole tests were not performed at the same time and the locations differed slightly but were generally within 10 to 15 ft. In this chapter, the 3-D sensor and dummy cone called a seismic cone is introduced and described in detail because this research focuses on seismic CPT testing. An electrical circuit trigger system and two, 3-D sensors were used as triggers. Their output signals were captured using two, 16-channel signal analyzers that used software called SignalCalc Mobilizer. In this chapter, the three major components are described in detail.

3.2 DOWNHOLE SENSOR

Profiles of shear and compression wave velocities are used to characterize layered soil masses. Therefore, a seismic sensor used to measure the S- and P-wave velocities

must be able to track the soil particle motions created by the passage of each body wave. The sensors used in this research had to fit the following requirements. First, the sensor had to be small enough to fit inside a case that then could be lowered into a borehole with an internal diameter of 4 inch. Second, the signal-to-noise ratio of the sensor must be large enough for accurate monitoring and trustable data reduction. Third, the seismic sensor and cable must be waterproof. Fourth, the sensor must be durable and retrievable. Fifth, two 3-D downhole sensors must be able to be connected to measure true-interval velocity. Finally, the sensor package must be able to be attached to an orientation system (orientation rods in this application) so that the orientation of the sensor could be controlled which then allowed maximized and polarized signals of shear waves generated by a reversible impulsive source.

The one, 3-D sensor and two, 3-D sensors were used to measure pseudo-interval and true interval velocities of body waves, respectively. The two, 3-D sensor package simply consisted of two of the same 3-D sensor and the connecting system could be lengthened or shortened to adjust the interval of the two 3-D sensors. All sensors are described below.

The one, 3-D sensor consists of three, 1-D geophones in an acrylic case as shown in Figure 3.1. Each 1-D geophone is composed of a coil-spring-magnet system housed in a protective case. Photographs of an assembled and disassembled 1-D geophone are shown in Figures 3.2a and 3.2b, respectively. The electrical coil is attached to the leaf spring which is supported by the geophone case. The magnet is also attached to the geophone case. Thus, when the geophone case moves along with the borehole, the

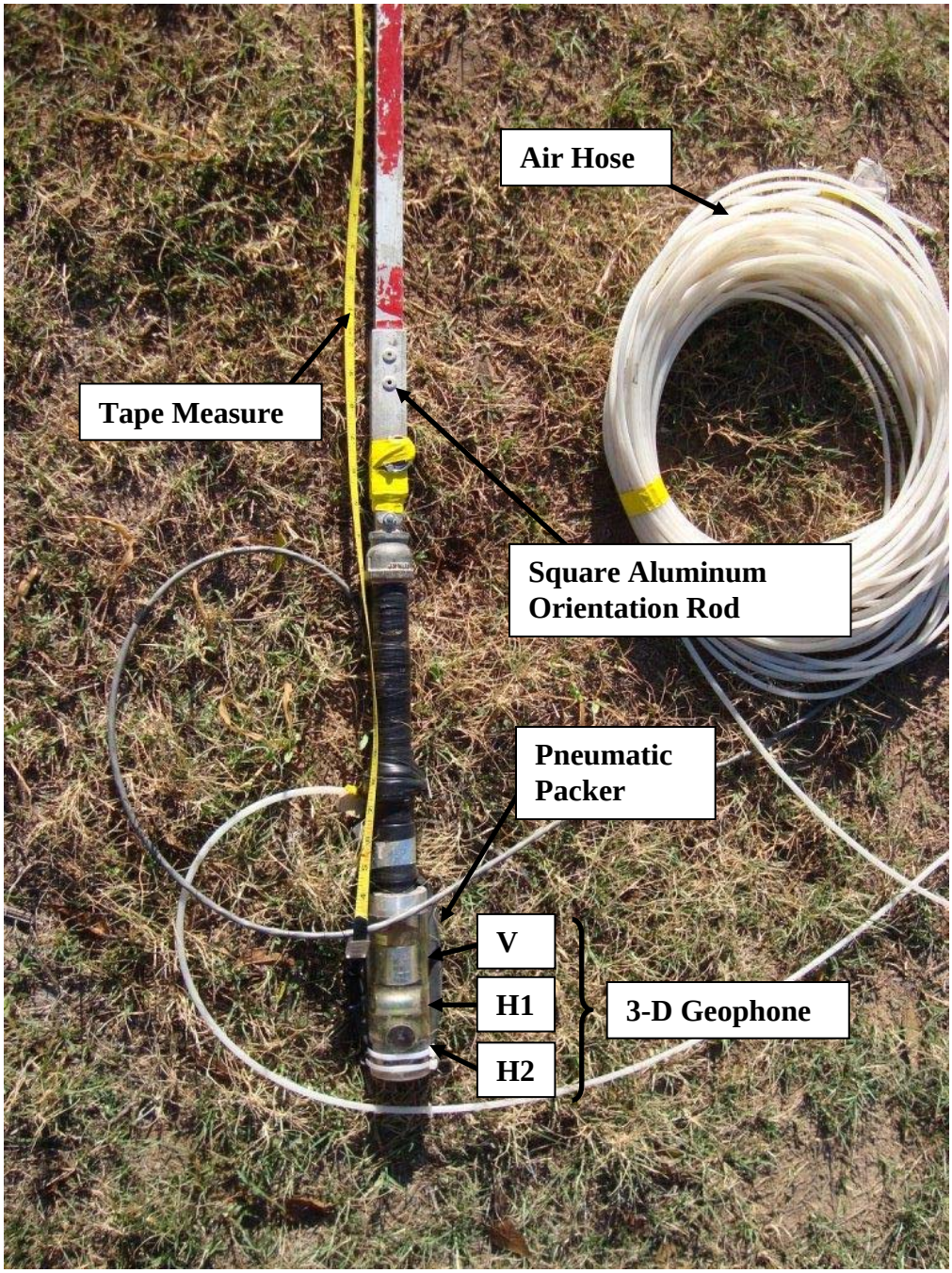

Figure 3.1: Three-Dimensional Receiver (one, 3-D Sensor) Used in Typical Downhole Testing

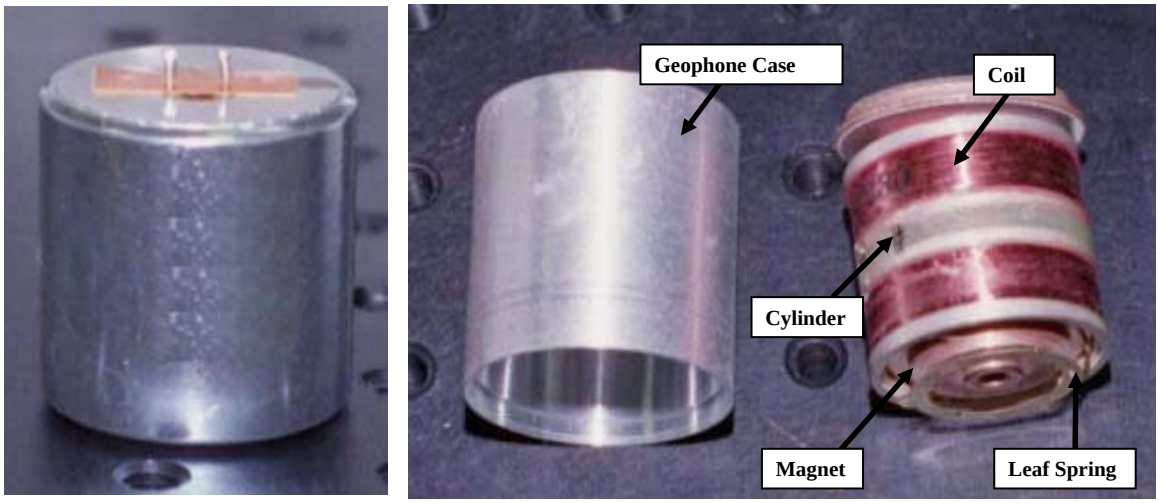

(a) Conventional Geophone **(b) Dissembled Geophone Components**

Figure 3.2: Conventional Geophone and the Dissembled Geophone Components (from Barzilai, 2000)

Table 3.1: Characteristics of the Individual Geophones in a 3-D Receiver and of the Completed 3-D Receiver (from Stokoe et al., 2009a)

Geophone	
Type	Geospace 101 LT
Natural Frequency	14 Hz
Coil Resistance	900 Ω
Damping	50% of critical
Height	1.47 in. (3.73 cm)
Diameter	1.01 in. (2.56 cm)
Weight	2.9 oz (83 g)
Acrylic Case (with 3-D geophones)	
Height	6.75 in. (17.15 cm)
Diameter	2.25 in. (5.72 cm)
Total Weight	~2 lb (0.9 kg)

suspended coil tends to remain stationary. The relative motion between the magnetic field and coil induces a voltage proportional to the velocity of motion for movements with frequencies above the natural frequency (f_n) of the spring-coil system (f_n = 14 Hz in these geophones). These geophones generate non-distorted, linear output signals over a frequency range from about 30 to 800 Hz. The frequency range of the downhole tests in this research is well within this frequency range. Specifications of the geophones used in the downhole tests are presented in Table 3.1.

Geophones were used to monitor wave propagation and particle motions in the soil and rock in this research for the following four reasons.

1. Geophones are robust sensors because of the simple single-degree-of-freedom (SDOF) coil-magnet system. As a result, the calibration factor is quite stable over many years unless the geophone experiences serious mechanical or temperature damage.
2. Geophones work properly over wide ranges in frequency (up to 800 Hz) so they work well for soil and rock testing.
3. Geophones do not require a signal conditioner or power supply and produce relatively large outputs.
4. Geophones used in this research are not expensive. The cost of the geophones was less than $ 100 per geophone.

The three, 1-D geophones used in each 3-D sensor were connected to the 16-channel dynamic signal analyzer using an electrical cable composed of three, shielded pairs of wires. When the 3-D sensor is lowered to significant depths in a borehole (say more 100 ft), noise increases and the signal-to-noise ratio of the body waves decreases. To maximize the signal-to-noise ratio, each pair of conductors in the cable were

individually twisted and shielded. The PVC jacket of the cable protected the conductors from water and normal handling.

Each downhole sensor contained three, orthogonally-oriented, 1-D geophones mounted in an acrylic case as shown in Figure 3.1. A close-up of a 3-D sensor is shown in Figure 3.3. The 3-D sensor monitors waveforms in the vertical (V), transverse horizontal (H1) and radial horizontal (H2) directions. The vertical geophone is need to monitor vertically propagating compression waves (P_v). Both the transverse and radial horizontal geophones are need to monitor vertically propagating and horizontally polarized shear waves (S_{vh} waves). The relative size of a 14-Hz geophone compared with other geophones is shown in Figure 3.4.

As seen in Figure 3.1, a 1.0-ft length of steel pipe is connected to the top of each 3-D downhole sensor. Square aluminum orientation rods are then connected to the top of the steel pipe to control the orientation of the downhole sensor. The pipe and orientation rods enable operators to: (1) orient the 3-D sensor in the borehole at the test depth, (2) lower or raise the sensor, and (3) attach the tape measure (for measurement of sensor depth) to the sensor and rods. When downhole tests were performed without orientation rods, a rope was used to lower or raise the 3-D sensor in this research. As shown in Figures 3.1 and 3.3, a pneumatic packer and an air hose were also attached to the downhole sensor or sensors. When the downhole sensor was lowered to the proper depth, the pneumatic packer was inflated to couple the sensor to the borehole casing. After completing a seismic test at a given depth, the pneumatic packer was deflated and the sensor was lowered to the next depth. The borehole casing typically had a 4-inch inside diameter and thus the size of the sensor, including the inflated packer was reasonable.

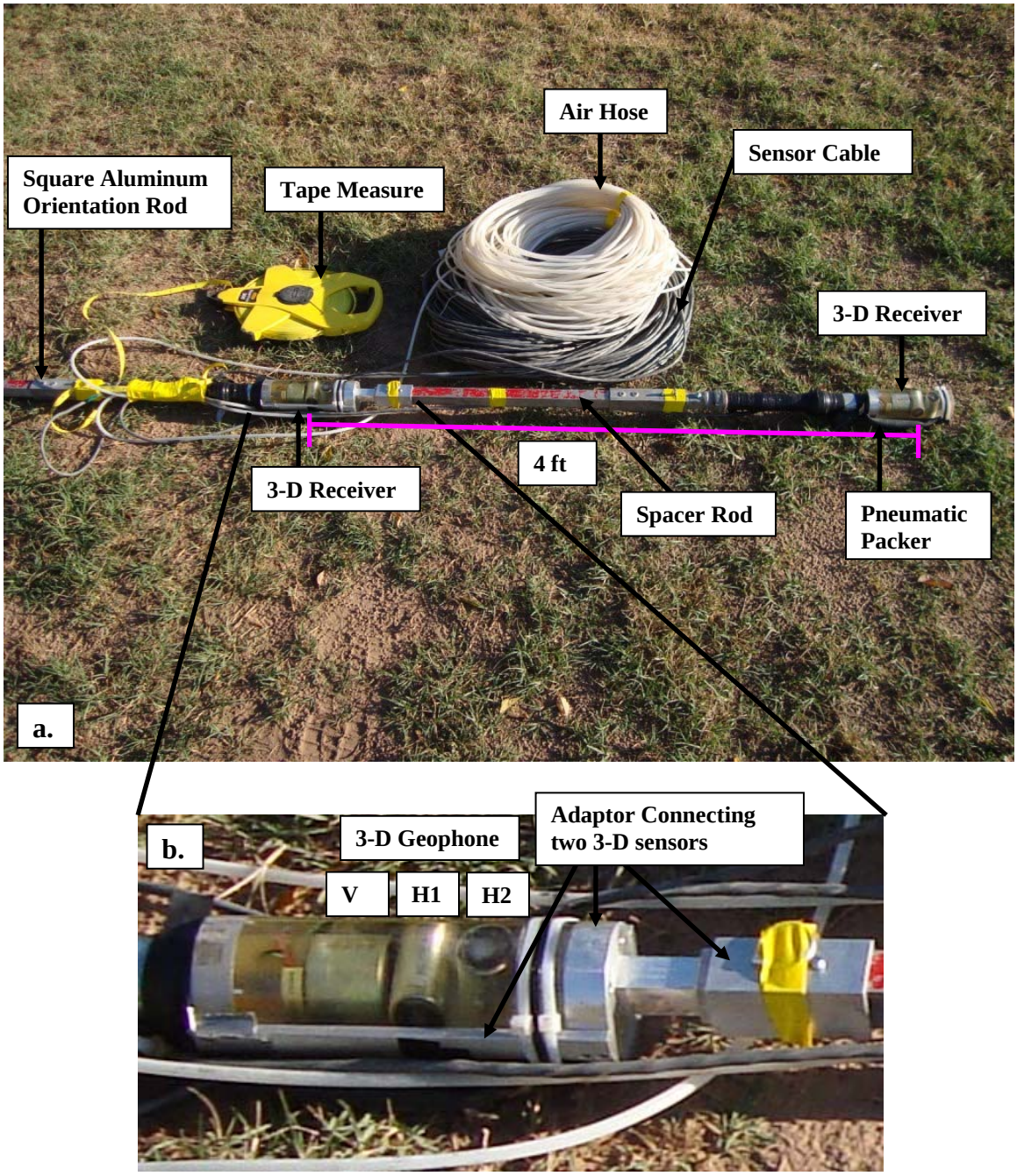

Figure 3.3: Two, 3-Dimensional Receivers Connected by an Adopter Rod Ready for Use in the Downhole Test

Figure 3.4: Examples of 1-D Geophones with Different Natural Frequencies Used for SASW (1 and 4.5 Hz), Downhole (4.5 and 14 Hz) and SCPT (24 and 28 Hz) Tests

The sensors used in the downhole test were connected directly to the 16-channel dynamic signal analyzers at the ground surface. Each geophone in the 3-D sensor was monitored without any disconnecting/reconnecting operations.

Two, 3-D sensors were connected together using an aluminum spacer rod as shown in Figure 3.3a. This set-up with two, 3-D receivers allowed measurement of true-interval velocities over a 4 ft interval. The length of the spacer rod is adjustable, which could be important in considering wavelength or frequency of body waves in very stiff or soft materials. The spacer rod firmly connects the two, 3-D sensors and thus the two 3-D

sensors are automatically synchronized for monitoring soil particle motions. Each component of the two, 3-D sensors is oriented in the same direction.

3.3 SEISMIC CONE PORTION OF SCPT

An SCPT body consists of CPT sensors and a seismic sensor. Thus the CPT test and downhole seismic test are able to be performed sequentially in SCPT testing. The focus in this research is on the seismic part of the SCPT test. A 3-D seismic sensor in a dummy cone, called a seismic cone hereafter, were developed and used for the in-situ seismic testing.

A seismic cone consists of a sensor and housing. There are several issues to be considered in the design of a seismic cone. First, the sensor must be small enough to be fit inside the model of a CPT cone with the larger of the two cone diameters (ASTM D5778-07, 2007), 44 mm (1.73 inch). Second, the sensor and housing of a seismic cone must be robust enough to withstand large stresses during pushing the seismic cone. Third, a seismic cone must be waterproof. Fourth, the signal-to-noise ratio must be large to collect high-quality data. Fifth, the directions of sensors inside a seismic cone should be known so that, at least the orientation is known at the start of the installation procedure. Sixth, the seismic cone is normally installed from the ground surface. Finally, a seismic cone must be retrievable after the seismic tests are completed. These issues are discussed below.

3.3.1 Sensors (28-Hz Geophone vs. 24-Hz Geophone)

Accelerometers, MEMS sensors or geophones can be used as sensors in a seismic cone. Accelerometers and MEMS sensors are more expensive than geophones and need charge amplifiers including extra wires in a small housing. Geophones have been widely

used as a seismic sensor in the SCPT since Campanella et al. (1986), Robertson et al (1986a), Karl (2005) and Butcher et al (2005). A GEO GS-14 28-570 L3 type geophone manufactured by GeoSpace has been used. This geophone has a natural frequency of 28-Hz, a damping ratio of 18 %, and a coil resistance of 570 ohms. It is simply called a 28-Hz geophone in this study. Figure 3.4 shows a 28-Hz geophone along with other common types of geophones. As shown in Figure 3.4, the geophone is small enough to be fit into a seismic cone, extremely rugged so that it can withstand the handling and operational stresses and it operates correctly in any orientation. However, additional damping to reduce free vibrations after body-wave passage could not be added to 28-Hz geophones due to the low output signal of 28-Hz geophones. The low output voltage signal of 28-Hz geophones may result in low signal-to-noise ratios when a seismic cone is located at deep depths below the ground surface.

In this research, GEO GS-14 24-3400 L3 (called 24-Hz geophone) that has a natural frequency of 24 Hz, a damping ratio of 25 %, and a coil resistance of 3400 ohms was chosen for comparison with the 28-Hz geophone. A 24-Hz geophone has been produced and used by GeoSpace for research purposes. A 24-Hz geophone has the same shape, size and weight as a 28-Hz geophone. However, a 24-Hz geophone may be slightly less robust than a 28-Hz geophone under large stresses because the leaf springs of a 24-Hz geophone are thinner than the 28-Hz geophone to create the lower natural frequency (from 28 Hz to 24 Hz).

A 24-Hz geophone with a damping ratio of 40 % can be created by adding a resistor. This more highly damped 24-Hz geophone and a 28-Hz geophone with a damping ratio of 18 % were calibrated in the Soil and Rock Dynamic Laboratory at The University of Texas at Austin. The calibration set-up is shown in Figure 3.5. The specific calibration procedure is described in Section 3.3.2. Calibrations of two geophones were

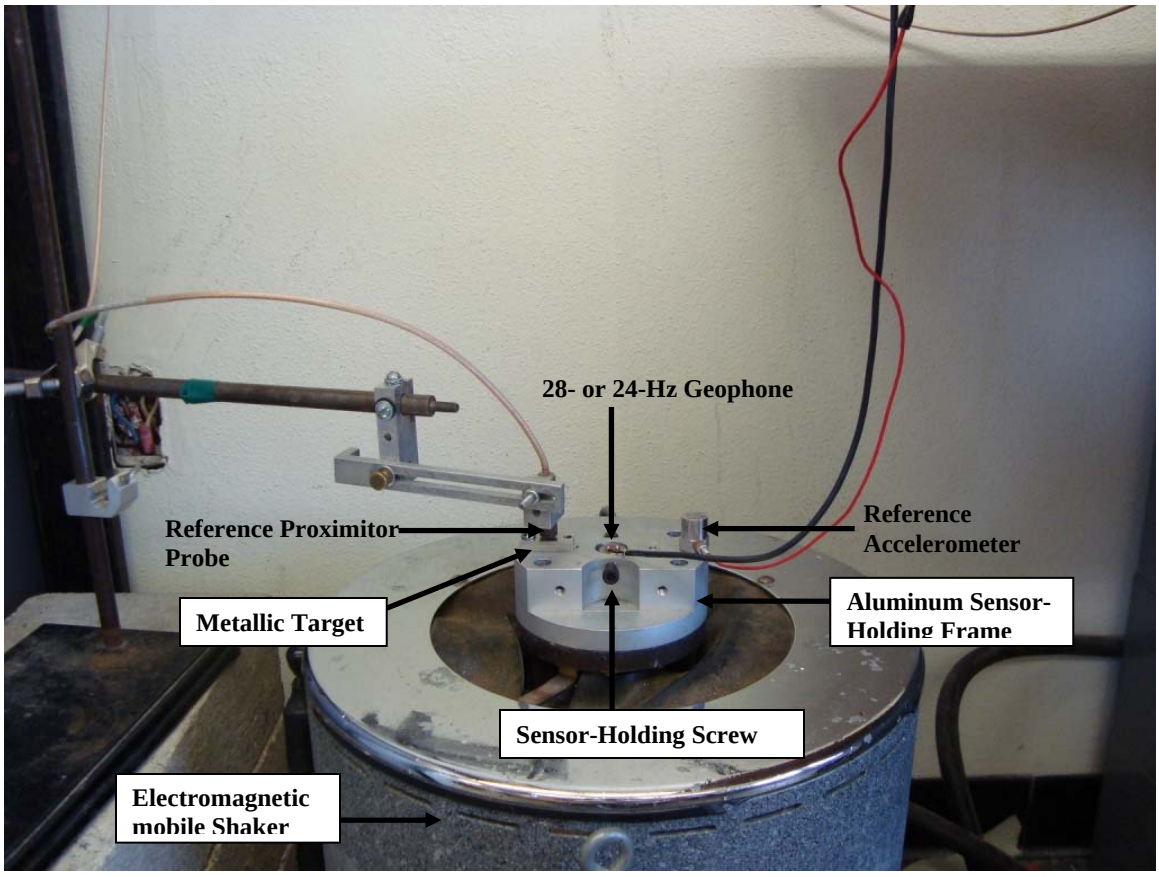

Figure 3.5: Experimental Set-up Used to Calibrate 28- and 24-Hz Geophones: Reference Accelerometer and Proximitor Used to Measuring Motion Created by a Shaking Table

conducted before and after a shock test to ensure that the two geophones were robust enough under large stresses. The 28- and 24-Hz geophones were strongly shaken by hand for 7 minutes. After being strongly shaken for 7 minutes, the geophones were calibrated from over the frequency range of 0.5 to 300 Hz in the vertical direction with a 50-mV, peak-to-peak driving voltage using a stepped sine-wave sweep.

The output signals of both geophones were consistent before and after being strongly shaken for 7 minutes as shown in Figure 3.6. This test and comparison shows that both geophones are robust under large stresses. A 24-Hz geophone was then chosen

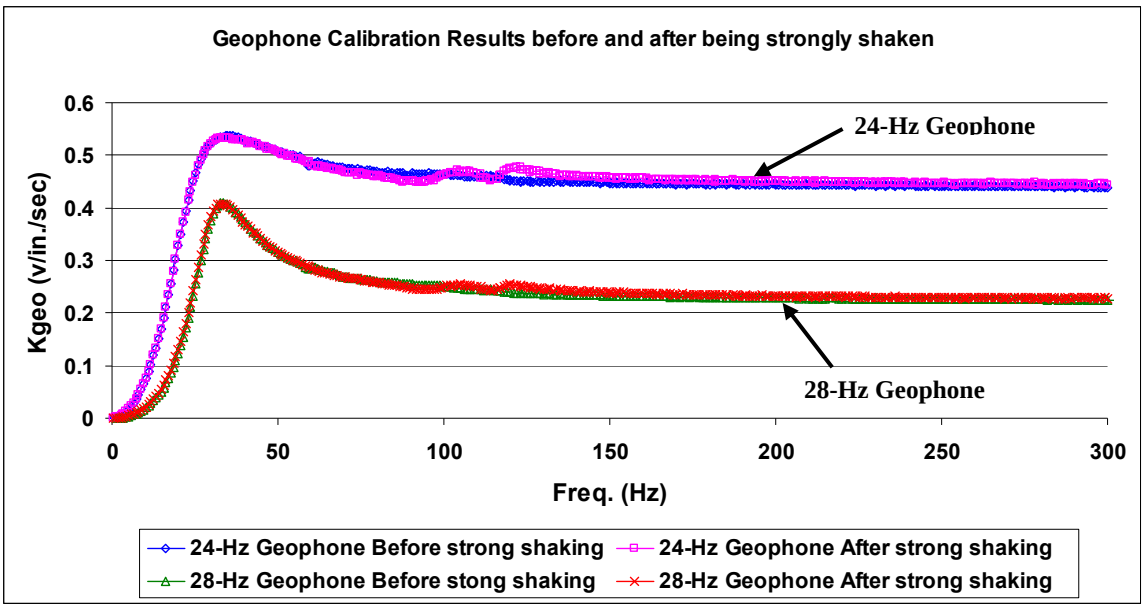

Figure 3.6: Frequency Response Curves of 28- and 24-Hz Geophones Calibrated from 0.5 to 300 Hz Using an Accelerometer as a Reference

as the sensor for the seismic cone because the 24-Hz geophone with a damping ratio of 40% generates a larger signal with a more reasonably constant output over a large frequency range. The increased damping minimizes the effect of the resonant frequency as seen in Figure 3.6.

Also importantly, annoying oscillations of the sensor that makes recognizing the first arrival time of the shear wave difficult was significantly reduced for the 24-Hz geophone with a damping ratio of 40 %.

3.3.2 Sensor Housing

A sensor housing with rods that connect to the CPT pushing mechanism attached to the back bumper of T-Rex is used to push the seismic cone into the ground. The sensor housing consists of a Teflon inner housing and an outer metal housing. Three component geophones were mounted in the inner Teflon housing. The Teflon housing was mounted

in the outer metal housing so that the Teflon housing would be protected from significant stresses during installation of the seismic cone.

The geophones, Teflon housing and metal housing of a seismic cone must be properly connected to correctly record seismic motions of the soil. The three, 24-Hz geophones that had been individually calibrated were securely assembled in the Teflon housing using a marine epoxy. The inner Teflon housing with 3, 24-Hz geophones is shown in Figure 3.7. In the Teflon housing, three small holes and several vertical routing holes were drilled in which to mount the small geophones and electric wires, respectively. Teflon is an excellent material for delicately machining the holes and routes.

The marine epoxy was used to water proof and secure the three geophones mounted inside the housing. The three geophones were connected to three pairs of electrical cables, with each pair individually twisted and shielded to reduce noise. The cable carried the signals from the three geophones to the dynamic signal analyzer at the ground surface. The jacket of the larger cable is made of polyurethane which is extremely tough, flexible and waterproof. The larger cable goes through the hollow push rods.

The three-component sensor in the seismic cone is used to monitor seismic waveforms in the vertical (V) and two horizontal directions (H1 and H2) just as a downhole sensor does (Figure 3.7). The vertical component geophone monitors vertically propagating compression waves (P_v). The two horizontal component geophones monitor vertically propagating and horizontally polarized shear waves (S_{vh}-waves). The output from each horizontal geophone depends on the orientation of the geophone relative to the orientation of the shear wave motion.

The Teflon housing must be protected during penetration. A strong metal housing is used for this purpose. A stainless steel rod was used as the material of the metal housing. The metal housing consists of three pieces (cone, body and cap) as shown in

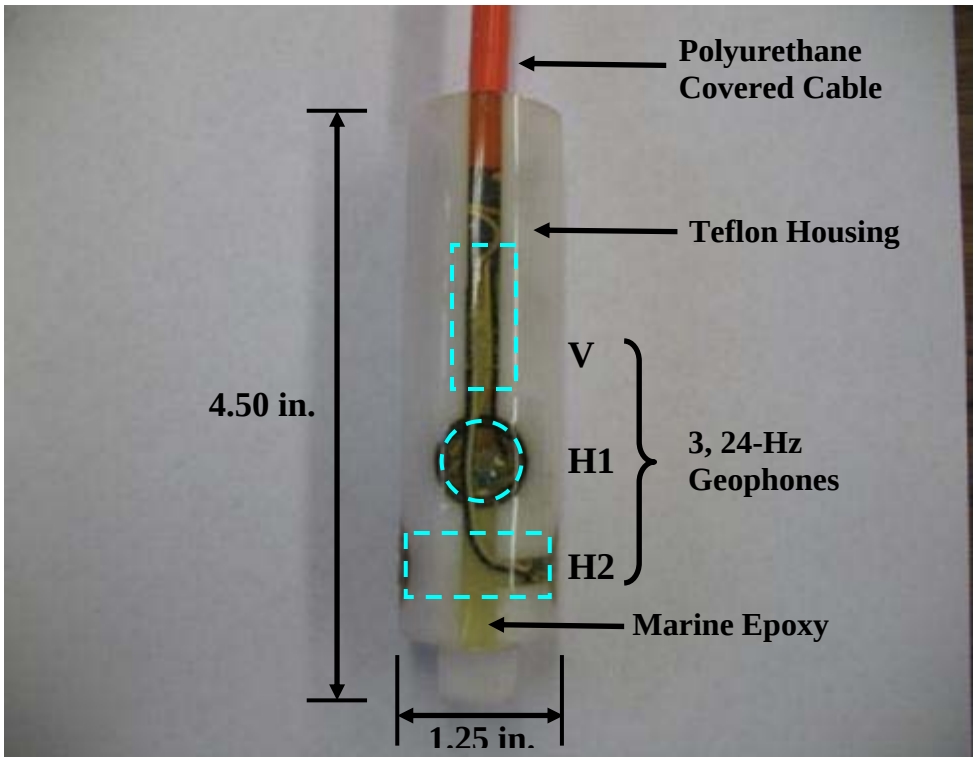

Figure 3.7: Three-Component, 24-Hz Geophone Securely Assembled in a Teflon Housing with Marine Epoxy

Figure 3.8a. The Cone tip has the nominal dimensions of ASTM D5778-07 (2007). The ideal size and shape of cone are that the base diameter gives a projected cone base area of 1500 mm^2 while maintaining a 60 apex angle and at height and diameter of 38.2 mm (1.5 in.) and 43.7 mm (1.72 in.) respectively. The cone designed for this research follows the ideal dimensions and shape of a cone as shown in Figure 3.9. A cone enables the SCPT device to penetrate the ground effectively. The cone part has two reference marks such as one hole or two holes on the surface of a cone to designate the directions of the orthogonally mounted horizontal components. The steel body protects the Teflon housing from horizontal earth pressure. A stainless steel ring was mounted inside the body by using a specially designed installation tool which was inserted into the stainless steel ring

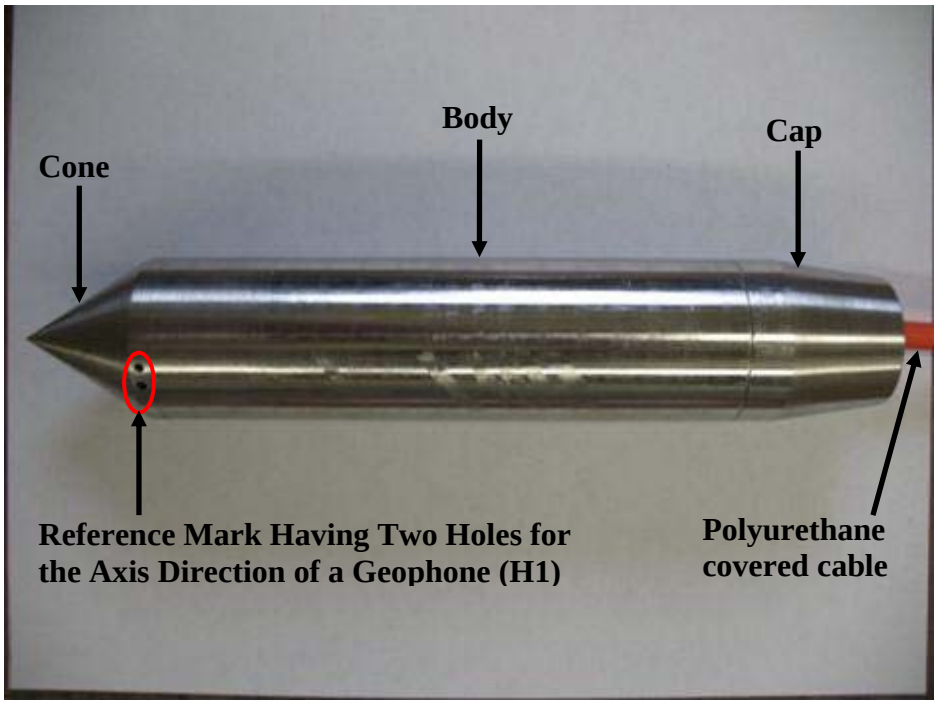

(a) The Metal Housing Assembled from 3 Stainless Steel Pieces

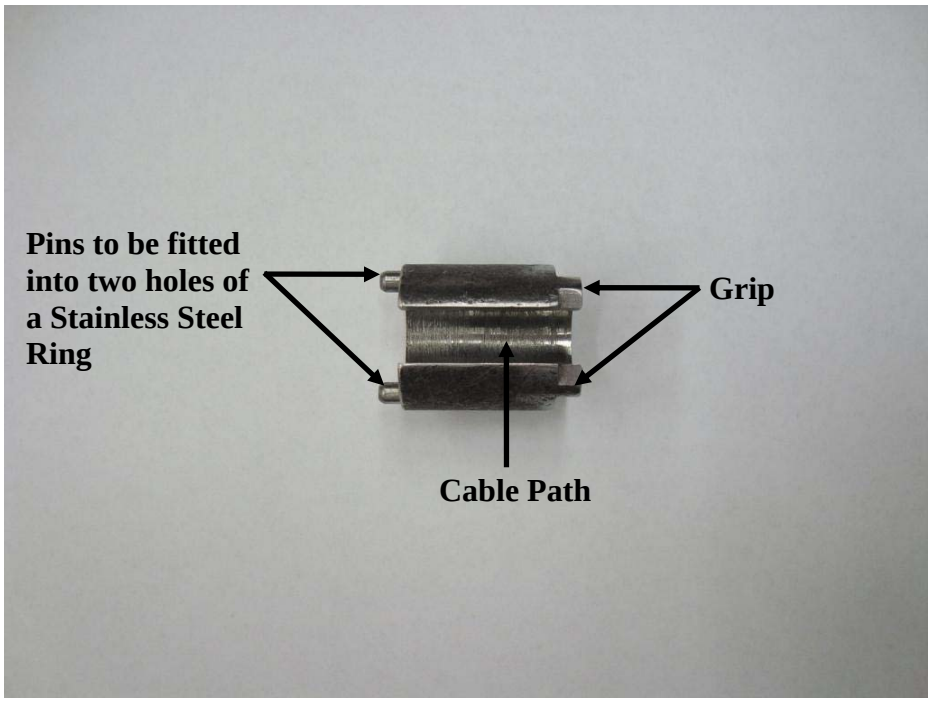

(b) An Installation Tool Mounting a Stainless Steel Ring inside the Metal

Figure 3.8: The Metal Housing and Installation Tool

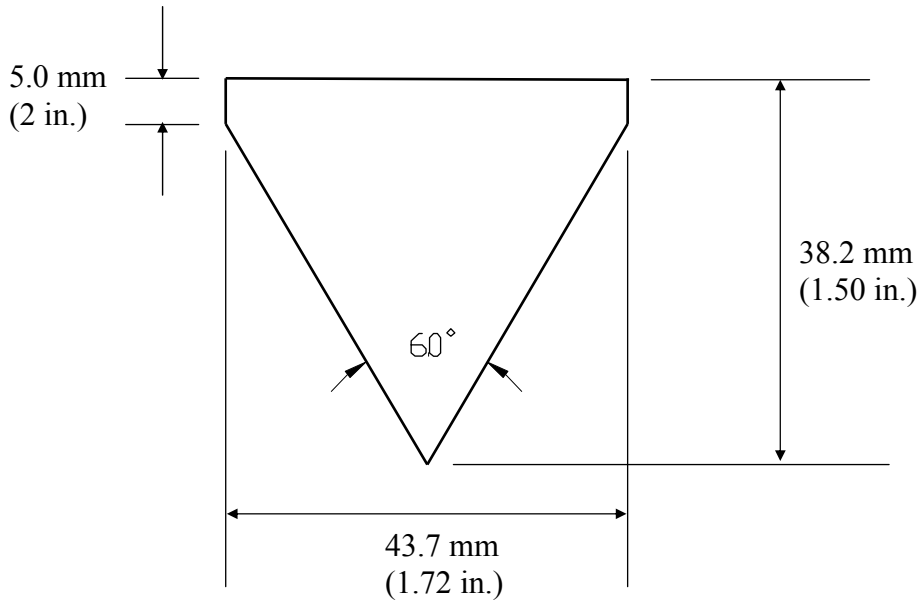

Figure 3.9: Dimensions and Shape of the Cone Tip Used in the Seismic Cone in this Research; Dimensions follow the Ideal Dimension of ASTM D5778-07

and used to screw the ring down tightly on the Teflon housing. The installation tool is shown in Figure 3.8b. The stainless steel ring with a rubber ring inside the body pushes and fixes the Teflon housing downward to make the Teflon housing move with the metal housing. The male thread of a cap is connected to the female thread of the body without touching the breakable Teflon housing. The female thread of the cap is connected to a push rod to install and retrieve the seismic cone.

The vertical and horizontal geophones in the seismic cone were calibrated with an accelerometer and a proximitor as the references. An electromagnetic shaker using stepped sine waves was used to excite the motion over the frequency range from 5 to 300 Hz. This set-up is shown in Figures 3.10a and b for vertical and horizontal geophone calibrations, respectively. The frequency response curves of each geophone in the seismic cone were plotted and compared with the frequency response curves of three geophones calibrated individually before assembly. Figure 3.11 shows the frequency response curves

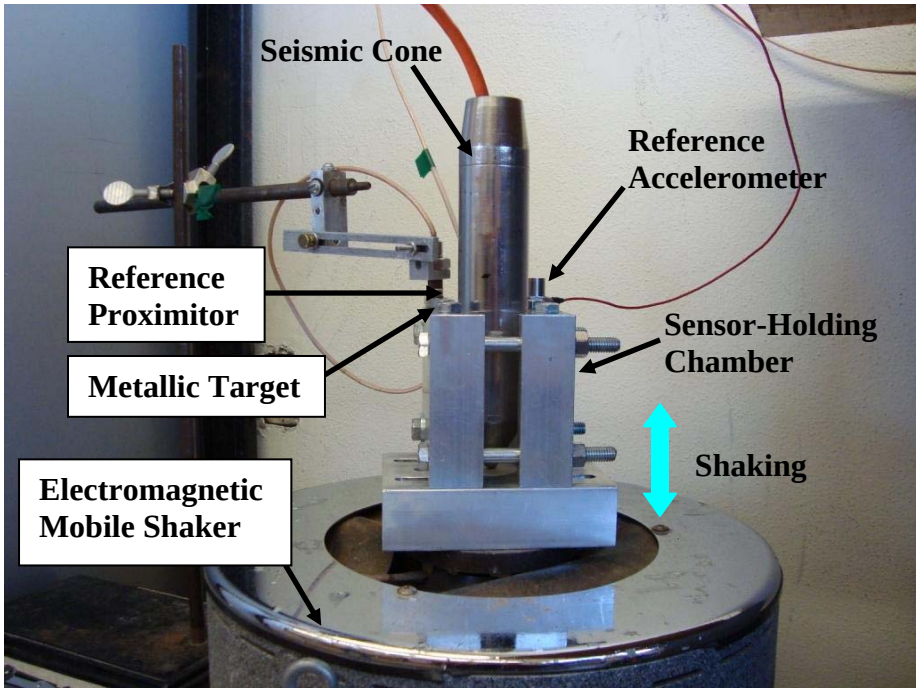

(a) Calibration of the Vertical Geophone

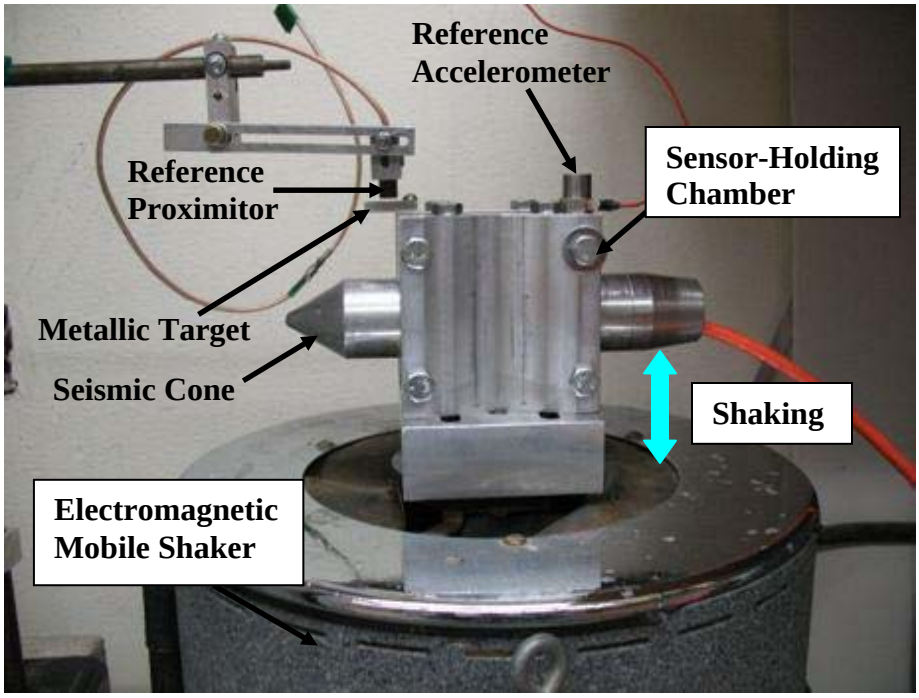

(b) Calibration of One of the Horizontal Geophones

Figure 3.10: Geophones in Seismic Cone Calibrated Using an Accelerometer and Proximitor as references on an Electromagnetic Shaker

for the vertical component geophone. The amplitudes of geophone output signals before and after assembly in Figure 3.11a are normalized by the reference accelerometer. The phase differences between the geophone and accelerometer signals were measured before and after assembly and the phase difference after assembly was subtracted from the phase difference before assembly. The calculated phase difference is less than 5 degrees in the frequency range of 5 to 300 Hz as shown in Figure 3.11b. The response curves were very similar before and after assembly because the vertical geophone, Teflon housing, and metal housing acted in phase during the vibration time of the electromagnetic shaker. The response curves of the other component geophones are similar to the response curves of the vertical component geophone and are shown in Figures 3.12 and 3.13 for the horizontal component geophones (H1 and H2).

3.4 TRIGGER SYSTEM

Different triggers were used in the downhole and SCPT tests. An electrical trigger was used with the sledge-hammer impacting source. This trigger connects the impulsive sources, the steel P-wave plate and the aluminum S-wave plank. In this case, the sledge hammers and P-wave plate and S-wave plank were at the ground surface. Two, triggering 3-D sensors were buried at 3.3 ft below the ground surface. These buried geophones were used to measure when the signals generated by the impulsive sources and a vibroseis truck called Thumper past the 3.3 ft depth level. The specification of two different triggers is discussed in detail below.

3.4.1 Electrical Trigger

An electrical trigger system with a 9-V battery and a 2-KΩ resistor was constructed. The electrical triggering is shown in Figure 3.14. The electrical trigger was

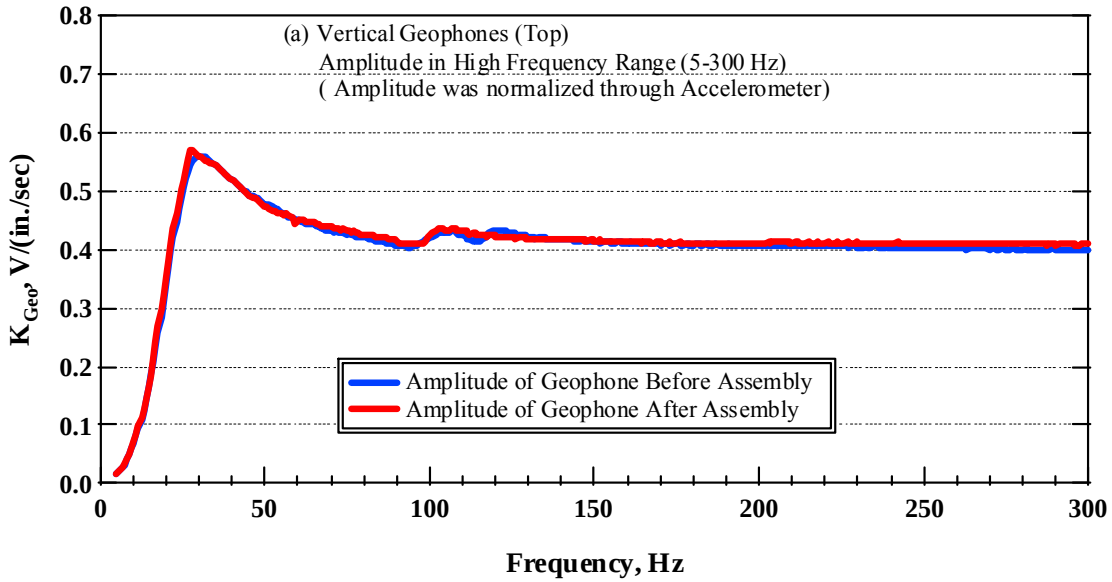

(a) The Amplitudes of the Same Vertical Geophone Before and After Assembly

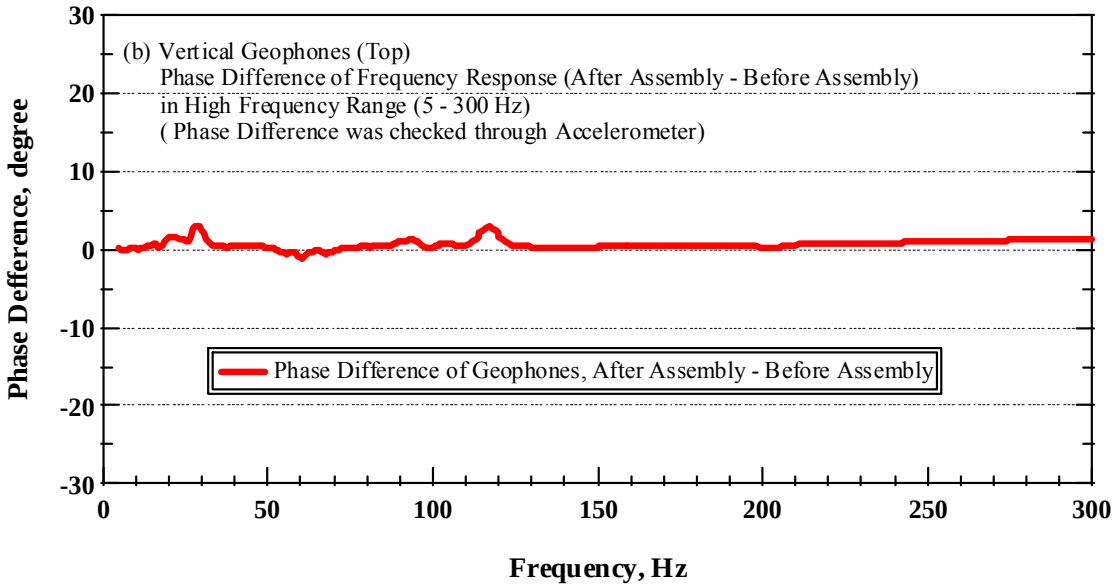

(b) Phase Difference of the Same Vertical Geophone Before and After Assembly

Figure 3.11: Response Curves of the Vertical Geophone at the Top of the Teflon Housing; Calibrations over the Frequency Range of 5 to 300 Hz

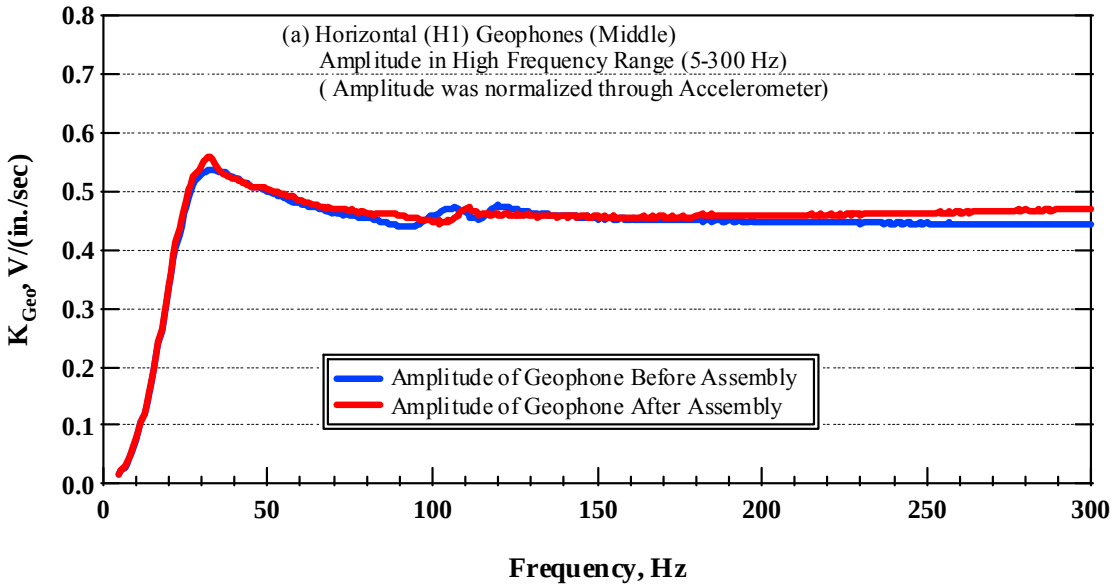

(a) The Amplitudes of the Same Horizontal (H1) Geophone Before and After Assembly

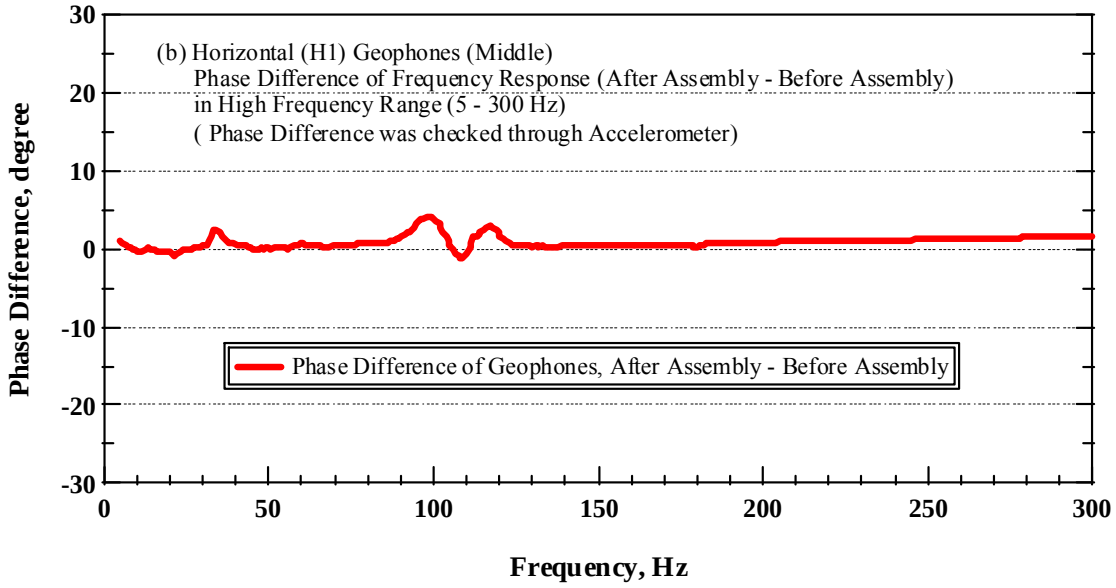

(b) Phase Difference of the Same Horizontal (H1) Geophone Before and After Assembly

Figure 3.12: Response Curves of the Horizontal (H1) Geophone at the Middle of the Teflon Housing; Calibrations over the Frequency Range of 5 to 300 Hz

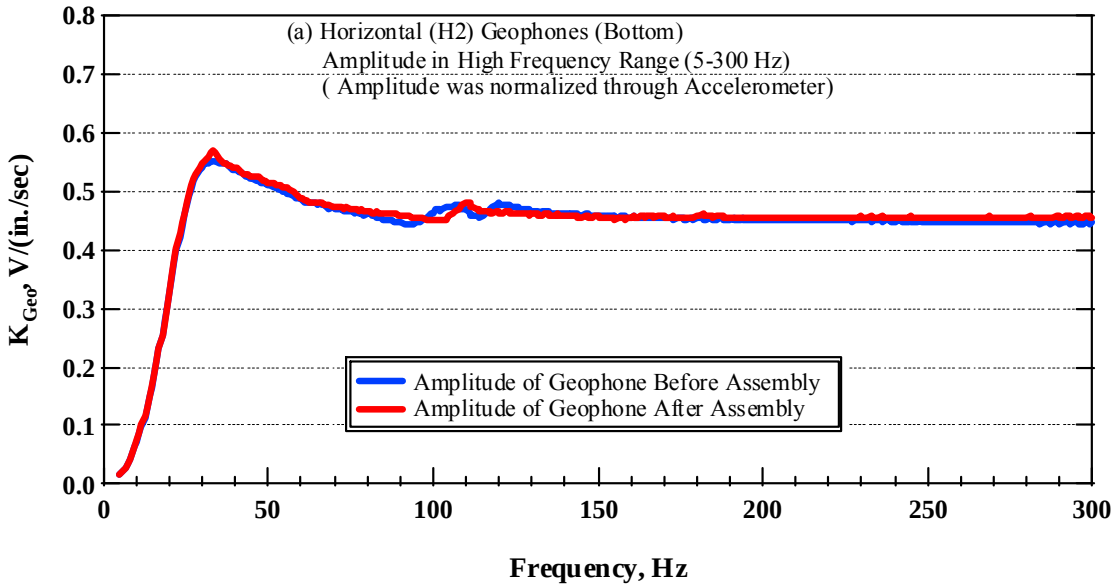

(a) The Amplitudes of the Same Horizontal (H2) Geophone Before and After Assembly

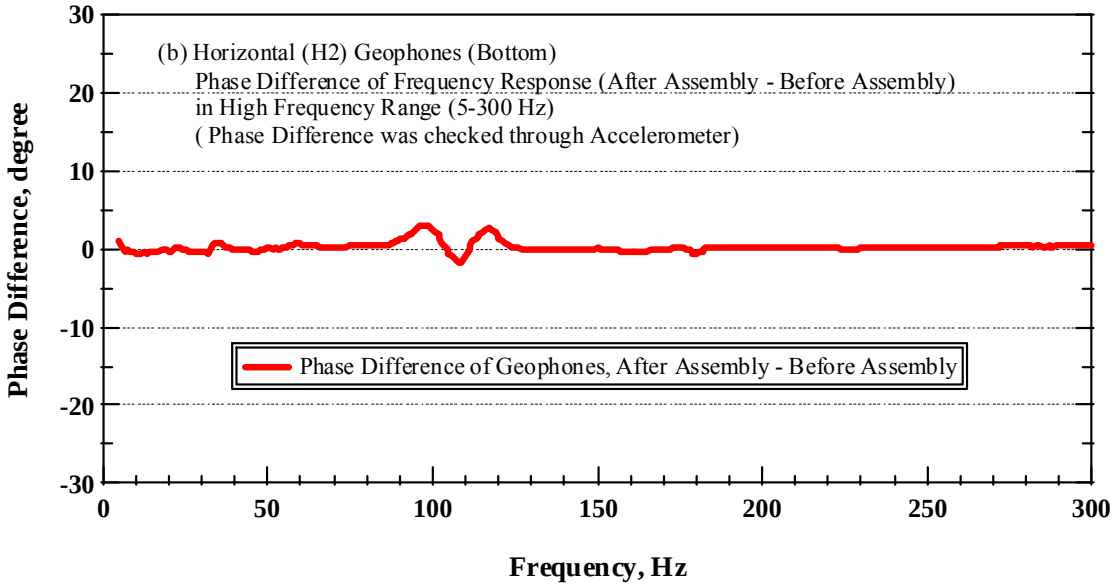

(b) Phase Difference of the Same Horizontal (H2) Geophone Before and After Assembly

Figure 3.13: Response Curves of the Horizontal (H2) Geophone at the Bottom of the Teflon Housing; Calibrations over the Frequency Range of 5 to 300 Hz

connected to a sledge hammer, an aluminum S-wave plank and a P-wave steel plate with electric wires. The electrical trigger was also connected to the dynamic signal analyzer. When the aluminum plank or steel plate was struck by the sledge hammer, current flowed into the trigger system through the electrical wires with a peak 9 volts at a certain time on a computer screen connected to the dynamic signal analyzer. The delay triggering time was minimized with settings of D-C coupling and positive slope setting on the signal analyzer. The electrical trigger setting on the analyzer records the electrical signal as a zero time at 3 volts when the steel plate or aluminum plank were used to generate compression waves or shear waves, respectively, at the ground surface. The delay triggering times were considered in analyzing travel-time data obtained from downhole and SCPT tests.

3.4.2 3-D Reference Sensors

Two, 3-D reference sensors were constructed so that they could be buried at a depth of 3.3 ft below the ground surface. A 3-D reference sensor was located between a steel P-wave plate at the surface and a seismic cone at depth. Another 3-D reference sensor was located between the vibroseis truck and the seismic cone at depth. The 3-D reference sensors consist of three orthogonally mounted 24-Hz geophones assembled in a cube of marine epoxy. This 3-D reference sensor is shown in Figure 3.15. The 3-D reference sensors use the same geophones and epoxy as the seismic cone to minimize the phase and amplitude differences between 3-D reference sensors and the seismic cone for each component. These triggers were mostly used to analyze the phase velocity and damping ratio of body waves from impulsive sources or the vibroseis truck. The phase and amplitudes of the 3-D reference sensor were calibrated using the same system

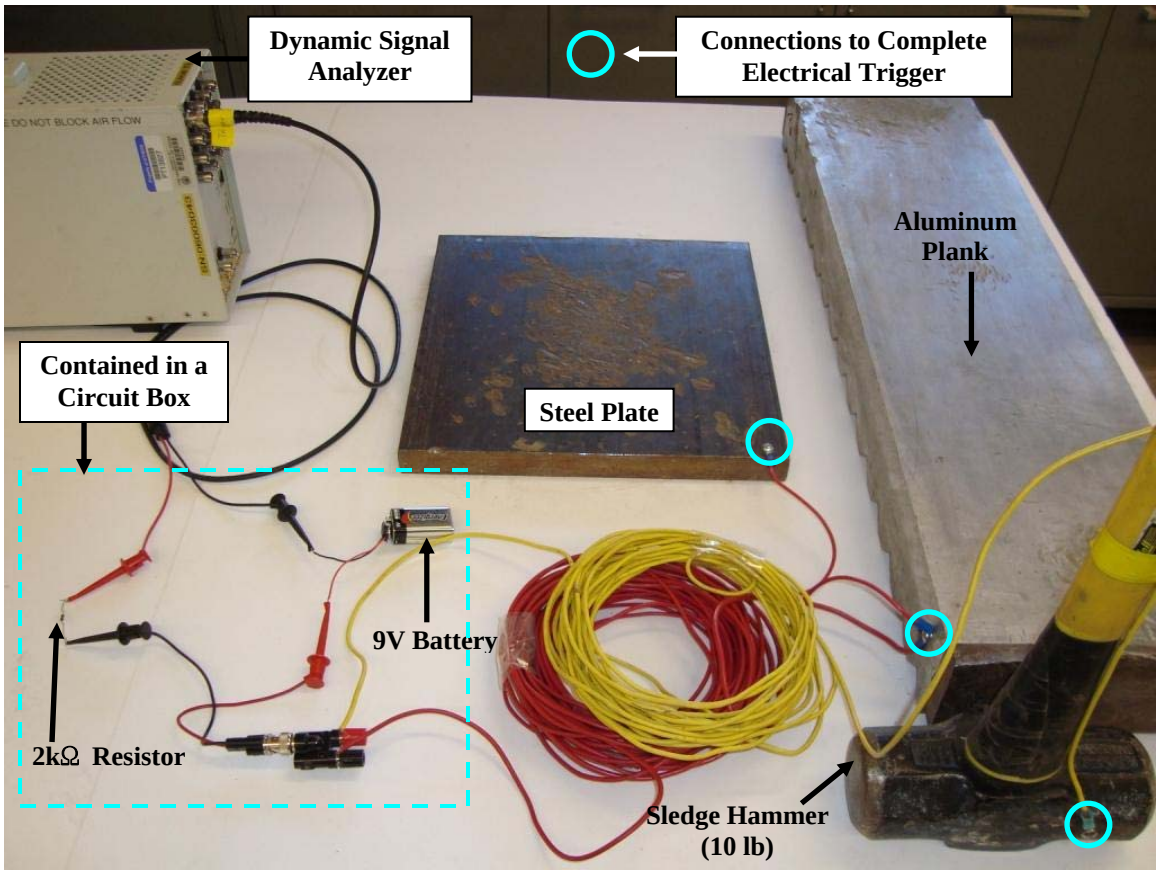

Figure 3.14: Electrical Trigger System with a 9-V Battery and a 2-KΩ Resistor Connected to a Sledge Hammer and then connected to an Aluminum S-Wave Plank and to a Steel P-Wave Plate with Electric Wires

(an accelerometer, a proximitor, the shake table and the same for input sinusoidal motions) used to calibrate the geophones in the seismic cone. This set-up with 3-D reference sensors is shown in Figure 3.16. Differences in the phase and amplitude quantities between the trigger and seismic cone were then evaluated.

As shown in Figure 3.16, the input sinusoidal motions were generated by the electromagnetic shaker. The accelerometer and proximitor were used as reference sensors during calibration of the 3-D reference sensor. The sensor calibrations are reliable because the reference sensors have been calibrated annually with equipment traceable to

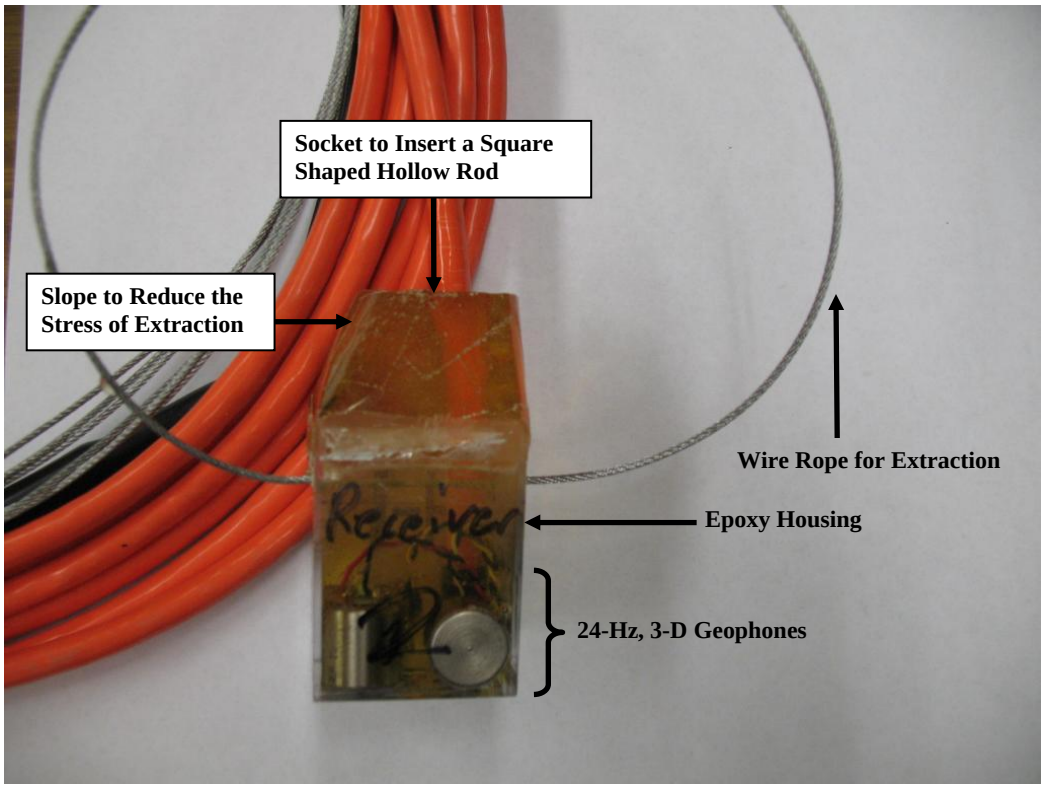

Figure 3.15: 3-D Reference Sensor Consisting of Three, 24-Hz Geophones

the National Institute of Standards and Technology (NIST). The accelerometer (Columbia 3021 and charge amplifier 4102M) is an acceleration transducer operating in the high-frequency range (5 to 5000 Hz). The proximitor (Bently-Nevada 19049) is a displacement transducer operating well at frequencies below 100 Hz. The electromagnetic shaker vertically generates sinusoidal motion in a stepped sine mode over two frequency ranges (600 to 40 Hz for the accelerometer reference sensor and 50 to 5 Hz for the proximitor reference sensor). Each component of 3-D reference sensor was calibrated in the assembled piece that was installed in the ground with cable connections, wire rope and epoxy housing as shown in Figure 3.16. The dynamic signal analyzer was used to record the responses of the 3-D reference sensor, accelerometer and proximitor in the two frequency ranges.

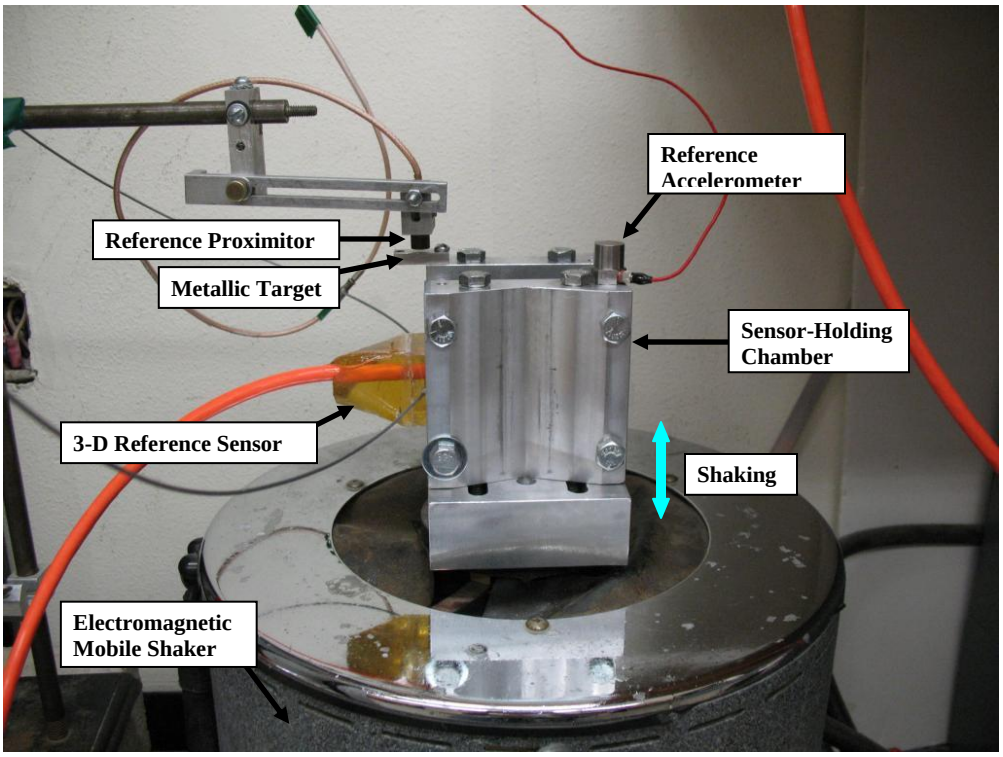

Figure 3.16: 3-D Reference Sensor Calibrated with an Accelerometer and Proximitor on an Electromagnetic Shaker

Figure 3.17 shows a typical example of the calibration response curves from the seismic cone and 3-D reference sensor. In this example, the transverse horizontal geophone (H-1) of the seismic cone and the same geophone in the 3-D reference sensor were checked with the reference sensors (an accelerometer over the frequency range of 600 to 40 Hz and proximitor over the frequency range of 50 to 5 Hz). The phase response of the H-1 geophone in the seismic cone was subtracted from the phase response of the H-1 geophone in the 3-D buried receiver. These results are shown in Figure 3.17a and c for the high and low frequency ranges, respectively. The maximum phase difference is less than 5 degrees in the frequency range from 5 to 600 Hz. This difference can be disregarded because the phase difference is still small at the smallest phase measurement of 90˚; about 5.5 %. The small phase differences of each component of the seismic cone

and 3-D reference sensor enable operators to calculate the correct phase velocity of body waves. The H-1 geophones of the seismic cone and 3-D reference sensor were normalized through the reference sensors. Figure 3.17 (b) and (d) show the response curves over the high (40 to 600 Hz) and low (5 to 50 Hz) frequency ranges respectively. The differences of the amplitude response curves of two sensors are small.

3.5 DATA ACQUISITION SYSTEM

Two Data Physics Analyzers with a software called SignalCalc Mobilizer were used to record the voltage signals generated by sensors during seismic testing. This set-up is shown in Figure 3.18. Each dynamic signal analyzer had the capacity to record signals from 16 channels simultaneously with a sampling rate up to 100 kHz (100,000 samples per second) per channel. Typical frequencies of the seismic signals during the downhole and SCPT tests were less than 500 Hz. The dynamic signal analyzers collected signals without any aliasing frequency based on the sampling theorem because the frequency range of the signals was always less than 40% of the sampling rate. The maximum frequency was high enough to collect signals without aliasing them.

Each dynamic signal analyzer was used with a different trigger, one with the electrical trigger and the other with the 3-D reference sensor. The accuracies of the two dynamic signal analyzers are critical to obtain wave velocities estimated from time and phase differences in these seismic tests. Both signal analyzers were calibrated for timing accuracy using function generators traceable to the National Institute of Standards and Technology (NIST). The calibration was performed by inputting square waves from a function generator into the 16 channels of each dynamic signal analyzer, recording with a computer connected to the analyzer and measuring the time duration over 14 cycles of the

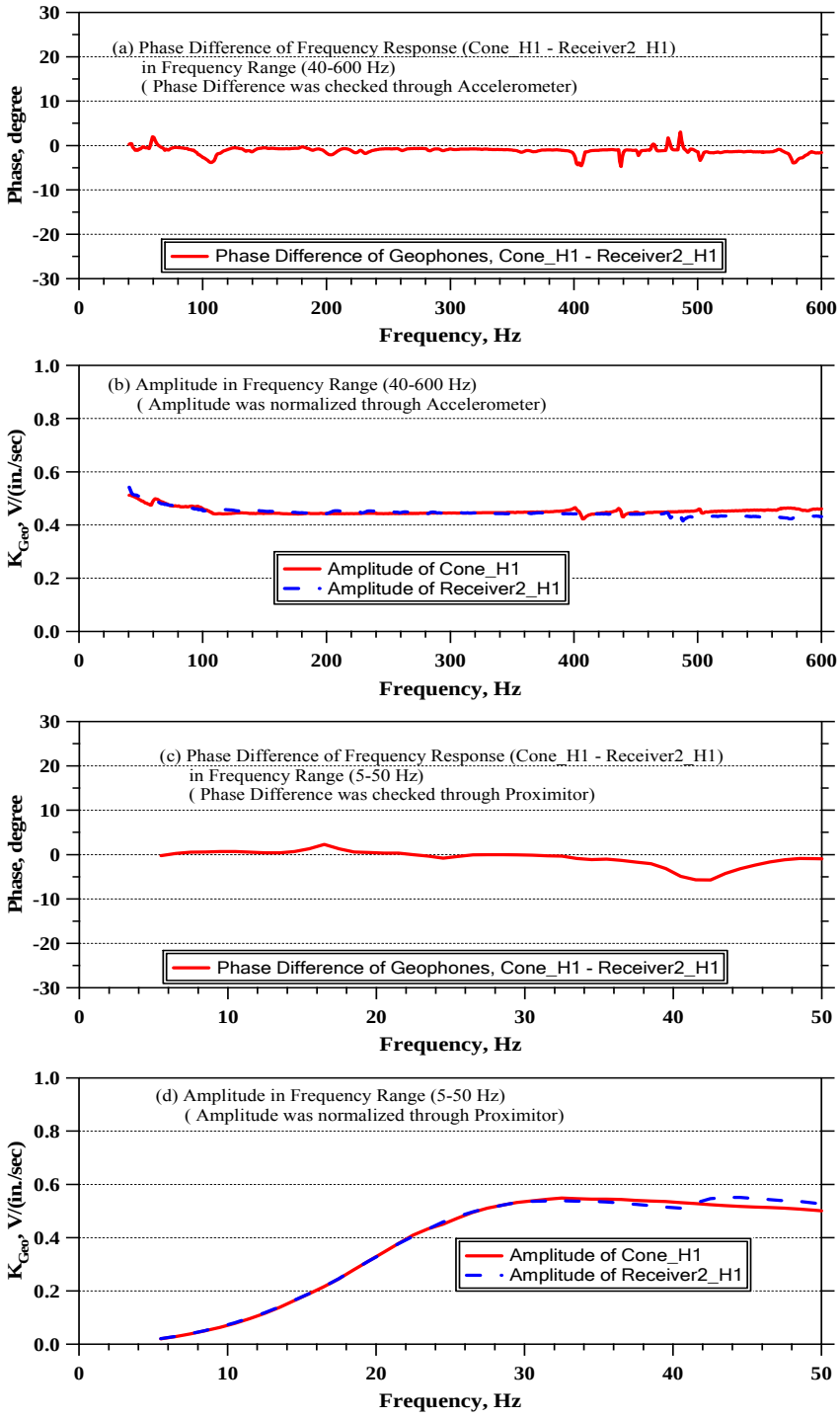

Figure 3.17: Phase Differences and Amplitude between the Seismic Cone and a 3-D Reference Sensor Evaluated with an Accelerometer in the High Frequency Range (40-600 Hz) and a Proximitor in the Low Frequency Range (5-50 Hz)

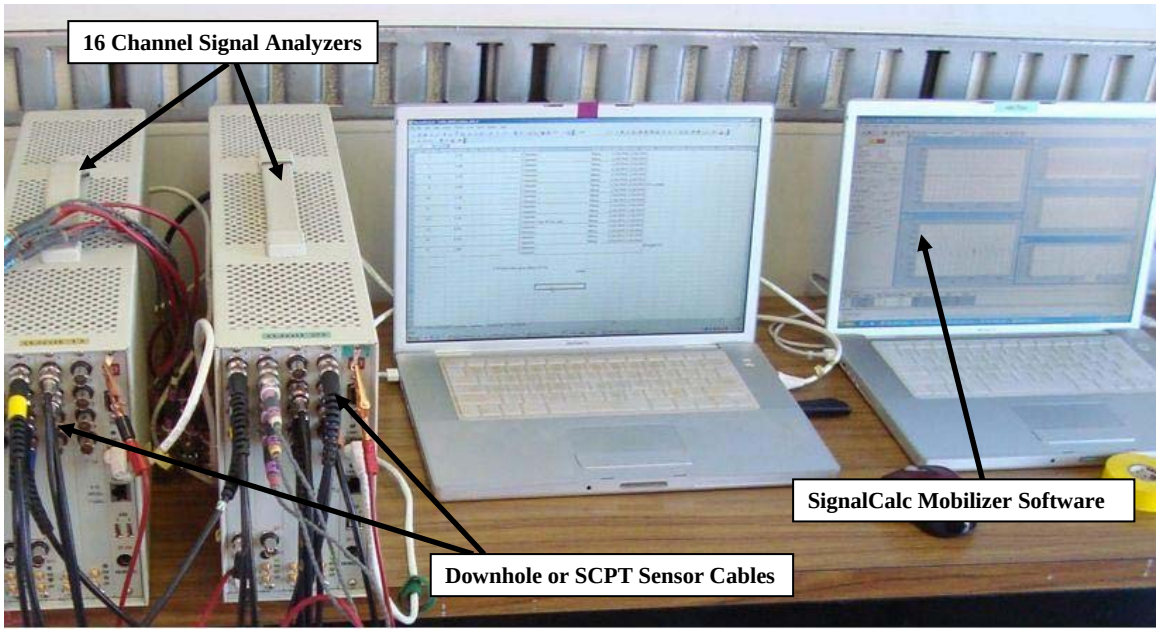

Figure 3.18: Data Acquisition System for Downhole or SCPT Testing

square-wave signal.

The measured time duration was then compared with the expected time duration for the given input frequency. Square waves with frequencies of 10 Hz, 100 Hz, 1 kHz and 10 kHz were used as input, and the frequency spans of the analyzer were set to the same values typically used in the field in downhole and SCPT testing. These calibrations showed that any differences in the timing measurements of each channel were less than 0.02 milliseconds (ms), which is within an acceptable tolerance for this study. Table 3.2 presents an example showing the result from square wave calibration for channels 1 through 16 for one analyzer.

Table 3.2: Example Calibration Records of the Data Physics Dynamic Signal Analyzer for Channels 1 through 16; 10-kHz Square Wave Input

Input Frequency	Square Wave 10 KHz			
Channel No.	Frequency	Input Amplitude	Expected Δt	Measured Δt
	Hz	V	ms	ms
1	10000	0.1	0.10000	0.09998
2	10000	0.1	0.10000	0.09998
3	10000	0.1	0.10000	0.09998
4	10000	0.1	0.10000	0.09998
5	10000	0.1	0.10000	0.09998
6	10000	0.1	0.10000	0.09998
7	10000	0.1	0.10000	0.09998
8	10000	0.1	0.10000	0.09998
9	10000	0.1	0.10000	0.09998
10	10000	0.1	0.10000	0.09998
11	10000	0.1	0.10000	0.09998
12	10000	0.1	0.10000	0.09998
13	10000	0.1	0.10000	0.09998
14	10000	0.1	0.10000	0.09998
15	10000	0.1	0.10000	0.09998
16	10000	0.1	0.10000	0.09998

3.6 SUMMARY

The instrumentation used in the downhole and SCPT tests is described in this chapter. Proper seismic sources, receivers, triggers and data acquisition systems are critical to generating, monitoring and recording body wave signals. A 3-D receiver with three, 14-Hz geophones orthogonally mounted in an acrylic housing was used to monitor vertically propagating compression waves (P_v) and vertically propagating and horizontally polarized shear waves (S_{vh}-waves) in the downhole test. Two, 3-D receivers were separated over a known distance (usually 4 ft) by an aluminum adaptor and a length

of adjustable square rods. This 2-receiver set-up was used to measure true-interval velocities over a range of frequencies in the downhole test.

In the seismic cone test, 24-Hz geophones were used as the sensors. These sensors were used instead of 28-Hz geophones due to larger output and an increased frequency range with a constant calibration factors. The three, 24-Hz geophones were connected to an electrical cable containing three pairs of twisted and shielded sensor cables. The electrical cable was protected with a Polyurethane jacket which is extremely tough, flexible and waterproof. The three, 24-Hz geophones with electrical cables were mounted in a Teflon inner housing. This inner housing was mounted in a metal housing with the shape of a cone (a dummy cone) following the nominal dimensions of ASTM D5778-07. The inner Teflon housing is protected from significant stress during the penetrating procedure. The three-component receiver in the two housings formed the seismic cone. The seismic cone was calibrated before and after assembly using a shake table and reference sensors (an accelerometer traceable to NIST and a proximitor calibrated with equipment traceable to NIST).

An electrical trigger system with a 9-V battery and a 2-KΩ resistor was constructed for use with the P-wave and S-wave seismic sources. Time delays associated with the downhole and seismic cone tests were determined. Two 3-D reference sensors with three, 24-Hz geophones mounted in marine epoxy housing were also constructed. These triggers were buried at a 3.3-ft depth below the ground surface and used to measure the phase difference of the same frequencies propagating between the trigger and the seismic cone. The 3-D reference sensor and seismic cone can be installed and retrieved due to their design and ruggedness structure.

Voltage signals generated by the sensors were recorded with two, 16-channel dynamic signal analyzers. The sampling rate of each signal analyzer was high enough to

collect the wave signals propagating through the soils in the downhole and SCPT tests. The dynamic signal analyzers were calibrated for timing accuracy with function generators which input square waves with frequencies of 10 Hz, 100 Hz, 1 kHz and 10 kHz. The timing difference was within tolerance for this research.

Chapter 4: Field Test Procedures for Downhole and SCPT Testing

4.1 INTRODUCTION

In this research, the field test procedures used in the downhole and SCPT tests can be divided into five categories. These categories consist of: (1) testing setup, (2) installation of 3-D reference sensors, (3) installation of downhole sensor or pushing the seismic cone, (4) generation of body waves, and (5) extraction of the downhole sensor or seismic cone, and the 3-D reference sensors. The five categories are discussed below.

4.2 TESTING SETUP

The typical testing set-ups used in the downhole tests are shown in Figure 4.1 and 4.2. The typical testing setup used in the SCPT tests is shown in Figure 4.3. The testing set-ups of the downhole and SCPT tests shared the same seismic sources; the impulsive sources and the vibroseis truck called Thumper. While the impulsive sources and Thumper were located at the same position in downhole testing, the sources were located at two different positions in SCPT testing because a seismic cone could not be installed at the same location. As a result, the downhole tests with the different installation tools, downhole sensors, and sources were performed at the same location. SCPT tests, which do not need the (expensive) borehole, were performed at many different locations.

A borehole was prepared and the rear bumper of Thumper was located 6 ft away from the borehole as shown in Figure 4.1a. An aluminum S-wave plank with a steel plate on each end was located under the rear bumper of Thumper as shown Figure 4.1b. A hand-operated hydraulic jack was placed on an aluminum cylinder set on the center of the S-wave plank. The hydraulic jack was used to apply a static hold-down force on the plank. The hold-down force reacted against the rear bumper of Thumper and created

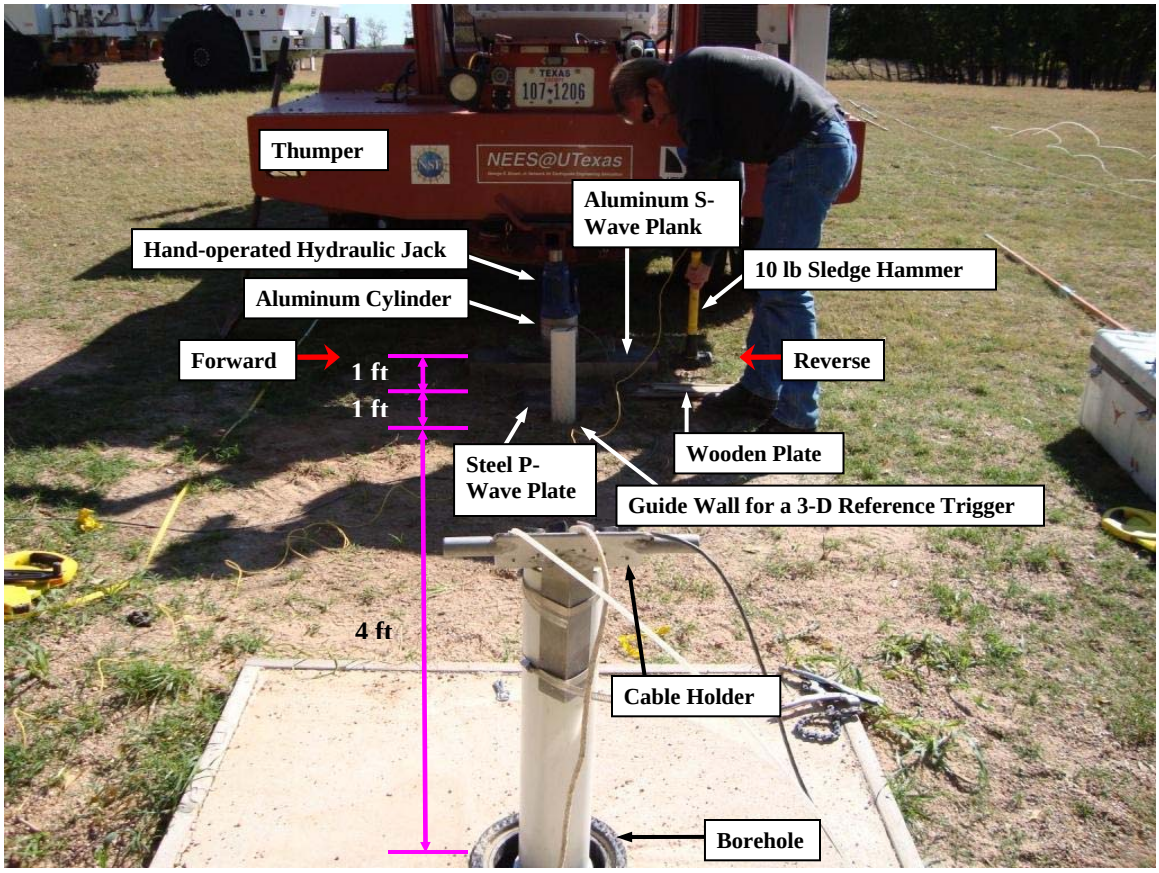

a. Testing Setup of Downhole Test with Impulsive Sources

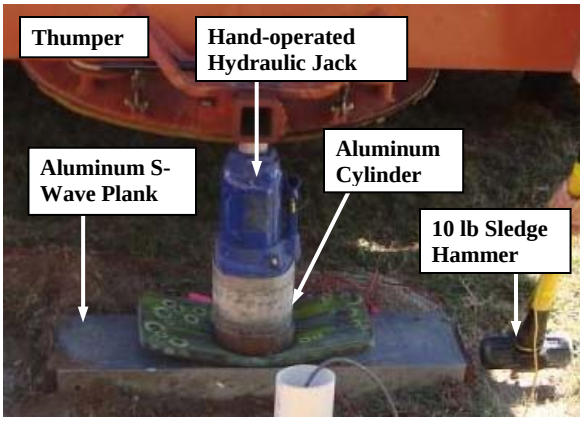

b. S-wave Plank Horizontally Struck with a Sledge Hammer

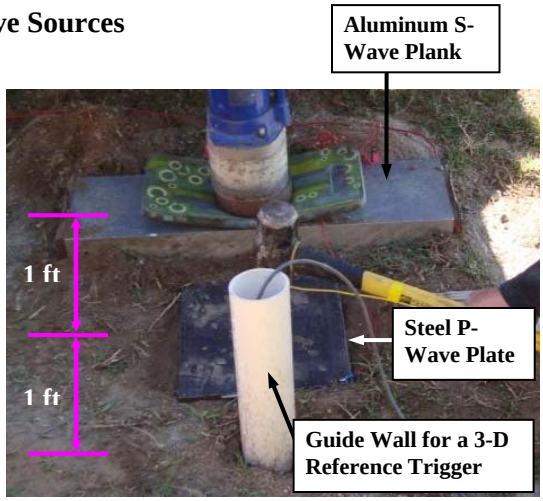

c. P-wave Plate Vertically Struck with a Sledge Hammer

Figure 4.1: Photographs of the Testing Setups Used in Downhole Testing with Impulsive Seismic Sources

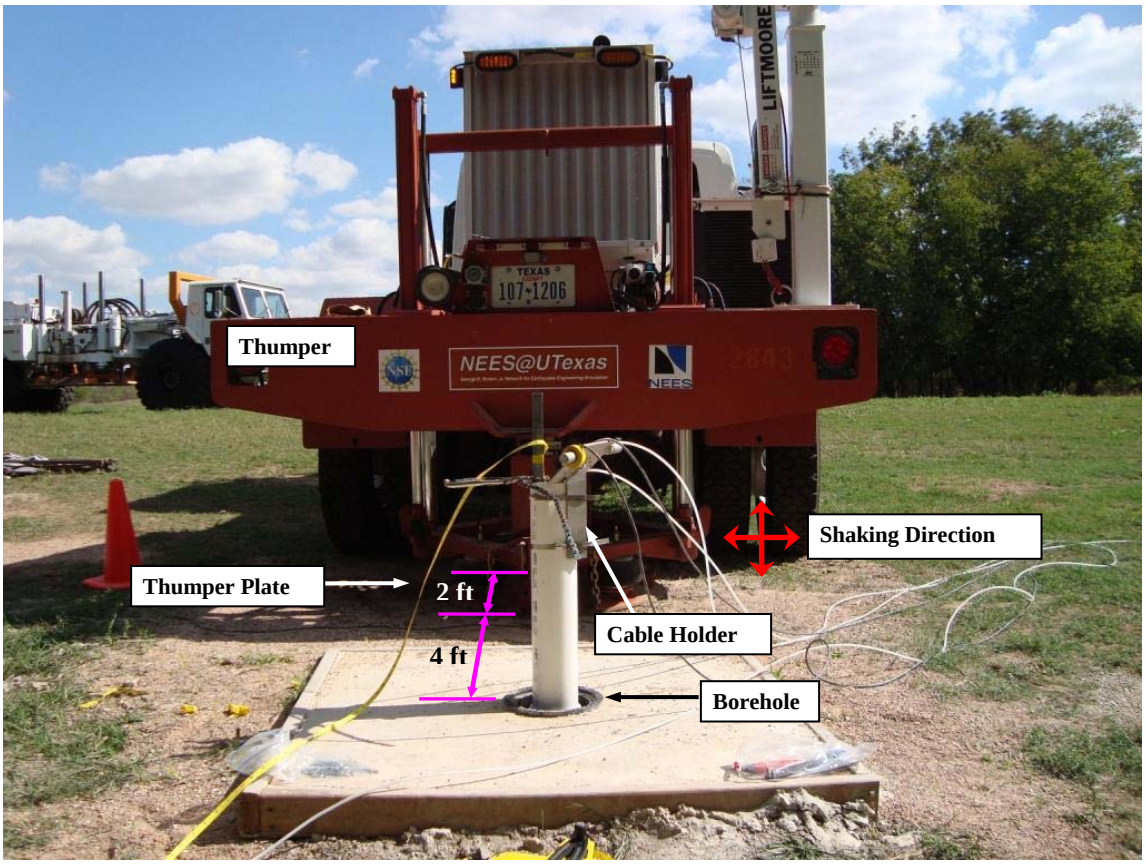

a. Testing Setup of Downhole Test with a Vibroseis Truck

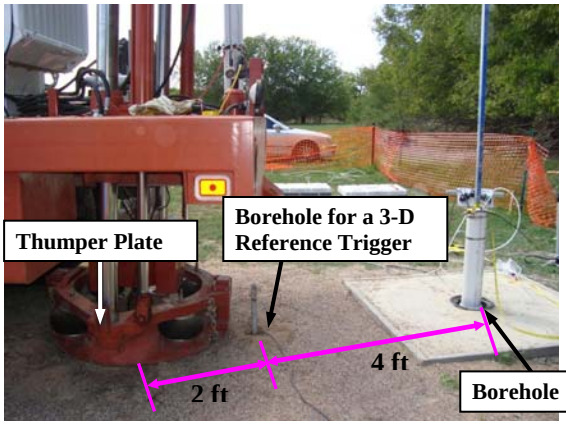

b. Side View of Testing Setup for Downhole Test with a Vibroseis Truck

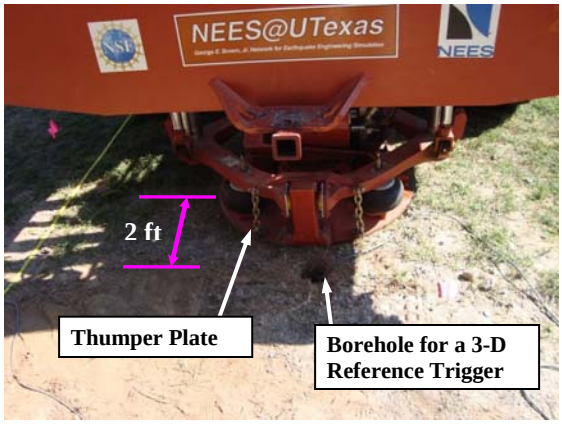

c. Front View of Testing Setup for Downhole Test with a Vibroseis Truck

Figure 4.2: Photographs of the Testing Setups Used in Downhole Testing with a Vibroseis Truck

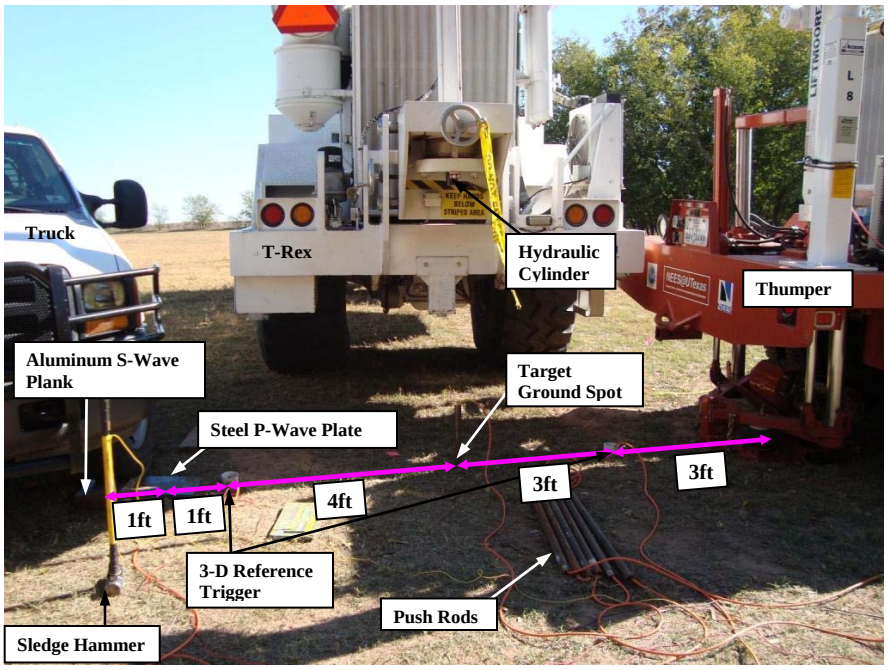

a. Photograph of the Testing Setup of SCPT

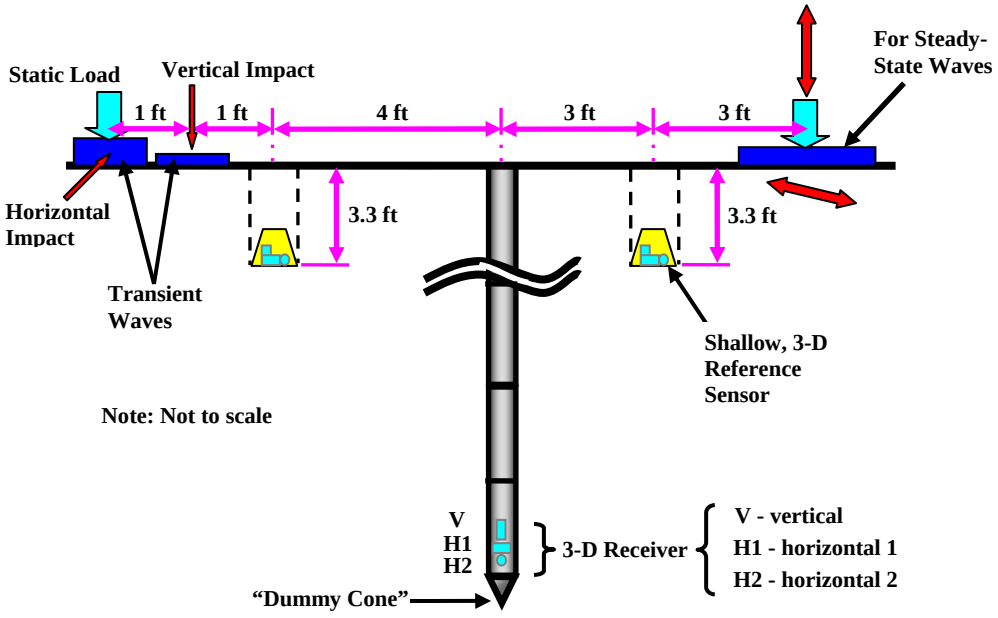

b. Profile View of the Testing Setup for SCPT

Figure 4.3: Photograph and Profile View of the Testing Setup Used in SCPT Testing

excellent coupling between the ground and the S-wave plank. A steel P-wave plate was located 1ft in front of the center of the aluminum plank (see Figure 4.1c). A 3-D sensor that acted as the reference sensor was buried 3.3 ft deep at a distance about 4 ft away from the borehole. When Thumper was used as the source, the center of the Thumper plate was located 6 ft away from the borehole instead of the aluminum S-wave plank and steel P-wave plate, and the 3-D reference sensor was not relocated as shown in Figure 4.2.

SCPT tests were performed at different locations. Figures 4.3a and b show a photograph and profile view, respectively of the testing setup. The target location of the seismic cone was chosen and the hydraulic cylinder on the rear bumper of T-Rex was located 6 ft away from this spot. The aluminum S-wave plank and steel P-wave plate used in downhole testing were located 6 ft and 5 ft away, respectively from the target spot. Thumper and the S-wave plank were located diametrically opposed to each other. The tire of a truck was located on top of the aluminum S-wave plank to make good coupling between the ground and the S-wave plank. A trailer which has a data acquisition system was located facing the rear bumper of T-Rex as a control center. One, 3-D reference sensor was buried 3.3 ft deep and 3 ft away from the Thumper and another reference sensor was 4 ft away from the target spot as shown in Figure 4.3b.

4.3 INSTALLATION OF 3-D REFERENCE SENSOR

A 3-D sensor just like the downhole 3-D sensor used in the borehole was used as a 3-D reference sensor for downhole testing. This sensor is shown in Figure 3.1. The purpose of this reference sensor was to give a reference “time zero” in all downhole (and SCPT) tests. The 3-D reference sensor was embedded in the ground at a distance of 4 ft

from the borehole. A hand-augered borehole was carefully created for the 3-D reference sensor. Insuring the exact location and orientation are the key points when installing the 3-D reference sensor. A square-shaped, hollow aluminum rod was prepared and used as a guide rod to position the sensor properly. The orientation of the reference sensor was controlled and adjusted while installing the 3-D sensor with the square guide rod. The 3-D sensor has a square shaped socket. The square shaped top portion of the sensor was inserted in the square-shaped, hollow guide rod during placement. The installation procedure of the reference sensor in the downhole tests was the same as the installation procedure of the reference sensor in SCPT tests. The specific installation procedure of the sensor in the SCPT tests is illustrated below.

Two, 3-D reference sensors in the SCPT tests were embedded 3 ft away and 4 ft away from the target spot of the SCPT as shown in Figure 4.3b. The two reference sensors were used to determine reference time zero and to monitor body waves that the impulsive sources and Thumper generated in downhole testing. Two boreholes (about 3.7 in. in diameter) were hand-augered 3.3 ft deep (see Figure 4.4) and the reference sensors were placed in them. The installation procedure for the reference sensors is shown in Figure 4.5. The 3-D sensor was oriented and placed using a square hollow rod that was colored red on one side. The soil around the sensor was compacted with solid steel rods that had different cross-sectional areas. The soil that was removed with the hand auger was used in the backfilling and compaction operation. This backfilling process was performed while the square rod held the 3-D sensor in the borehole. After the sensor was secured in position and the backfilling process was completed, a plastic pipe (3.5 in. in diameter and about 3 ft in length) was placed in the hole as a guide wall to prevent the soil wall from loosening and collapsing. The bottom of the plastic pipe was about 3 in. above the sensor. Finally, the square shaped hollow rod was detached by using a solid

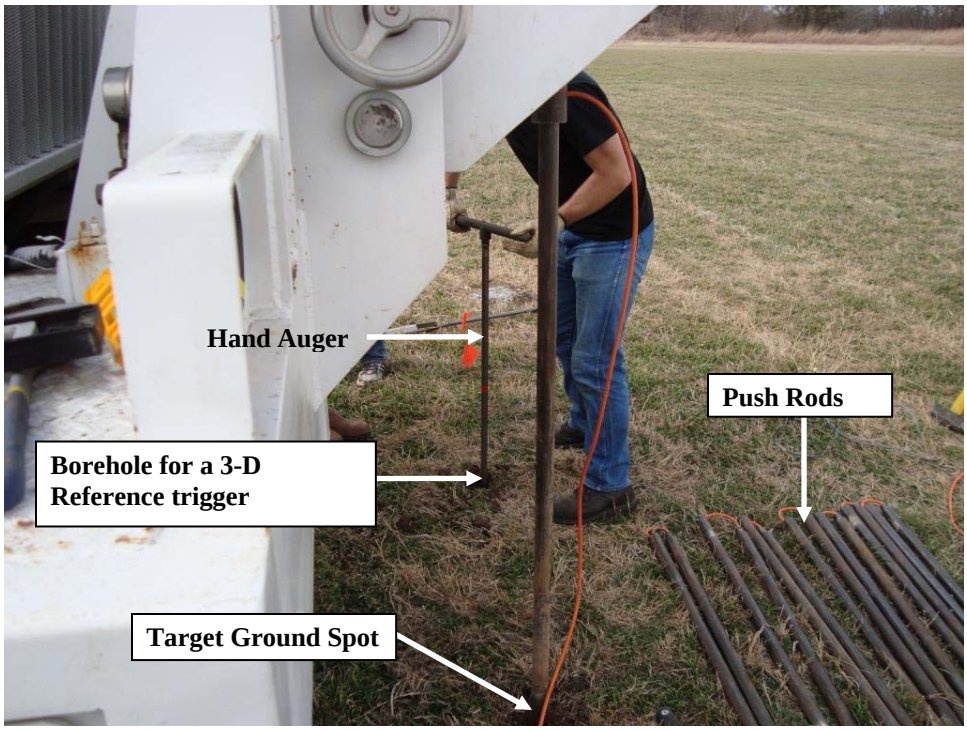

Figure 4.4: Preparation of a Borehole for a 3-D Reference sensor

steel rod to keep the sensor in place and the soil above the sensor was gently re-compacted.

4.4 SEISMIC SENSOR INSTALLATION

The sensor installation procedures for the downhole and SCPT tests are different. While downhole testing requires a borehole in which the downhole sensor is located, SCPT testing requires a hydraulically-operated machine and push rods to advance the seismic cone into the ground. Each installation method has advantages and disadvantages. Downhole tests can be performed without heavy equipment once the borehole has been constructed and can be repeated at different times in the same location. The profiling depth is not limited due to a stiff layer or bedrock. SCPT tests cannot be

a. Placement of 3-D Reference trigger using a Square, Hollow Rod with One Red Colored Side

b. Compaction around the 3-D Reference trigger using Various Solid Steel Rods that have Different Cross-Sectional Areas

c. Placement of Protection Wall to Prevent the Soil from Loosening and Collapse

d. Extraction of Square Hollow Rod

Figure 4.5: Illustration of Procedure Used to Install 3-D Reference sensor

repeated at the exact same location because the seismic cone pushed into the ground with the machinery and push rods disturbs the soil layers with a small area. In addition the profiling depth is limited when a seismic cone reaches a stiff layer or bedrock. However, using CPT machinery and push rods is much cheaper and faster than preparing and using a borehole. As a result, downhole tests were performed in this research at different times in the same borehole. SCPT tests were performed at various locations around the test site,

thus enabling one to create a two-dimensional profile. The installation procedures used in the downhole and SCPT tests are discussed below.

4.4.1 Downhole Borehole and Sensor Installation

In this research, a borehole was drilled and cased at the Hornsby Bend site. At the borehole location, the material profile was sampled using thin-wall Shelby tubes, standard penetration tests and a double-tube core barrel sampler before the borehole was drilled. The upper soil material in the profile was continuously sampled with a thin-wall Shelby tube from the ground surface to 10 ft deep. The thin-wall Shelby tube was used to sample the soil in increments of 5 ft from 10 to 40 ft. Standard penetration tests were performed to sample the mixture of sand and gravel over the depth range of 40 to 50 ft. Below soil, shale exists and between 50 to 75 ft, the shale was sampled continuously with a double-tube core barrel. The profile obtained from the soil and rock samples of the borehole is presented in Appendix B.

As shown in Figure 4.6, a dry borehole was constructed to avoid seismic waves that would be transmitted through a water column in the borehole. The borehole, with a diameter of 9.25 in. and a depth of 75 ft was drilled with minimum sidewall disturbance (Figure 4.6a). Bentonite was used as the drilling mud. After drilling was completed, the bentonite was pumped out and then the borehole was partially filled with a grout mixture of bentonite and cement up to a depth of about 35 ft. A 4-in., inside-diameter PVC pipe filled with water was carefully installed in the borehole as shown in Figure 4.6b. The volume of the PVC pipe pushed the mixture of bentonite and cement in the borehole up to the ground surface. The PVC pipe was centered and set up vertically by using spacers. The casing was held with a griper and the rear bumper of the drilling rig. The upper space surrounding the borehole was grouted with the mixture. When shrinkage occurred as

a. Drilling Borehole

b. Installation of a PVC Pipe Filled with Water so that the Casing Can be Grouted In Place

c. Pumping Water out of the PVC Casing after the Grout Hardened

d. Bailing Remnant Water from bottom of PVC Casing

Figure 4.6: Preparation of a Borehole for Downhole Testing

shown near the top of the borehole, additional grout was filled in this zone. The density of the grout mixture was approximately the same as the density of the surrounding in-situ, geotechnical materials after solidification of the grout. After solidification of the grout, water was pumped out of the casing as shown in Figure 4.6c. The remaining water was removed out by using a bailing tool as Figure 4.6d.

After the dry, PVC-cased borehole was constructed, downhole testing using one, 3-D sensor or two, 3-D sensors was performed. The 3-D sensors were installed with either square, aluminum, orientation rods or simply a rope attached to the sensor package on a 2-ft section of square rod. Two, 3-D sensors with two pneumatic packers and a tape measure are shown in Figure 4.7. The two, 3-D sensors were oriented with square orientation rods so that a horizontal geophone of each 3-D sensor was parallel to the long axis of the aluminum S-wave plank used to generate vertically propagating and horizontally polarized shear waves (S_{vh}-waves) (shown in Figure 4.8). The orientation rod was constructed in 5-ft lengths which were connected with two pins as the surveying depth increased and additional rod was needed. Then the ring of each pin was taped to the orientation rod to eliminate loss of the pins (see Figure 4.8a). A depth measuring tape was attached to the orientation rods to locate correctly the depth of the downhole sensor (s). After the two, 3-D sensors were positioned at the desired depth by lowering and orienting the rods, two pneumatic packers attached to the sensors were inflated using a hand pump at the surface to a net air pressure of about 10 psi (41 kPa) as shown in Figure 4.8b. The inflated pneumatic packers provided good coupling between the downhole sensor and the PVC casing. Two air hoses and two electrical cables were arranged and fixed using a cable holder as shown in Figure 4.9. A foam cushion was placed below a gripping tool (see Figure 4.9) that held the orientation rods. The foam cushion was used to minimize noise that could be transmitted from the ground surface or air. After

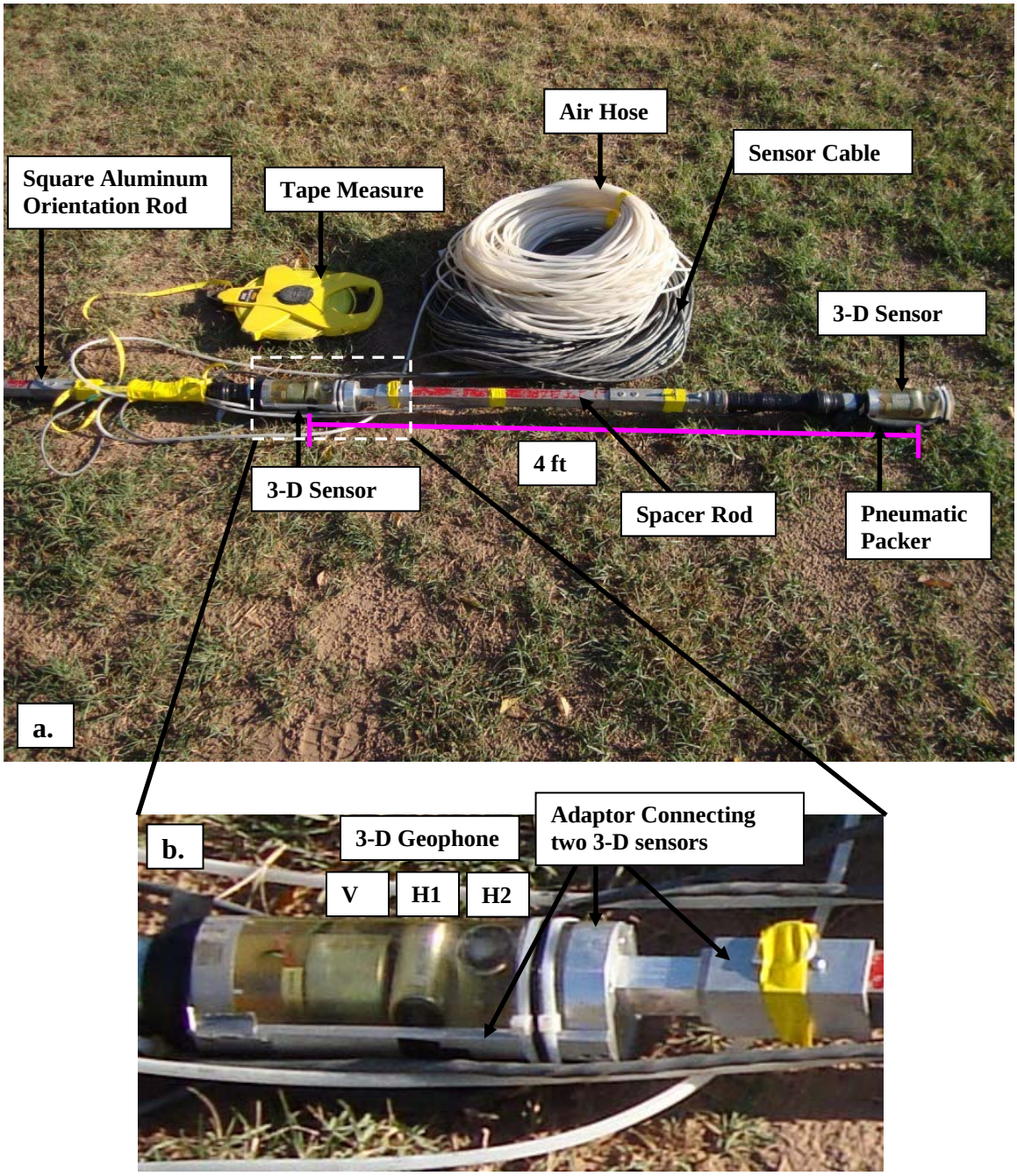

Figure 4.7: Two, 3-Dimensional Sensors Connected by an Adopter Rod Ready for Use in the Downhole Test

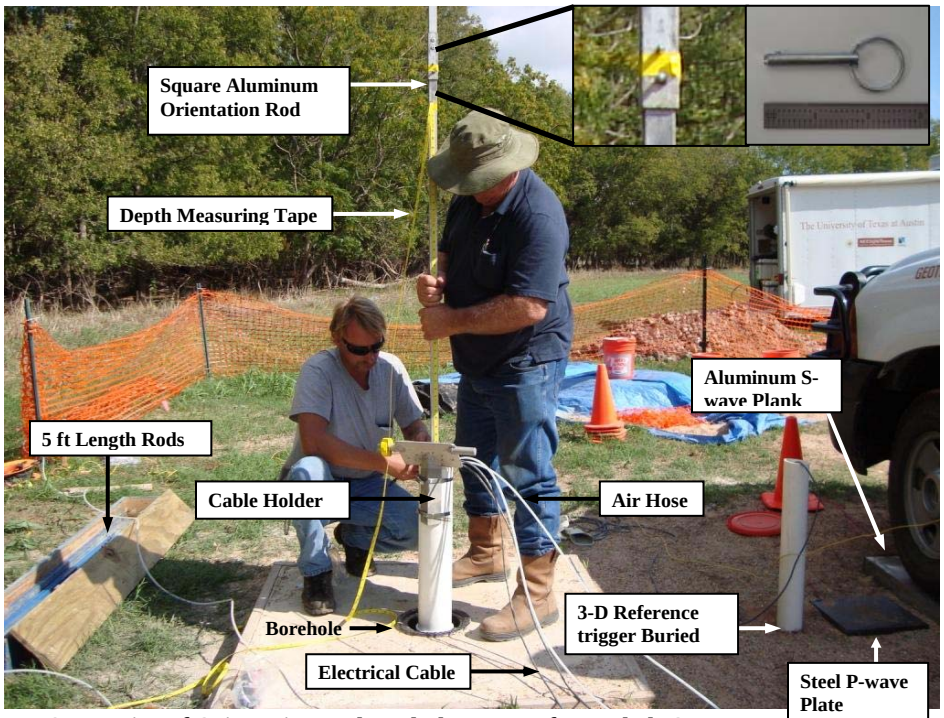

a. Connection of Orientation Rods and Placement of Downhole Sensor

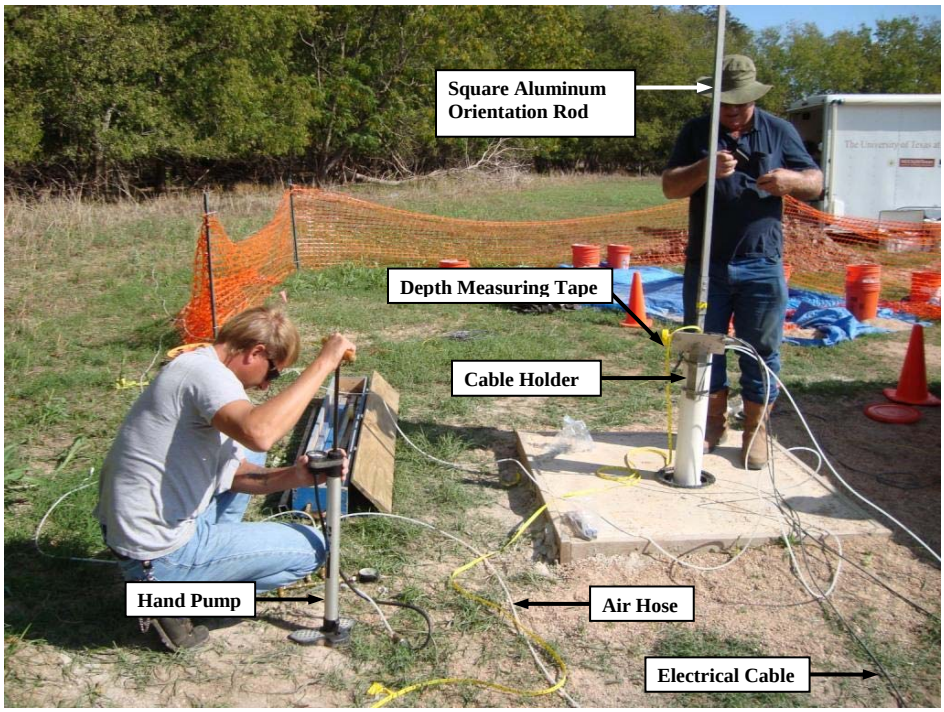

b. Inflation or Deflation of Pneumatic Packer for the Placement or Relocation of Downhole Sensor

Figure 4.8: Procedure Used to Install Downhole Sensor (s)

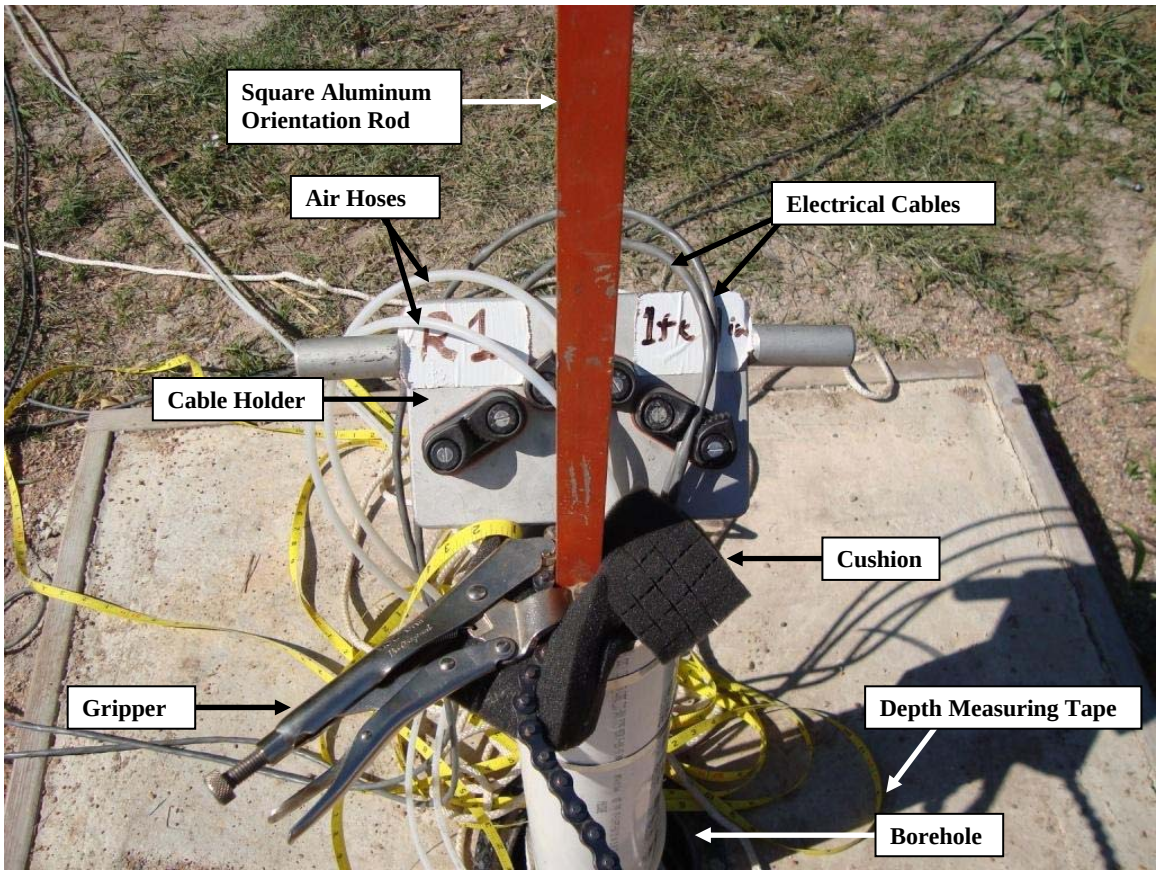

Figure 4.9: Photograph Showing a Cable Holder with Two, 3-D Sensors in the PVC-Cased Borehole

downhole testing was completed at a given depth, the air pressure in the pneumatic packers was released and the pneumatic packers deflated, allowing the sensor (s) to be moved to next test depth.

As shown in Figure 4.10, a rope instead of continuous orientation rods was used to lower or raise the one, 3-D sensor. The installation procedure using a rope was similar to the installation procedure using the orientation rods illustrated in Figure 4.8. A short square rod was connected to the 3-D sensor. The rope was connected to the end of the short rod that had holes for the two pins. Orientation of this single 3-D sensor could not be controlled with the rope. A depth measuring tape attached to the short rod was used to

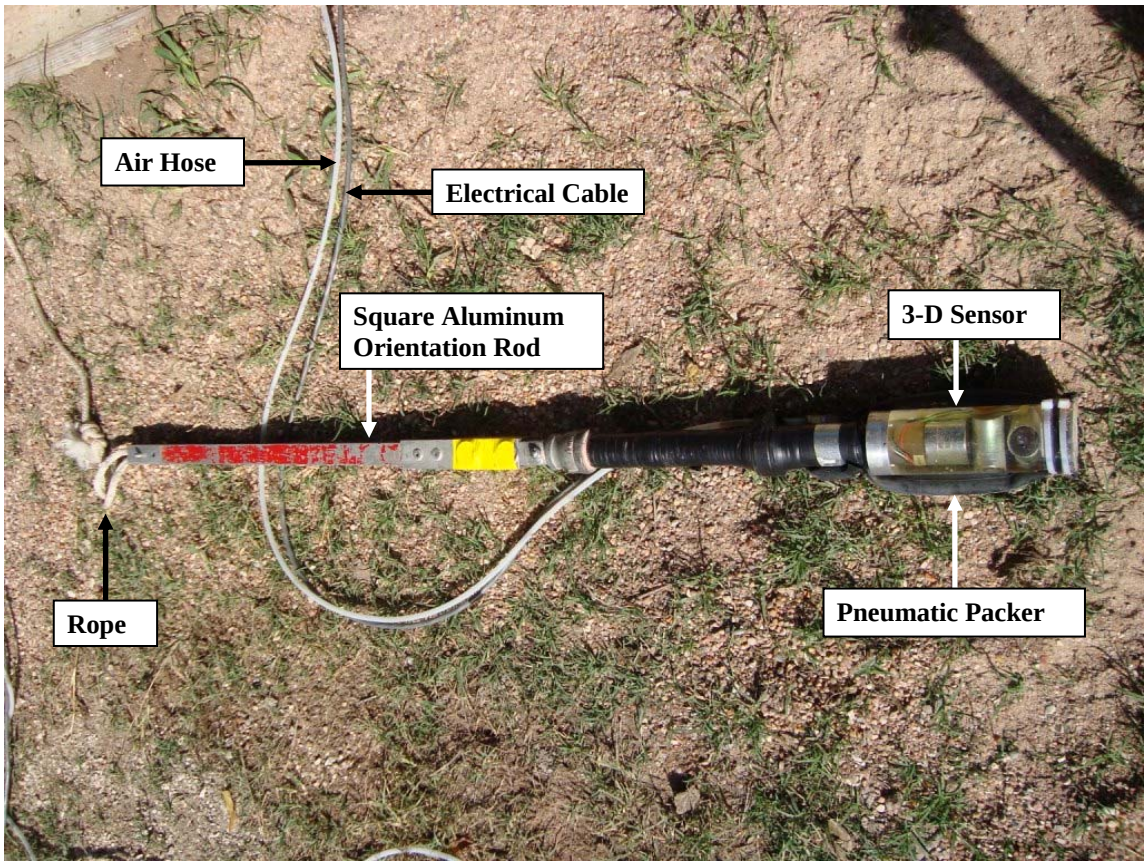

Figure 4.10: Photograph Showing Rope Attached to One, 3-D Sensor with a Short Rod

locate the depth of the downhole sensor. A pneumatic packer was inflated or deflated to fix or change the location of the downhole sensor in a borehole by using a hand pump shown in Figure 4.8b.

4.4.2 Seismic Cone Installation

The design and construction of the seismic cone are discussed in detail in Chapter 3. In this section, pushing the seismic cone into the ground is discussed. The seismic cone is shown in Figure 4.11 for review purposes. As seen in the figure, the cylindrical Teflon housing includes three, 24-Hz geophones fixed with marine epoxy. The Polyurethane cable jacket is extremely tough, flexible and waterproof so that the cable is able to go

through hollow push rods to the ground below water level. The Teflon housing was mounted in the metal housing, (see Figure 4.11b) and thus the Teflon housing was protected from significant stress during pushing the seismic cone. Two reference marks denoted the orientation of the orthogonally mounted, two, horizontal components (one hole and two holes show the axis directions of H1 and H2, respectively). Using female threads of the cap at the top of the seismic cone, a push rod was connected to the cap to begin the installation process.

The heavy-walled, hollow, steel push rods of the CPT and the hydraulic cylinder on the rear bumper of T-Rex were used to install the seismic cone as shown in Figure 4.12. The hydraulic ram is capable of operating at variable speeds and pushing with a maximum force of 20,000 lb (59 kN). The push rods, also called CPT or Dutch Cone Penetrometer rods, are 3.3 ft (1 m) long, with an outside diameter of 1.5 in. (3.8 cm) and an inside diameter of 0.5 in. (1.3 cm). One of the push rods was cut to make 11-in. (28 cm) long sections to aid in seismic cone installation process.

Pushing and pulling adaptors, shown in Figure 4.13 were used to connect the push rods to the hydraulic cylinder on the rear bumper of T-Rex. Both adaptors were simply connected and disconnected, as needed, to the hydraulic cylinder. The pushing adaptor was coupled to the push rods with a simple compression fit. The sides of both adaptors have a slot that allows the seismic cone cable to exit the adaptors without being damaged when the cone and rods are pushed or pulled. The pulling adaptor consists of a top piece and a bottom piece. The bottom piece that has a male threaded section on top and a lower hollow body with a slot is capable of moving up and down, and rotating within the top piece. The mechanical capability enables the male thread of the bottom piece to be connected to the female thread of each push rod. When the top piece of the pulling adaptor is loaded in tension, the bottom piece is firmly coupled to the top piece. Thus the

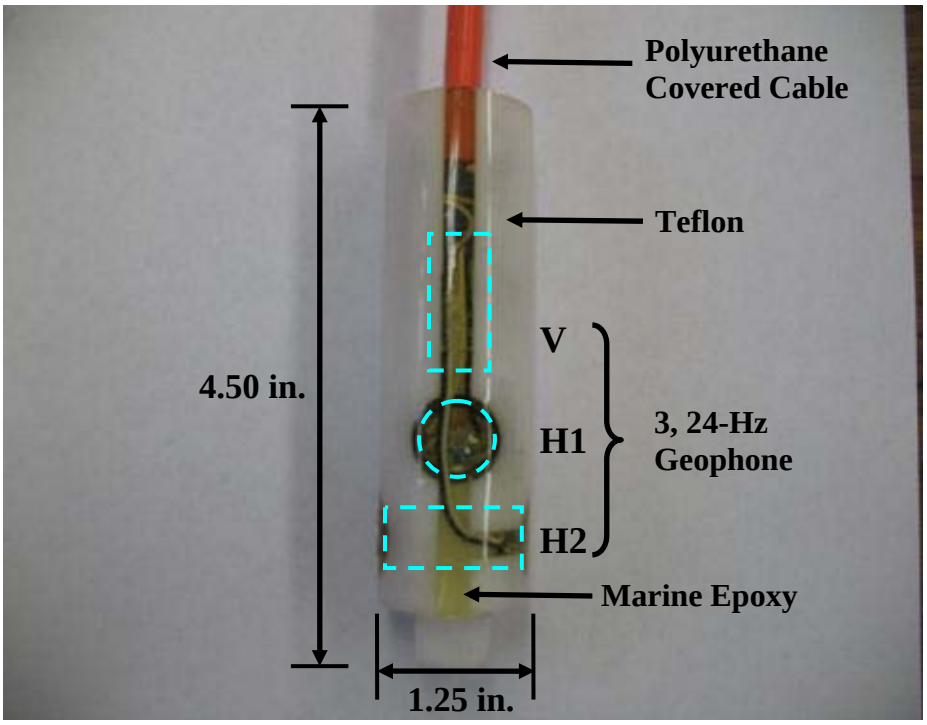

(a) Three-Component, 24-Hz Geophones Securely Assembled in a Teflon Housing with Marine Epoxy

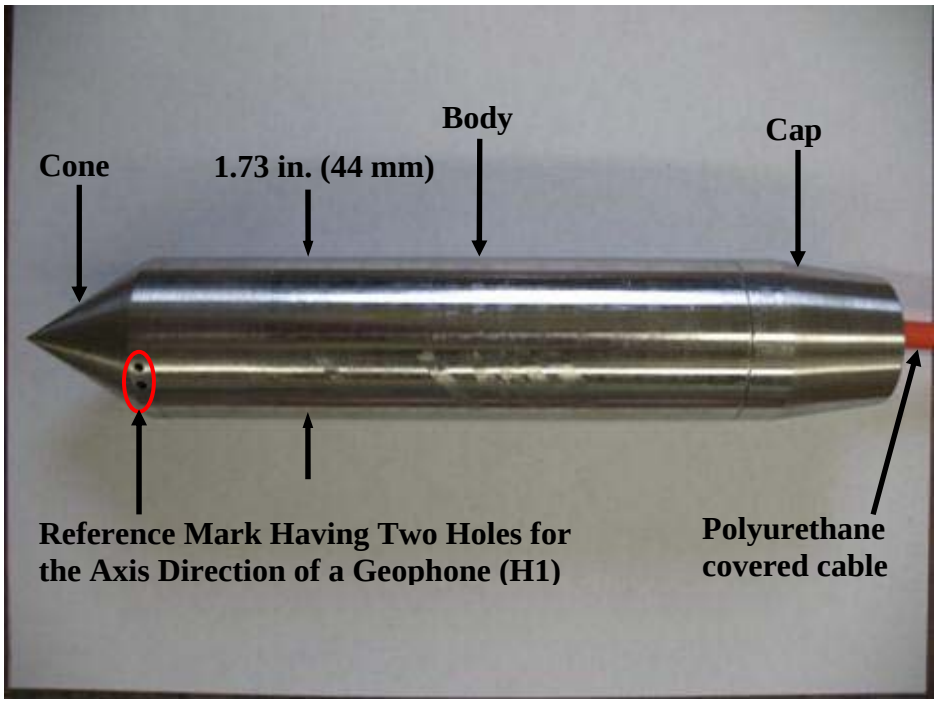

(b) Outer Metal Housing Composed of Assembled by 3 Stainless Steel Pieces

Figure 4.11: Photographs Showing a Seismic Cone with Three, 24-Hz Geophones

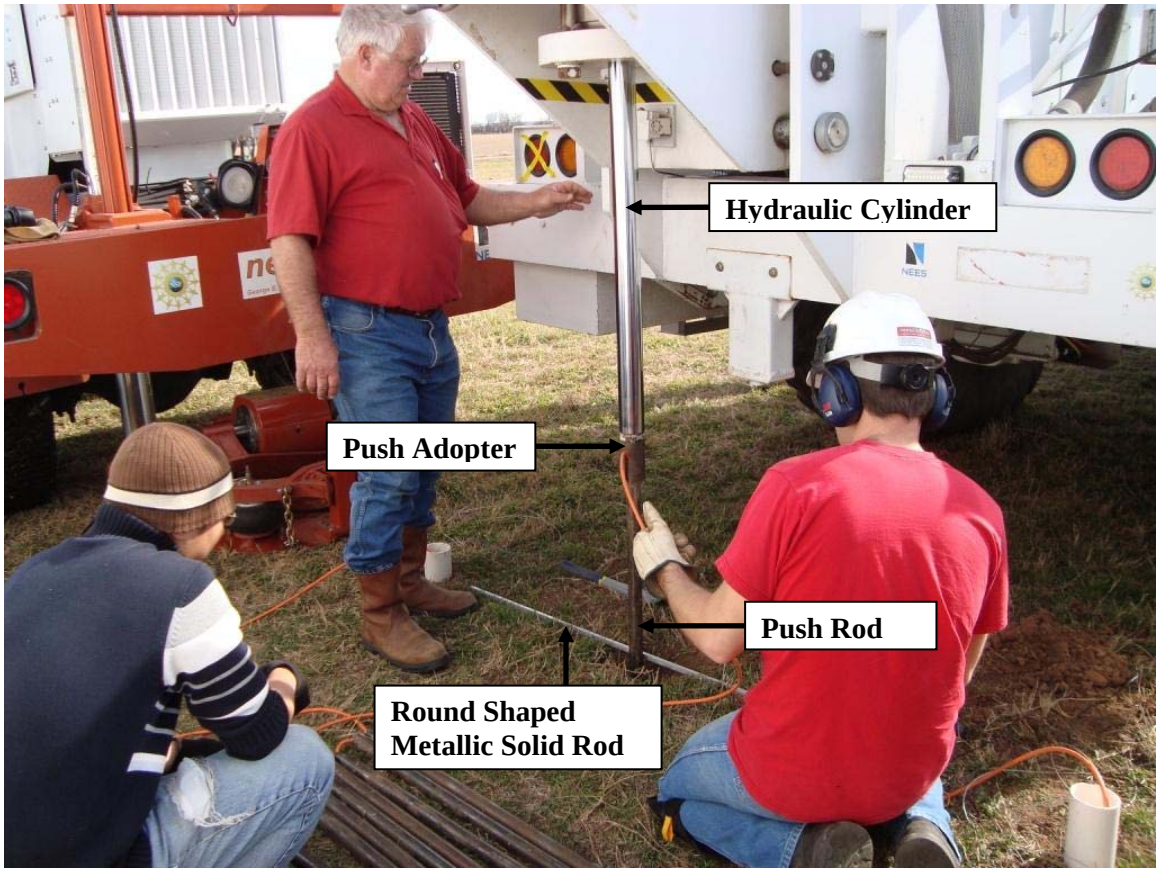

Figure 4.12: Installation of a Seismic Cone using the Hydraulic Cylinder on the Rear Bumper of T-Rex connected to a Push Rod

rods are pulled out of the ground.

The verticality of the push rods are measured with an air bubble level to maintain verticality in the rods at all times, at least at the surface. The verticality of the push rods enables one to estimate the location of the cone and, hence, the distance that the body waves travel. The hydraulic cylinder with the pushing adaptor is used to the seismic cone in 3.3-ft intervals through the soil. Seismic testing was performed in 1 m (3.3 ft) depth intervals. Push rods were always decoupled from the pushing adaptor before any seismic testing was performed. The decoupling of the push rods ensures that the dynamic movement of the seismic cone will not be influenced by noise from T-Rex traveling

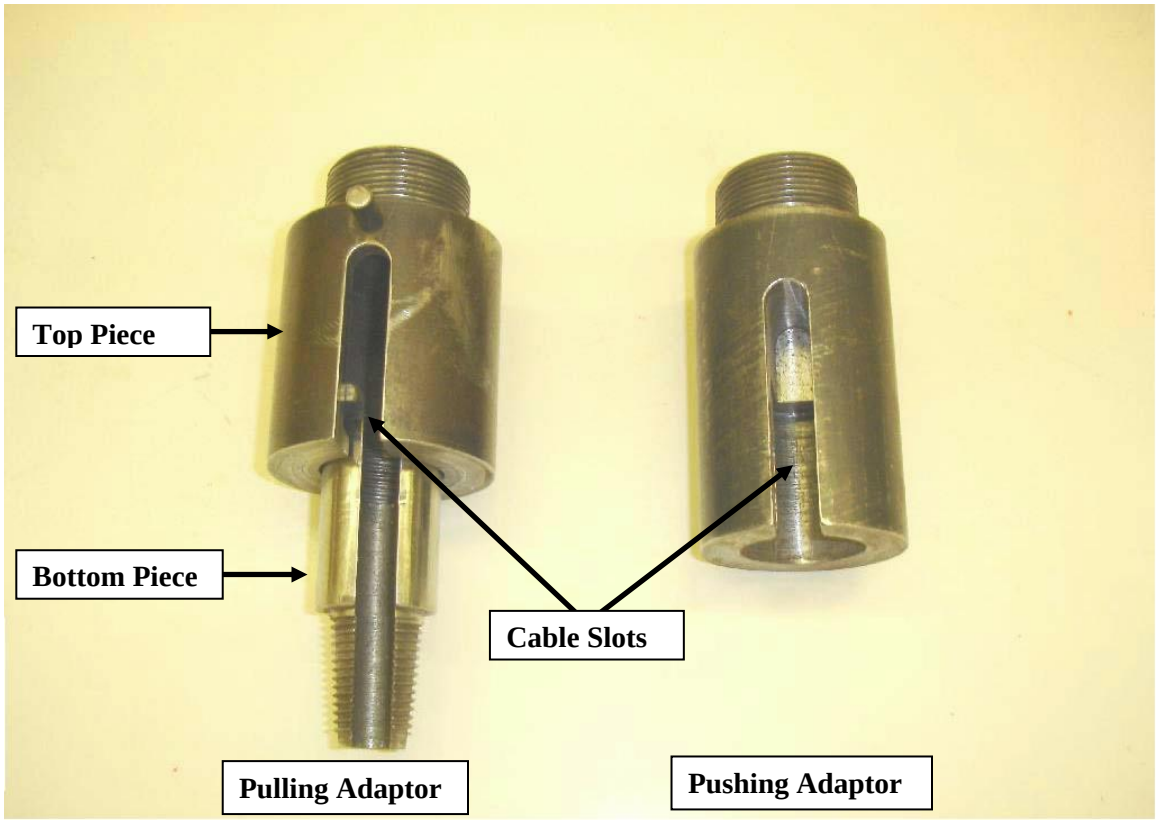

Figure 4.13: Photograph of the Pushing and Pulling Adaptors that Connect the Hydraulic Cylinder on the Rear Bumper of T-Rex to the Push Rods (from Cox, 2006)

directly down the rods.

4.5 GENERATION OF BODY WAVES

In this research, two different types of sources were used to generate shear and compression waves. The sources consisted of impulsive sources generating transient body waves and a vibroseis truck (called Thumper) generating sinusoidal waves in a stepped sine mode.

An aluminum S-wave plank was set up as shown in Figure 4.14. The hold-down force against the rear bumper of Thumper or the weight of a truck located on the aluminum S-

wave plank created excellent coupling between the ground and the heavy aluminum plank which has a saw-teeth pattern on the bottom. Good coupling guaranteed maximum S wave generation when the plank was horizontally struck by the sledge hammer. The result was generation of strong, clean S_{vh}-waves. Each side of the aluminum S-wave plank was covered by a rectangular steel pad to prevent damage to the aluminum plank. Each side of the plank was struck with a 10-lb sledge hammer to generate polarized S_{vh}-waves which were used to create a butterfly shape. The two impacting directions are called "forward" and "reverse" in this study. In each direction, the tests were repeated 5 to 10 times or more if needed to obtain a low-noise record. As the testing depth increased, the number of blows with a sledge hammer increased. Even with more averaging, the signal-to-noise ratio in the records increased somewhat with the increasing depth. An electrical trigger system with a 9-V battery and 2-KΩ resistor was connected between the sledge hammer and the aluminum plank. The electrical trigger system is discussed in Chapter 3.

A steel plate, with the weight of 40 lb, which was vertically impacted, was used to generate P waves as shown in Figure 4.14. The center of the steel plate was 1 ft away from the center of the aluminum S-wave plank. The edges of the S-wave plank and P-wave plate did not touch. Any grass or weeds between the plate and ground surface were removed and the ground surface was leveled with a shovel. When the P-wave plate was vertically struck by a sledge hammer, a person stood on the plate to minimize rebounding and to ensure good coupling between the plate and ground. Seismic tests with the steel plate involved striking the plate 5 to 10 times or more if needed to obtain consistent data. Similarly, the S-wave plank was struck multiple times at each measurement depth. The signal-to-noise ratios of body wave trains increased with the increasing number of impacts. The same electrical trigger system connected to the S-wave plank was also

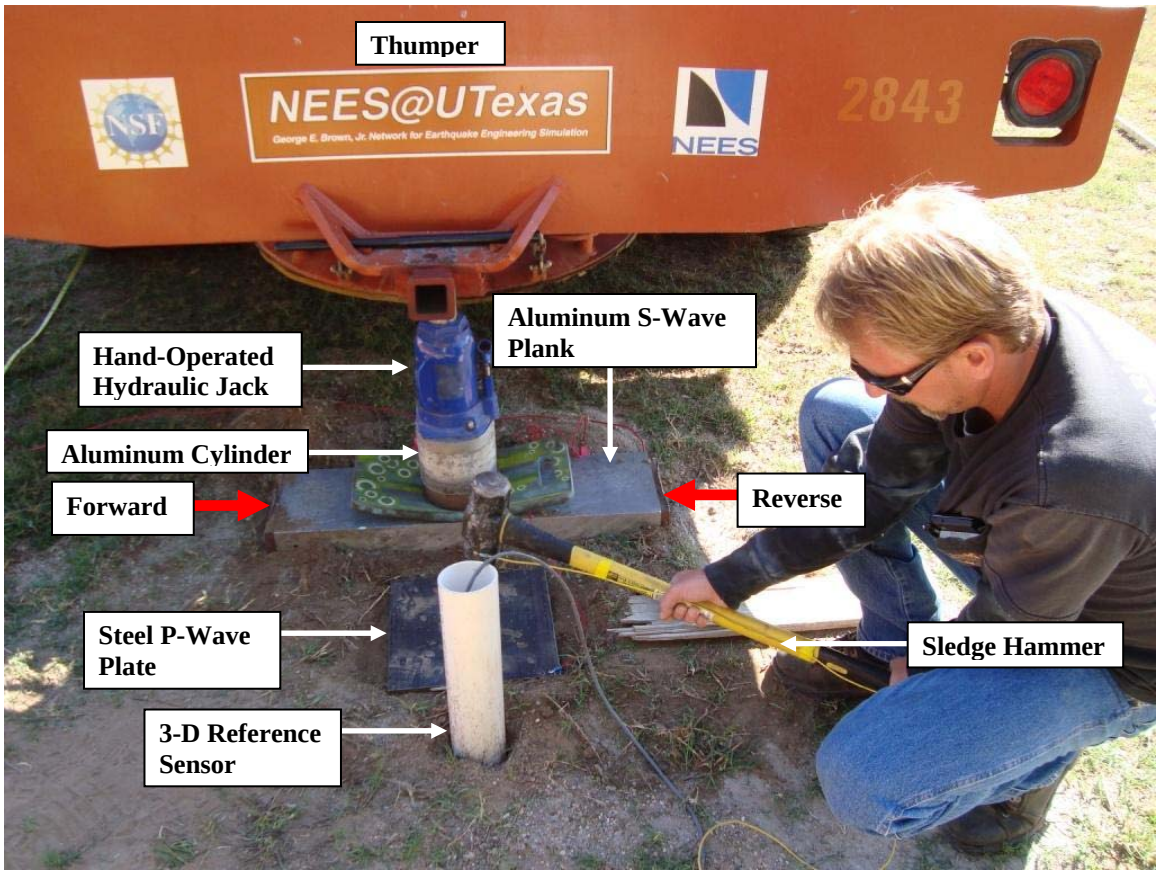

Figure 4.14: Setup of Impulsive Sources Used to Generate Shear and Compression Waves

connected to P-wave plate.

Thumper was used as a wide-band frequency source. Thumper is shown in Figure 4.15. Thumper was operated in a stepped-sine mode. The loading plate of Thumper has two vibration orientations, vertical and horizontal. The vibration orientations of the loading plate enabled S_{vh}-waves and P_v-waves to be generated. The frequency range covered by Thumper is generally 20 to 200 Hz which is the frequency range over which the constant maximum force is generated as shown in Figure 4.16. Shear-wave measurements ranged from 50 to 500 Hz with Thumper on the ground surface. This range was used to study the dispersive characteristics of body waves in the SCPT testing.

Figure 4.15: Thumper Used to Generate Shear and Compression Waves (from http://nees.utexas.edu/Equipment-Thumper.shtml)

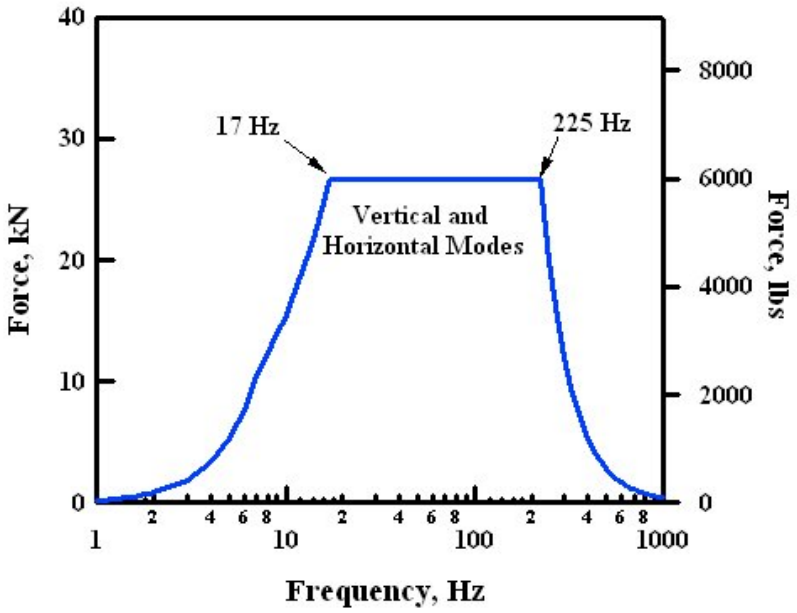

Figure 4.16: Theoretical Force Output of Thumper (from http://nees.utexas.edu/Equipment-Thumper.shtml)

However, body waves with short wavelengths (frequencies above 300 Hz) did not have enough energy to propagate to the seismic cone through soil layers at comparatively deeper depths (depths greater than about 15 ft in this study). The average value of 5 sinusoid signal cycles generated by Thumper was recorded in each measurement frequency. A 3-D reference sensor embedded 3.3 ft below the ground surface was used as a reference sensor to calculate the phase velocities.

4.6 EXTRACTION OF SENSORS

The extractions of downhole sensors, a seismic cone and 3-D reference sensors were easily performed with the same tools used to install the sensors.

4.6.1 Extraction of Downhole Sensors

The downhole sensor connected to the square aluminum rods were simply extracted by pulling the square aluminum rods out of the borehole. The pneumatic packers attached to the downhole sensors had to be deflated by opening the air valve before the downhole sensor was pulled up by hand. As each square rod was extracted out of the borehole, it was disconnected from a square rod below it by pulling the two pins out of the connector. Once disconnected from other square rods, the rods were returned to the wooden storage box for next testing.

A downhole sensor tied with a rope could be extracted by simply pulling the rope after deflating the pneumatic packer.

4.6.2 Seismic Cone Extraction

After SCPT testing was completed, the seismic cone and pushing rods had to be recovered from the ground. The pulling adapter connected to a hydraulic cylinder on the rear bumper of T-Rex was used to withdraw the push rods connected to the seismic cone,

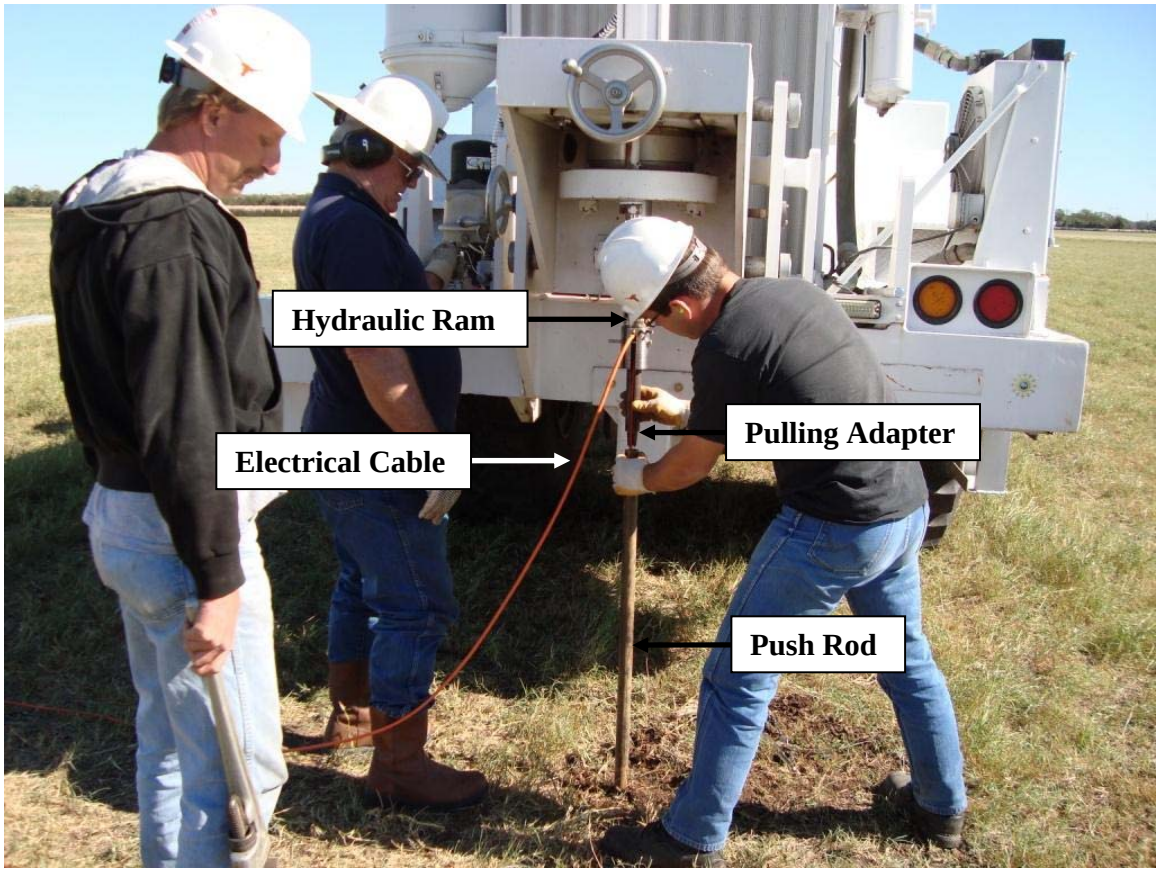

Figure 4.17: Extraction of a Seismic Cone using the Pulling Adapter Coupled to the Hydraulic Cylinder on the Rear Bumper of T-Rex

as shown in Figure 4.17. The bottom piece of the pulling adapter has the same threads as the push rods. The bottom piece with a slot was able to move up and down, and rotate within the top piece. This mechanical capability allowed the male thread of the bottom piece to be connected to the female thread of the push rod. The bottom piece was engaged by the top piece when the top piece was pulled upward with the hydraulic piston. The push rods were continuously pulled out of the ground and disconnected.

4.6.3 Extraction of 3-D Reference sensors

After SCPT testing was completed, the two, 3-D reference sensors were extracted. A pre-attached wire rope was used to extract each 3-D reference sensor buried in 3.3 ft below the ground surface. After the protection wall was pulled out of the shallow borehole, each 3-D reference sensor was withdrawn out pulling the wire. The conical top of the 3-D reference sensor minimized the earth pressure that would damage the sensor when the wire rope was pulled.

4.7 SUMMARY

The procedures used in downhole testing and SCPT testing are discussed in this chapter. The procedures can be subdivided into five categories. These categories are: (1) testing setup, (2) installation of 3-D reference sensor, (3) sensor installation, (4) generation of body waves, (5) extraction of 3-D reference sensors, downhole sensors and seismic cone. Steps (3) and (4) were repeated at increased depths in 1-m (3.3-ft) intervals until the seismic cone reached the final depth and at 5-ft depth intervals in the downhole tests.

Chapter 5: V_S and V_P Profiling in the SCPT Test with Conventional and Advanced Testing and Analysis Procedures

5.1 INTRODUCTION

Conventional profiling in the SCPT test with only V_S measurements is presented in Appendix A. This work was performed primarily to confirm that the 3-D SCPT sensor worked properly and to obtain experience with SCPT testing. Following this work, a series of tests was performed to investigate V_S and V_P profiling with the SCPT test using conventional and advanced testing and analysis procedures. These tests are presented in this chapter. All SCPT testing was performed in the time domain as done in conventional SCPT testing. This work also formed the wave velocity data with which the new SABW method results presented in Chapter 6 are compared. It should be noted that the SABW method is a frequency-domain method much like the SASW method discussed in Chapter 2. The SCPT testing was performed at Platt 4 at Hornsby Bend. The SCPT testing consisted of CPT and seismic cone tests that were performed in slightly different locations at slightly different times.

A horizontal geophone (H-2) in the 3-D seismic cone was used to monitor vertically propagating and horizontally polarized shear waves (S_{vh} waves) that were generated by an S-wave source. The other horizontal geophone (H-1) and a vertical geophone (V) in the 3-D seismic cone were used to monitor vertically propagating compression waves (P_v waves), which were generated by a P-wave source. A dynamic signal analyzer was used to record signals from the 3-D geophone. Three waterfall plots which consisted of the recorded output signals were plotted and analyzed to calculate the S- and P-wave velocities.

To analyze the data, waterfall plots were used to identify first-arrival times or times of other reference points on the shear and compression waveforms in the time domain. In the data analyses, picking first arrival times or times of other reference points of S_{vh} and P_v waves is important in calculating body wave velocities. The body wave velocities calculated using times of different reference points and also using cross correlation of signals are discussed in this chapter. While signals that were generated by the S-wave source were cross correlated without a window, signals that were generated by the P-wave source were cross correlated without and with a rectangular window. The importance of windowing P-wave signals is clearly shown and discussed.

The testing site, Platt 4 at the Hornsby Bend, is briefly described in this chapter. The testing site is described in detail in Appendix B.

5.2 SCPT TESTING SET-UP

Traditional SCPT testing consists of an S-wave source at the ground surface and a 1-D, horizontal receiver positioned above the cone portion of the CPT device as introduced in Chapter 2. In this testing, CPT and downhole testing are performed sequentially during the pushing process. In contrast to traditional SCPT testing, the SCPT testing conducted in this research was performed in two separate steps. The first step was simply a CPT test using the CPT device described in Appendix A. In the second step, a dummy 15-cm^2 cone was used in which a 3-D sensor was installed just above the cone as described in Chapter 3. The two-step testing process resulted in the CPT and seismic cone tests being performed at slightly different times and at slightly different surface locations. The testing times were within a week and the locations were within 15 ft.

The set-up for the seismic cone test as performed in this research is shown in Figure 5.1 and consisted of shear (S) and compression (P) wave sources, a 3-D receiver in the dummy cone. An aluminum S-wave plank and a steel P-wave plate were located about 6 ft and 5 ft away, respectively, from the seismic cone surface location. To maximize the recorded amplitude of the S_{vh}-waves, the orientation of the H2 horizontal geophone in the 3-D seismic cone receiver was aligned parallel to the direction of the horizontal impacts applied to the S-wave aluminum plank. This orientation was checked following the procedure discussed in Appendix A.5 and the miss-alignment was never more than 3 degrees. The H1 horizontal geophone, which was oriented perpendicular to the direction of the horizontal impacts applied to the S-wave plank and thus minimized the recorded amplitude of the S_{vh}-waves, was used to record P waves. For measurements near the surface, the axial direction of the H1 geophone maximized the recorded amplitude of the P_v-waves that were generated by the P-wave source. These P waves that were generated by vertical impacts also were recorded by a vertical geophone in the 3-D receiver, which maximized the recorded amplitude of the P_v-waves at deeper depths. The 3-D receiver in the seismic cone was used to monitor motions of the body waves that traveled from the impulsive sources and propagated past the 3-D receiver as illustrated in Figure 5.1.

5.3 SCPT TESTING AT HORNSBY BEND

The SCPT testing in this portion of the research was also performed at the Hornsby Bend site described in Appendix A. The site is located on a historical farm about 10 miles from the University. The area of Hornsby Bend where these tests were performed differs from the testing presented in Appendix A. In this case, the SCPT tests

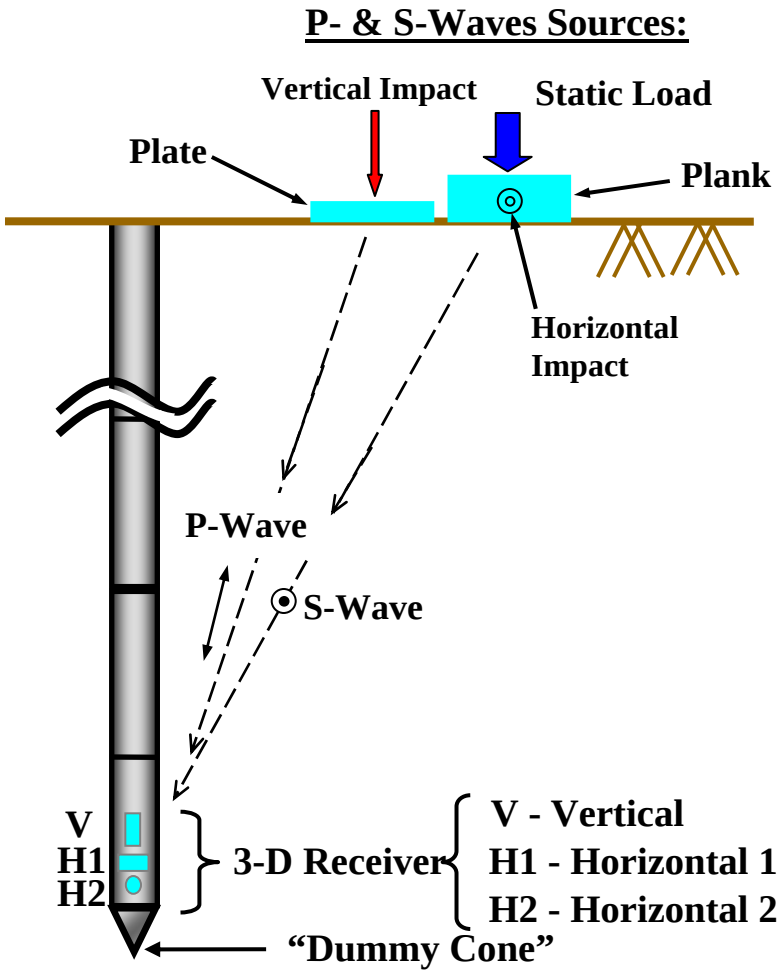

Figure 5.1: Setup for SCPT Testing Performed in This Research Using a 3-D Receiver and Measuring P and S waves.

were performed in an area called Platt 4 as shown in Figure 5.2. Ten Cone Penetration Tests (CPT) were performed around Platt 4 to characterize the subsurface profile before any seismic cone testing was conducted. The CPT testing took about 3 days. Cone resistance and friction ratio were used with the classification chart published by Robertson et al. (1986b) to interpret the geotechnical profile. All results of the CPT tests are described and grouped into areas with the similar geotechnical profiles in Appendix B. In this chapter, the results at one location where the SCPT tests were performed are

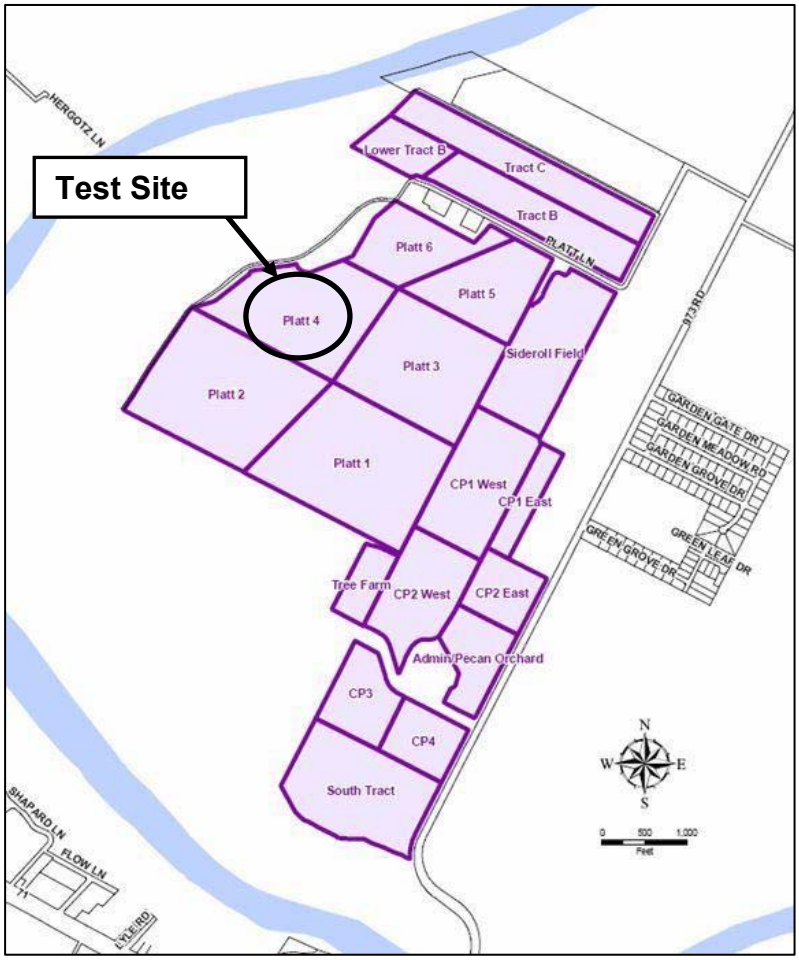

Figure 5.2: Platt 4 at Hornsby Bend

plotted in Figure 5.3. The interpreted soil profile from the ground surface to a depth of 42.4 ft consists of six layers. The thickest layers are a silty sand layer in the depth range of about 3.0 to 14.5 ft and a clay layer in the depth range of about 14.5 to 26.0 ft. These two layers and the rest of the soil profile are used in this chapter to study the P- and S-wave velocity measurements. In addition, this site is used to demonstrate the SABW method and some of the additional resolving capabilities that clearly differentiate the layers in Chapter 6.

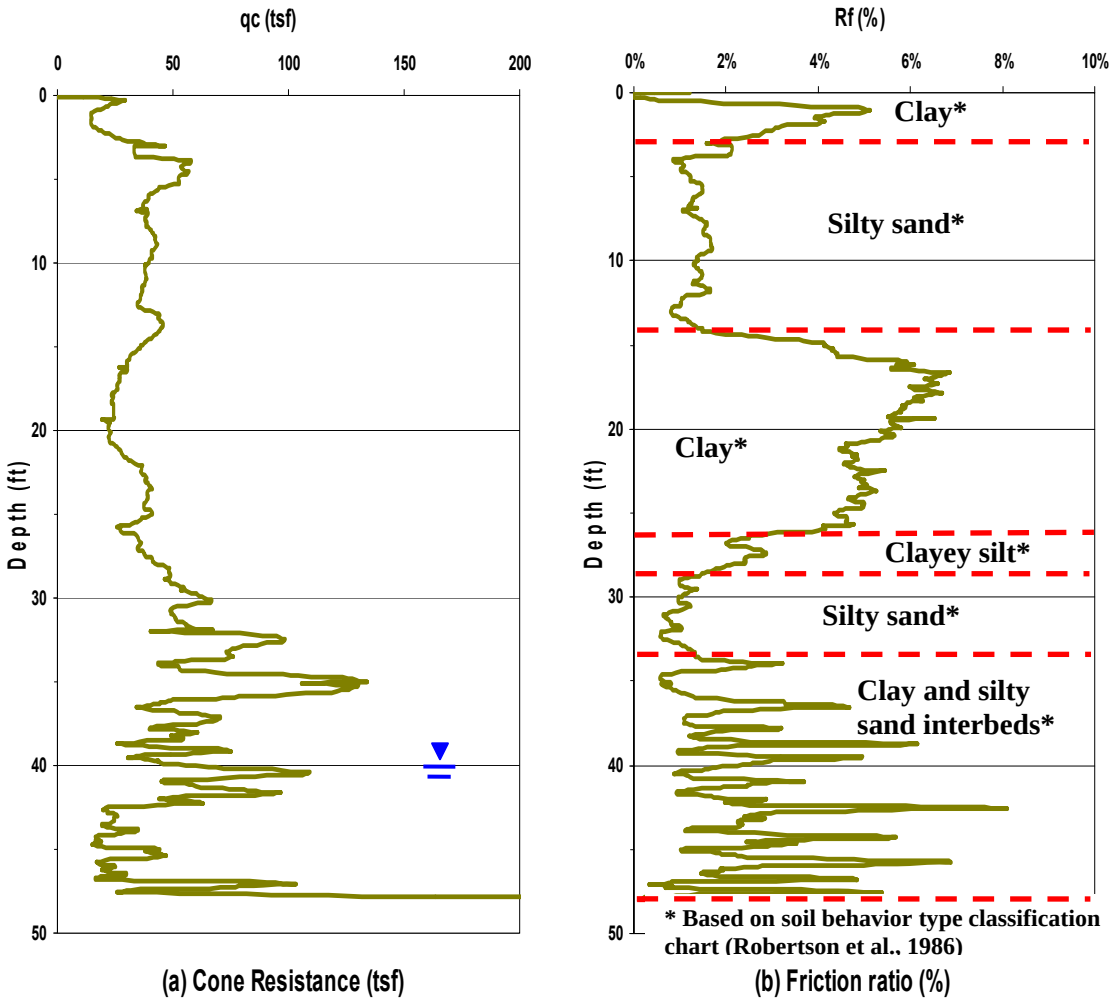

Figure 5.3: Typical CPT Profile at Platt 4 of the Hornsby Bend Site

5.4 V_S Measurements Using Time-Domain Methods from Seismic Cone Testing

Seismic cone testing was initially performed using conventional data collection and analysis procedures at Platt 4. The field setup is shown in Figure 5.1. All data were collected in the time domain. The output from an electrical trigger was recorded on Channel 1 of the waveform recorder. The electrical trigger signal was used to mark a

"zero time" which represented the instant when the aluminum S-wave plank or the steel P-wave plate were struck by the sledge hammer and shear or compression waves were generated at the ground surface, respectively. A trigger delay time of 0.0305 ms was determined by calibrating the hammer-plank-electrical trigger-recorder system. This trigger delay was used in analyzing the travel-time waveforms obtained from seismic cone tests by adding the delay time to each first-arrival time.

5.4.1 V_S measurements based on first arrivals

A waterfall plot of the shear waveforms that were monitored at 3.3-ft (1-m) depth intervals is presented in Figure 5.4. The electrical trigger is plotted at a depth of zero feet in the figure. The trigger time was recorded at each measurement depth and is marked as zero time. One set of average S_{vh} waveforms generated at each depth for forward and reverse impacts to the S-wave plank are shown. The S_{vh} waves were monitored with the transverse horizontal geophone (H-2) in the 3-D receiver. Each average S_{vh} waveform was generated by striking the S-wave plank five times. The measurements were performed over the depth range of 3.0 to 42.4 ft (0.93 to 12.93 m).

The first-arrival times of S_{vh}-waves were carefully picked at each depth. The first-arrival picks are denoted by the triangles in Figure 5.4. These travel times represent travel times along inclined paths. Using the direct travel-time method introduced in Appendix A, all travel times were corrected to the travel time in the vertical path. The corrected travel times were then best-fit with straight-line segments by changing the slopes of the lines to approach a value of R^2 close to 1 for each segment. For this data set, three straight lines were used as shown in Figure 5.5. As seen, the first straight line actually was fit using "judgment" because the layer was so thin that two measurements points were not located in this layer. The straight lines represent three S_{vh} velocity layers, with

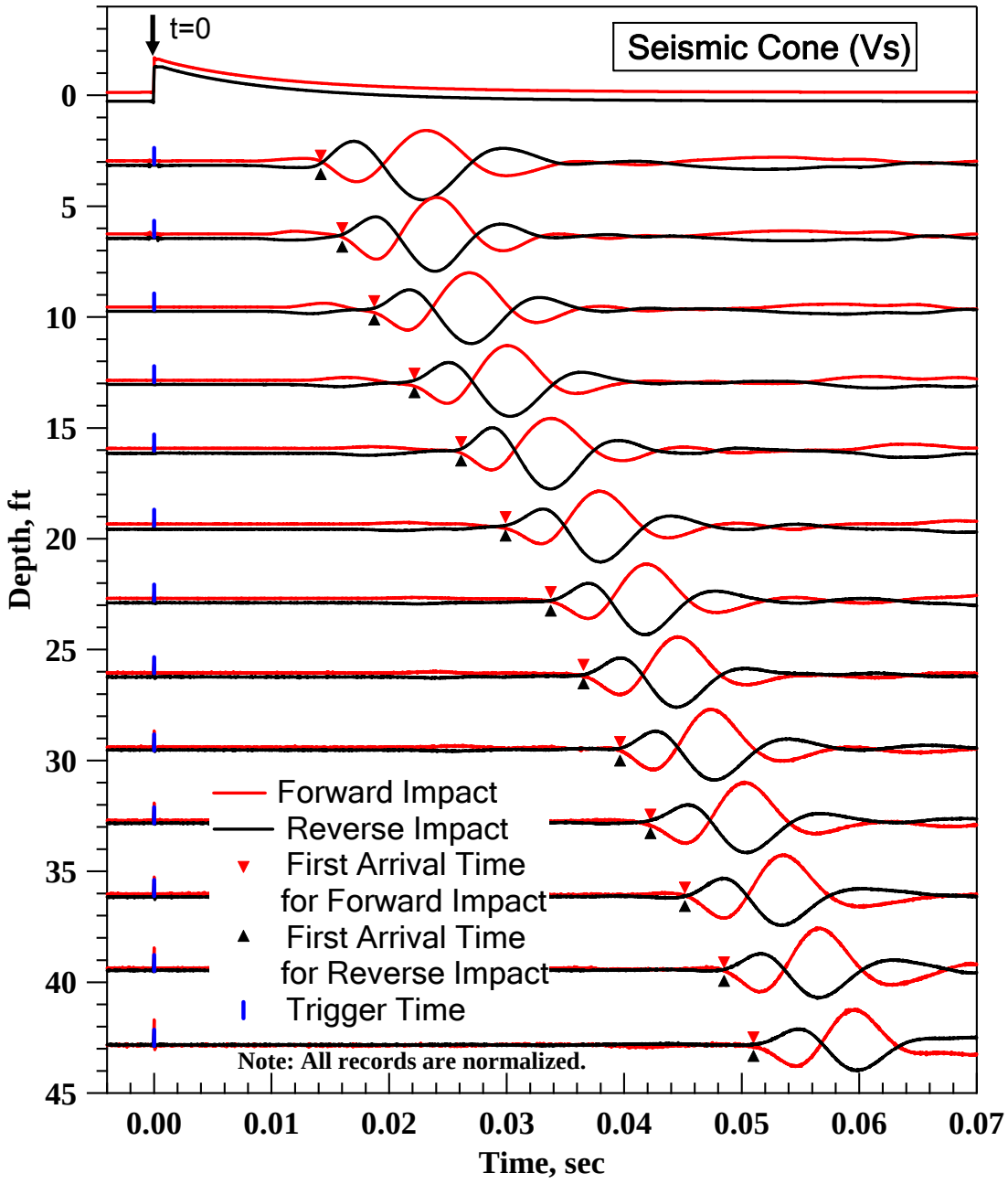

Figure 5.4: Waterfall Plot of Polarized S-Wave Signals Recorded by a Horizontal (H2) geophone in the 3-D Receiver of the Seismic Cone Obtained 15 ft away from the CPT Profile Shown in Figure 5.3

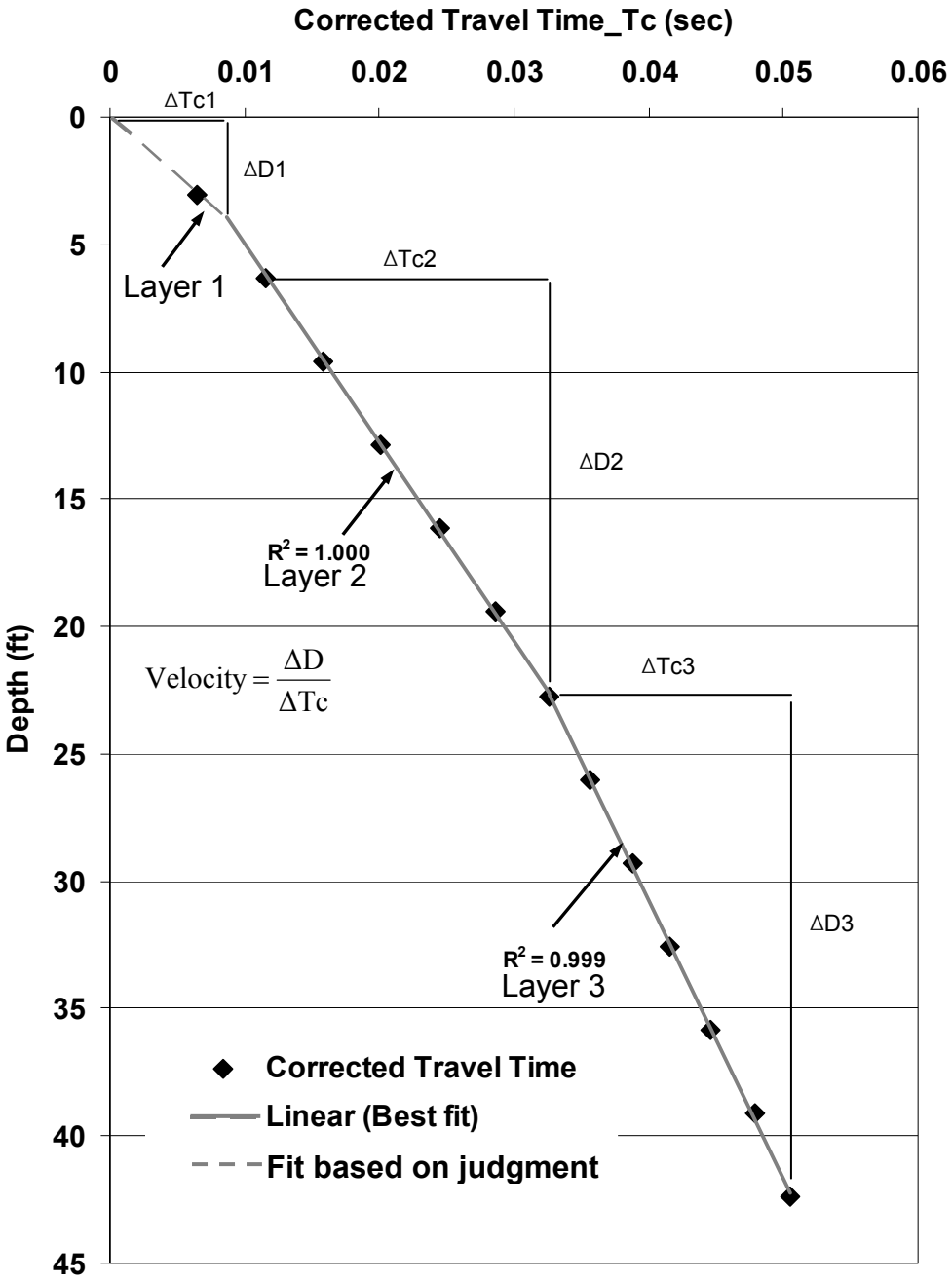

Figure 5.5: S-Wave Travel Time Corrected to the S-wave Travel Time in the Vertical Path versus Depth Obtained 15 ft away from the CPT Profile Shown in Figure 5.3

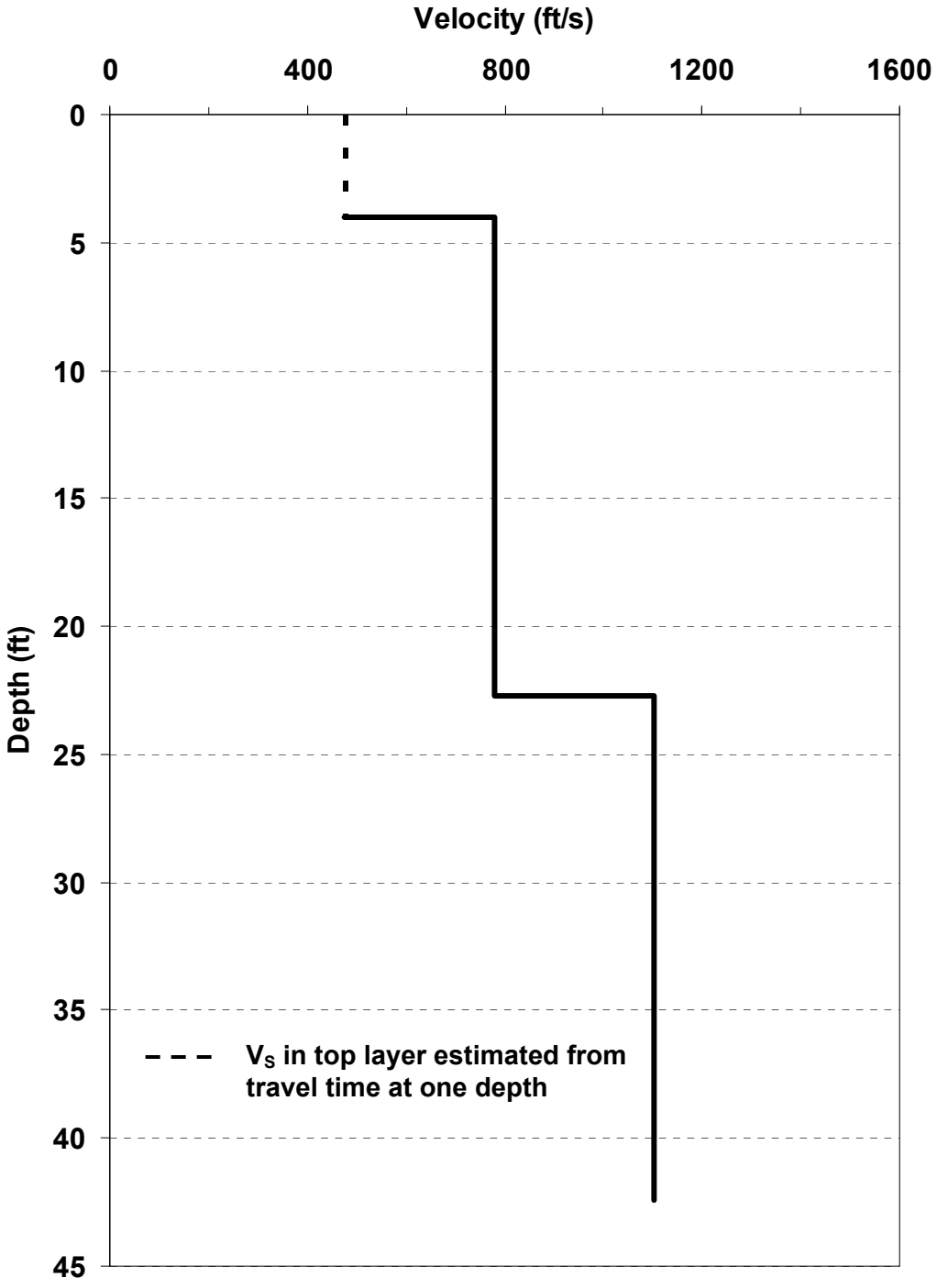

Figure 5.6: V_S Profile Calculated from the Slopes of the Three Best-Fit Lines Shown in Figure 5.5

each layer having a uniform velocity. The resulting S_{vh} velocities are: (1) Layer 1, V_S = 474 ft/s, (2) Layer 2, V_S = 781 ft/s, and (3) Layer 3, V_S = 1102 ft/s. The resulting S_{vh}-velocity profile is presented in Figure 5.6.

5.4.2 Advanced time-domain V_S measurements based on interval travel times and various time-domain reference points

As discussed in Appendix A, picking first-arrivals is a critical task in time-domain analysis because picks control the final shear wave velocities. However, picking these points in time records is not always easy because of low signal-to-noise ratios, especially in the case of shear waves which arrive later in the time record. To avoid picking first arrivals, or to "confirm" the first-arrival picks, other reference points such as the first trough, first cross-over point or first peak can be considered to measure the incremental travel times. This procedure was studied in theses SCPT tests. The reference points are shown in Figure 5.7. Two signals generated by the S-wave plank struck in the forward direction are shown. The 3-D sensor was located at depths of 16.2 ft and 26.0 ft. The reference points are marked in Figure 5.7. Picking these reference points can be easily identified and automated because the S_{vh} waveforms recorded by the H2 geophone have a large signal-to-noise (S/N) ratio and are polarized. The large S/N ratio of the S_{vh} waveforms enables the operator to readily pick the first troughs and first peaks of the recorded signals. The polarized form of the S_{vh} waves also helps the operator to pick the first cross-over point in the recorded signals.

As shown above, four reference points were picked in the S_{vh} waveform recorded at each depth. The time interval determined with each reference point was used to calculate the incremental travel time. The incremental travel distance along inclined paths was also calculated (see Figure 2.6). With these two values, the interval S-wave velocity was calculated by:

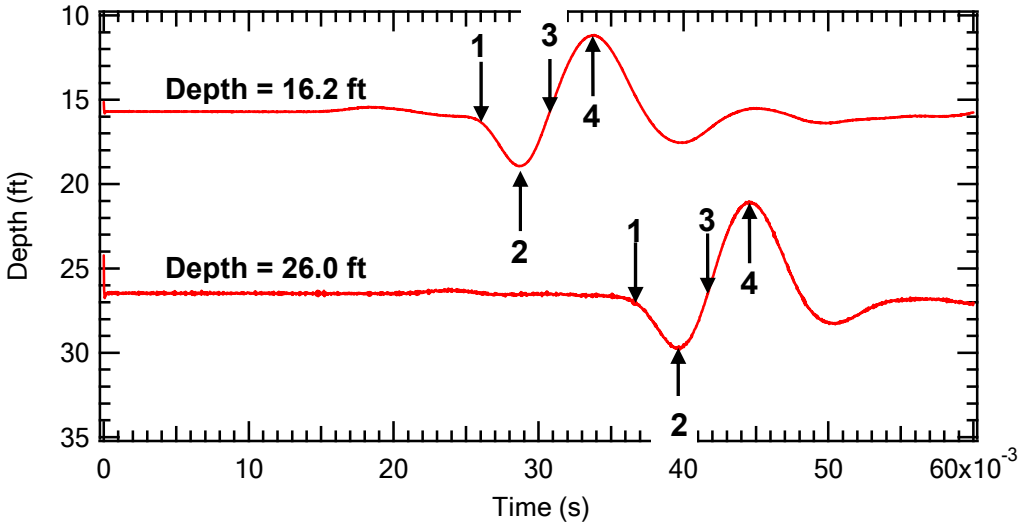

Figure 5.7: Reference Points Identified on Two Signals Generated with Impacts in the Forward-Direction (1: First Arrival; 2: First Trough; 3: First Cross-Over Point; and 4: First Peak)

$$\text{Interval Velocity} = \frac{R_2 - R_1}{T_2 - T_1} \tag{5.1}$$

where: R_1 = distance from the source to the upper receiver,

R_2 = distance from the source to the lower receiver,

T_1 = wave travel time between the source and the upper receiver, and

T_2 = wave travel time between the source and the lower receiver.

This method is called an interval measurement (Mok, 1987). The interval velocities of the S_{vh} waves were calculated with each reference point and the results are shown in Figure 5.8. The V_S profiles calculated by the interval measurement method with the four reference points are also compared to the V_S profile calculated by the slopes of three linear lines best fit.

As shown in Figure 5.8, the V_S profile of the first arrival is most scattered because of the human subjectivity for picking the reference point. The V_S profile of the first cross-

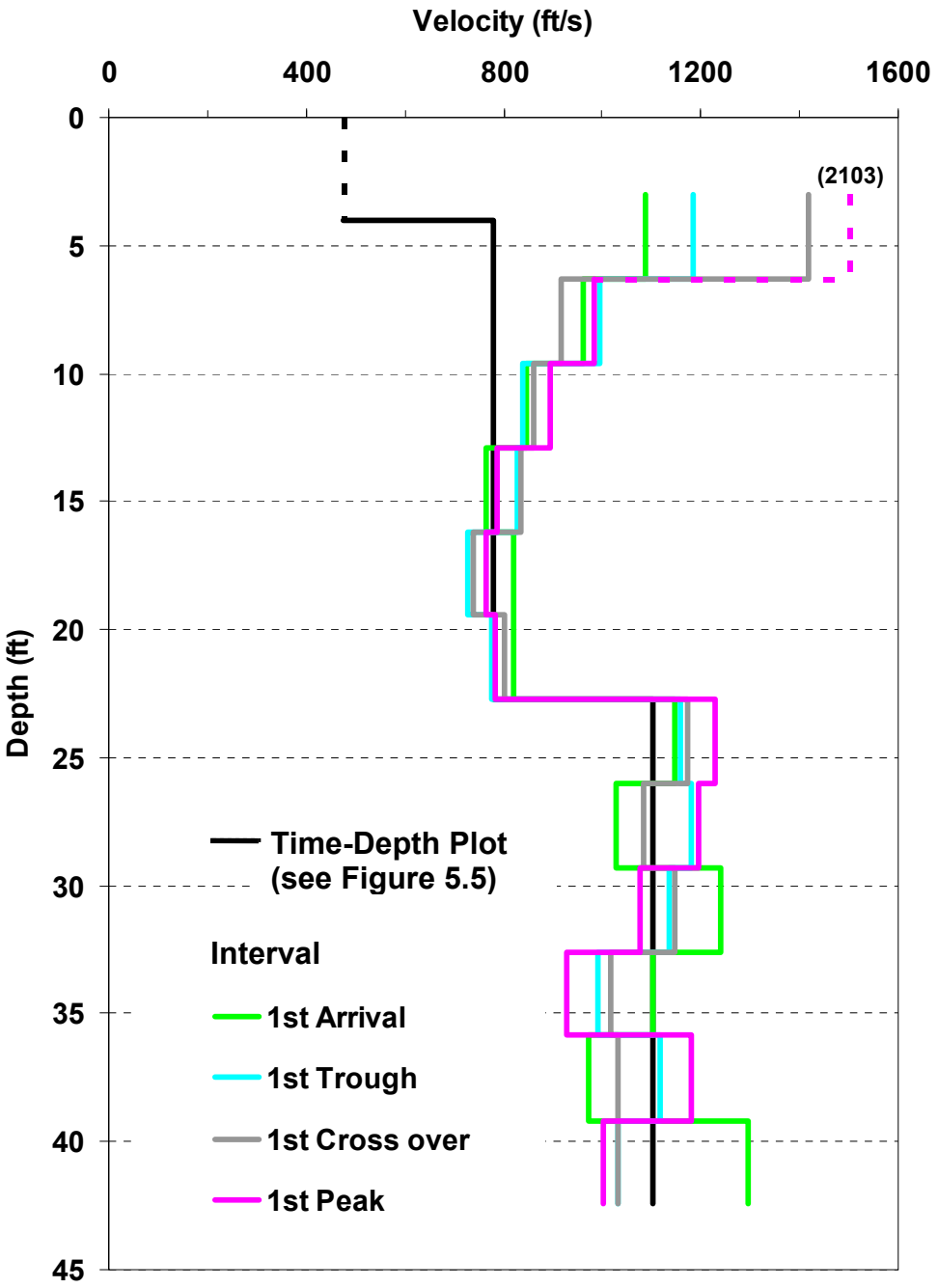

Figure 5.8: Comparison of the V_S Profiles Calculated with 4 Reference Points of Signals for Entire Depth and V_S Profile Calculated by the Time-Depth Plot Shown in Figure 5.6

over is less scatter than the V_S profiles of the first tough and first peak because while the V_S profiles of the first tough and first peak were calculated with the impact of the only forward direction, the V_S profile of the first cross-over was calculated with the averaged value of the forward and reverse impacts. The V_S profile of the averaged first arrivals is median as shown in Figure 5.8.

5.4.3 Advanced V_S measurements based on interval travel times and cross correlation

Cross correlation of two signals in the time domain has been used in geophysics because the method is an automation method and reference points on the waveforms do not have to be identified (Bendat and Piersol, 1986). Cross correlation uses the time shift of two similar waveforms that results in the maximum correspondence. This time shift is taken as the interval time of two S_{vh}-waves. The two S_{vh}-waveforms shown in Figure 5.7 were cross correlated and the resulting cross-correlation function is shown in Figure 5.9. The time shift between the two waves is the time at which the peak in function occurs; hence 10.835 ms. The resulting V_S is 872 ft/s for the clay layer in the depth range of 16 to 26 ft (see Figure 5.3).

As shown in Figure 5.10, the V_S profile that is calculated by cross correlation is similar to the V_S profile of the averaged first arrival. The V_S profile of cross correlation is less scatter than other V_S profiles using reference points because while other V_S profiles rely on only one reference point to calculate the time interval of two signals, the V_S profile calculated by cross correlation uses all data of the signals to calculate the time interval of two similar signals. The V_S profile calculated by averaging the interval velocities of 4 reference points is very similar to the V_S profile calculated with the cross-correlation method in Figure 5.11.

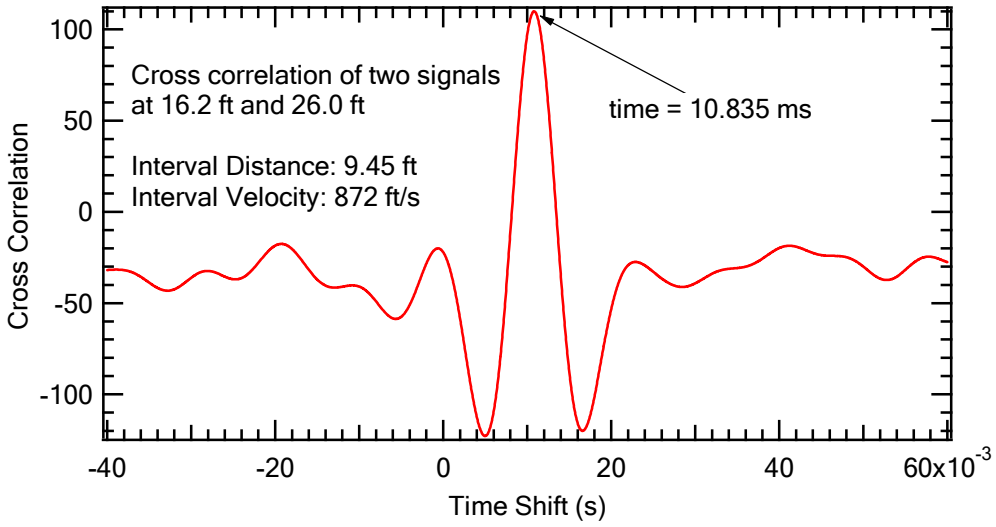

Figure 5.9: Cross Correlation of the Two, S_{vh} Signals Shown in Figure 5.7

5.5 V_P MEASUREMENTS USING TIME-DOMAIN METHOD FROM SEISMIC CONE TESTING

5.5.1 V_P measurements based on first arrivals

In seismic testing with a 3-D receiver, P-wave measurements can also be performed. Two waterfall plots of compression waveforms that were monitored at 3.3-ft (1-m) depth intervals are presented in Figures 5.12 and 5.13. The waterfall plots in these figures are the waveforms that were recorded by the vertical geophone and the horizontal H-1 geophone, respectively. Both figures show the electrical trigger at a depth of zero feet to mark zero time. An average P_v waveform was generated at each depth by striking the P-wave plate in the vertical direction with a sledge hammer. As noted earlier, P_v waves can be monitored with the vertical (V) and horizontal (H1) geophones in the 3-D receiver in the seismic cone depending on the depth. The measurements were performed with a depth increment of 3.3 ft (1 m) over the depth range of 3.0 to 42.4 ft (0.93 to 12.93 m).

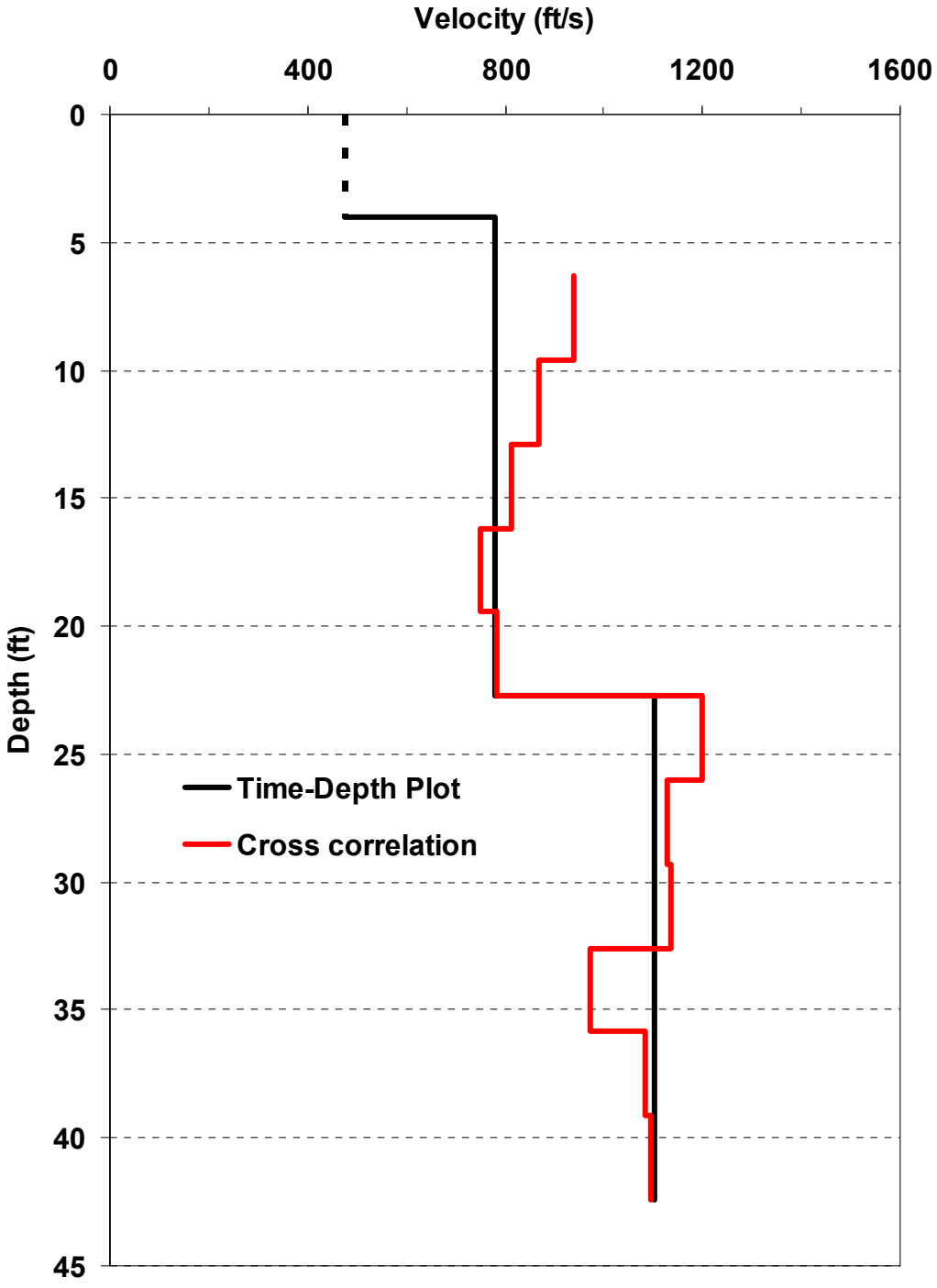

Figure 5.10: Comparison of the V_S Profile Calculated by the Time vs. Depth Plot and V_S Profile Calculated by Cross Correlation of Signals

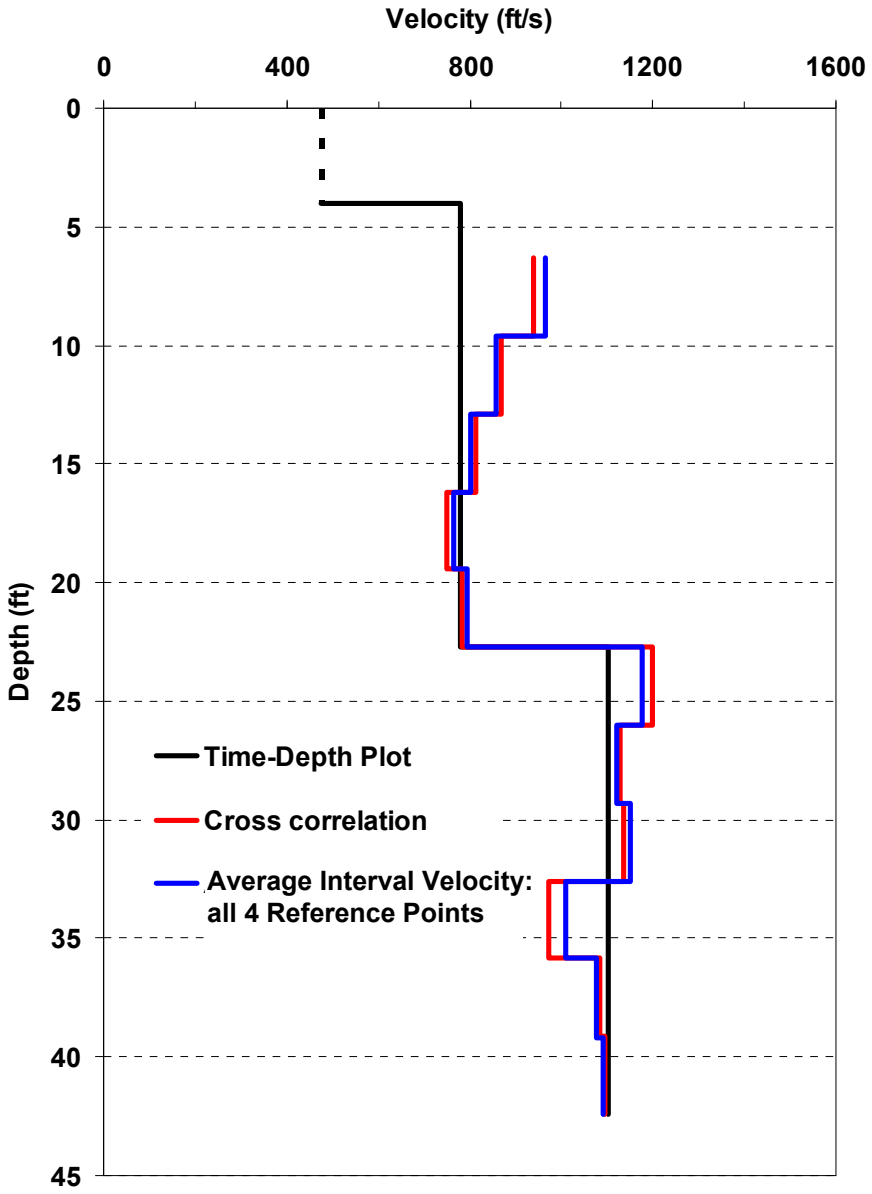

Figure 5.11: Comparison of the V_S Profiles Calculated with (1) the Time vs. Depth Plot, (2) Cross Correlation of Signals and (3) the Average Interval Velocity of all 4 Reference Points

The first-arrival times of P_v-waves were carefully picked at each depth. The first-arrival picks are denoted by the circular dots shown in Figures 5.12 and 5.13. By using the waterfall plots recorded by both the vertical geophone and the horizontal H1 (radial) geophone, it is easier to find a consistent P_v wave arrival in the soil and compensate for the disadvantage of each geophone. The waterfall plot of the vertical geophone shows high signal-to-noise ratios in the depth range of about 6 to 26 ft while the waterfall plot of the horizontal H1 geophone shows high signal-to-noise ratios in the depth range of about 3 to 23 ft and then rather low signals below this depth which required significant amplification, resulting in lower signal-to-noise ratios. However, the waterfall plot of the horizontal H1 geophone, unlike the vertical geophone, does not show early-arriving waveforms before the arrival of compression waves. These early arrivals result from P waves in the water. By using both waterfall plots, the possibility of picking the correct times of first-arrival P waves in soil can be maximized. In Figures 5.12 and 5.13, the arrival times in both records are the same.

Picking the first-arrival times of P_v-waves, which were recorded by the vertical geophone, was not easy for depths ranging from 32.6 ft to 42.4 ft. The layer ranging from 32.6 ft to 42.4 ft consists of clay and silty sand interbeds as shown in Figure 5.3. The initial portions of the waveforms recorded by the vertical geophone at depths 39.1 ft and 42.4 ft are expanded in the vertical and horizontal directions in Figure 5.14. The interval travel times of the first arrivals, first peaks and second peaks average around 0.67 ms for the incremental travel distance of 3.25 ft. The calculated V_P is about 4800 ft/s and close to the V_P in water or saturated soil. The waveforms recorded by the vertical geophone highlighted the saturated zone around the depth of the water table.

The direct travel-time method that was introduced to analyze the S_{vh}-waves was also used to analyze the P_v data. The analysis procedure for the V_P profiles is same as the

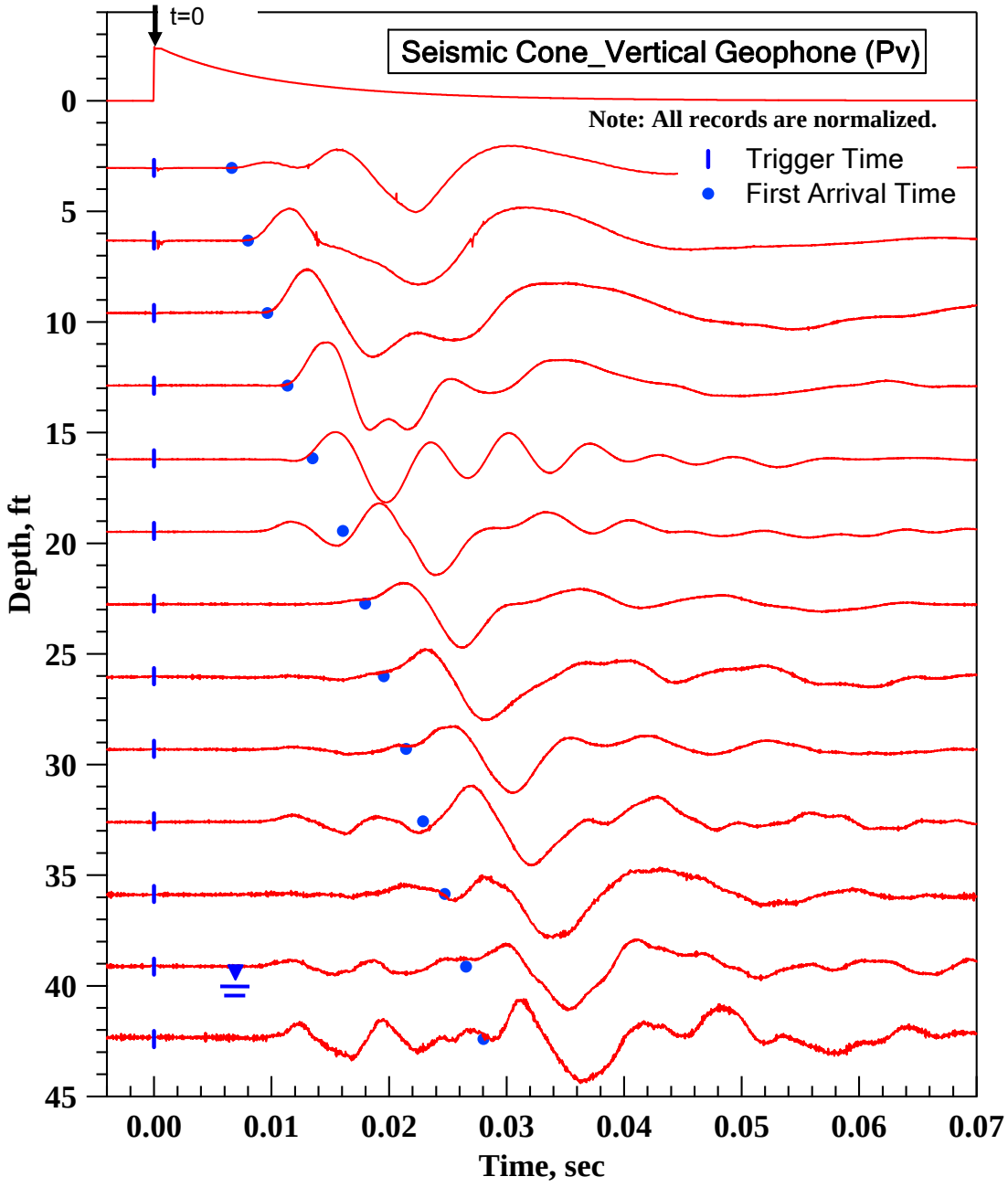

Figure 5.12: Waterfall Plot of Signals Recorded by the Vertical (V) Geophone in the 3-D Receiver of the Seismic Cone Obtained 15 ft away from the CPT Profile Shown in Figure 5.3

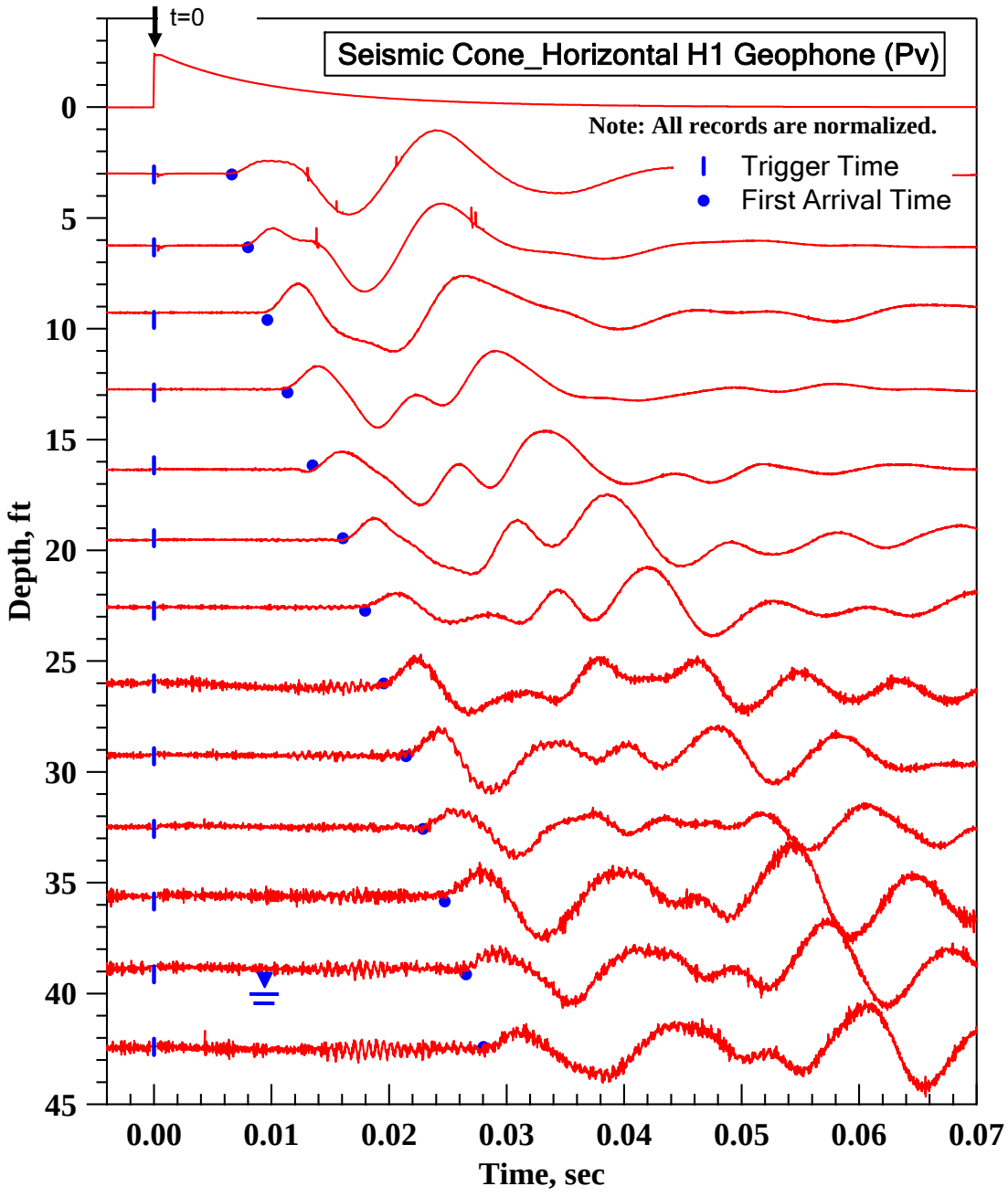

Figure 5.13: Waterfall Plot of Signals Recorded by the Horizontal (H1) Geophone in the 3-D Receiver of the Seismic Cone Obtained 15 ft away from the CPT Profile Shown in Figure 5.3

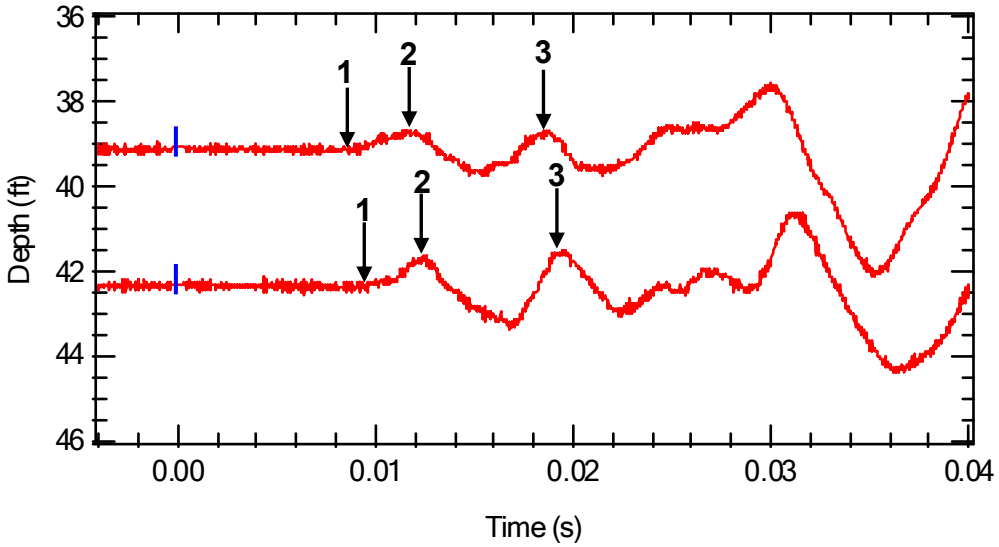

Figure 5.14: The First Arrivals, First Peaks and Second Peaks of Two Waveforms Recorded by the Vertical Geophone at Depths of 39.1 ft and 42.4 ft (1: First Arrival, 2: First Peak, and 3: Second Peak)

analysis procedure for the V_S profiles which was described above. Three layers that were determined for the V_P profile are the same layers as the three layers of V_S profile as shown in Figure 5.15. The R^2 of two straight lines is close to 1. The resulting P_v velocities are: (1) Layer 1, V_P = 884 ft/s, (2) Layer 2, V_P = 1454 ft/s, and (3) Layer 3, V_P = 1912 ft/s. The V_P profile that consists of three layers is shown in Figure 5.16.

Poisson's ratios of the three layers can be calculated using the relationship between V_S and V_P by:

$$\nu = \frac{V_P^2 - 2 \cdot V_S^2}{2 \cdot (V_P^2 - V_S^2)} \tag{5.2}$$

where: ν is Poisson's ratio, and

V_s and V_p are shear and compression wave velocities, respectively.

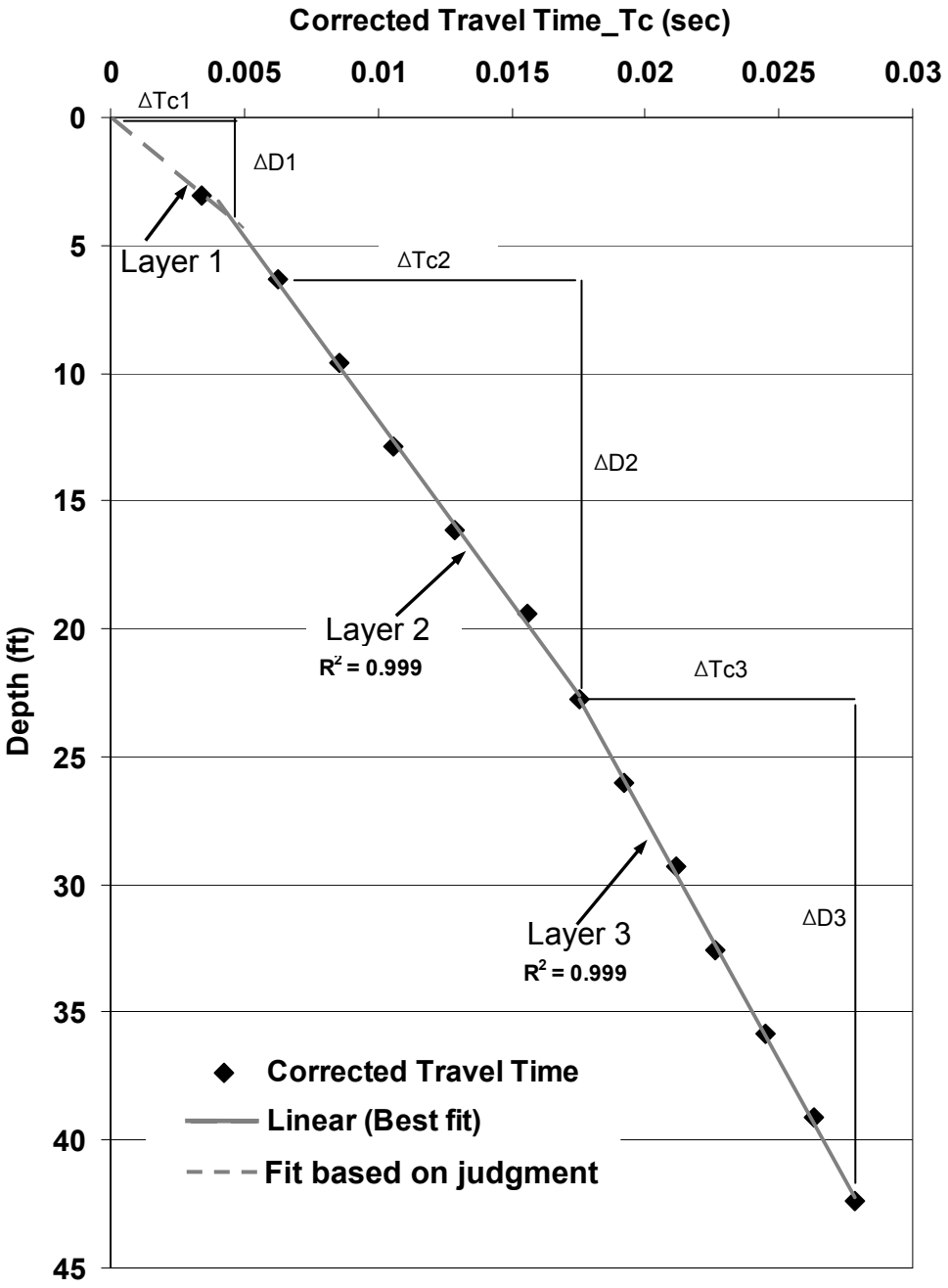

Figure 5.15: P-wave Travel Time Corrected to the P-wave Travel Time in the Vertical Path versus Depth Calculated from First Arrivals Show on the Waterfall Plot in Figure 5.13

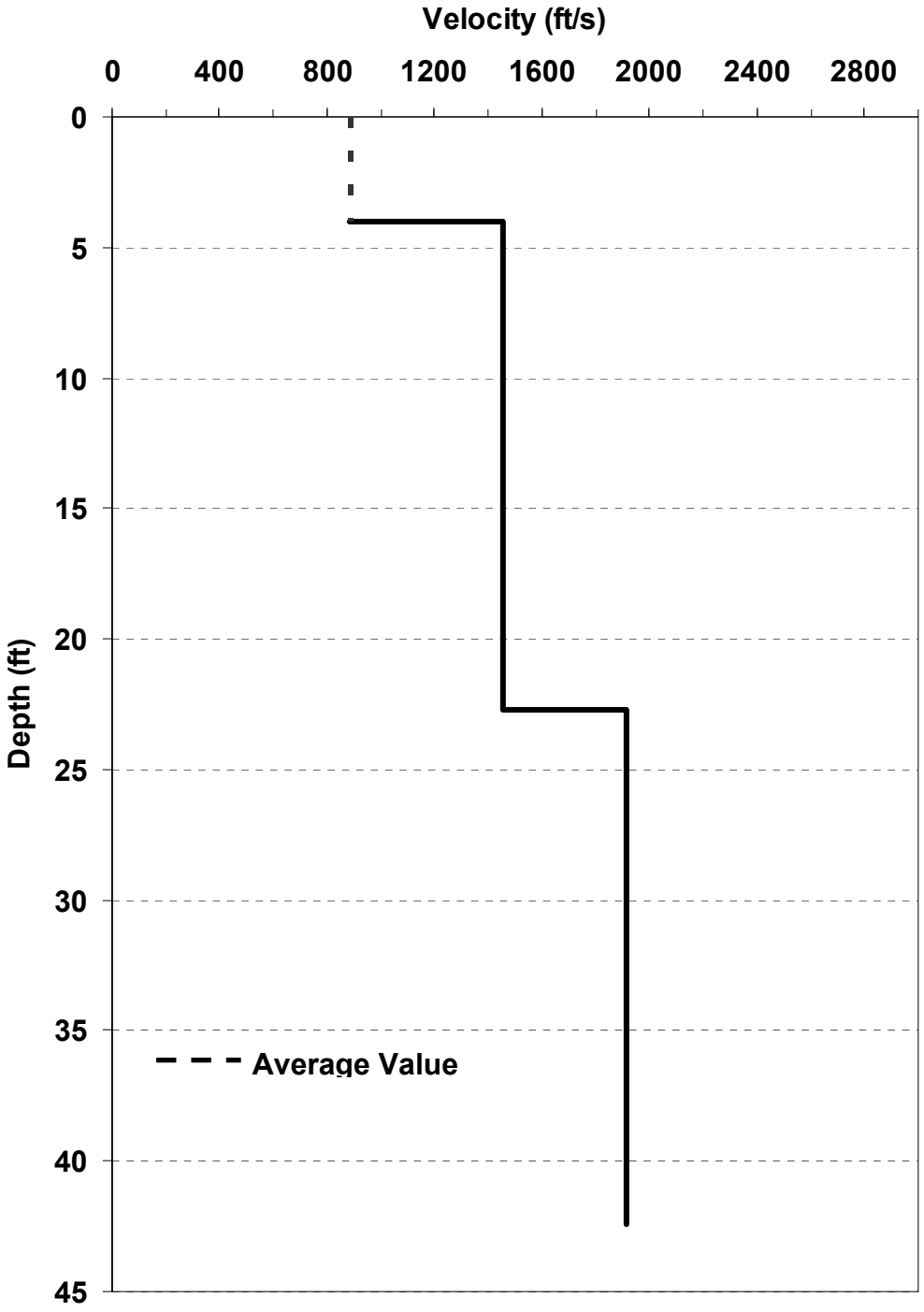

Figure 5.16: V_P Profile Calculated from the Slopes of the Three Best-Fit Lines Shown in Figure 5.15

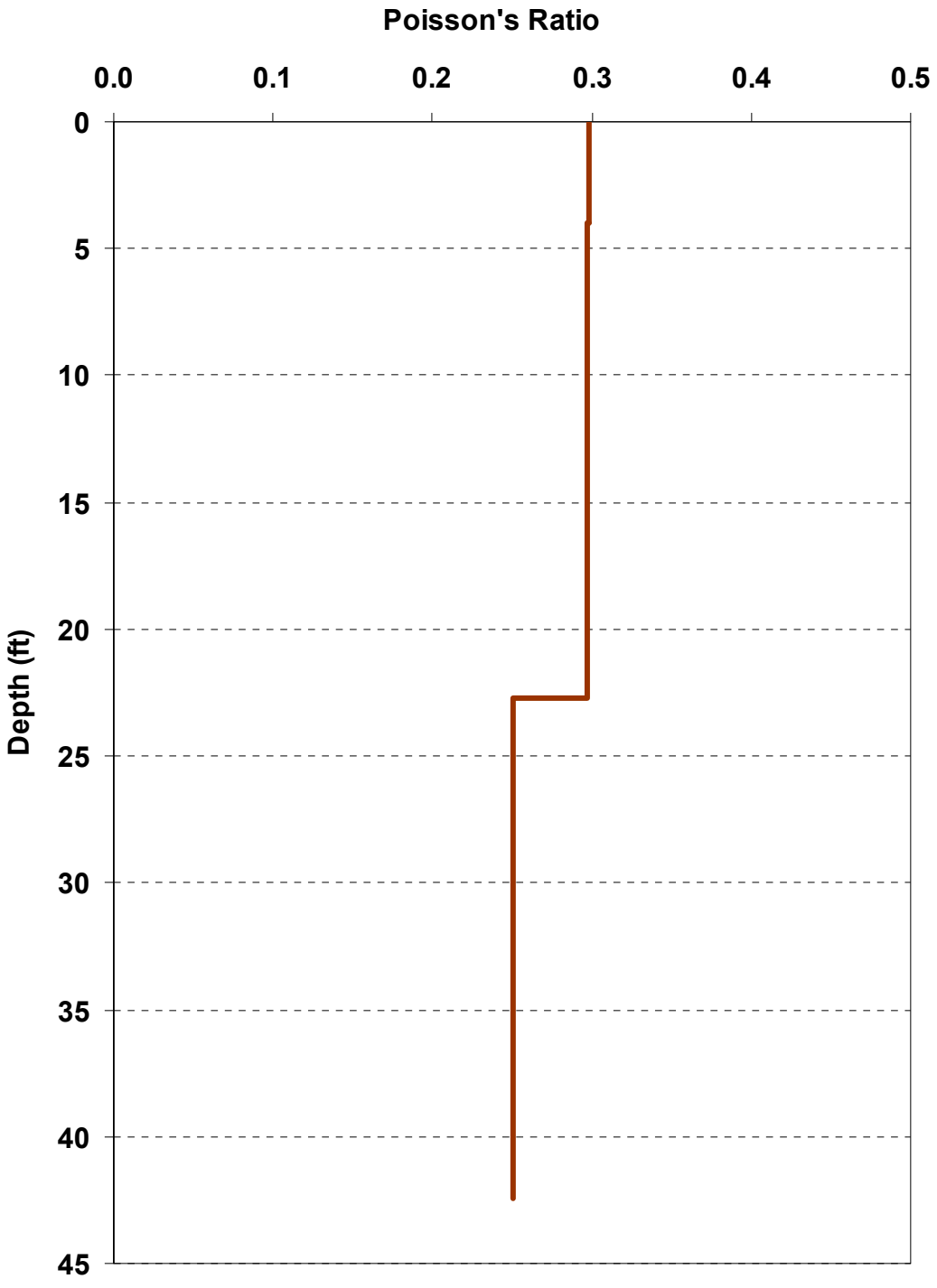

Figure 5.17: The Profile of Possion's Ratios Calculated from the Relationship between V_S and V_P Values Shown in the Profiles Shown in Figures 5.6 and 5.16

The resulting Poisson's ratios are: (1) Layer 1, ν = 0.30, (2) Layer 2, ν = 0.30, and (3) Layer 3, ν = 0.25. These Poisson's ratios are typical values for soil. The profile of the Poisson's ratios is plotted as shown in Figure 5.16.

5.5.2 Advanced V_P measurements based on interval travel times and various time-domain reference points

Unlike S_{vh} waves, P_v waves generated by the P-wave source cannot be polarized to help clarify the reference points in the waveforms. The P waveforms can easily be distorted by the only slightly later arriving S-waves that also may have greater amplitudes. As a result, the first peak and trough may be distorted by the slower S-waves with greater amplitude at the depth ranging from the ground surface to about 10 ft. The distortion is most serious at shallow depths because waves have not travelled far enough to separate. The P- and S-waves were clearly separated below the depth of about 10 ft in Figures 5.18 and 5.19. Picking the first arrivals of P-waves recorded by the vertical and horizontal geophones can help to minimize any mistake that would be caused by distortions in the waveforms.

5.5.3 Advanced V_P measurements based on interval travel times and cross correlation

The waveforms generated by the P-wave source were recorded by the vertical and horizontal H-1 geophones and were correlated within each set of waveforms to calculate the time shift between waves. The waveforms shown in Figures 5.12 and 5.13 were correlated and the P-wave velocities were calculated using the interval measurement method. The excessively low and high velocities shown in Figures 5.20 and 5.21 prove that the V_P profiles obtained by cross-correlating full waveforms are not reasonable. These unreasonable velocities occur because the larger, slower S-waves that are included

in the waveforms distort the records. The V_P profile that is calculated by cross correlation is not similar to the V_P profile of the time vs. depth plot.

To minimize the distortion of the waveforms, the signals recorded by two geophones are windowed with a rectangular window with a time of 0.01 seconds as shown in Figures 5.18 and 5.19 by the vertical dashed lines. In this case, the windowed waveforms below a depth of about 12 ft include no waveform associated with the far-field shear wave. The windowed waveforms were correlated and the P-wave velocities were calculated using the interval measurement method. The V_P profiles obtained by the windowed waveforms exhibit less scatter than the V_P profiles obtained by cross-correlating the full waveforms as shown in Figures 5.20 and 5.21. Interestingly, the interval velocities calculated using first arrivals and cross correlation of signals are better (more reasonable) when using the horizontal H-1 geophone than the vertical geophone as seen in Figure 5.21.

5.6 SUMMARY

SCPT testing which consists of CPT testing and seismic cone tests with a 3-D receiver was performed at Platt 4 of Hornsby Bend in Austin. The ground profile was characterized with the cone resistance and friction ratio. The S- and P-wave velocities were determined by testing and analysis procedures used in SCPT testing. S_{vh} waves generated by an S-wave source were recorded by a horizontal H-2 geophone in the 3-D receiver. Two sets of polarized waveforms were generated by impacting the S-wave plank in opposite directions. The polarized waveforms enabled the operator to easily pick the first arrival and other reference points in the S-wave signals. Cross correlation of signals generated with the S-wave source was a very useful method of calculating the

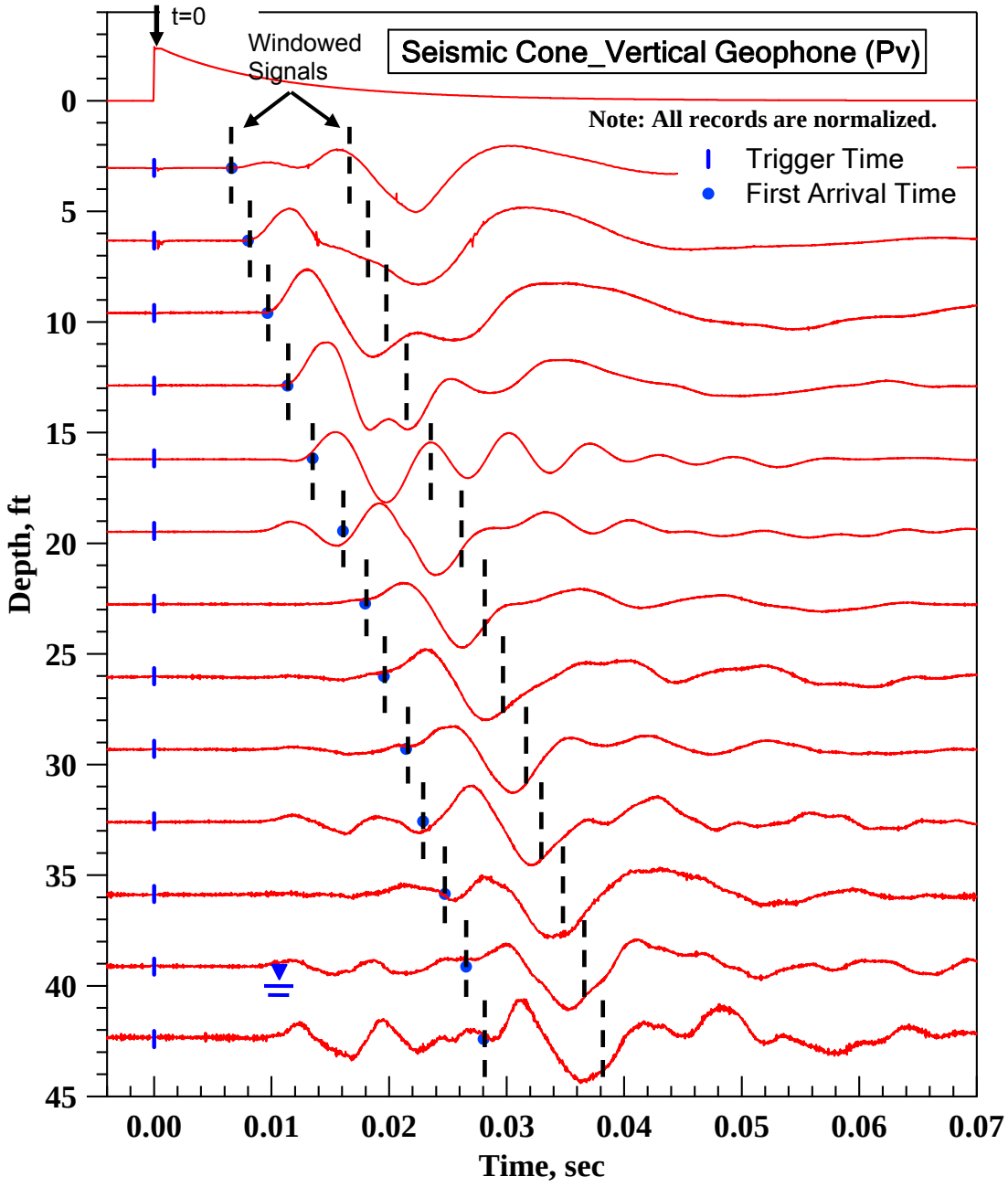

Figure 5.18: Waterfall Plot of Signals Recorded by the Vertical (V) Geophone in the 3-D Receiver of the Seismic Cone in Figure 5.12 and P Waves Windowed by a Rectangular Window with the Time Period of 0.01 Seconds

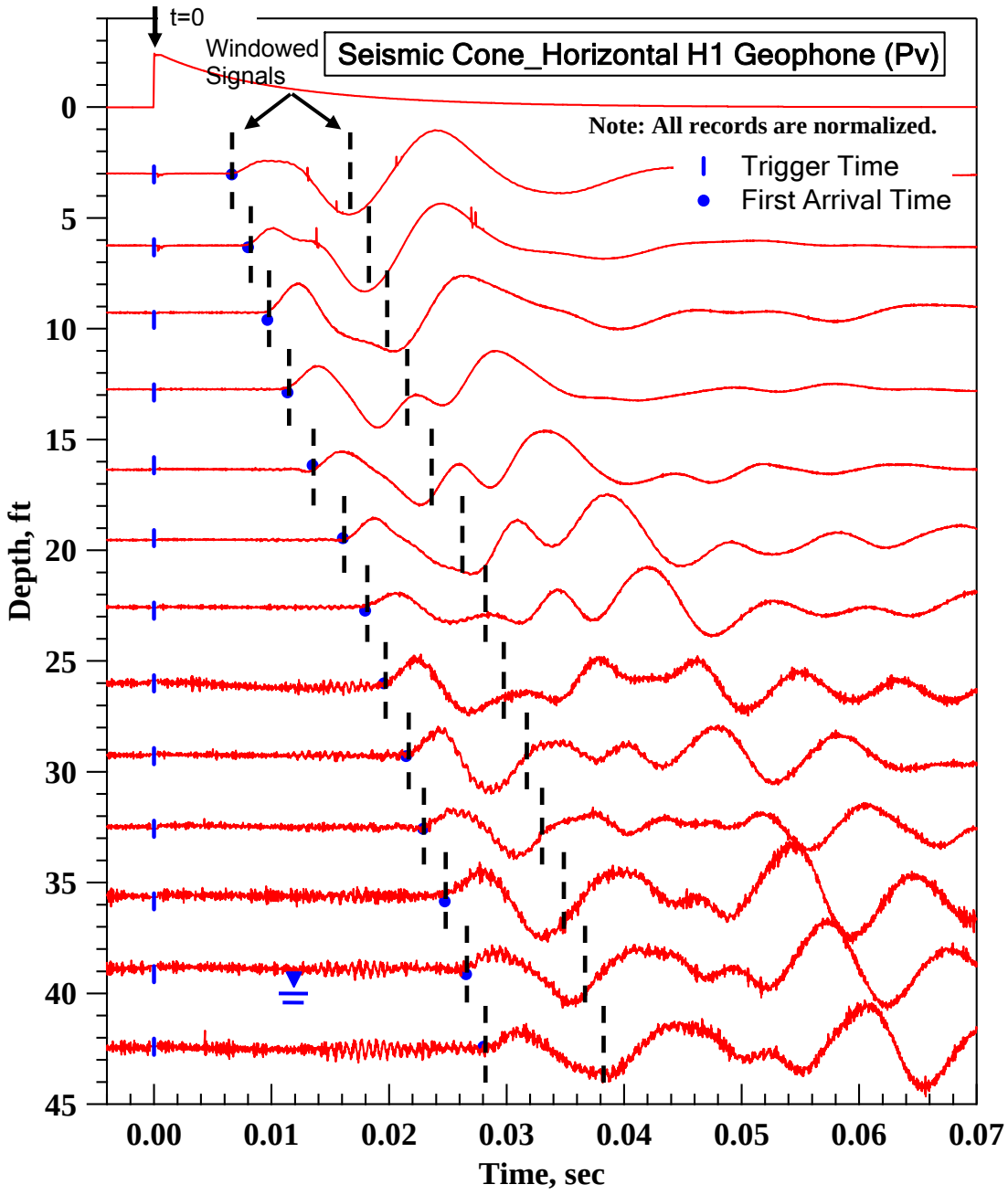

Figure 5.19: Waterfall Plot of Signals Recorded by the Horizontal (H1) Geophone in the 3-D Receiver of the Seismic Cone in Figure 5.13 and P Waves Windowed by a Rectangular Window with the Time Period of 0.01 Seconds

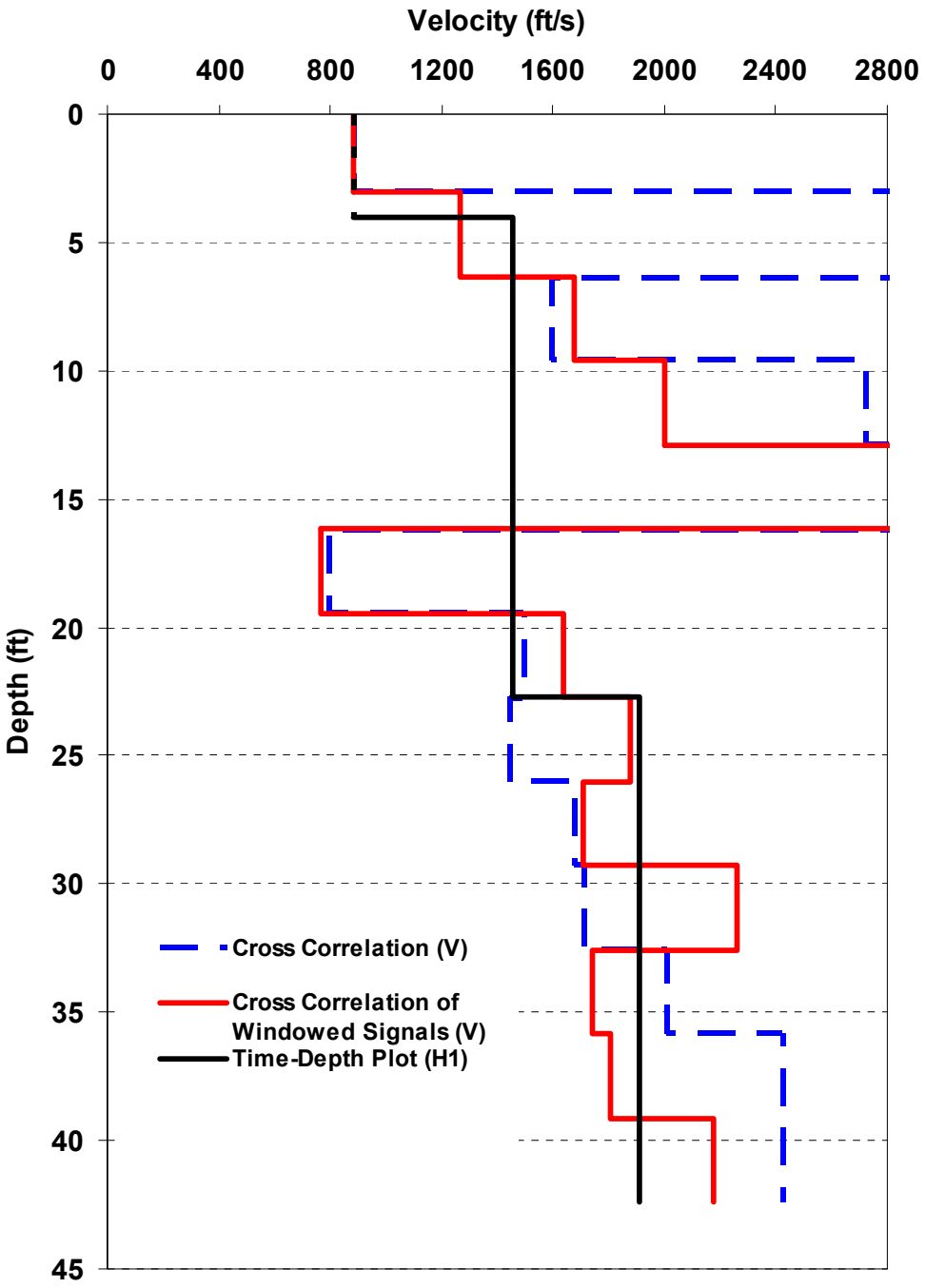

Figure 5.20: Comparison of the V_P Profiles Calculated by Cross Correlation of Signals and Windowed Signals Recorded to the Vertical (V) Geophone, and the V_P Profile Calculated by the Averaged 1st Arrivals

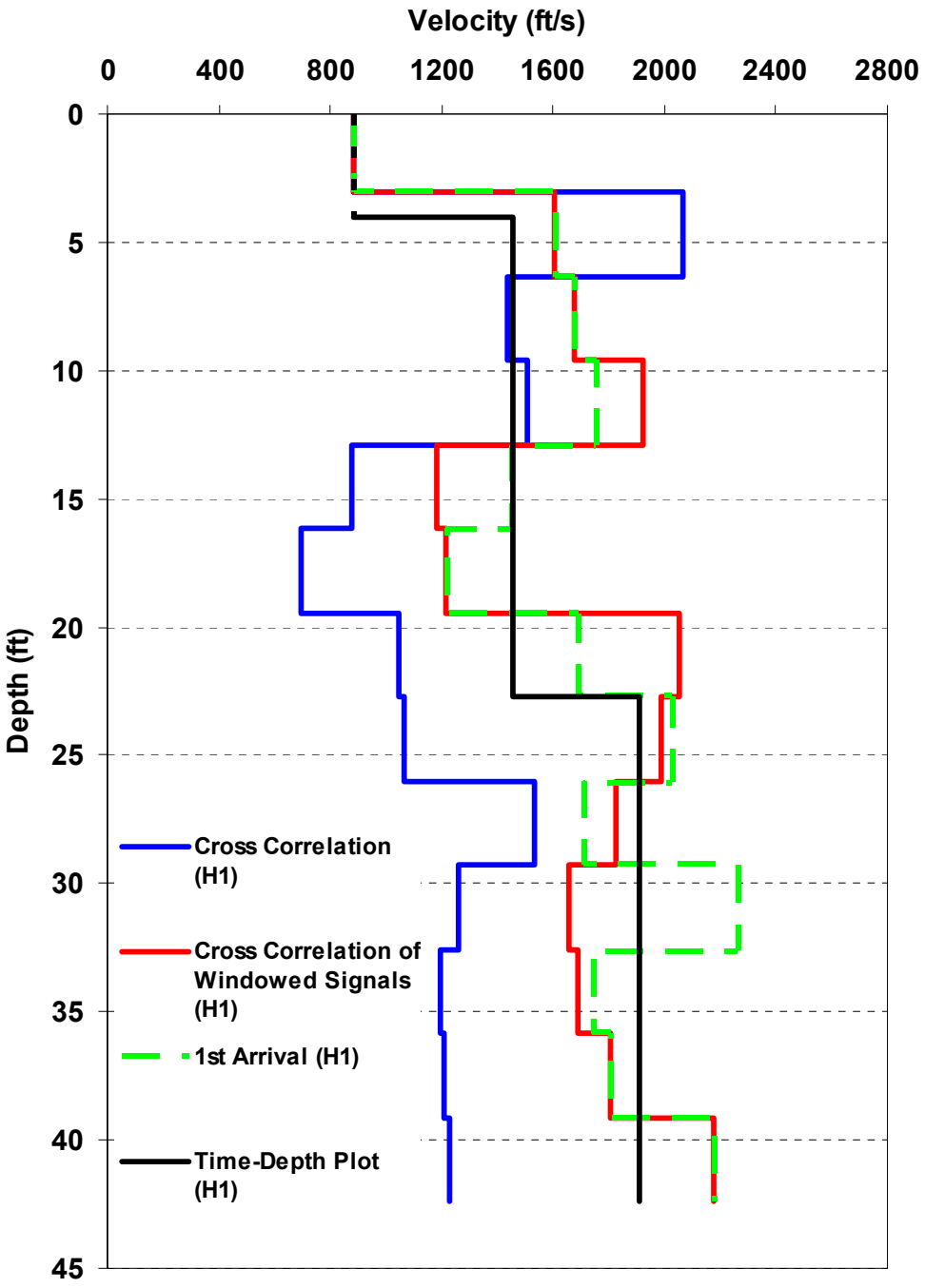

Figure 5.21: Comparison of the V_P Profiles Calculated by Cross Correlation of Signals and Windowed Signals Recorded to the Horizontal (H1) Geophone, the V_P Profile Calculated by the 1st Arrivals, and the V_P Profile Calculated by the Time-Depth Plot

interval travel times of the S waves. The V_S profile obtained by cross correlation of full waveforms exhibited less scatter than other V_S profiles obtained by the first arrival and other reference points. Cross correlation, unlike picking first arrivals or other reference points, utilizes all the waveform to calculate the time shift in the time domain because full-waveform cross correlation minimizes distortion in the waveform and operator biases. However, if V_S profiles are obtained with larger intervals, both cross correlation and reference points show more similar V_S profiles losing the resolution to find thin layers.

P_v waves generated by a vertical-impact source (P-wave source) were recorded by a vertical geophone and a horizontal H-1 geophone to maximize the likelihood of picking the correct first arrivals of P-waves. The waterfall plot obtained by the vertical geophone informed the existence of saturated soil by showing waves before the arrival of P-waves in soil. Picking other reference points was not easy because of the slow, larger S-waves after the first arrival of P waves. Waveforms windowed by a rectangular window of 0.01 seconds could be correlated and the V_P profiles obtained by cross correlation and the first arrival of signals are similar.

In next chapter, the SABW method is introduced and the V_S profile calculated with the SABW method is compared to the V_S profiles calculated in the time domain shown in this chapter. The calculation procedures for material damping measurements and the dispersive characteristic of S-wave velocities and material damping ratios are presented in Chapter 6.

Chapter 6: Development of the Spectral-Analysis-of-Body-Waves (SABW) Method

6.1 INTRODUCTION

In this chapter, the Spectral-Analysis-of-Body-Waves (SABW) method is introduced. The testing and analysis procedures of the SABW method are described using test data collected from a site at Hornsby Bend. The site is the same site that is presented in Chapter 5. The seismic data collected from this site was analyzed in the time domain. The S- and P-wave velocities at each depth were calculated with different analysis methods and the velocity profiles are those that are presented in Chapter 5. Two V_S profiles obtained by using time-depth plots based on first arrival times and on cross correlation of time-domain waveforms are compared with the V_S profile of the SABW method in this chapter.

The same CPT profiles shown in Chapter 5 are presented again in Figure 6.1 for reference purposes. The soil profile consists of 6 layers ranging from the ground surface to 42.4 ft. The thickest layers marked in blue dashed circles are a silty sand layer in the depth range of about 3.0 to 14.5 ft and a clay layer in the depth range of about 14.5 to 26.0 ft. The thickness of both layers is about 11.5 ft. The layers differ by soil types. These two layers are used in an example measurement to demonstrate the SABW method. Additional characteristics such as damping ratios and soil-type evaluations are obtained by the SABW method in these two layers.

6.2 TESTING SET-UP FOR SABW TESTING WITH IMPACT SOURCES

The set-up for seismic cone testing is shown in Figure 6.2 and consisted of shear (S) and compression (P) wave sources and a 3-D receiver in the dummy cone. The

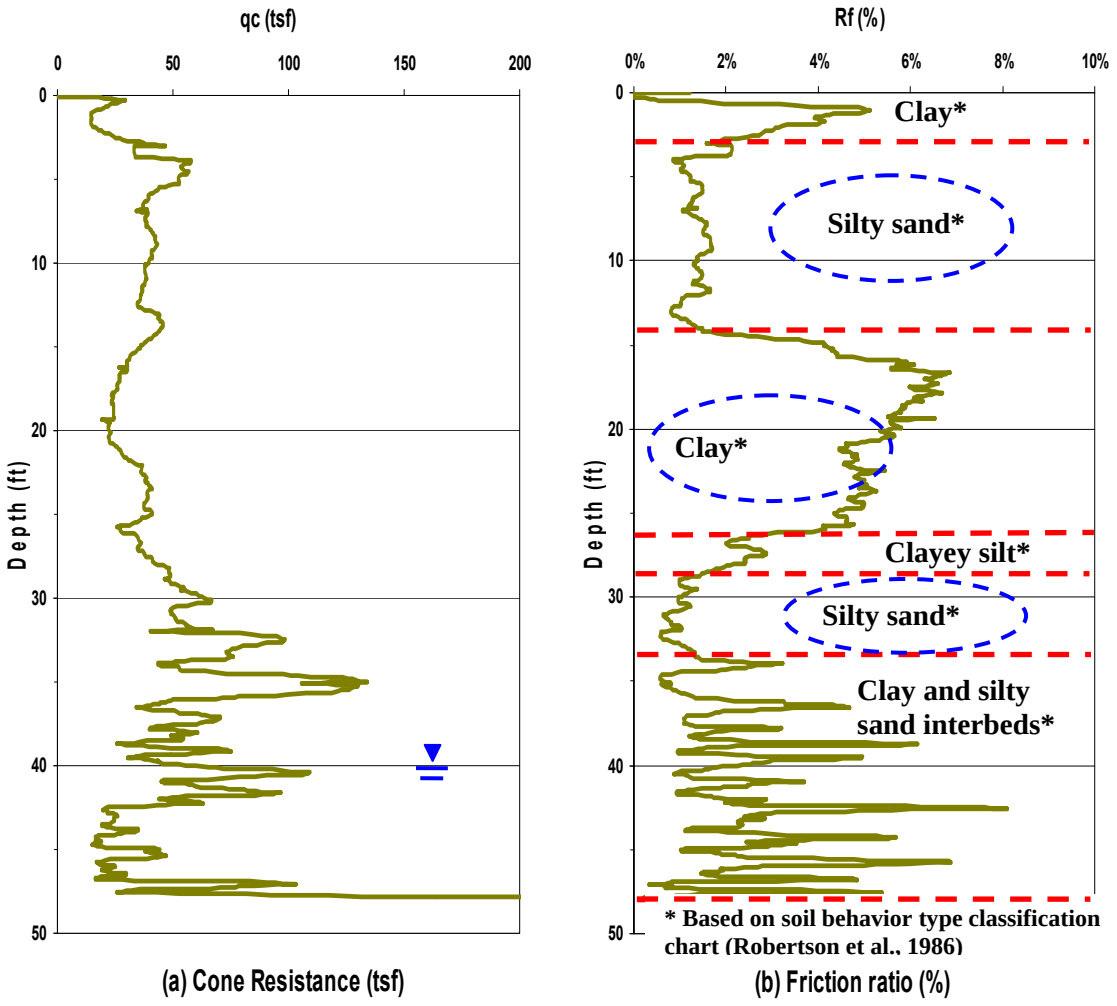

Figure 6.1: CPT Profiles Showing Clay and Sand Layers at SCPT Test Site at Hornsby Bend

location of the sources was described in Chapter 5. While an electrical trigger was utilized to record zero time in the seismic cone testing described in Chapter 5, a 3-D reference sensor buried at a shallow depth of 3.3 ft was used to calculate the phase difference between the 3-D receiver in the seismic cone and the 3-D reference sensor. In this case, the orientation of the geophone in the reference sensor was the same as the companion geophone in the 3-D receiver.

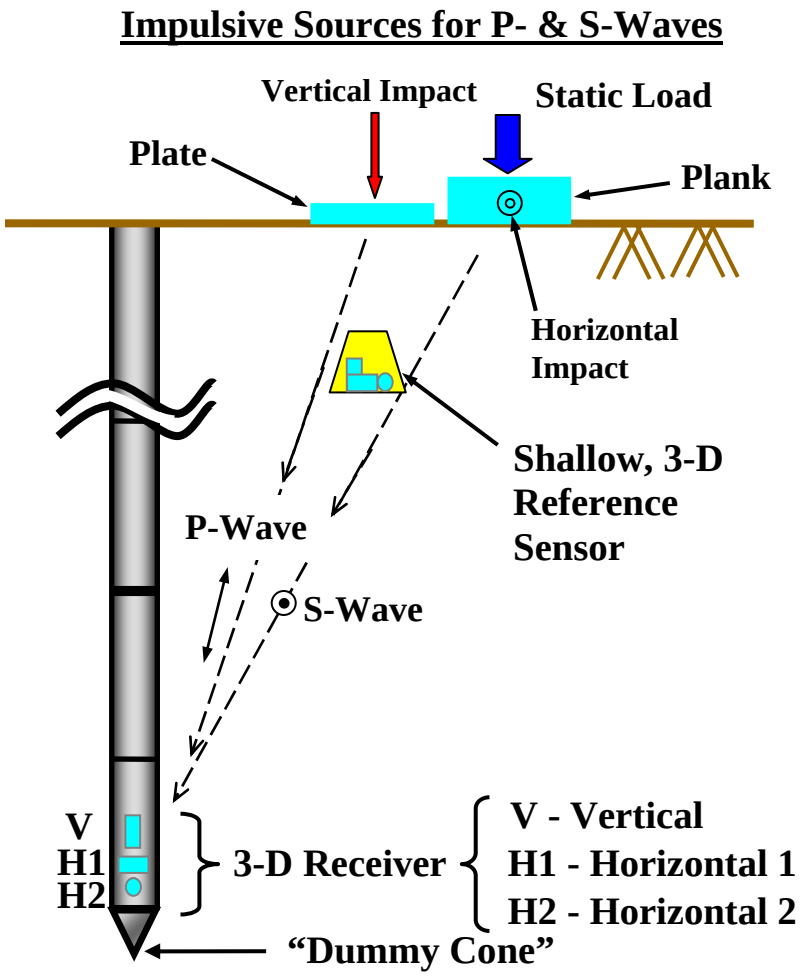

Figure 6.2: Setup for SCPT Testing Using Impulsive Sources

A steel P-wave plate and an aluminum S-wave plank were located about 5 ft and 6 ft away, respectively, from the seismic cone surface location. The 3-D reference sensor was buried about 3.3 ft deep at a distance about 4 ft away from the cone location. The orientations of each H2 horizontal geophone in the 3-D seismic cone receiver and 3-D reference sensor were aligned parallel to the direction of the horizontal impacts applied to the S-wave aluminum plank to maximize the recorded amplitude of the S_{vh}-waves. Phase differences of P waves generated by vertical impacts were also recorded by the two

vertical geophones in the 3-D seismic cone and the reference sensor, which generally maximized the recorded amplitude of the P_v-waves at depths greater than about 10 ft.

6.3 Analysis Procedures for S-Wave Phase Velocity, Material Damping and Dispersion

In Chapter 5, the interval times of waves collected at different measurement depths were determined by picking the first arrival times or other reference points or by using the cross-correlation method. Interval velocities determined by cross correlation or by time-depth plots based on first arrivals exhibit the least scattering in the V_S profiles as shown in Chapter 5. Therefore, V_S profiles determined by these two methods are compared in this chapter with V_S profiles obtained by the SABW method.

The interval time of two S_{vh}-waves is shown as a time shift between the two signals in a cross-correlation plot in Figure 6.3. The interval time of two S_{vh}-waves that travel from a depth of 16.2 ft to a depth of 26.0 ft is 10.83 ms and the inclined interval travel distance is 9.45 ft. By dividing the inclined interval distance by the interval time, a shear wave velocity of 872 ft/s is calculated.

Frequency-dependent V_S (V_P) called dispersion and also frequency-dependent D_S (and D_P) is also called dispersion in this research. This handling of the term dispersion is common in geophysics in terms of velocity but not in terms of material damping.

6.3.1 Analysis procedure for S-wave phase velocity measurements

The Spectral-Analysis-of-Body-Waves (SABW) method for shear and compression wave velocity measurements follows the same data recording and phase velocity calculations of the Spectral-Analysis-of-Surface-Waves (SASW) method presented by Stokoe et al. (1994). The measurements are performed between pairs of

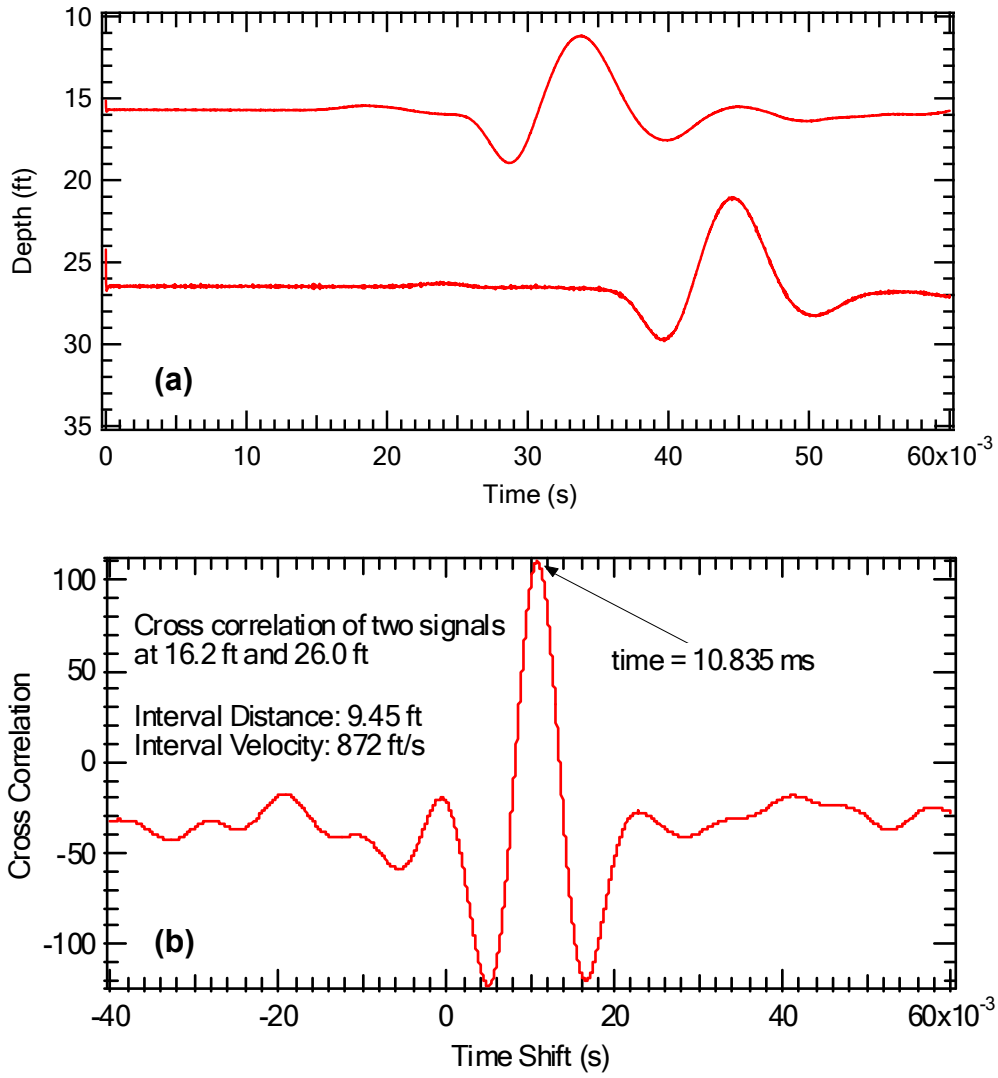

Figure 6.3: Cross Correlation of Signals: (a) Two Signals from Depths of 16.2 ft and 26.0 ft that were Generated by a S-wave Plank Struck by a Sledge Hammer in the Forward Direction and (b) Cross Correlation of the Two Signals

receivers. For the SCPT testing illustrated in Figure 6.2, the pair of sensors is the H2 geophone in the 3-D reference sensor that was embedded at some depth (3.3 ft in this case) below the ground surface and the H2 geophone in the 3-D receiver inside the seismic cone.

The time-domain records (r(t) and s(t)) collected from the H-2 geophone in the 3-D reference sensor and the H-2 geophone in the 3-D seismic cone at each depth are transformed into the Laplace form (R(s) and S(s)) by the dynamic signal analyzer. Then the transfer function, H(s), of the two frequency domain-signals (R(s) and S(s)) is calculated and displayed by the dynamic signal analyzer in real time. The internal calculation procedure of the dynamic signal analyzer can be outlined as:

$$R(s) = L\{r(t)\} = \int_0^\infty r(t)e^{-st}dt \tag{6.1}$$

$$S(s) = L\{s(t)\} = \int_0^\infty s(t)e^{-st}dt \tag{6.2}$$

$$H(s) = \frac{S(s)}{R(s)} \tag{6.3}$$

$$G(\omega) = \frac{|S|}{|R|} = |H(j\omega)| \tag{6.4}$$

$$\phi(\omega) = \arg(S) - \arg(R) = \arg(H(j\omega)) \tag{6.5}$$

where: r(t) and s(t) collected by a reference sensor and a seismic cone, respectively are the time domain records, R(s) and S(s) are the Laplace forms of r(t) and s(t), $H(j\omega)$ is the transfer function of the frequency-domain signals , $G(\omega)$ is the amplitude spectrum of the transfer function, and $\phi(\omega)$ is the phase difference. The changes of the sinusoid signals for every frequency, ω, are described by the frequency response, $H(j\omega)$.

Phase velocity can be used to plot the V_S profile of shear wave velocities in the ground. Figure 6.4 shows the transfer function between the H-2 reference geophone at a depth of 3.3 ft and the H-2 receiver geophone inside the seismic cone at a depth of 16.2 ft. The differences of phase angles between the H-2 reference geophone and the H-2

receiver geophone inside the seismic cone were calculated in real time by the dynamic signal analyzer and simultaneously displayed in terms of wrapped phase. The wrapped and unwrapped phases are shown in Figures 6.4a and b, respectively. If a complicated response exists in the frequency domain, that portion of the frequency range in the unwrapped phase can be deleted by referring to the wrapped phase plot as shown in Figure 6.4b. The unwrapped phase difference (ϕ) and the distance (d) that the S waves travelled were used to calculate the wavelength (Equation 6.6). The wavelength was plotted in the frequency domain as shown in Figure 6.4c. Finally, the phase velocity of the S wave ($V_{S,PH}$) can be calculated using Equation 6.7.

$$V_{S,PH} = f \times \frac{d}{\phi / 360°} \tag{6.6}$$

$$= f \times \lambda \tag{6.7}$$

The resulting phase velocities are plotted in Figure 6.4d. As seen in Figure 6.4c, wavelengths of the S wave range from about 30 ft to at a frequency of 20 Hz to 2 ft at a frequency of 300 Hz. As seen in Figure 6.4d, the associated phase velocities of the S wave range from about 30 ft at a frequency of 20 Hz to 2 ft at a frequency of 300 Hz. As seen in Figure 6.4d, the associated phase velocities of the S wave range from about 610 ft/s at 25 Hz to 700 ft/s at 300 Hz, with the velocity essentially constant (independent of frequency) at 680 ft/s above 55 Hz; hence $\lambda \leq 13$ ft. These characteristics are discussed in more detail later in this section.

In the same calculation procedure, Figures 6.5a and b show the wrapped and unwrapped phases between the H-2 reference geophone at a depth of 3.3 ft and H-2 geophone receiver inside the seismic cone at depth of 26.0 ft. Data with a low signal-to-noise ratio above 280 Hz were eliminated as shown in Figure 6.5b. The wavelength and

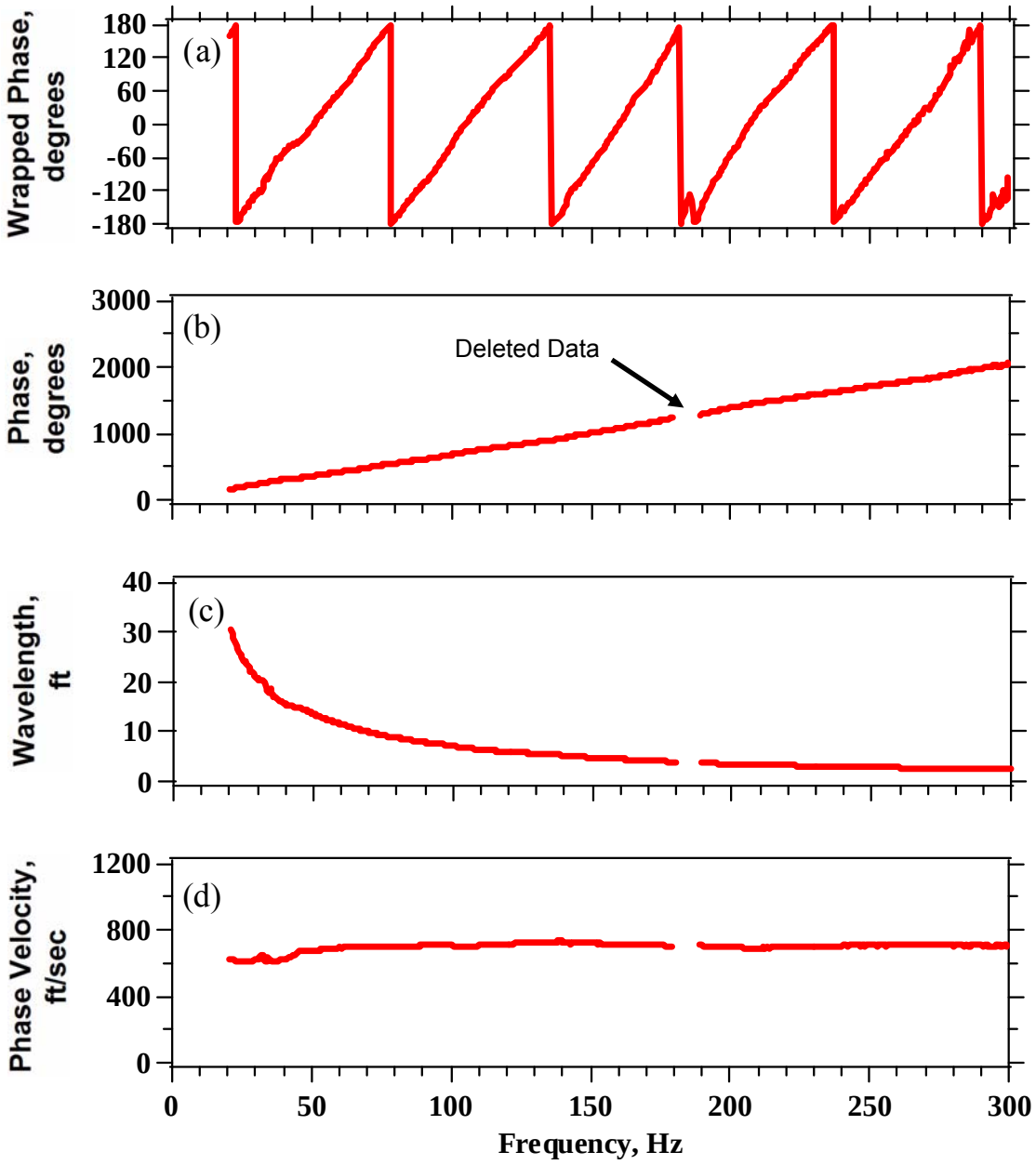

Figure 6.4: S-Wave Phase Velocity from Analysis of the Transfer Function between the Embedded Reference H-2 Receiver at a Depth of 3.3 ft and the Seismic Cone H-2 Receiver at a Depth of 16.2 ft

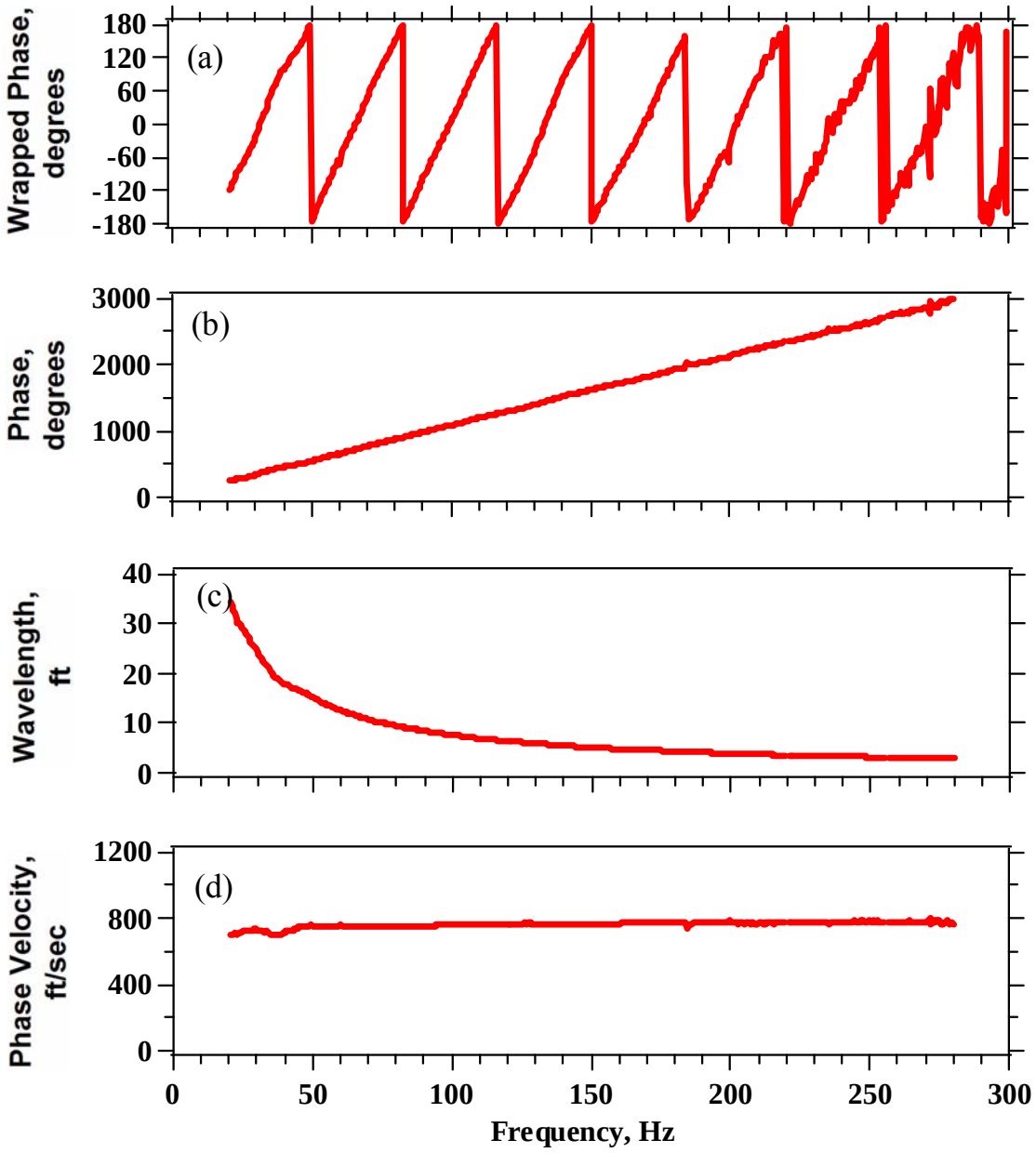

Figure 6.5: S-Wave Phase Velocity from Analysis of the Transfer Function between the Embedded Reference H-2 Receiver at a Depth of 3.3 ft and the Seismic Cone H-2 Receiver at a Depth of 26.0 ft

phase velocity of the shear wave were calculated and plotted as illustrated in Figures 6.5c and 6.5d, respectively.

The phase velocities shown in Figure 6.5 are shear wave velocities over a large interval ranging from 3.3 to 26.0 ft. To calculate the phase velocity of S waves propagating through the clay layer ranging from 16.2 to 26.0 ft (see Figure 6.1), the phase angles between the H-2 receiver geophone of the seismic cone at depth of 16.2 ft and the same H-2 receiver geophone at depth of 26.0 ft. In this case, the H-2 reference geophone of a 3-D reference sensor embedded at depth of 3.3 ft is used as the common reference as follows:

$$H_U(s) = \frac{S_U(s)}{R_U(s)} \tag{6.8}$$

$$H_L(s) = \frac{S_L(s)}{R_L(s)} \tag{6.9}$$

$$H_{L/U}(s) = \frac{H_L(s)}{H_U(s)} \tag{6.10}$$

$$\phi_{L/U}(\omega) = \arg(H_L) - \arg(H_U) = \arg(H_{L/U}(j\omega)) \tag{6.11}$$

where: R_U(s) and S_U(s) are the Laplace forms of time-domain data collected with the reference sensor and the seismic cone receiver at the upper location, respectively, $H_U(j\omega)$ is the transfer function of the frequency-domain signals, (R_U(s) and S_U(s)), R_L(s) and S_L(s) are the Laplace forms of time-domain data collected with the a reference sensor and the seismic cone receiver at the lower location, respectively, $H_L(j\omega)$ is the transfer function of the frequency-domain signals, (R_L(s) and S_L(s)), and $\phi_{l/U}(\omega)$ is the phase difference between the two transfer functions ($H_U(j\omega)$ and $H_L(j\omega)$), the changes of the

sinusoid signals for every frequency, ω, are described by the frequency response, $H_{L/U}(j\omega)$.

The transfer functions (H_U(s) and H_L(s)) between the outputs of the H-2 reference geophone and the H-2 geophone in the seismic cone at the upper and lower locations were calculated with Equations 6.8 and 6.9, respectively. The transfer function (H_L(s)) obtained from the lower location can be divided by the transfer function (H_U(s)) from the upper location as described by Equation 6.10. Because the H-2 reference geophone is embedded at the same depth regardless of the movement of the seismic cone, the transfer function of the lower location can be reasonably normalized with the transfer function of the upper location. As shown in Equation 6.11, the phase of the normalized transfer function is the phase of lower transfer function minus the phase of upper transfer function because the equation of wave motion is an exponential function. The phase of the normalized transfer function at depths of 16.2 ft and 26.0 ft was calculated. The wrapped and unwrapped phases are plotted in Figures 6.6a and b. As described above, the wavelengths and phase velocities were calculated with Equations 6.6 and 6.7. These results are plotted in Figures 6.6c and d, respectively. The average phase velocity in the frequency ranging from 20 Hz to 270 Hz is 876 ft/s.

The velocity (also called group velocity) determined by cross correlation of two signals traveling the same interval distance ranging from 16.2 to 26.0 ft is 872 ft/s in Figure 6.3. The group velocity is shown by the blue dashed line in Figure 6.6d so it can be compared with the phase velocities as shown in Figure 6.6d. The difference of average phase velocity and the velocity from cross correlation is very small (0.6 %). With this data collection procedure, the phase velocities of any interesting soil layers can be calculated without using an expensive SCPT sensor that has two or more 3-D receivers. The length of interval is controllable with the 3-D reference sensor. This length control

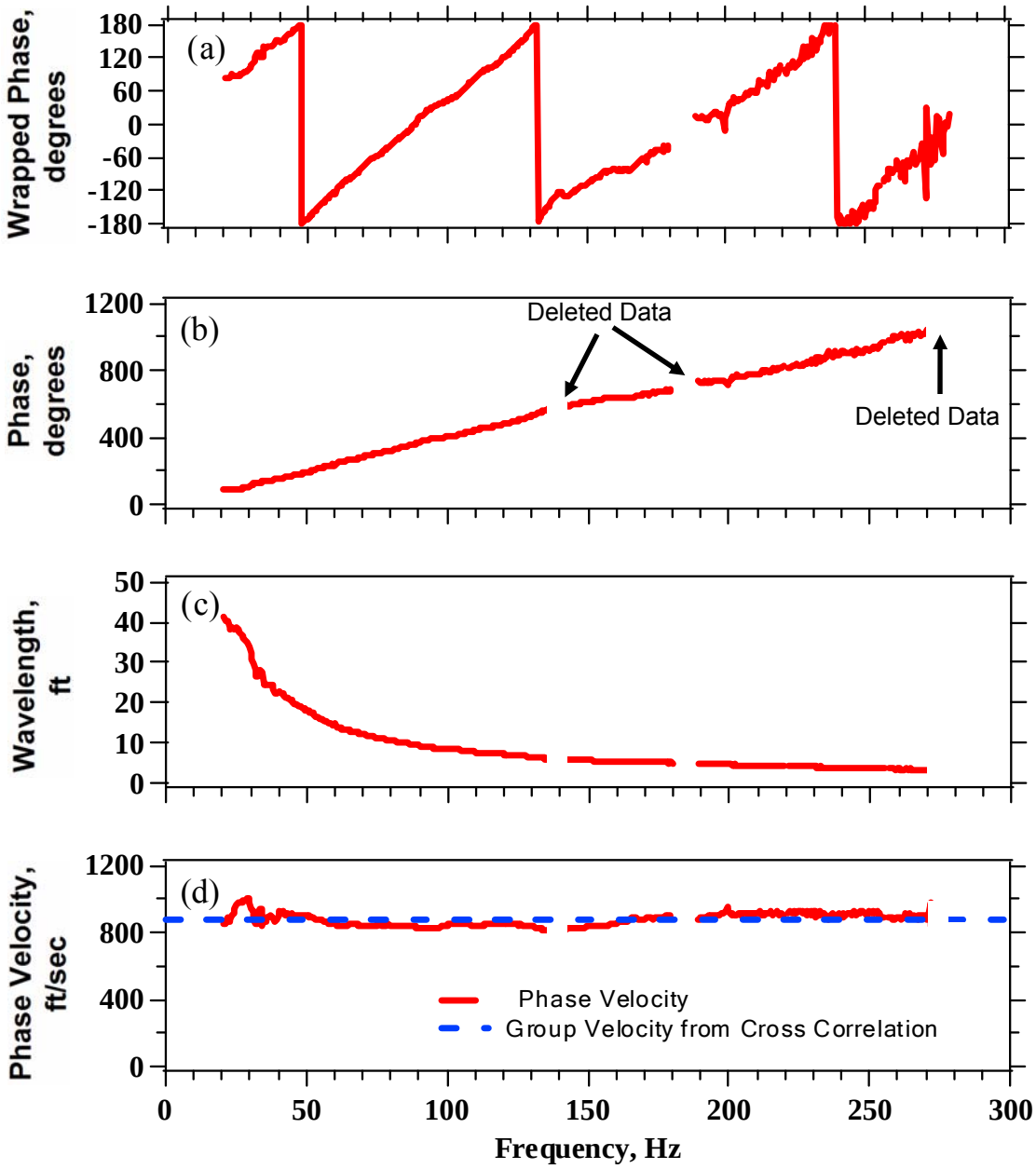

Figure 6.6: S-Wave Phase Velocity from Analysis of the Transfer Function between the H-2 Geophone in the Seismic Cone at a Depth of 16.2 ft and the Same H-2 Geophone in the Seismic Cone at a Depth of 26.0 ft

enables one to avoid possible estimation errors that fixed short intervals cause and to increase the resolution of interesting intervals.

Using the analysis procedure presented above, the average S-wave phase velocity over the frequency range of 50 to 250 Hz was calculated for each depth interval (interval distance is 3.3 ft). Hence, interval average phase velocities were determined which can be compared with the interval velocities presented in Chapter 6. Also, the frequency range of 50 to 250 Hz was selected because this range minimizes the inclusion of near-field and low S/N ratio data. The interval average phase velocities are plotted as in Figure 6.7. The average phase velocity at the shallowest depth range of 3.0 to 6.3 ft was 550 ft/s. The wavelength of waves with 100 Hz is 5.5 ft. Because the inclined travel distance of waves at the depth of 6.3 ft is 8.7 ft, the travel distance is 1.6 times longer than the wavelength at 100 Hz. Phase velocity averaged in the frequency range from 100 to 250 Hz were calculated and plotted to be compared with the phase velocity averaged in frequency range from 20 to 280 Hz in Figure 6.7. The two velocity profiles are very similar.

V_S profiles that were determined from the time-depth plot using first-arrival times, from cross correlation of two signals and from phase differences are compared in Figure 6.8. The three wave velocity profiles are globally similar. The wave velocity profiles using cross correlation and phase difference are very similar with the interval distance of 3.3 ft because the calculation procedures do not need human subjectivity for picking the first arrival time or other reference and cross correlation smoothes the time-domain waveforms.

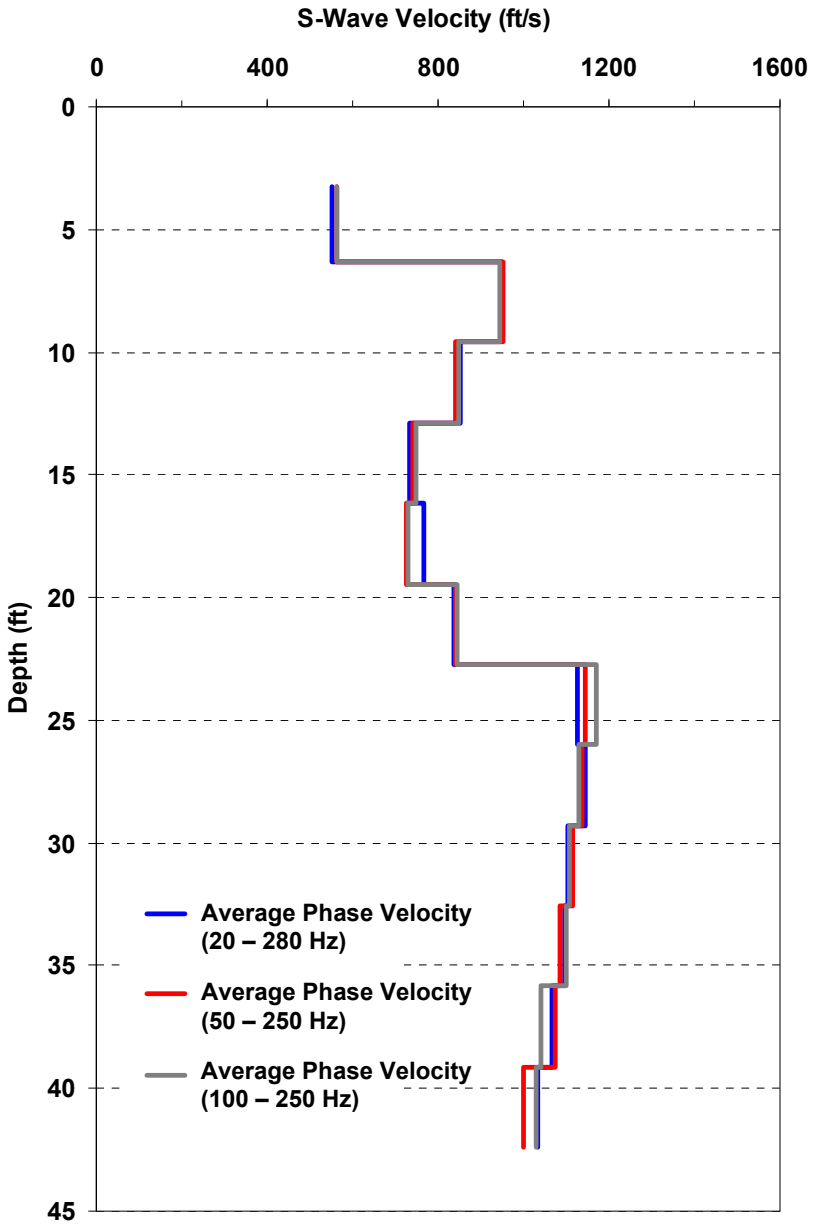

Figure 6.7: Comparison of V_S Profiles of Average Interval Phase Velocity for Frequency Ranges of Analysis Ranging 20 to 280 Hz, 50 to 250 Hz and 100 to 250 Hz

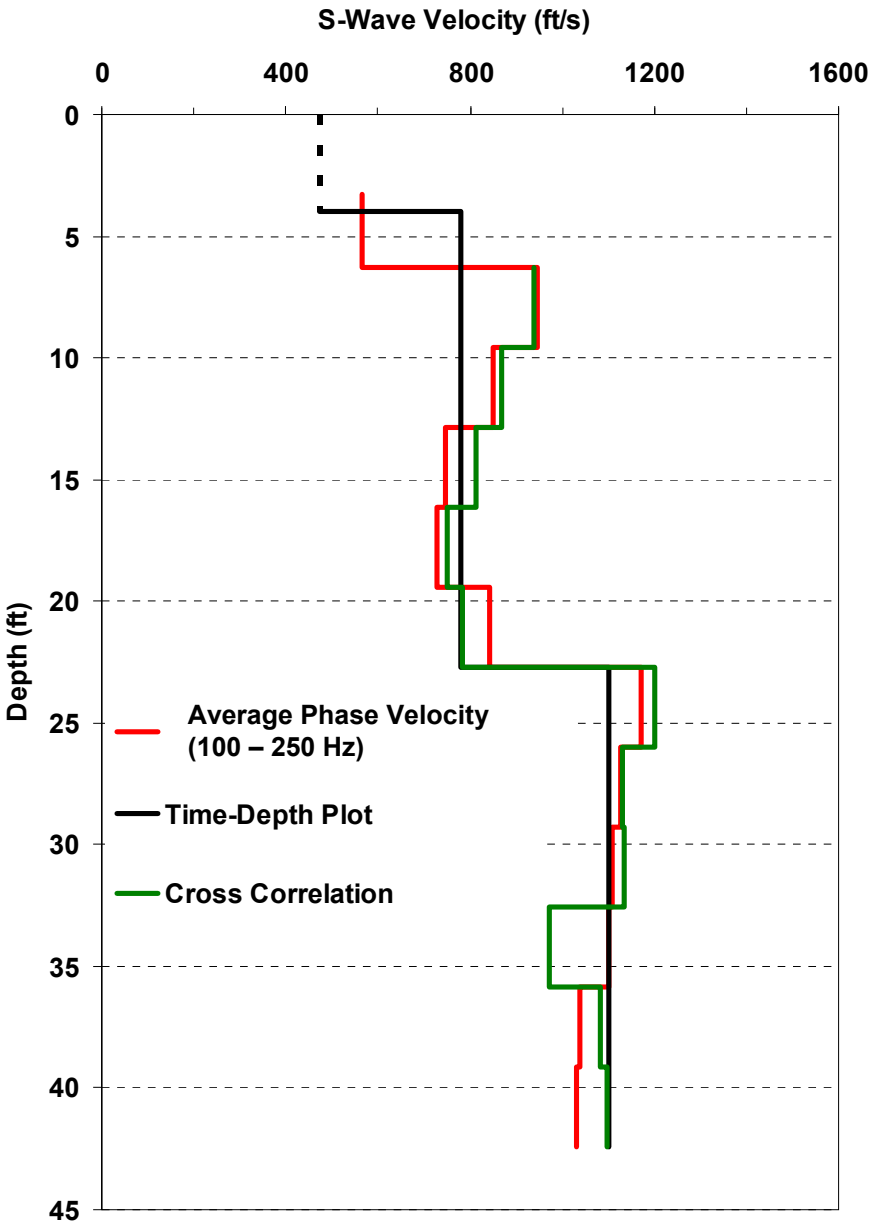

Figure 6.8: Comparison of V_S Profiles from Three Analysis Methods

6.3.2 Analysis procedure for S-wave material damping measurements

Material damping ratio in shear is an important property in characterizing soil and materials. While material damping ratios of geotechnical materials have been actively studied in the laboratory by numerous investigators, field material damping ratios have only been studied with limited success by small number of engineers and scientists such as Redpath et al. (1982), Redpath and Lee (1986), Mok (1987), Mok et al. (1988), Stewart (1992) and Karl (2005). The primary reasons are that measurement of damping ratios in field seismic testing requires: (1) an understanding of various factors that affect attenuation, (2) separation of these factors and (3) precise measurements of particle motion.

A spectral ratio method has been developed and used by Mok et al. (1988) for in-situ material damping measurements with the crosshole seismic method. Stewart (1992) and Karl (2005) applied the spectral ratio method to downhole tests to determine field material damping ratios. In this study, the spectral ratio method is improved and used for the measurements of material damping in shear in the field. In this research, the spectral ratio method in SCPT measurements is only used for S_{vh} waves propagating along inclined ray paths in the same soil layer. Therefore, it is assumed that the measured wave amplitudes at different depths are not affected by refracted and reflected waves, and, since the soil at this research test site ranges from sands to clays, backscattering does not affect the measurements.

The motion of S_{vh} waves away from a source in a 3-dimensional homogeneous isotropic soil is described as (see Chapter 2.3):

$$A(r,t) = \frac{A_0}{r} \cdot e^{i(k_r r - \omega t)} \cdot e^{-\alpha r} \tag{2.10}$$

where r is the radial distance from the source, e is the base of the natural logarithm, k_r is the real part of the wave number, $e^{-\alpha r}$ is the attenuation factor due to material damping. Equation 2.10 is the equation of motion for S_{vh} waves propagating along the radial direction at a velocity equal to $\frac{\omega}{k_r}$ $(= f \cdot \lambda)$ and a decreasing amplitude caused by the geometric spreading $(\frac{A_0}{r})$ and material damping $(e^{-\alpha r})$ in a homogeneous, isotropic visco-elastic material.

The amplitude of a sinusoidal wave that propagates through an infinite homogeneous medium attenuates with increasing distance from the source and due to material damping in the visco-elastic medium. Equation 2.10 can be used to describe the factors that change the amplitude of wave as it propagates from r_1 to r_2 by:

$$\frac{A_2}{A_1} = \frac{r_1}{r_2} \cdot e^{-\alpha(r_2 - r_1)} \tag{6.12}$$

where r_1 is the distance from the source to the first receiver at depth, r_2 is the distance from the source to the second receiver at a deeper depth, A_1 is the wave amplitude at distance r_1 from the source, A_2 is the body wave amplitude at distance r_2 from the source, α is the attenuation coefficient. The ratio A_2/A_1 is called a spectral ratio. The terms r_1/r_2 and the exponential function are related to geometrical spreading and material damping, respectively.

If the source is an impulsive source and if the wave amplitudes vary with frequency, the spectral ratio becomes a function of frequency as:

$$\frac{A_S(f)}{A_R(f)} = \frac{x_R}{x_S} \cdot e^{-\alpha(x_S - x_R)} \tag{6.13}$$

where x_R is the distance from the source to a reference geophone at a shallow depth, x_S is the distance from the source to a geophone in the seismic cone at a deeper depth, A_R is the body wave amplitude at the reference geophone at distance x_R from the source, A_S is the body wave amplitude at the geophone in the seismic cone at distance x_S from the source, and α is the attenuation coefficient.

However, calculation of material damping ratio from Equation 6.13 is based on a global soil layer ranging from the reference geophone at a fixed shallow depth to a geophone in the cone at a deeper depth. To calculate material damping over depth intervals of interest, the amplitudes of the seismic cone at the upper and lower locations are divided by the amplitude of the reference geophone used in the upper and lower measurements, respectively. The normalized spectral ratio is written as:

$$\frac{\left(\frac{A_{SL}(f)}{A_{RL}(f)}\right)}{\left(\frac{A_{SU}(f)}{A_{RU}(f)}\right)} = \frac{x_{SU}}{x_{SL}} \cdot e^{-\alpha(x_{SL}-x_{SU})} \tag{6.14}$$

where x_{SU} is the distance from the source to the seismic cone at the upper location, x_{SL} is the distance from the source to the seismic cone at the lower location, A_{RU} and A_{SU} are the body wave amplitudes of the reference geophone and the geophone in the seismic cone at the upper location, respectively, and A_{RL} and A_{SL} are the body wave amplitudes of the reference geophone and the geophone in the seismic cone collected at lower location, respectively.

By rearranging Equation 6.14, the attenuation coefficient, α, can be expressed as:

$$\alpha(f) = \frac{\ln\left(\frac{A_{SU}(f)/A_{RU}(f)}{A_{SL}(f)/A_{RL}(f)} \cdot \frac{x_{SU}}{x_{SL}}\right)}{x_{SL} - x_{SU}} \tag{6.15}$$

The attenuation coefficient can also be expressed using Equation 2.4 as:

$$\alpha(f) = \frac{2 \cdot \pi \cdot f \cdot D(f)}{V(f)} \tag{6.16}$$

where $\alpha =$ attenuation coefficient, $f =$ frequency, $D(f) =$ damping ratio for each frequency and $V(f) =$ phase velocity for each frequency. By combining Equations 6.15 and 6.16, material damping ratio can be expressed as:

$$D(f) = \frac{V(f)}{2 \cdot \pi \cdot f} \cdot \frac{\ln\left(\frac{A_{SU}(f) / A_{RU}(f)}{A_{SL}(f) / A_{RL}(f)} \cdot \frac{x_{SU}}{x_{SL}} \right)}{x_{SL} - x_{SU}} \tag{6.17}$$

To use Equation 6.17, the following assumptions are made: 1. any additional near-field effects on wave amplitude can be neglected, 2. reflection and refraction of body waves on boundary is negligible for amplitude in the similar layer, and 3. material damping is dependent on frequency and the result of the spectral amplitude ratios at small strains (less than 10^{-3} percent).

The field material damping ratio of a clay layer was calculated with Equation 6.17 as an example. The shear wave velocity should be reasonably constant in the clay layer and the location of the layer should be away from the ground surface to minimize any near-field effects. With these constraints, the example clay layer ranges from 16.2 to 22.7 ft in depth. The friction ratio profile and V_S profile of the clay layer are shown in Figures 6.1b and 6.8, respectively.

The material damping ratio determined using Equation 6.17 is dependent on frequency. As shown in Figure 6.9a, the amplitudes of the power spectrum of the H-2 geophone inside the seismic cone were calculated in the frequency domain at depths of

16.2 and 22.7 ft. As discussed in Appendix A, the nonlinear amplitude data in the frequency range of 20 to 60 Hz are affected by the nonlinear calibration factor around the natural frequency of 24 Hz of the geophones and, thus, are not used in Equation 6.17. As shown in Figure 6.9a, the signal-to-noise ratios of the amplitude power spectrum in the frequency range above 180 Hz are low and data above 180 Hz are not considered in the material damping ratio evaluation. As shown in Figure 6.9b, the inclined travel distance between the depths of 16.2 ft and 22.7 ft is divided by the wavelengths of the S waves so that the amplitude power spectrum versus interval distance/wavelength can be plotted. To calculate interval distance/wavelength scale, unwrapped phase was plotted and a linear equation was best fit to the unwrapped phase plot. The linear fit is shown in Figure 6.10. The layer between depths of 16.2 and 22.7 ft should have wavelengths that are shorter than the inclined travel distance to minimize the effect from other material that longer wavelengths would include. This frequency is 125 Hz for an interval distance/wavelength of 1. As a result, the data of the frequency ranging from 125 to 180 Hz are available for the damping ratio measurement.

The attenuation coefficient, α, and field material damping ratio, D, were calculated with Equations 6.15 and 6.17. These results are plotted in Figures 6.11 and 6.12, respectively. The field material damping ratio is dispersive as expected for a soil with moderate plasticity. The dispersive field damping ratios at the frequency range of 140 to 180 Hz are averaged with a dashed blue line in Figure 6.12 because the damping ratios look like due to sand mixing in measurements. The average field material damping ratio of S-waves that propagate through the clay layer ranging from 16.2 to 22.7 ft is 4.67 %. It is within the damping ratio ranges of clay suggested by Sun et al. (1988) and Darendeli (2001).

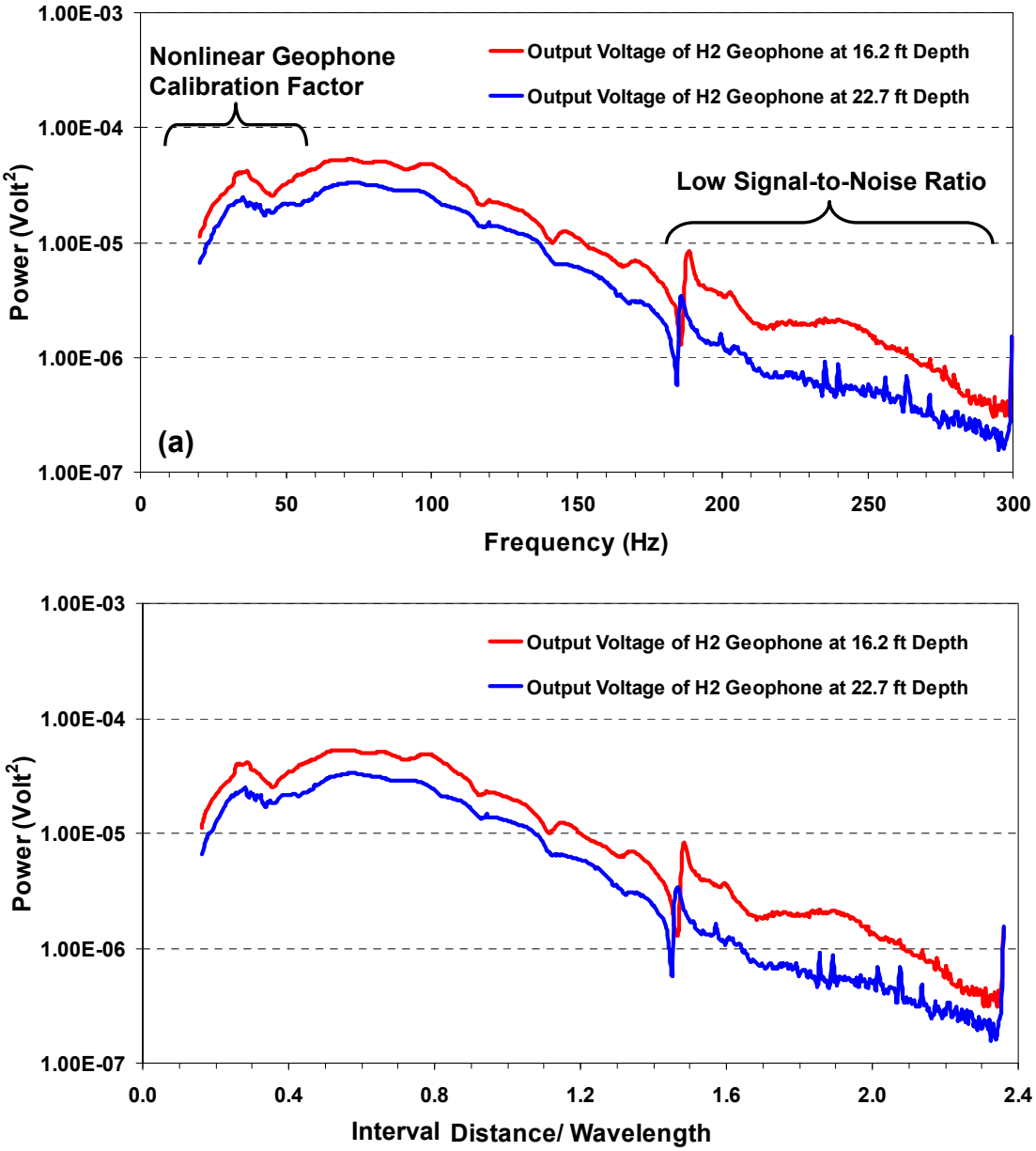

Figure 6.9: Variation in H-2 Geophone Output in the Seismic Cone with (a) Frequency and (b) Interval Distance/ Wavelength over the Useable Frequency Range for S-Wave Material Damping Ratio Measurements

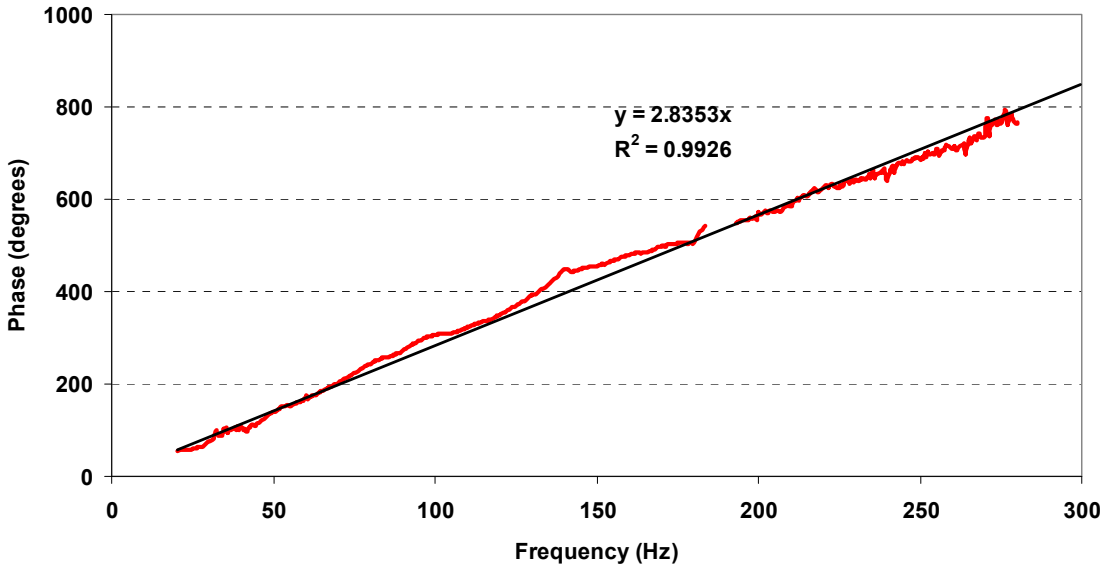

Figure 6.10: Best-Fit Straight Line through the Unwrapped Phase versus Frequency Relationship

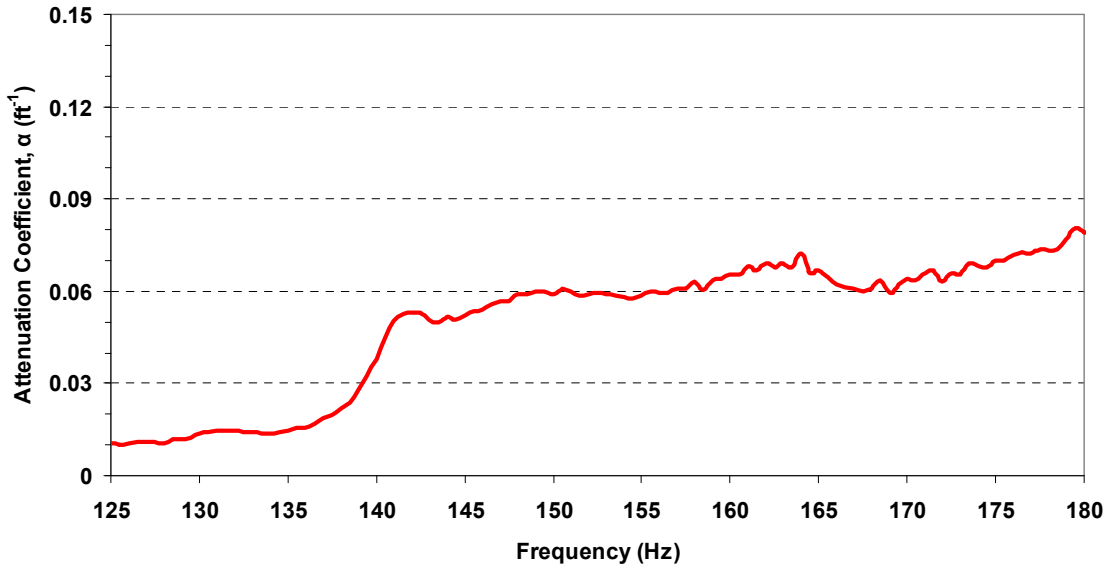

Figure 6.11: Attenuation Coefficient, α, Calculated from the Spectral Amplitudes of S-Waves Propagating through the Clay Layer in the Depth Range of 16.2 to 22.7 ft; Relationship Exhibits Dispersion

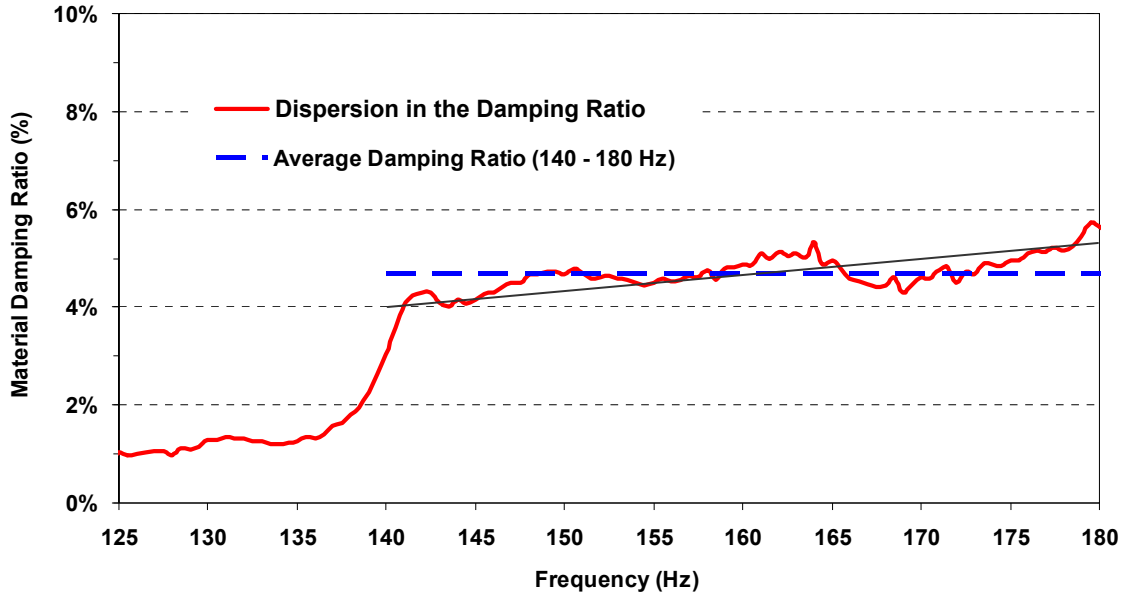

Figure 6.12: Plots Showing Dispersive Damping Ratio and Average Damping Ratio Calculated from the Spectral Amplitudes of S-Waves Propagating through the Clay Layer Ranging from 16.2 to 22.7 ft

6.3.3 S-wave dispersion measurements

V_S and $D_{S\,min}$ increase with the increasing excitation frequencies in clayey soils (Hardin and Drnevich, 1972 and Stokoe and Santamarina, 2000). The change in V_S and $D_{S\,min}$ with increasing frequency increase as the PI of soils increases (Hardin and Drnevich, 1972 and Stokoe and Santamarina, 2000). $D_{S\,min}$ is more affected than V_S over the same frequency range. As shown in Figure 6.13, the increase in V_S and $D_{S\,min}$ are dependent on the PI of the soil. In principle, the dispersive characteristics of V_S and $D_{S\,min}$ could be used to characterize soil layers according to general soil types with comprehensive field seismic measurements.

As an example of such measurements, consider the analytical study presented by Sanchez-Salinero et al. (1986). The following was considered in modeling a field crosshole test: (1) the distance from the source to the second receiver (d_2) over the

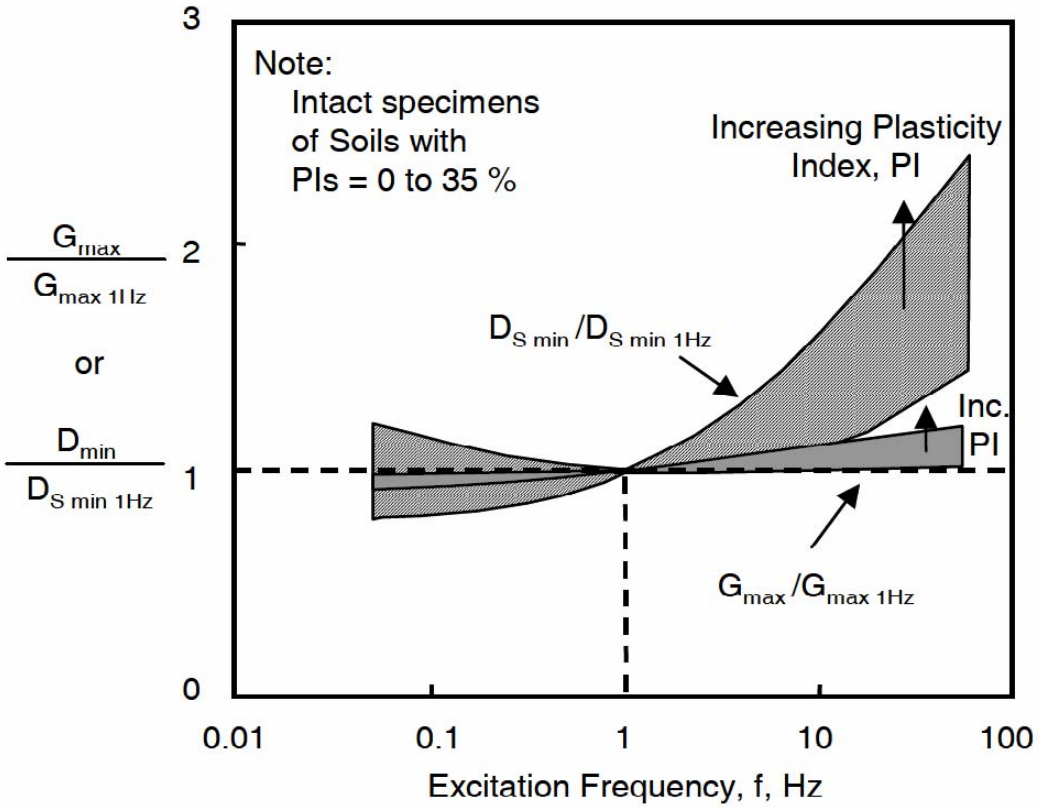

Figure 6.13: General Effect of Excitation Frequency on Small-Strain Shear Modulus, G_{max}, and Small-Strain Material Damping Ratio in Shear, $D_{S\ min}$ (from Stokoe and Santamarina, 2000)

distance from the source to the first receiver (d_1) is 1.5, (2) Poisson's ratio of the soil is 0.25, (3) the material damping ratio is 5 %, and (4) the shear wave velocity fluctuates within about 7 % of a constant velocity for d_1 divided by wavelength (d_1/λ) below 2.0 due to the near field effect. These values are similar to the values that were estimated in this field seismic testing. In the field testing, the inclined distance from the source to the seismic cone at a depth of 26.0 ft (d_2) divided by the inclined distance from source to the seismic cone at 16.2 ft (d_1) gives d_2/d_1 equal to 1.56. Poisson's ratio is about 0.25 ~ 0.30 for the ground profile as shown in Figure 5.16. The material damping ratio of the clay

layer in the depth range of 16.2 to 22.7 ft is 4.67 %. Using the estimated distance and phase velocities, the phase velocity versus frequency plot (Figure 6.14a) can be plotted in terms of phase velocity versus d_1/λ (Figure 6.14b). To minimize the near field effect, the data for d_1/λ below 2 were deleted. To use data having reasonable signal-to-noise ratios, the data in the frequency range above 250 Hz were eliminated. The phase velocities of two different soil layers are plotted as shown in Figure 6.14. In addition, the travel distance from a source to the seismic cone at the middle location of each layer is divided by wavelengths. The phase velocity versus the average S-R travel distance/ wavelength is plotted in Figure 6.14c. All the waves that propagate through the middle location of each layer have a wavelength less than travel distance (see Figure 6.14c). Phase velocities of shear waves that propagate through the silty sand layer (depth range of 3.3 to 16.2 ft) are constant in the frequency domain (see Figure 6.14a and c). However, phase velocities of shear waves that propagate through the clay layer ranging 16.2 to 26.0 ft gradually increases due to the dispersive characteristics of clayey soil as shown in Figure 6.14a and c. The dispersive characteristic of the phase velocities of shear waves propagating through the clayey soil shows additional information for the soil type. The information can be obtained by field seismic testing.

The dispersive characteristics were checked with small interval distances of 3.3 ft. The phase velocities of waves in two small interval distances ranging from 22.7 to 26.0 ft and from 29.3 to 32.6 ft depths are plotted in Figure 6.15a and b, respectively. While the phase velocities gradually increase in Figure 6.15a, the phase velocities do not increase in Figure 6.15b. It is because the first soil layer and second soil layer consist of clay and silty sand, respectively, as shown in Figure 6.1.

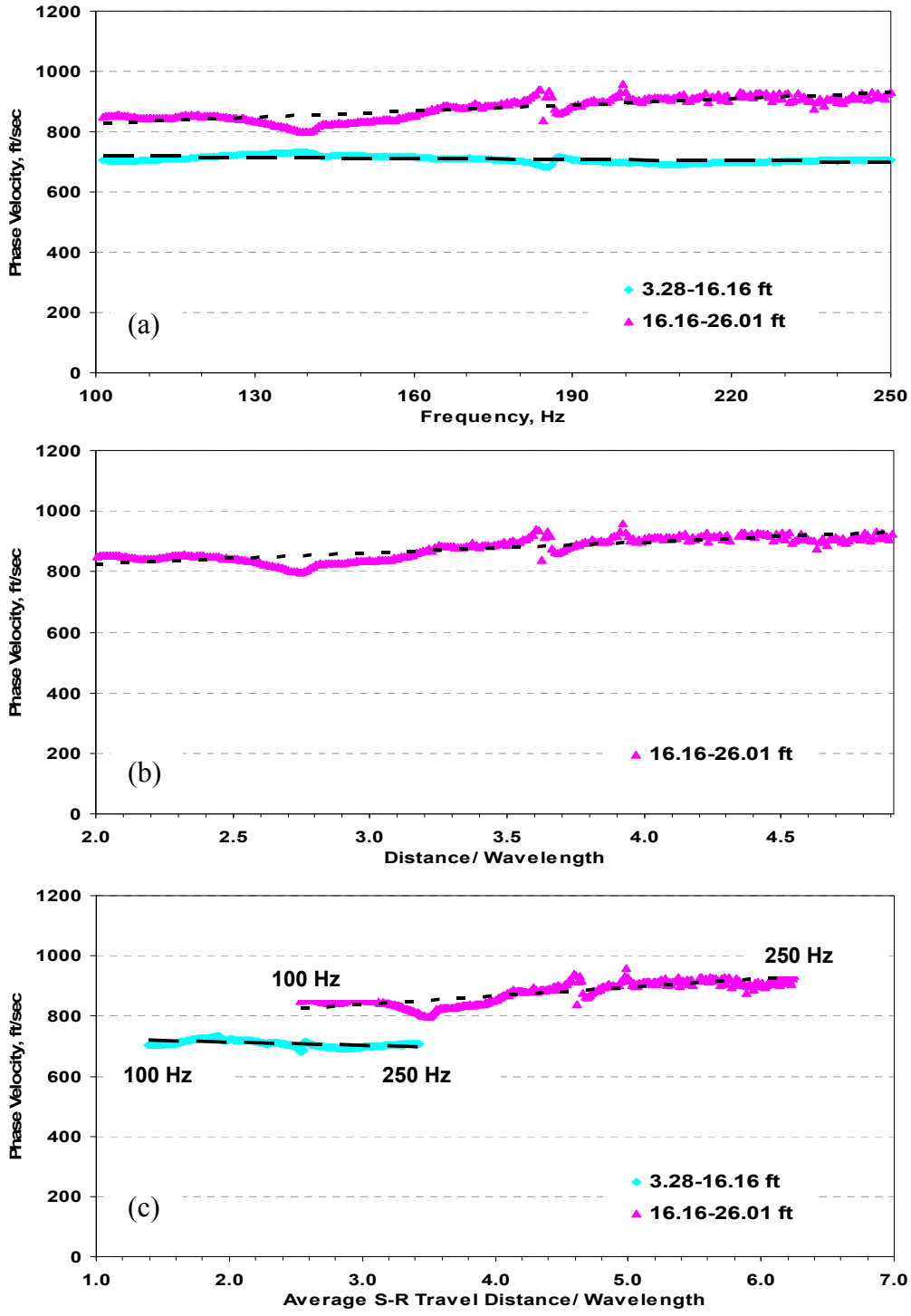

Figure 6.14: V_S Dispersion Curves Showing Two Different Soil Types

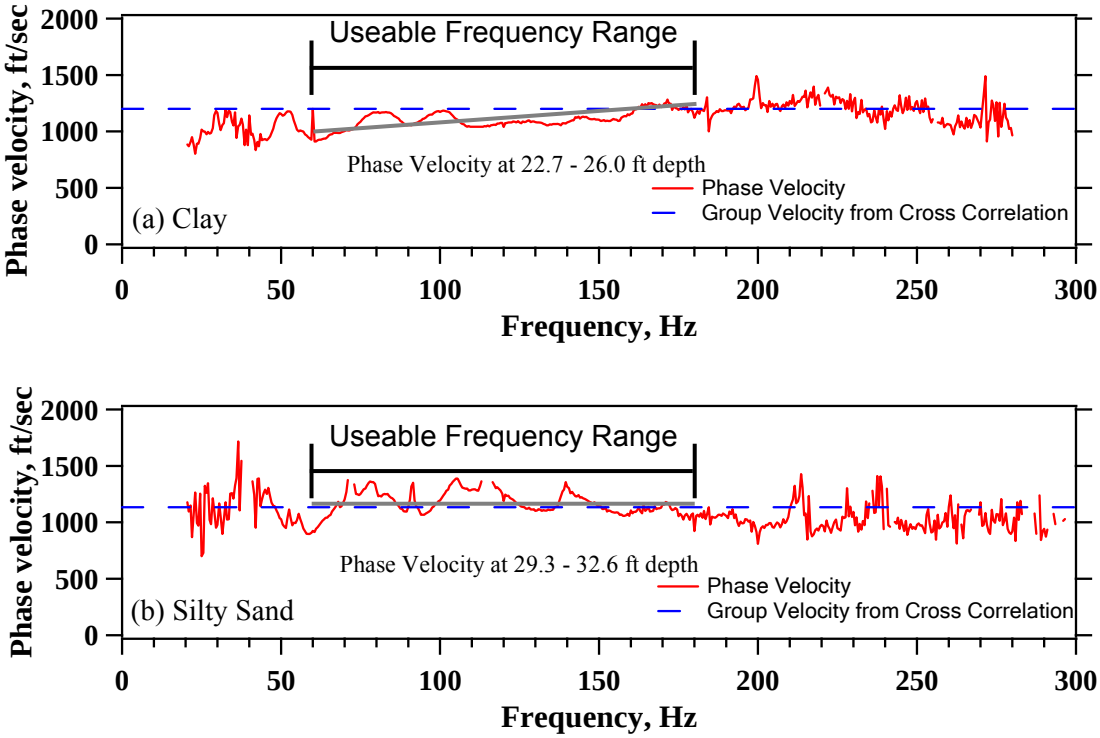

Figure 6.15: V_S Dispersion Curves Showing Different Soil Types at Two Soil Layers of the Same V_S

For dispersive characteristic of damping ratio over frequency in clay layer, that damping ratio increases as the frequency increases is shown in Figure 6.12. The increment rate of damping ratio is much larger than the increment rate of phase velocity.

6.4 Analysis Procedure for P-Waves

Application of the SABW method to P-wave velocity measurements was not as successful as the S-wave application for several records. First, P waves propagating through soil layers are easily converted to other waves. Second, the small amplitude of P-wave signals relative to the S-wave signals result in relatively low signal-to-noise ratios.

Third, interaction of vertically propagating P waves with the water table affects the waveform and spectrum of the P waves. Fourth, phase velocities of P waves exhibit a larger effect of near-field terms. Sanchez-Salinero et al. (1986) recommended using data that have d_1/λ above 10 when performing spectral analysis of P-wave to avoid the near-field effect. Fifth, generating P-waves with large amplitude in the high-frequency range is not easy. Therefore, it is recommended that application of the SABW method to P-wave measurements to be studied with numerical-simulation methods before applying the method to field measurements.

6.5 SUMMARY

Time-domain analysis methods for evaluation of body wave velocities usually require picking first arrival times or times of other reference points. This time-consuming analysis procedure also requires an experienced operator. The human subjectivity causes, at a minimum, scatter wave velocity profiles. To avoid this type time consuming effort and to minimize the human-subjectivity aspect, the cross correlation method has been introduced and is used in geophysics. However, the cross correlation method is only used to evaluate wave velocities, thereby losing other valuable material-characterization information.

A frequency-domain method, called the Spectral-Analysis-of-Body-Waves (SABW) method has been developed. The wave velocity calculation procedure of the SABW method is similar to the wave velocity calculation procedure of the Spectral-Analysis-of-Surface-Waves (SASW) method. In the SABW method, the phase difference between the outputs of two sensors is determined from which the phase velocity is calculated. The phase difference can be automatically calculated in real time with the

internal calculation procedure of a dynamic signal analyzer. Vs profiles calculated with time-domain methods and the SABW method are compared in this research. The Vs profiles are essentially the same, with the exception that additional information about the body wave is present in the SABW results.

In addition, a frequency-domain method with which material damping ratio is determined has been developed. This method uses the spectral ratio method that has been used at the University of Texas in crosshole testing. The equation of wave motion was modified for frequency dependency of material damping ratio and a reference 3-D geophone used to normalize signals from the seismic cone at two measurement depths. A frequency range (hence, a wavelength range) is suggested for use with the equation. The damping ratio of one clay layer at the Hornsby Bend site was calculated and plotted. The estimated field material damping ratio, 4.67 %, is within the range obtained from laboratory testing of clay.

Lastly, the SABW method has the potential to be used to identify general soil type based on the dispersive characteristic of stress wave velocities. As an example, the phase velocity and material damping ratio obtained from field testing increased with increasing frequency in a clay layer. However, phase velocity in silty sand layer was constant.

Chapter 7: Application of the SABW Method Using a Sinusoidal Source

7.1 INTRODUCTION

As part of the development of SABW method, SCPT testing with a sinusoidal source was also investigated. The SCPT test in this case involved a CPT test and a seismic cone test using Thumper as a sinusoidal source. This testing was performed at Platt 4 of the Hornsby Bend site. The CPT test was performed earlier than the seismic cone test. In addition, a seismic cone test using an impulsive source, as described in Chapter 6 was conducted for comparison purpose. These tests were finished within several days. The CPT profile is plotted in Figure 7.1.

The seismic cone tests using sinusoidal and impulsive sources were each performed about 25 ft away from the location of the CPT test in a triangular pattern. The V_S profiles obtained from the two different sources are compared and discussed in this chapter.

7.2 TESTING SET-UP FOR SCPT WITH SINUSOIDAL AND IMPULSIVE SOURCES

The seismic cone test using a sinusoidal source was set up and performed as shown in Figure 7.2a. This test was performed with Thumper. Another seismic cone test was performed 25 ft away from the location of the first seismic cone test using an impulsive source in Figure 7.2b. The specifications of Thumper are described in Chapter 4.

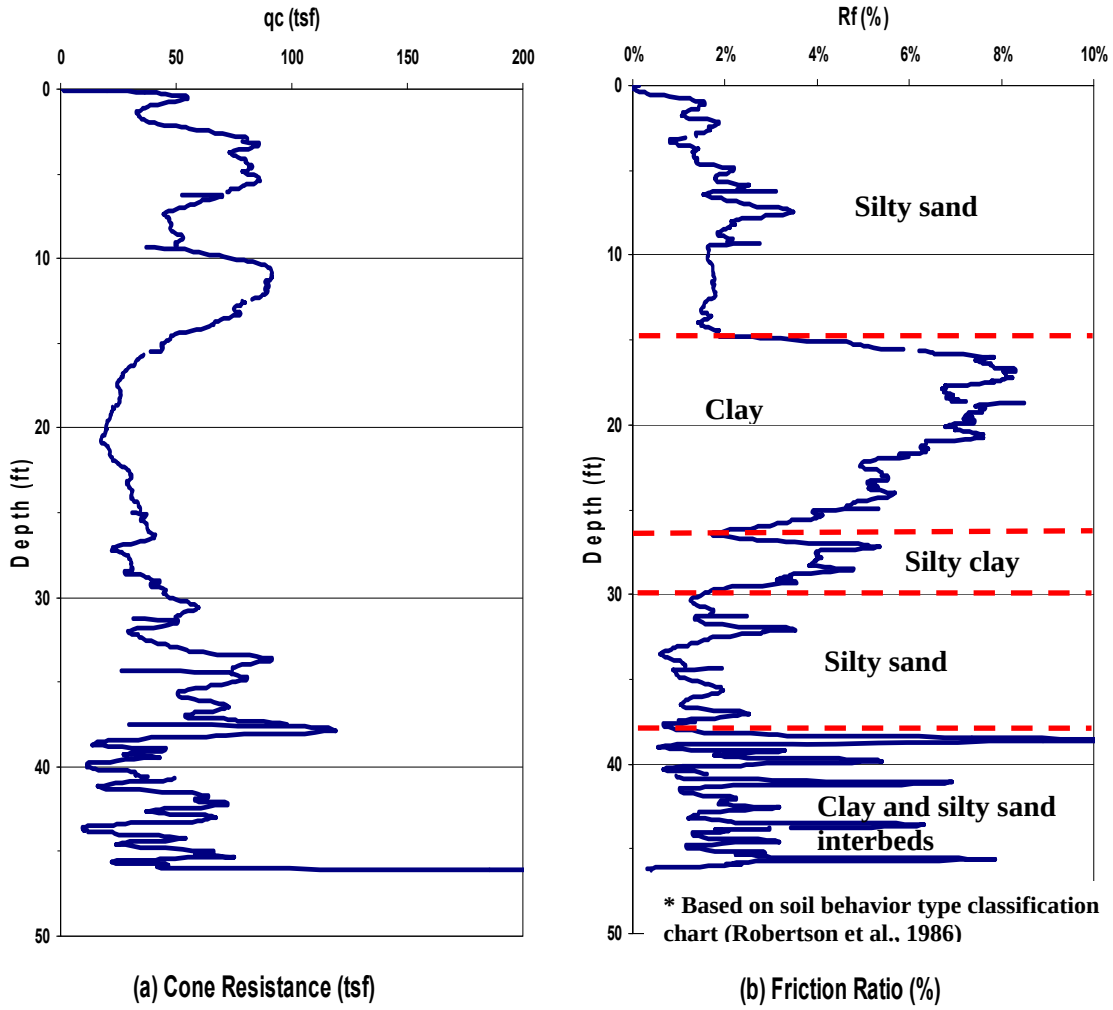

Figure 7.1: CPT Profiles for Seismic Cone Tests Using Two Different Sources at Platt 4 of the Hornsby Bend

7.3 V_S PROFILING WITH SINUSOIDAL SOURCE

The focus of this work was on V_S profiling dispersion in shear wave velocity and not material damping measurements.

Thumper was used as the sinusoidal source over the frequency range of 20 to 200 Hz in these tests. This frequency range was selected because the theoretical output force

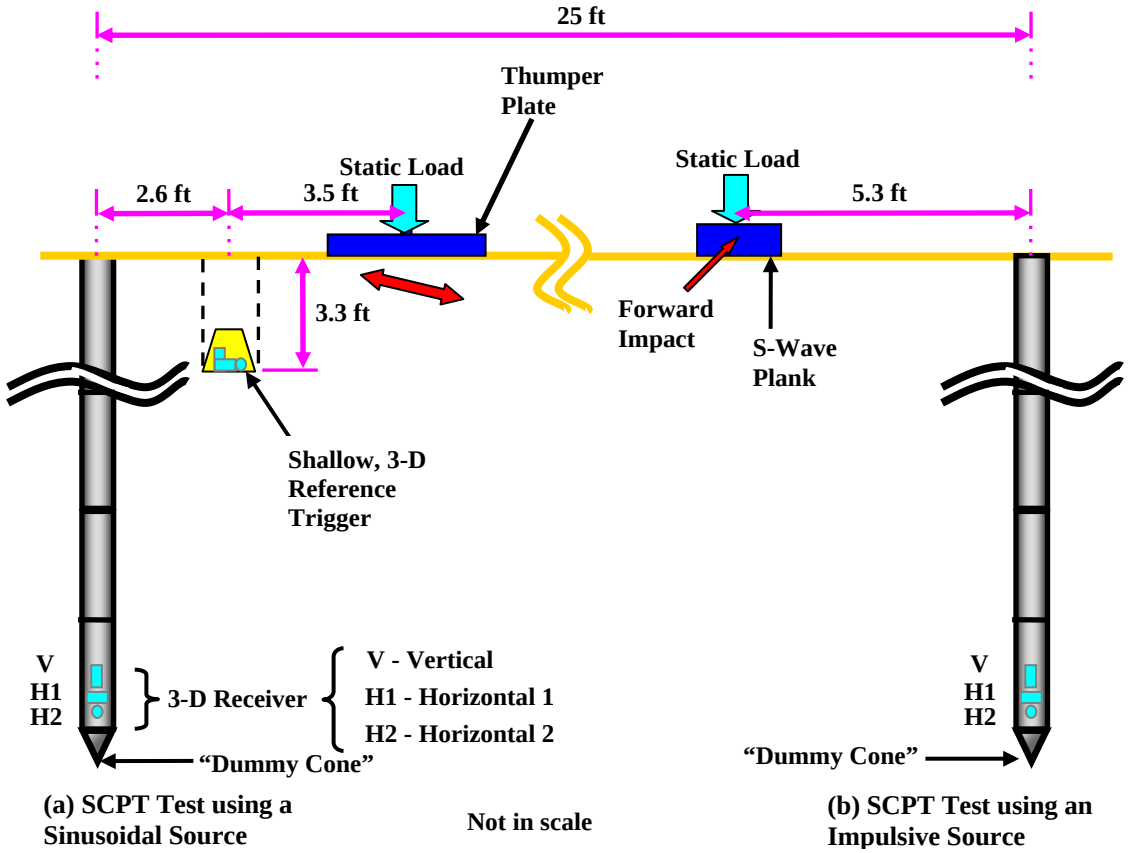

Figure 7.2: Testing Setup Used in SCPT testing with an Impulsive Source and Sinusoidal Source

is a constant maximum force. The phase between the H-2 horizontal geophone in a shallow, 3-D reference sensor at depth of 3.3 ft and the H-2 horizontal geophone in a seismic cone at depth of 30.4 ft were calculated with the internal calculation procedure of a dynamic signal analyzer in real time as shown in Figure 7.3a. The unwrapped phase is plotted in Figure 7.3b. The phase velocity is calculated with the calculation procedure described in Chapter 6 and plotted in Figure 7.3c. In the same procedure, the transfer function between two sensors was calculated in Figure 7.4 when the seismic cone was located at depth of 36.9 ft. The transfer function between the H-2 horizontal geophone in the seismic cone at depths of 30.4 and 36.9 ft is calculated and plotted in Figure 7.5.

The waveform signals collected with the seismic cone test with an S-wave plank struck by a sledge hammer were cross correlated in the time domain as described in Chapter 5. The V_S profile was used to be compared with the V_S profile obtained with Thumper.

V_S profiles obtained with two different sources are plotted in Figure 7.6. The profiles are quite similar except in depth range of 40 to 47 ft. In this range, the cross-correlation results show significant differences. The reason (s) for the differences are unknown but it is likely that reflections of the shale at a depth of about 50 ft contribute to these differences. Thumper can be useful source when testing at deeper depths because the force output is much larger than a sledge hammer (see Figure 4.16). Output voltages of H2 geophone excited by S-waves generated with Thumper and a sledge hammer at 47.9 ft Depth are compared in Figure 7.7.

7.4 SUMMARY

The phase velocities of S-waves generated by a sinusoidal source (Thumper) were calculated and the V_S profile was compared with V_S profile calculated with cross correlation of S-waves generated by an impulsive source (S-wave plank with a sledge hammer). Both profiles show overall similar V_S profiles. Thumper can be a useful source in deeper depth due to the larger out force.

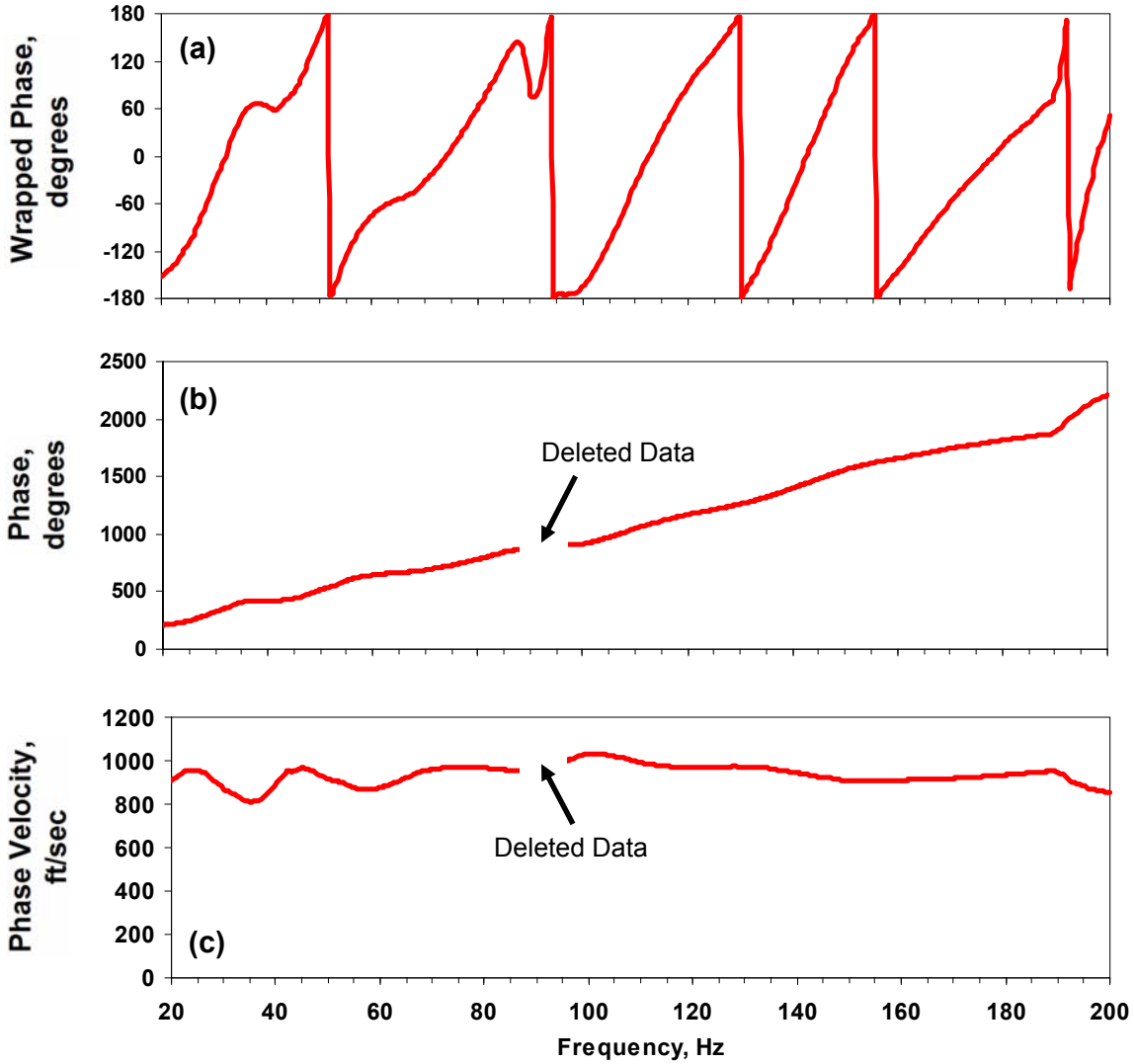

Figure 7.3: Analysis of the Transfer Function of Two Waves Recorded from Embedded Reference Sensor at Depth of 3.3 ft and Seismic Cone at Depth of 30.4 ft at the Same Time (Source: Thumper): (a) Wrapped Phase, (b) Unwrapped Phase, and (c) Phase Velocity

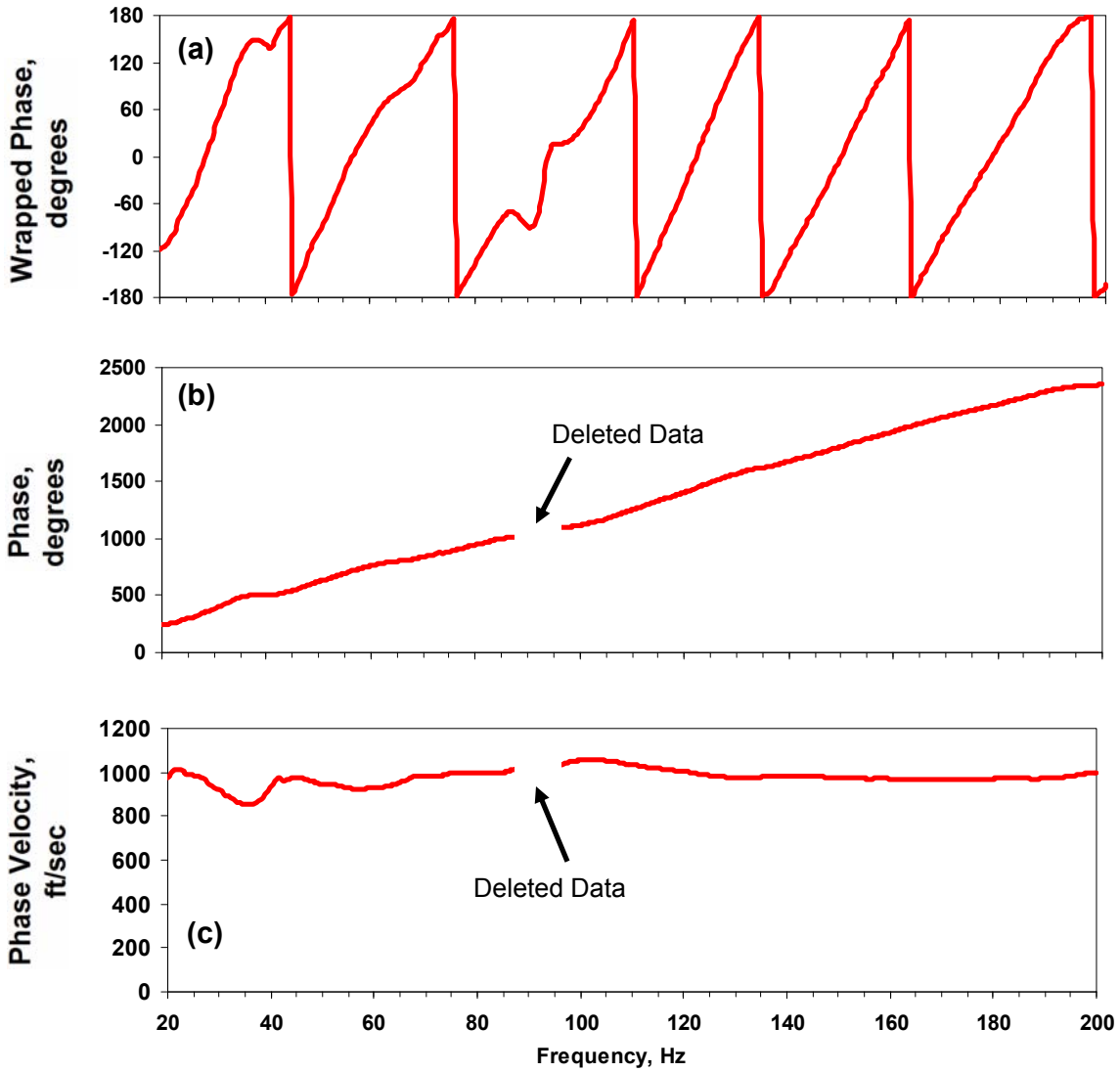

Figure 7.4: Analysis of the Transfer Function of Two Waves Recorded from Embedded Reference Sensor at Depth of 3.3 ft and Seismic Cone at Depth of 36.9 ft at the Same Time (Source: Thumper): (a) Wrapped Phase, (b) Unwrapped Phase, and (c) Phase Velocity

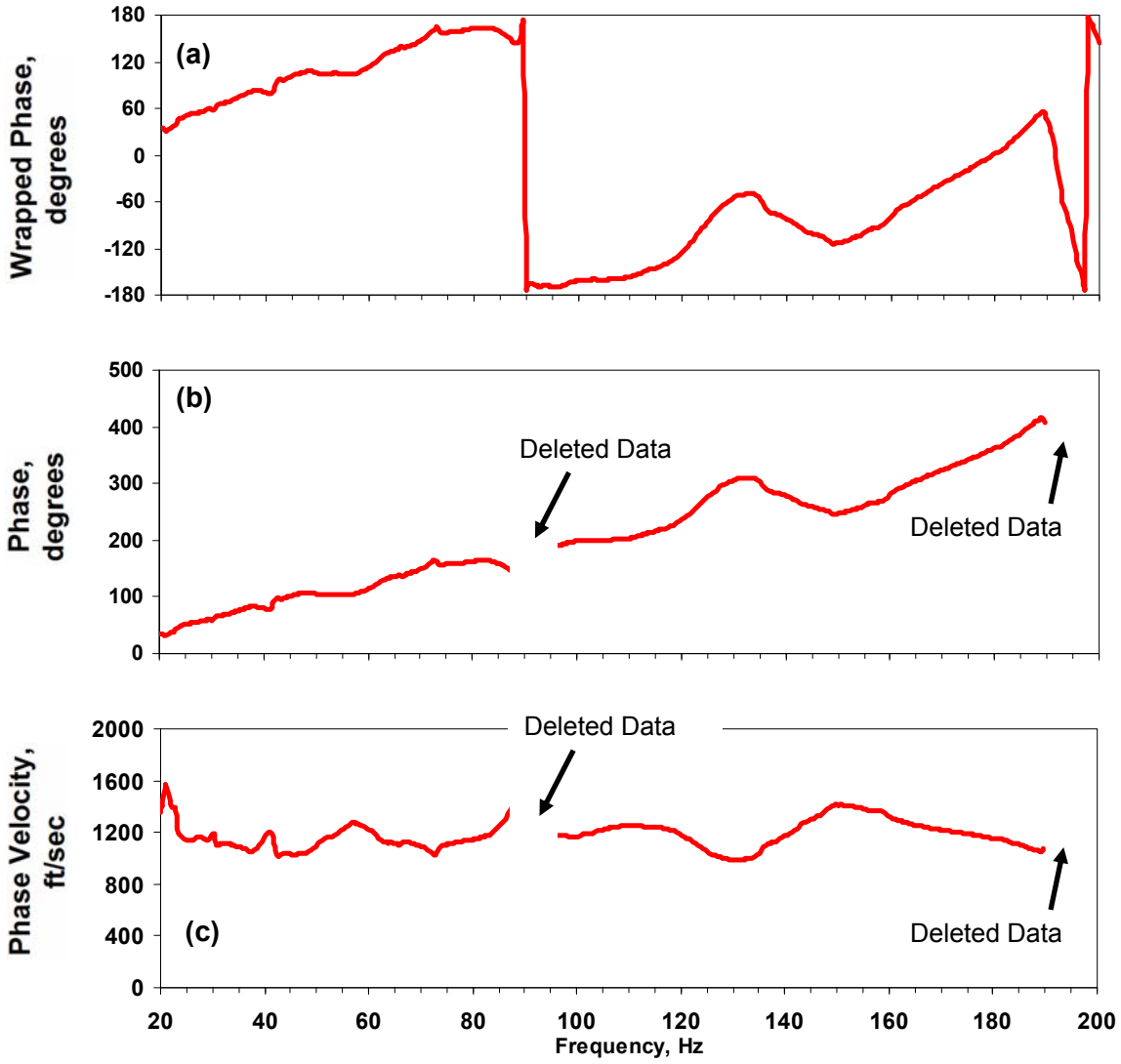

Figure 7.5: Analysis of the Transfer Function of Two Waves Recorded from Seismic Cone at Depth of 30.4 ft and Seismic Cone at Depth of 36.9 ft in Different Time (Source: Thumper): (a) Wrapped Phase, (b) Unwrapped Phase, and (c) Phase Velocity

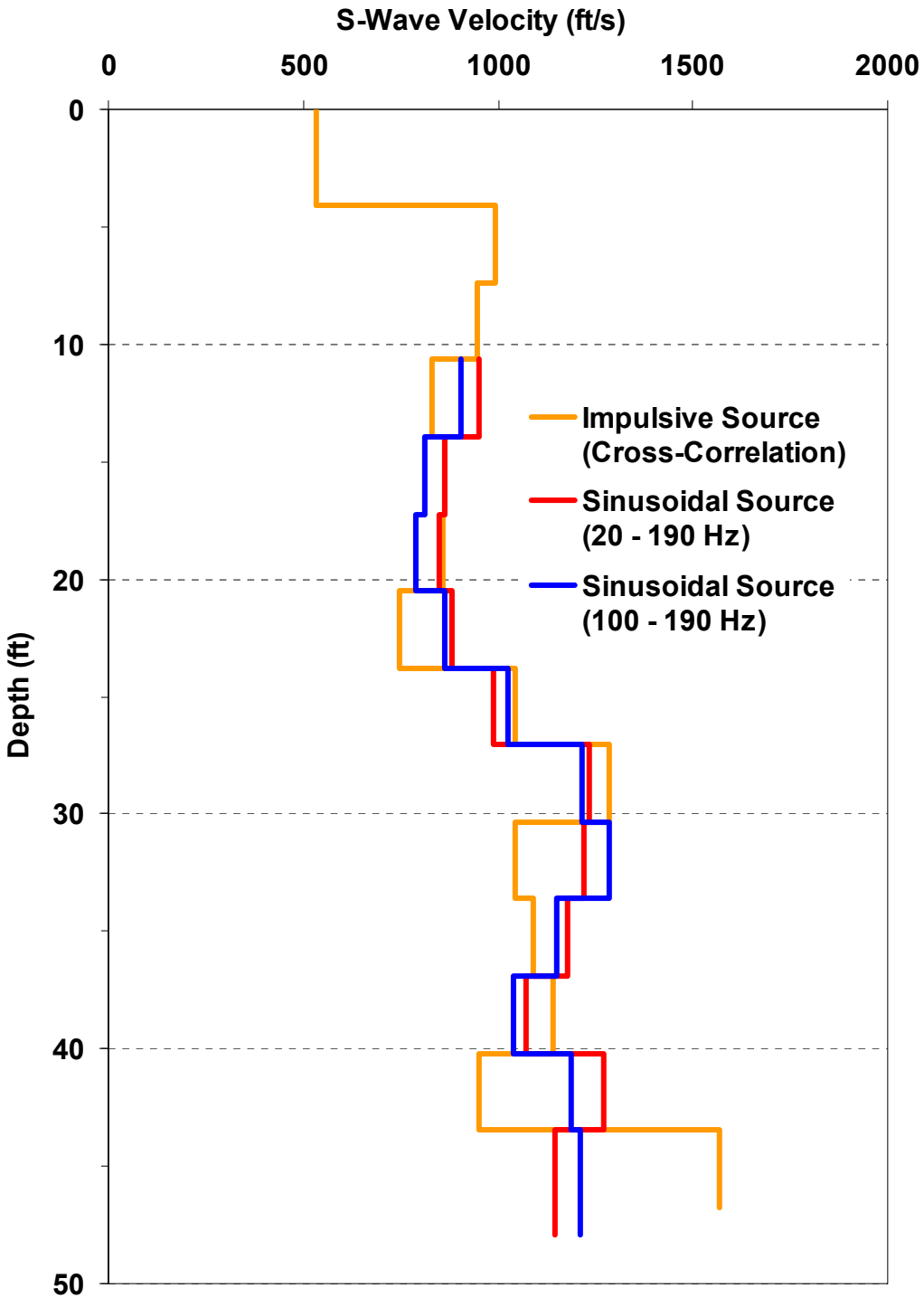

Figure 7.6: Comparison of V_S Profile Comparison for Shear Waves Generated by Thumper and an S-Wave Plank Struck a Sledge Hammer at Platt 4

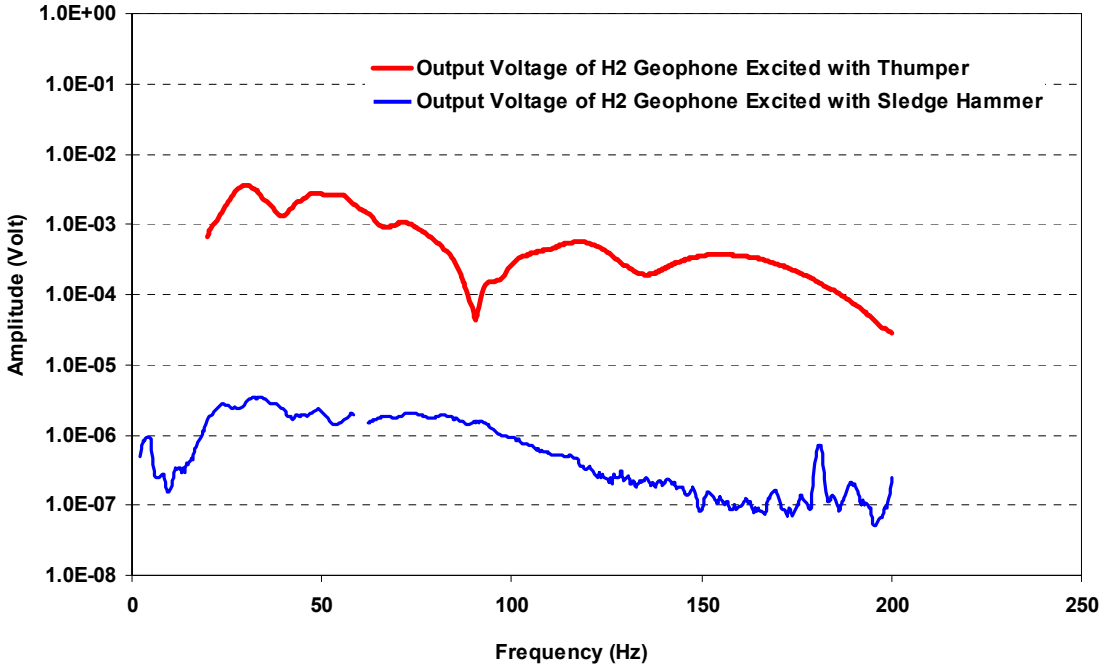

Figure 7.7: Comparison of Output Voltages of H2 Geophone Excited by S-Waves Generated with Thumper and a Sledge Hammer at 47.9 ft Depth.

Chapter 8: Summary, Conclusions and Recommendations for Future Work

8.1 SUMMARY

Body wave velocities and material damping ratios are important dynamic soil properties in characterizing soil and rock profiles for all types of loading and profiling situations. Wave velocities and material damping ratios are determined by performing in-situ seismic tests and dynamic laboratory tests. Normally, the in-place soil dynamic properties at small strains, especially the soil stiffness, can only reliably obtained with in-situ seismic tests. In-situ measurements of shear and compression wave velocities have been widely used in civil engineering for more than four decades. As a result, testing and analysis procedures of the in-situ seismic tests have been generalized. The best examples of these measurements are the traditional crosshole and downhole seismic tests. The downhole seismic test has been adapted to include seismic cone penetration testing (SCPT) in the 1980's. There have been little changes in the SCPT since the 1990's, with the same sensors, sources, test procedures, and analytical methods being employed. In this research, the sensors, sources, test procedures and analytical methods of downhole seismic testing are discussed and improved.

The instrumentation used in the downhole and SCPT tests is one of the essential components to improve. Using proper seismic sources, receivers, triggers and data acquisition systems is important in generating, monitoring and recording P- and S-wave signals. Downhole or SCPT testing with two, 3-D receivers is the preferred method so that true-interval velocities can be measured in time-domain and frequency-domain recordings.

A seismic cone following the nominal dimensions of ASTM D5778-07 was designed and developed. The seismic cone includes a 3-D receiver consisting of 24-Hz

geophones in a Teflon inner housing protected by a metal housing in a dummy cone. The three, 24-Hz geophones were connected to an electrical cable protected with a Polyurethane jacket. The seismic cone was calibrated before and after assembly using a shake table. This seismic cone was successfully used in SCPT testing in this research. Two, near-surface, reference sensor triggers were constructed. These reference trigger had three, 24-Hz geophones mounted in marine epoxy housing. They were generally buried at a depth of about 3.3 ft (1 m) below the ground surface. The reference triggers were used to perform spectral analysis of body waves (SABW) for use in investigating dispersive phase velocities and dispersive material damping ratios in soil.

The procedures used in downhole and SCPT testing in this research are described. The testing setup, installation of sensors, generation of body waves using impulsive sources and a sinusoidal source, and extraction of sensors are discussed.

Seismic cone testing and CPT testing (equivalent to a single SCPT system) were performed close to each other at Lower Tract B at the Hornsby Bend site. The seismic cone testing was performed with the traditional downhole testing procedure using a horizontal geophone in a 3-D receiver and an S-wave plank struck by a sledge hammer. The collected data were presented in a waterfall-type plot over the entire test depth. The relative P-wave amplitude in the waterfall plot normalized using the peak S-wave amplitude increased with the increasing depth due to the rotation of the seismic cone. The rotated angle of the seismic cone was estimated using the relative difference of amplitudes of output signals of two horizontal geophones. The estimated rotation angles were compared with actual rotated angles in the laboratory set.

The data collected with the two-step SCPT test at Platt 4 at the Hornsby Bend site were analyzed in time-domain records to calculate S- and P-wave velocities. Polarized shear waveforms obtained with the properly oriented horizontal H-2 geophone were used

in these analyses of S-waves. S-wave velocities calculated using different reference points and cross correlation of wave signals were plotted versus depth. The V_S profiles are compared and discussed. Wave signals generated by a P-wave source were monitored with the seismic cone using the horizontal H-1 geophone and the vertical geophone. First P-wave arrival times and other references of the P-wave signals are discussed and used to calculate P-wave velocities from time-domain records. P-wave velocities were also calculated using cross correlation of the full waveforms as well as windowed waveforms. The V_P profiles are plotted, compared and discussed.

A frequency-domain method, called the Spectral-Analysis-of-Body-Waves (SABW) method has been developed in this research. The SABW method uses the same procedure for wave velocity calculations as the procedure used in the Spectral-Analysis-of-Surface-Waves (SASW) method. Both methods use the transfer function between the outputs of two sensors. The phase differences and amplitude differences between the outputs of the two sensors are used to calculate phase velocities and field material damping ratios. The phase and amplitude differences are calculated and plotted in real time with the internal calculation procedure in a dynamic signal analyzer. Moreover, the phase velocity and material damping ratios over various depth intervals were calculated using a 3-D reference trigger buried at a shallow depth. Analysis of the dispersion curves of phase velocities and material damping ratios is shown to allow general characterization of soil types in terms of sand versus clay.

SCPT, SASW, and downhole tests were performed at Platt 4 and Lower Tract B of the Hornsby Bend site. The V_S profiles obtained using seismic cone tests with an impulsive source and a sinusoidal source are compared and discussed. The testing site at Platt 4 was investigated and sectioned into four areas. Cone resistance, friction ratio, V_S and V_P profiles obtained with the SCPT in the four areas are compared and discussed. A

2-D V_S profile is plotted with eight V_S profiles obtained at the test array of the straight line of 660 ft (200 m).

8.2 CONCLUSION

8.2.1 Improvement of SCPT sensor

For the SCPT sensor, a 3-D receiver package was selected to replace the 1-D horizontal receiver traditionally used. To choose the 1-D sensors to be mounted in the 3-D receiver package in the seismic cone, a GEO GS-14 24-3400 L3 geophone that has a natural frequency of 24 Hz, a damping ratio of 40 %, and a coil resistance of 3400 ohms was compared with a GEO GS-14 28-570 L3 geophone with a natural frequency of 28-Hz. The 28-Hz geophone has generally been used as the horizontal sensor SCPT. The 24-Hz geophone was selected for use instead of the 28-Hz geophone due to larger output and somewhat increased frequency range with a constant calibration factor. The seismic cone with the three, 24-Hz geophones was calibrated before and after assembly using a shake table and two reference sensors (an accelerometer traceable to N.I.S.T. and a proximitor calibrated with equipment traceable to N.I.S.T.). The phase difference between geophones is less than 5 degrees in the frequency range of 5 to 300 Hz and the response curves are very similar because the same type of geophones, Teflon housing, and metal housing acted in phase during testing on the electromagnetic shaker.

8.2.2 Estimation of Sensor Rotation in SCPT Testing

Rotation of the seismic cone due to connecting rods and during pushing was estimated using the amplitudes of the output signals of the two horizontal geophones in the 3-D receiver in the seismic cone. Estimates of the rotational angles evaluated during field testing were compared with actual rotated angles in a set of laboratory tests. The

estimated angles obtained from linear, best-fit equations were close to actual rotated angles of the seismic cone. Estimated angles determined over frequencies ranging from 5 to 15 Hz and 60 to 600 Hz gave the best comparisons for the seismic cone with the 24-Hz geophones with a damping ratio of 40 %.

8.2.3 Comparison of SASW and SCPT test results

Shear wave velocity profiles determined by the SASW and seismic cone tests show good agreement in the V_S profiles at depth with V_S generally increasing with depth. However, the differences between the two test results did regularly occur near the ground surface, usually in the top 15 ft. The main reasons for this difference are attributed to the SCPT (and downhole) tests with the V_S profiles from the seismic cone tests showing larger S-wave velocities at these shallow depths. These differences occur primarily because of the following reasons.

1. Differences in distances that the body waves travel along inclined paths at two different depths in the top 10 ft is small at these shallow depths and the exact distance is difficult to estimate due to wave refractions so that (small) errors arise in the V_S and V_P calculations.
2. The soil layer or layers above the first downhole or SCPT measurement depth (top 3 to 5 ft) represents an average value in a zone that usually includes gradients and lateral variability.
3. Body waves generated in seismic cone testing generally are likely refracted near the surface and the travel path is unknown.
4. V_S profiles determined by SASW testing represent global measurements over lateral distances on the order of the test depth while results from SCPT testing represent localized measurements near the probe hole.

8.2.4 V_S and V_P measurements using time-domain methods in SCPT testing

S_{vh} waves generated by an S-wave source can be clearly recorded by a horizontal H-2 geophone (oriented parallel to the source impact) in the 3-D receiver using two sets of polarized waveforms generated by impacting the S-wave plank in opposite directions. The first arrival and other reference points (first peak, first trough and crossover points) can be picked in the polarized waveforms. Picking the other reference points can be automated unlike picking the first arrival.

Cross correlation of signals generated with the S-wave source is a very useful method of calculating interval travel times of the S waves. Cross correlation, unlike picking first arrivals or other reference points, utilizes the complete waveform to calculate the time shift in the time domain because full-waveform cross correlation minimizes distortion in the waveform and operator biases. As a result, the V_S profile obtained by cross correlation of full waveforms exhibited less scatter than other V_S profiles obtained by the first arrival and other reference points. The average value of S-wave velocities calculated from the first arrival and other reference points at each measurement depth is very similar to the velocity calculated with cross correlation.

Using a vertical geophone and a horizontal H-1 geophone can maximize the likelihood of picking the correct first arrivals of P-waves generated by a vertical-impact source (P-wave source). With the waterfall plot obtained by the vertical geophone, the existence of the water table could be identified by showing waves before the arrival of P-waves in soil. Picking other reference points is not easy because of distortions in the P waveforms. Using a proper window in analyzing P waveforms is critical for cross correlating the waveforms and calculating P-wave velocities.

8.2.5 V_S and material damping measurements, and soil type characterizations using the SABW method

The Spectral-Analysis-of-Body-Waves (SABW) method was developed as a frequency-domain method for use in downhole and SCPT testing. The SABW method uses the phase difference between the outputs of two sensors to calculate phase velocity just like the Spectral-Analysis-of-Surface-Waves (SASW) method. This frequency method has three key advantages.

1. The phase difference can be automatically calculated in real time with the internal calculation procedure of a dynamic signal analyzer. The V_S profiles calculated with cross-correlation in time domain method and the SABW method are very similar.
2. Field material damping ratios can be determined using the transfer function between the output amplitudes of monitoring sensors in the SABW frequency-domain analysis. The equation of wave motion used in the spectral-ratio method is modified for frequency dependency of material damping ratio and a reference, near-surface geophone is used to normalize the two signals of seismic cone that were recorded at different times and depths. A limited frequency range should be used in the equation. The frequency range depends on the output characteristics of the geophone sensor, the resulting wavelengths, and the distances from the source.
3. The SABW method can be used to form a general characterization of the soil type based on the dispersive characteristics of waves that propagate through the material. For instance, the phase velocity and material damping ratio obtained from field testing increased as the frequency increases in clay layer, while the phase velocity in a silty sand layer is nearly constant and the material damping ratio only increased slightly.

8.2.6 Characterization of soil profile using in-situ seismic tests

SCPT (consisting CPT and seismic cone tests), SASW and downhole tests were performed at different locations of the Hornsby Bend site and at different times as a part of this and other research projects. The findings are discussed below.

1. The phase of S-waves generated with a sinusoidal source (Thumper) can be calculated in real time. The V_S profile calculated with the phase exhibits similar values to the V_S profile calculated with cross correlation of S-waves generated by an impulsive source (S-wave plank and a sledge hammer). Thumper (or T-Rex) can be a useful source in deeper profiling due to the larger force that can be generated.
2. Shear wave velocity profiles obtained along a test array with seismic cone tests were useful in creating a 2-D profile that interpolates the velocity profiles at other locations that tests are not performed.
3. The SASW test shows better resolution than the SCPT test at shallow depths (top 15 to 20 ft). However, the seismic cone test shows better resolution in the depth range of 20 to 40 ft that was tested in this research, with small inversions formed.

8.3 RECOMMENDATIONS FOR FUTURE WORK

Three main areas are worthy of additional research. The first area deals with improving the SCPT 3-D sensor. The improvements should be:

(1) Assembling the CPT portion of the test in the seismic cone. Then uncertainties with differences in testing locations and testing times would be eliminated.

(2) Using geophones with a lower natural frequency and higher damping ratio would increase the useable frequency range where the calibration factor is constant.

(3) Making additional 3-D seismic cones would permit the operator to embed a 3-D reference receiver (seismic cone) at deeper depths to avoid possible near-field effects.

(4) Develop a seismic cone system that has multiple 3-D receivers located a set vertical distances in one probe rod, say spaced at 1-m intervals.

The second main area deals with studying soft ground at deeper depths and with high PI material to evaluate dispersion curves of phase velocity and damping ratio with various sources. The final area deals with developing the SABW method to measure P-wave velocities and material damping ratios in compression. Numerical modeling should also be used to study the parameters that influence phase velocity and damping ratios in compression. Various windows and filters can be designed for use in the P-wave analyses.

Appendix A: V_S Profiling following Conventional SCPT Testing and Analysis Procedures

A.1 INTRODUCTION

To begin this research, SCPT testing was performed following conventional testing and analysis procedure at Lower Tract B, Hornsby Bend, Austin, Texas. The focus of this work was on: (1) developing a set of data with which the SCPT testing using the SABW method could be compared, (2) evaluating the functionality of the 3-D sensor, (3) determining S-wave velocities based on first arrivals, (4) comparing V_S profiles from SCPT and SASW tests and (5) investigating sensor rotation resulting from connecting rod and pushing the probe forward. The SCPT testing consisted of CPT testing and seismic cone testing that were performed in slightly different locations. A horizontal geophone (H-2) in the 3-D seismic cone was used to monitor vertically propagating and horizontally polarized shear waves (S_{vh} waves). A dynamic signal analyzer was used to record the output signals from the geophone.

Seismic cone testing was performed at depth intervals of 3.3 ft (1 m). The output signals recorded in the time domain were plotted together for all depths where seismic measurements were performed. The group of time-domain output signals recorded for all depths was plotted and analyzed. This time-domain plot is called a waterfall plot. The waterfall plot was used to find the first-arrival times of shear waves. In conventional in-situ test data analyses, picking the first-arrival times of shear waves is critical in calculating the correct shear wave velocities. A horizontal geophone oriented parallel to the plank source is used to maximize amplitudes of the output signals generated by the shear waves. However, the horizontal geophone might rotate little by little while the seismic cone is pushed further and further into the ground. Any rotations in the horizontal

geophone in the seismic cone were checked using a procedure described in this chapter. Rotations of the seismic cone were verified with laboratory tests.

The testing site, Lower Tract B of the Hornsby Bend, is briefly described in this chapter. The testing site is described in detail in Appendix B. The conventional SCPT data analyses are described in detail in this chapter.

A.2 TESTING SETUP

SCPT testing has enabled engineers to simultaneously perform CPT and downhole seismic testing in the same field setup. The traditional SCPT test consists of an S-wave source at the ground surface and a 1-D, horizontal receiver positioned above the cone portion of the CPT device as shown in Figure A.1 (Campanella et al., 1986). A simple plank source is used to generate shear (S) waves. The plank source is heavily loaded vertically so that it is well coupled to the ground. The plank is typically located about 2 to 3 m from the point where the SCPT is penetrating the ground. Each end of the plank is struck horizontally multiple times (normally 3 to 5) with a sledge hammer to generate shear waves and obtain average waveforms in the time domain. The shear waves are vertically propagating and horizontally polarized (S_{vh} waves), and are typically assumed to travel along a straight ray path from the source to the 1-D, horizontal receiver at a known depth. Impacts to the source in opposite directions are typically called "forward" and "reverse" impacts, with the forward direction arbitrarily chosen.

One benefit of the downhole configuration is that vertically propagating S_{vh} waves often travel downward with little conversion to other wave types due to the combination of nearly vertical propagation and often nearly horizontal layering. The S_{vh} waves generated by the source are monitored at depth by the 1-D horizontal receiver in

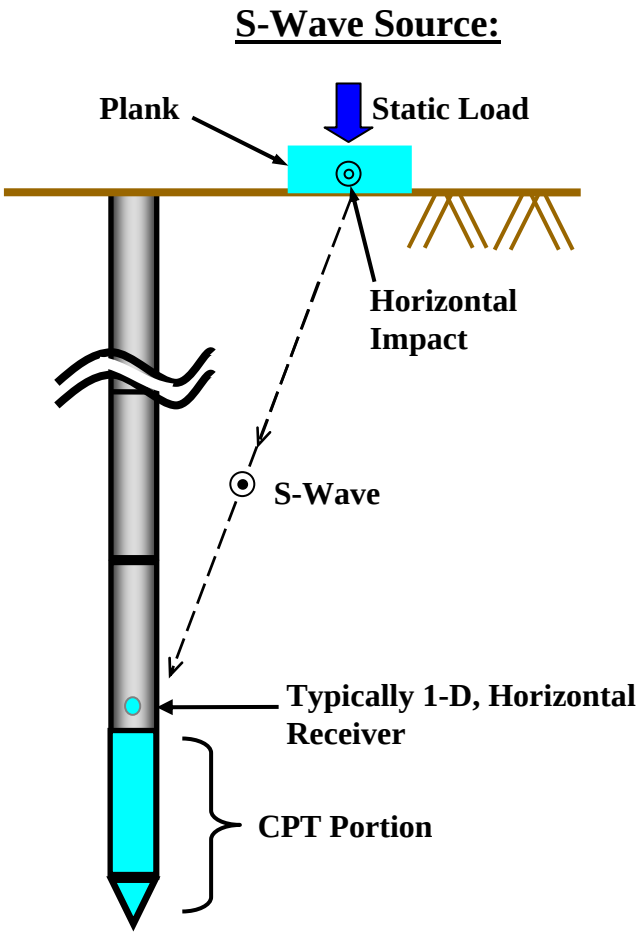

Figure A.1: Setup for V_S Profiling in Traditional SCPT Testing Using One Horizontal Receiver to Measure S waves

the SCPT and the time-domain waveforms are recorded. The straight-ray-path distance between the source and 1-D receiver is calculated from the setup geometry. Other wave paths that involve some refraction depending on the velocity profile can also be considered (Mok, 1987, Batsila, 1995 and Kim et al, 2004). The first-arrival times or the times of other reference points of the S_{vh}-waves are identified. The time difference of the S_{vh}-wave first arrivals (which are the only reference points used in this chapter) and the distance between the test depths are used to calculate the S_{vh}-wave velocities.

In this research, SCPT testing was performed in two separate steps. The first step was simply a CPT test. A Fugro, 15-cm^2 cone with a Fugro M1507501.EHE Digital Land Based CPT recording system was used in this step. In the second step, a dummy 15-cm^2 cone was used in which a 3-D geophone sensor was installed. The dummy cone was used because the first part of this study only involved developing a 3-D receiver that would work well in this application and a prototype (dummy cone) that could be easily and economically modified was needed in the developmental process. The second step is called the "seismic cone" herein and the combination of the first and second steps is loosely referred to as an SCPT test. The two-step testing process resulted in the CPT and seismic cone tests being performed at slightly different times and at slightly different surface locations. The testing times were generally within one day and the locations were within 15 ft.

The setup for the seismic cone test is shown in Figure A.2 and consisted of a shear-wave plank source and a 3-D receiver in the dummy cone. The S-wave plank was located about 7 ft (2.1 m) away from the seismic cone surface location. To maximize the recorded amplitude of the S_{vh}-waves, the orientation of the H2 horizontal geophone in the 3-D seismic cone receiver was aligned parallel to the direction of the horizontal impacts applied to the S-wave plank. This alignment was done at the ground surface at the start of testing. However, one complication is that this alignment can be inadvertently compromised during attachment of the first few rods during the advancement process as shown (subsequently in this chapter).

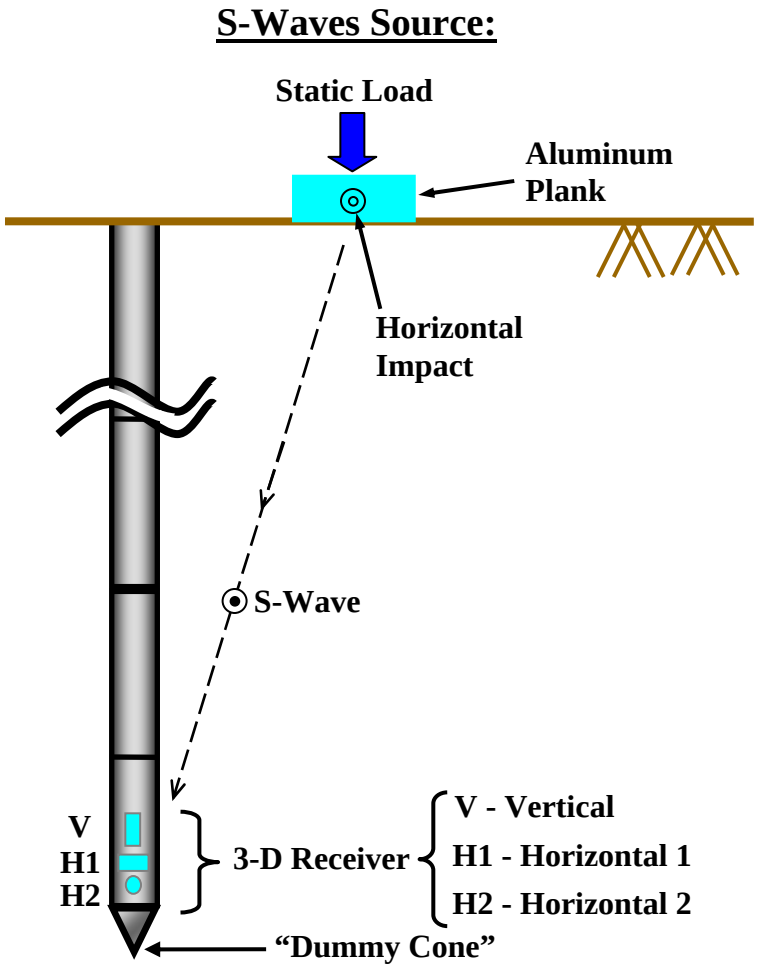

Figure A.2: Setup for V_S Profiling in SCPT Testing Performed in This Research

A.3 Results of CPT Testing

A test site in Austin, Texas was selected for this study based on the soil profile and its proximity to The University of Texas. The test site is called Hornsby Bend and it is located on a historical farm field near the Austin-Bergstrom International Airport, about 10 miles from the University as shown in Figure A.3. The short distance relative to the University of Texas enabled the heavy T-Rex vibroseis to be easily used in this research. T-Rex has a hydraulic cylinder on the back bumper that is used to perform CPT testing. The first SCPT test was performed at an area of Hornsby Bend that is called

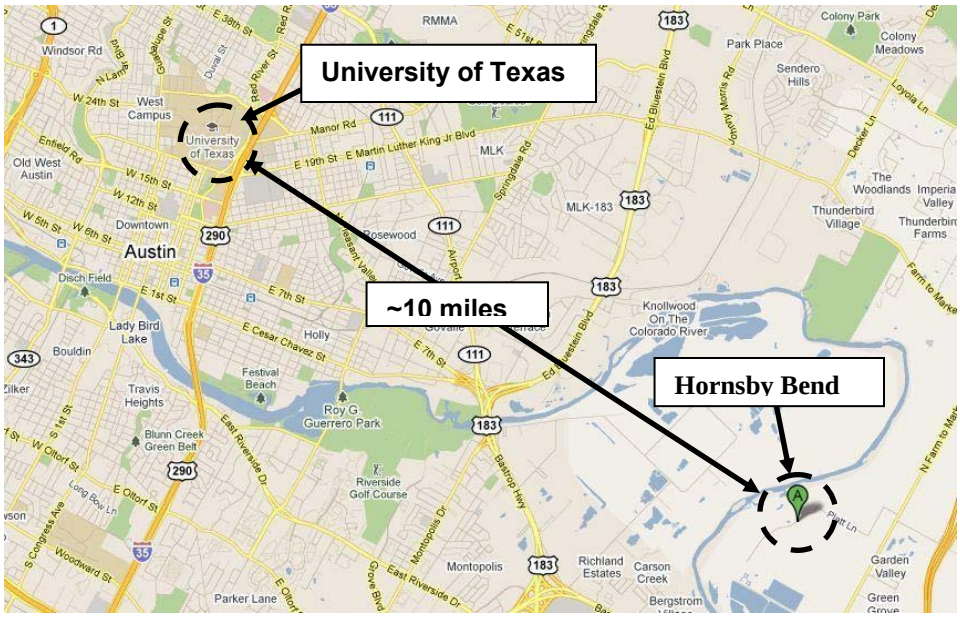

Figure A.3: Location of the Hornsby Bend Site Relative to University of Texas

Lower Tract B. Lower Tract B is shown in Figure A.4. Before any seismic cone testing was conducted, Cone Penetration Testing (CPT) was performed around the site to characterize the subsurface profile. Cone tip resistance and friction ratio were used with the classification chart published by Robertson et al. (1986b) to interpret the geotechnical profile. These results at one location are plotted in Figure A.5. The interpreted soil profile from the ground surface to a depth of 44 ft consists of five layers. The thickest layer is a silty sand layer in the depth range of about 8 to 30 ft. A soft layer consisting of clay and sand interbeds exists in the depth range of about 30 to 40 ft. These layers and the rest of the soil profile are used in the example SCPT measurements to compare the shear wave velocity and soil profiles obtained from the cone testing.

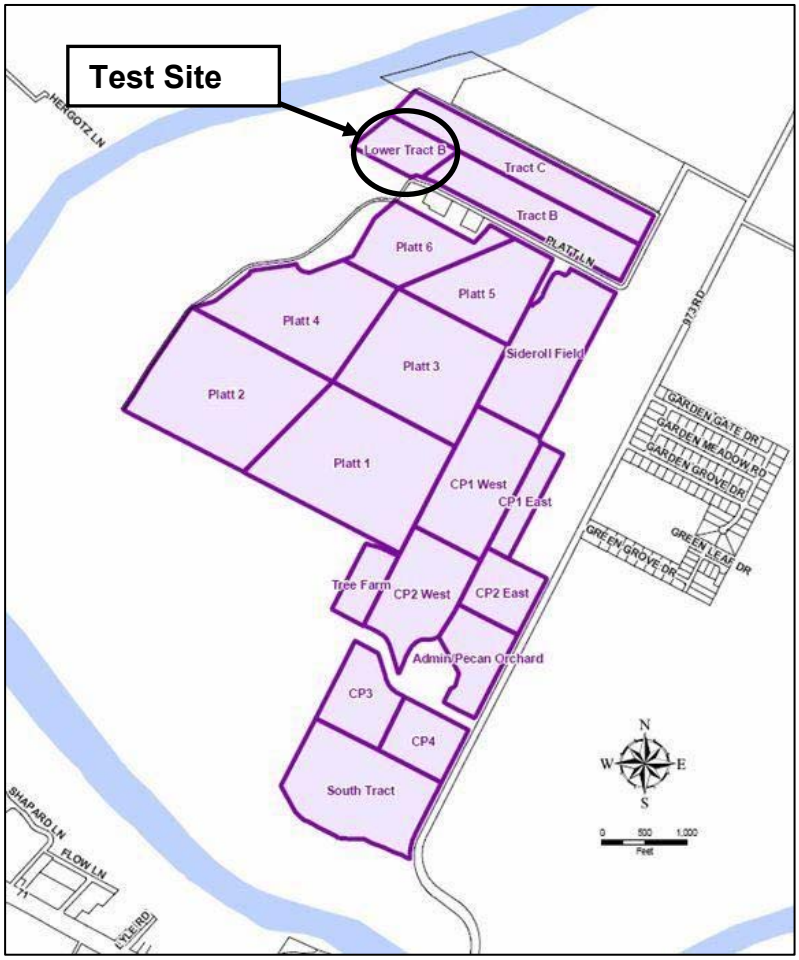

Figure A.4: Lower Tract B at the Hornsby Bend Site

A.4 RESULTS OF SEISMIC CONE TESTING

Seismic cone testing was initially performed using conventional data collection and analysis procedures at Lower Tract B. The field setup is shown in Figure A.2. All data were collected in the time domain. The output from an electrical trigger was recorded on Channel 1 of a waveform recorder. The electrical trigger signal was used to mark a "zero time" which represented the instant when the S-wave plank was struck by the sledge hammer and shear waves were generated at the ground surface. A trigger delay

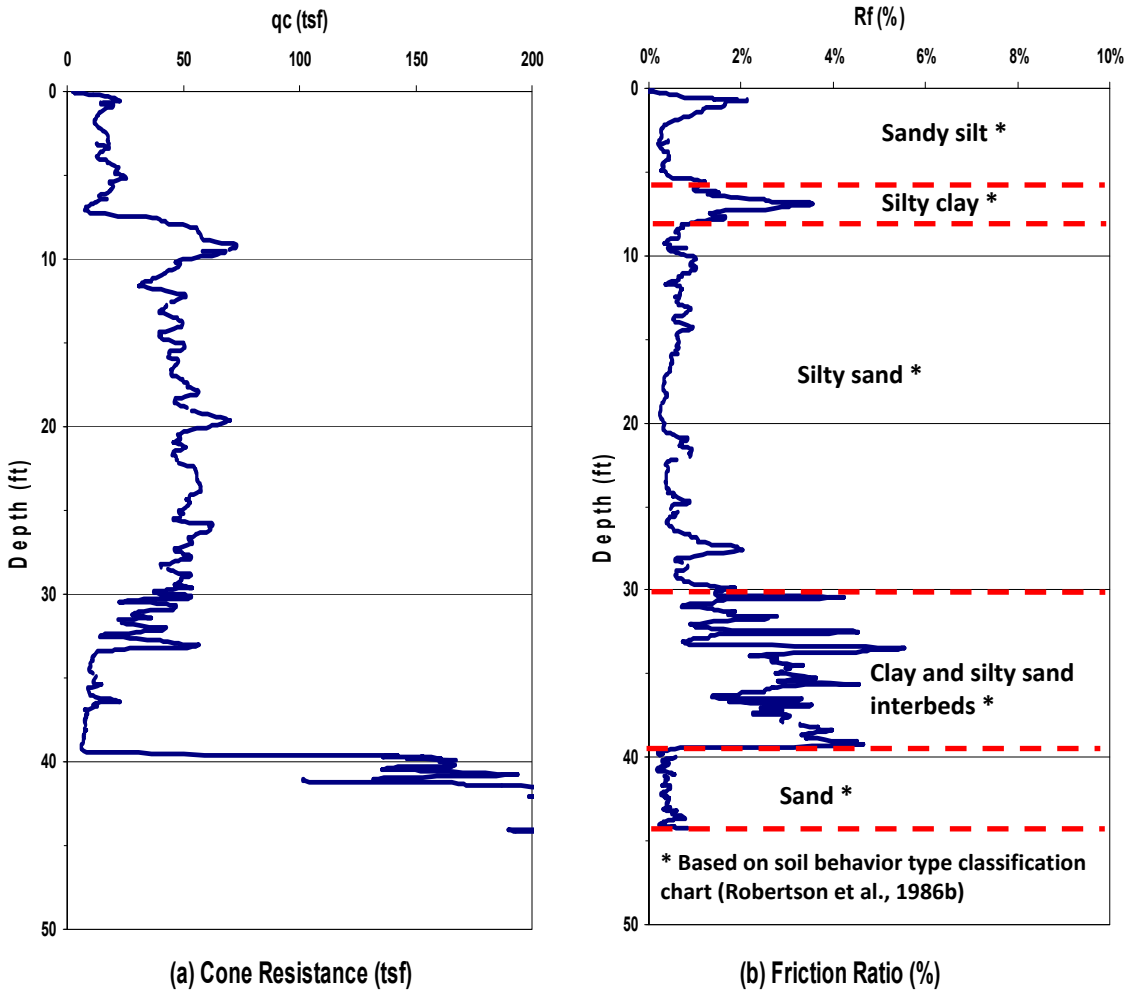

Figure A.5: One CPT Profile at the Lower Tract B Test Site at Hornsby Bend that is Used in the Analysis of the Near-by SCPT Results

time of 0.00465 ms was determined by calibrating the hammer-plank-electrical trigger-recorder system. This trigger delay was used in analyzing the travel-time waveforms obtained from seismic cone tests by adding the delay time to each first-arrival time. A waterfall plot of one set of average shear waveforms that were monitored at 3.3-ft (1-m) depth intervals is presented in Figure A.6. The electrical trigger is plotted at a depth of zero feet in Figure A.6. The trigger time was recorded at each measurement depth and is

marked as zero time. One set of average S_{vh} waveforms that was generated at each depth by striking the S-wave plank in the reverse direction is shown in Figure A.6. The time-domain waterfall plot in Figure A.6 presents the set of average S_{vh} waveforms generated by striking the S-wave plank five times with the sledge hammer in only one direction ("reverse" direction). Waveforms from only one direction are shown to simplify the results and also simplify the analysis of the effect of sensor rotation in seismic cone testing. In Chapter 6, the polarized shear waves generated with both forward and reverse impacts in the time-domain analyses are plotted and discussed in detail. The measurements presented in Figure A.6 were performed over the depth range of 3.9 to 40.0 ft (1.2 to 12.2 m).

The first-arrival times of S_{vh}-waves were carefully picked at each depth. The first-arrival picks are denoted by the red circular dots in Figure A.6. These travel times are presented in Table A.1 and represent travel times along inclined paths. All travel times were then corrected to travel times in the vertical path as conventionally done in downhole seismic testing. The corrected vertical travel times versus depths are plotted in Figure A.7. The four layers that corrected-vertical-travel-time proportionally increased as depth increased are tabulated in Table A.2. The corrected-vertical-travel-time versus depth plot was then best fit by changing the slopes of linear lines through the data to approach R^2 values close to 1. For this data set, four straight lines were used as shown

in Figure A.8. The straight lines represent four S_{vh} velocity layers, with each layer having a uniform velocity. As conventionally done, the shear wave velocity of each layer is simply the vertical interval distance divided by the corrected vertical interval travel time. The analytical method is called the direct travel-time method. The resulting S_{vh} velocities are: (1) Layer 1, V_S = 519 ft/s, (2) Layer 2, V_S = 679 ft/s, (3) Layer 3, V_S = 918 ft/s, and (4) Layer 4, V_S = 762 ft/s.

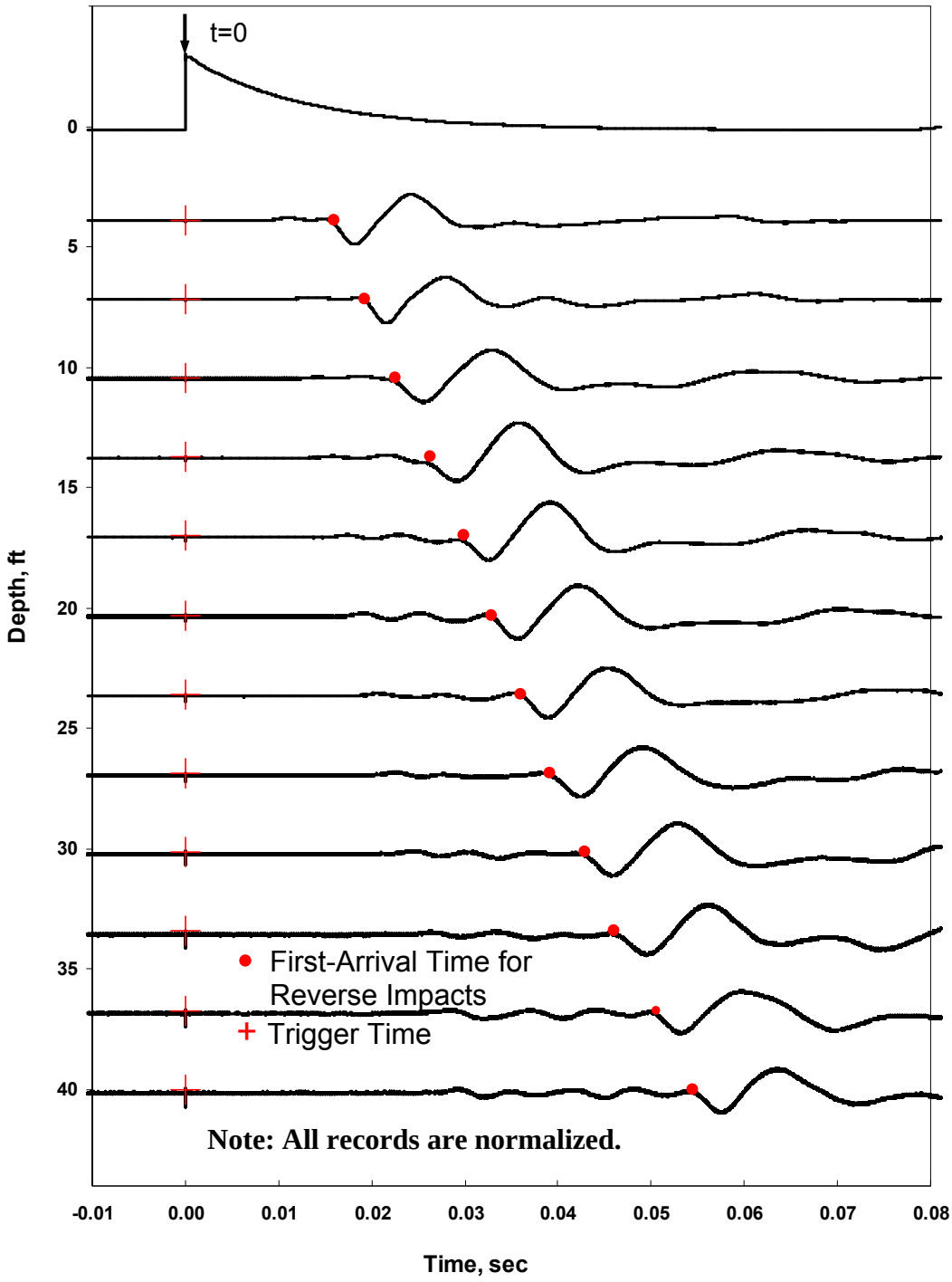

Figure A.6: Waterfall Plot of Average "Reversed" S-Wave Signals Recorded by the Horizontal H-2 Geophone in the 3-D Receiver of the Seismic Cone Obtained 15 ft away from the CPT Profile Shown in Figure A.5

Table A.1: Data Sheet Tabulation Showing the Procedure for Calculating Corrected Vertical Travel Time

Receiver Depth (also termed "Measurement Depth") (ft)	Corrected Inclined Travel Time* (ms)	Inclined Travel Path** (ft)	Vertical Travel Path*** (ft)	Corrected Vertical Travel Time+ (ms)
3.9	15.955	8.0	3.9	7.750
7.2	19.28	10.0	7.2	13.796
10.5	22.526	12.6	10.5	18.715
13.7	26.335	15.4	13.7	23.462
17.0	29.883	18.4	17.0	27.635
20.3	32.906	21.5	20.3	31.107
23.6	36.058	24.6	23.6	34.566
26.9	39.211	27.7	26.9	37.943
30.1	42.89	30.9	30.1	41.778
33.4	46.061	34.1	33.4	45.083
36.7	50.539	37.4	36.7	49.644
40.0	54.497	40.6	40.0	53.680

* Corrected inclined travel time equals total travel time (tt) plus 0.00465 ms
** Assumed straight-ray path between source and receiver
*** Equals receiver depth
\+ Equals (corrected inclined travel time) × (receiver depth) / (inclined travel path)

The resulting S_{vh} velocities of the four layers are shown in Figure A.9. Before the SCPT test was performed at this location in Lower Tract B, Spectral-Analysis-of-Surface-Waves (SASW) tests were performed 15 ft away from the location of the CPT cone. Thus, SASW testing was not be affected by any disturbance in the ground. The CPT testing performed between the locations of the seismic cone and SASW tests was assumed to represent a reasonably representative CPT profile for both seismic-testing locations.

The shear wave velocity profile evaluated by SASW testing near the location of

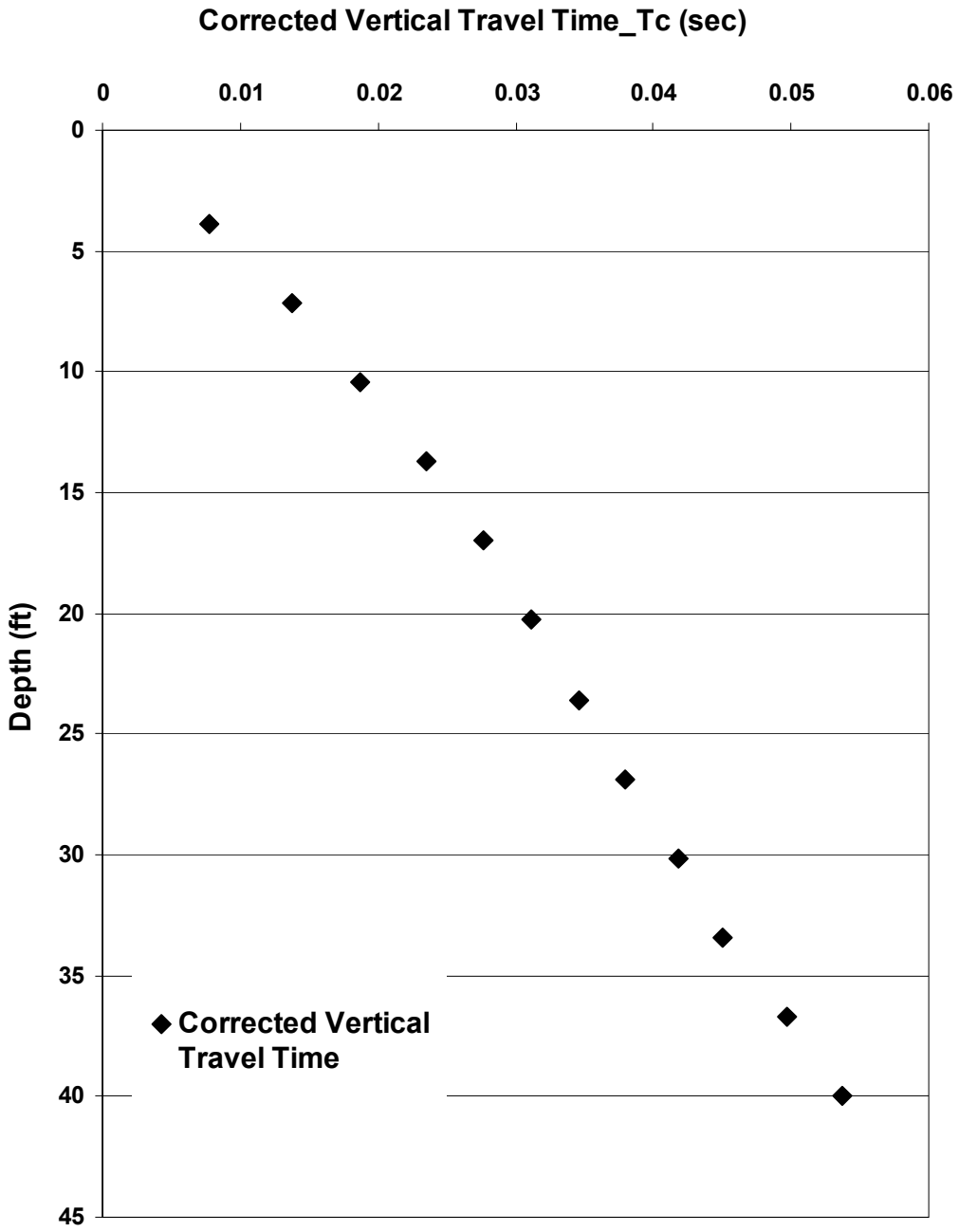

Figure A.7: S-Wave Travel Times Corrected to the S-wave Travel Time in the Vertical Path versus Depth Obtained 15 ft away from the CPT Profile Shown in Figure A.5

Table A.2: Data Sheet Tabulation Showing Four Layers that Corrected Vertical Travel Times Proportionally Increase as Depths Increase

Receiver Depth (also termed "Measurement Depth") (ft)	Corrected Inclined Travel Time* (ms)	Inclined Travel Path** (ft)	Vertical Travel Path*** (ft)	Corrected Vertical Travel Time+ (ms)
7.2	19.28	10.0	7.2	13.796
13.7	26.335	15.4	13.7	23.462
33.4	46.061	34.1	33.4	45.083
40.0	54.497	40.6	40.0	53.680

* Corrected inclined travel time equals total travel time (tt) plus 0.00465 ms
** Assumed a straight-ray path between source and receiver
*** Equals receiver depth
\+ Equals (corrected inclined travel time) × (receiver depth) / (inclined travel path)

seismic cone is compared to the SCPT velocity profile in Figure A.9. The shear wave velocity profiles evaluated by the SASW and seismic cone tests show very similar trends, with V_S increasing with depth. The small differences between the two test results are mainly attributed to the fact that the results of SASW testing represent global measurements over lateral distances on the order of the test depth while the results of SCPT testing represent localized measurements near the probe hole. In other words, SASW testing using comparatively low-frequency surface waves covers the spacing between each sensor pair located on the ground surface while seismic cone testing using S_{vh} waves between a source and a receiver, 5 to 10 ft apart (7 ft for this test) and depth increments of 3.3 ft (1 m). The difference between the two V_S profiles is largest at shallow depths, from the ground surface to 14 ft deep as shown in Figure A.9. The S_{vh} waves generated in seismic cone testing are likely refracted near the surface (top 5 ft). The black dashed line above the first measurement depth represents an average value in a

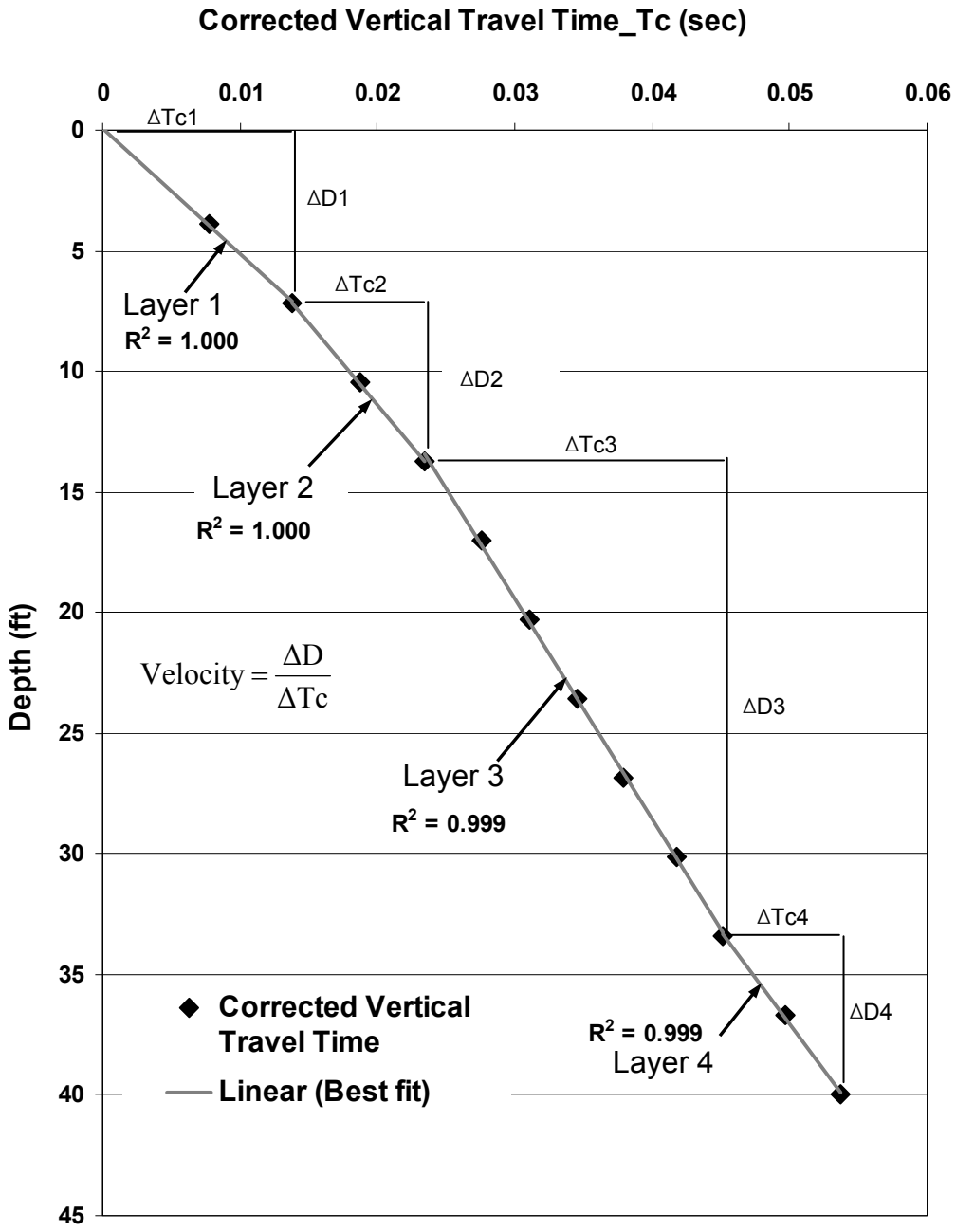

Figure A.8: Corrected Vertical Travel Time versus Depth Showing Four Straight Lines that Corrected Vertical Travel Times Proportionally Increase as Depths Increase

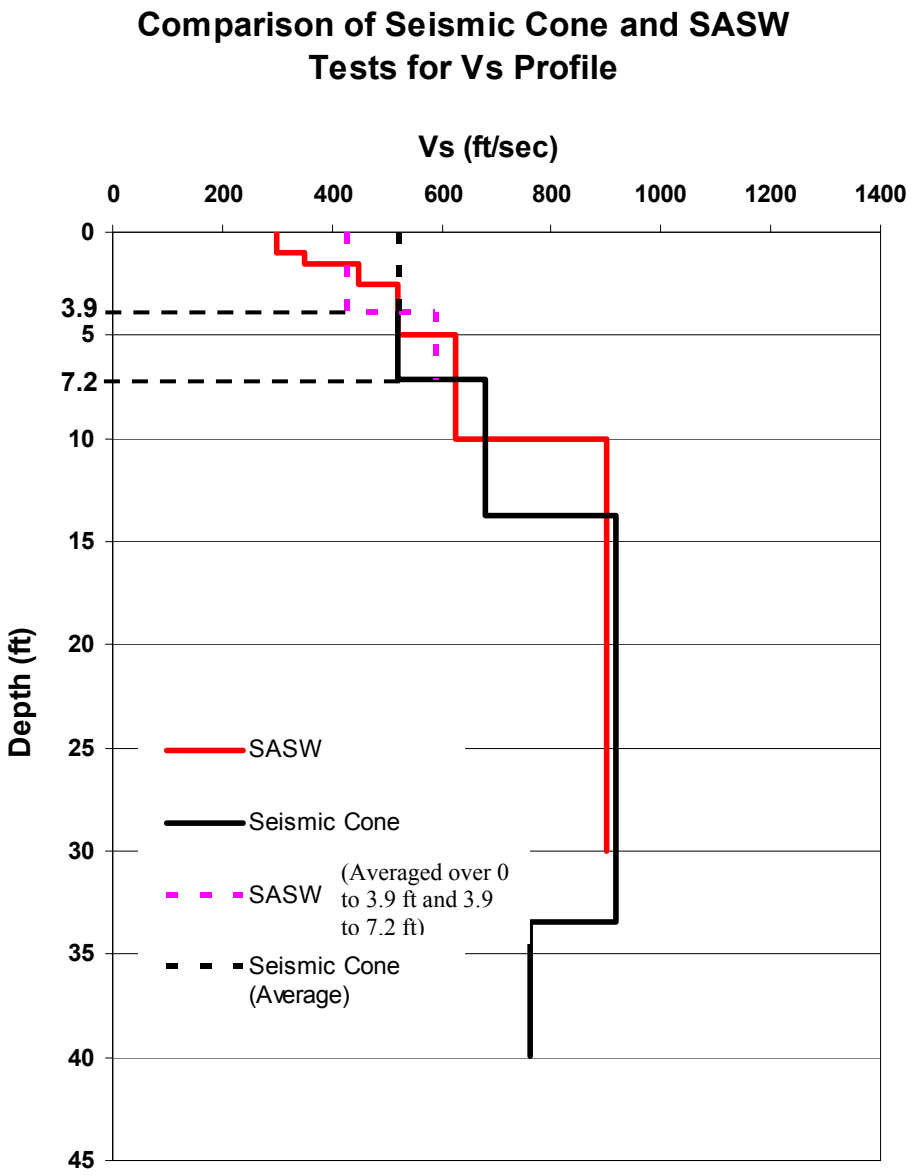

Figure A.9: Comparison V_S Profiles Evaluated by Near-by Seismic Cone and SASW Tests Performed at Lower Tract B; Interpreted Soil Profile Shown in Figure A.5

zone that likely includes gradients and capillary changes that could differ due to the time difference of a week between the two seismic tests. Also, it is difficult to correct for refraction in this zone because of too many unknowns. The pink dashed line above the depth of 7.2 ft in the V_S profile determined from SASW testing represents the averaged V_S profile at the top tow, SCPT measurement depths. The averaged V_S profile in the top 3.9 ft determined from SASW testing is smaller than the average velocity from seismic cone testing due to the effect of possible refraction.

The V_S profile from SASW testing was used to calculate equivalent to vertical travel times from downhole testing. The vertical travel times calculated with this approach are presented in Table A.3. The equivalent vertical travel time versus depth plot estimated by SASW testing is shown in Figure A.10. The corrected vertical travel times obtained by SASW testing are slightly greater than the values obtained by seismic cone testing at shallow depths (0 to 14 ft). However, the equivalent vertical travel times calculated from the SASW V_S profile essentially overlap the travel times from the SCPT testing below the depth of 14 ft. This comparison supports the point that uncorrected refraction near the surface in the SCPT tests resulted in overestimates of the near-surface V_S values.

A.5 CONSIDERATION OF SENSOR ROTATION

When a seismic cone is pushed into ground, the seismic cone can possibly rotate little by little with the increasing depth (hence, increasing rod length) because rotation is one type of distortional mode of an axially-loaded, long rod. Another reason is that the push rods can also be inadvertently rotated when one push rod is connected to the lower push rods with two adjustable wrenches.

Table A.3: Tabulation Showing the Equivalent SCPT Vertical Travel Times Calculated from the SASW V_S Profile Shown in Figure A.9

Depth* (ft)	V_S** (ft/s)	Equivalent Corrected Vertical Travel Time*** (ms)
1	300	3.333
1.5	350	4.762
2.5	450	6.984
5	520	11.792
10	625	19.792
16	900	26.458
30	900	42.014

* Equivalent measurement depth

** Shear wave velocity measured by SASW testing

*** Equals (vertical interval distance) divided by (SASW shear wave velocity) and accumulated with depth to give an equivalent vertical travel time

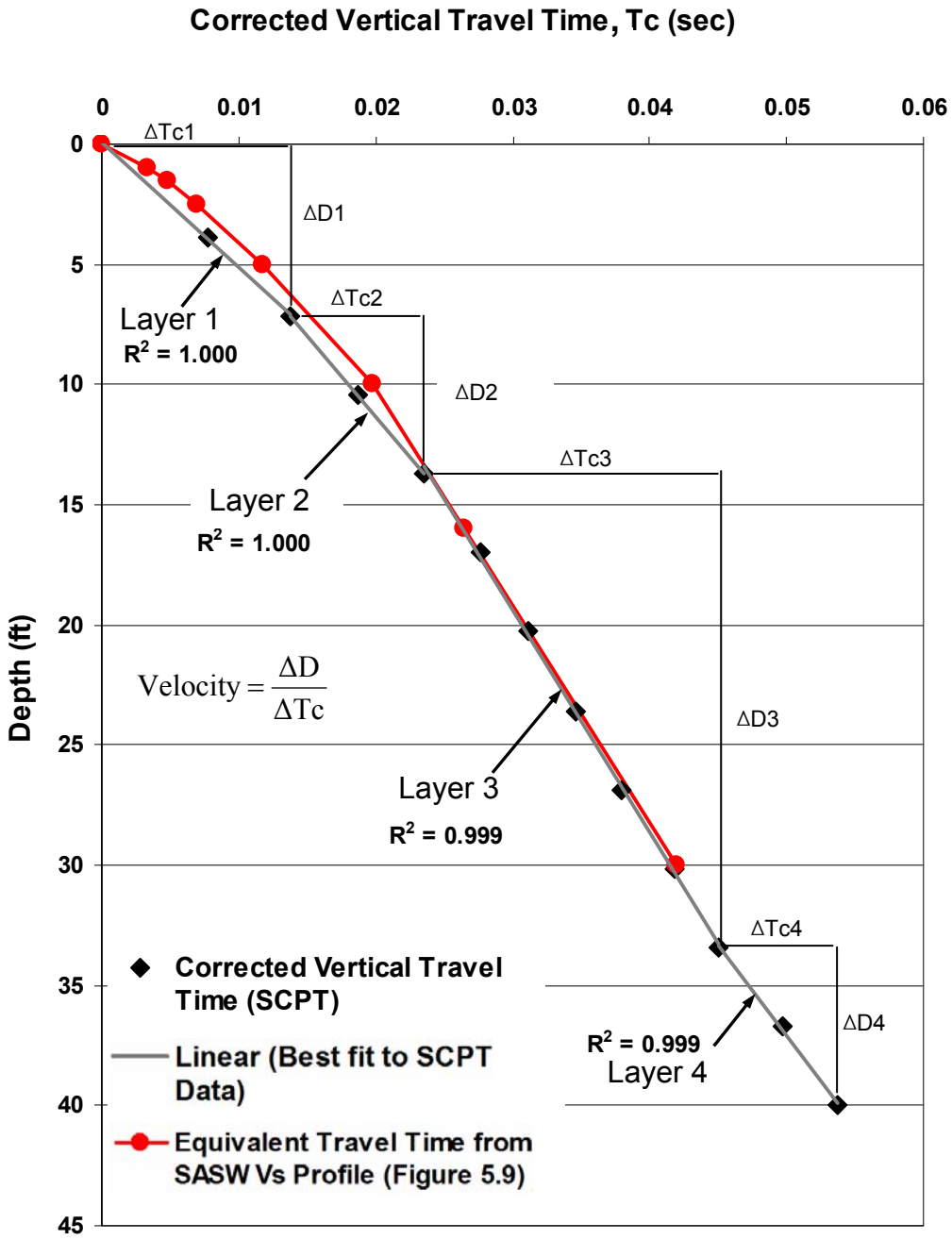

Figure A.10: Comparison of Vertical Travel Time versus Depth Plots Obtained by Seismic Cone and SASW Tests

To study possible rotation of the push rods, and hence rotation of the 3-D geophone near the end of the rods, the recorded body wave signals were normalized with the maximum S-wave amplitude at each depth. This normalization is shown in Figure A.11. The relative amplitudes of P-waves at the start of each waveform that were recorded with the horizontal geophone (H-2) (that was initially parallel to the S-wave plank) increased as the depth increased. This relative increase in P-wave amplitude indicates that the H2 geophone was rotating towards the source, hence towards the direction of P-wave particle motion. This result supports the assumption that the sensor was rotating with increasing depth. To estimate the amount of sensor rotation, the S_{vh} waves that were recorded with both horizontal geophones were windowed with a rectangular window that had a period of 0.02 seconds. This window is shown in Figure A.12.

The window shown in Figure A.12 that was applied to the H-2 geophone was also applied to the H-1 geophone. The window was applied to the H-1 geophone at exactly the same time (at each depth) as done in Figure A.12. These results are shown in Figure A.13 for the H-1 geophone. (It is interesting to note that large S wave amplitudes were also monitored on the H-1 geophone. This point is addressed in the next section.) The amplitudes of the windowed S_{vh} waves that were recorded with the two horizontal geophones were then plotted relative to each other in terms of H-1 on the vertical axis and H-2 on the horizontal axis. These plots are shown in Figures A.14 through A.17. Linear best-fit trends were plotted through the data at each depth. The R^2 values for these trends range from 0.89 to 0.97. The equations from the linear trends were used to calculate the rotational angles of the H-2 axis. The increasing angles of the trend lines for the H-2 axis mean that the sensor rotated as the depth of a seismic cone increased. As the penetration depth of a seismic cone increased from 3.9 ft to 40.0 ft, the seismic cone

rotated from an initial value of 30.2˚ at 3.9 ft to 61.1˚ at 40 ft as shown in Figure A.18. The rotation of the seismic cone shows a jump of 30.2˚ at the first depth. This rotation is attributed to initial, inadvertent rotation created during addition of the first rod. Refracted waves propagating along the ground surface may have exaggerated the estimated amount for the sensor rotation. However, the intent was to orient the axial direction of the horizontal H-2 geophone parallel to the impact direction of the S-wave plank on the ground surface. As discussed in Chapter 6, great care is required to keep from initially rotating the SCPT rods due to the very low confining pressures near the ground surface. The assumption is also discussed in the next section dealing with the laboratory tests.

Minimizing the effect of the sensor rotation can be important in identifying the first arrivals of the S-waves. The relative amplitude of the S-wave arrival decreases as the rotation of the transverse horizontal geophone increases. The amplitude of the P waves not included in the windowing of the S_{vh} waves was multiplied by the cosine value of the rotated angles. The relative amplitude of the windowed S_{vh} waves increased as shown in Figure A.19. As a result, the first arrival times of S_{vh} waves are more clearly identified with increasing depth.

All subsequent seismic cone tests have been carefully performed to minimize sensor rotation at Hornsby Bend since this first seismic cone test was performed. To remove the significant sensor rotation on the ground surface, a small shallow hand-augered borehole has been created to make confining pressure at the starting point. The each push rod has been carefully pushed with a hydraulic cylinder and connected to lower push rods with adjustable wrenches, and a mark on the surface of push rods has been drawn to trace and minimize the sensor rotation.

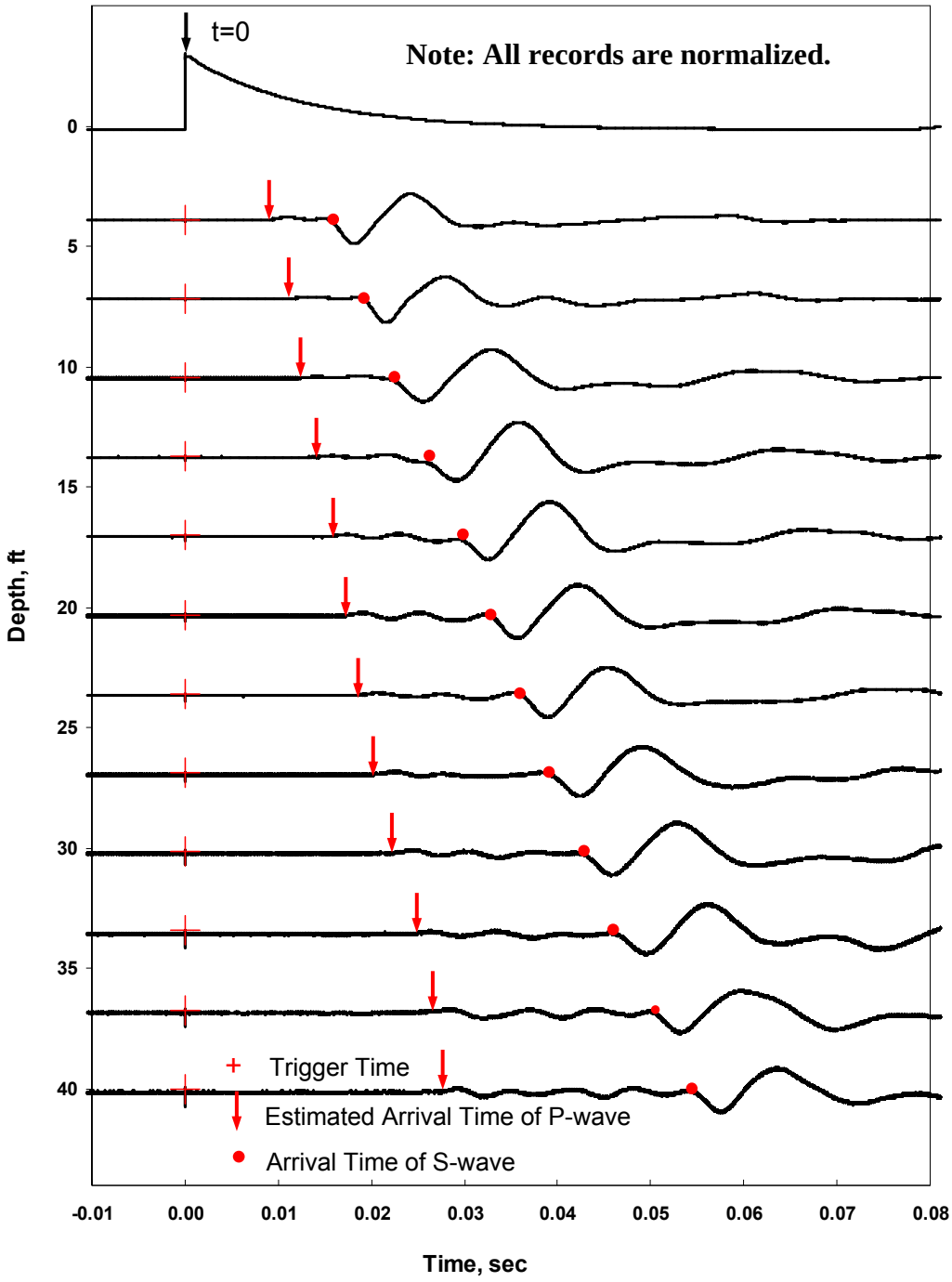

Figure A.11: Waterfall Plot of Signals Recorded by the Horizontal H-2 Geophone in the 3-D Receiver of the Seismic Cone in Figure A.6 and the Notation of P- and S-Waves

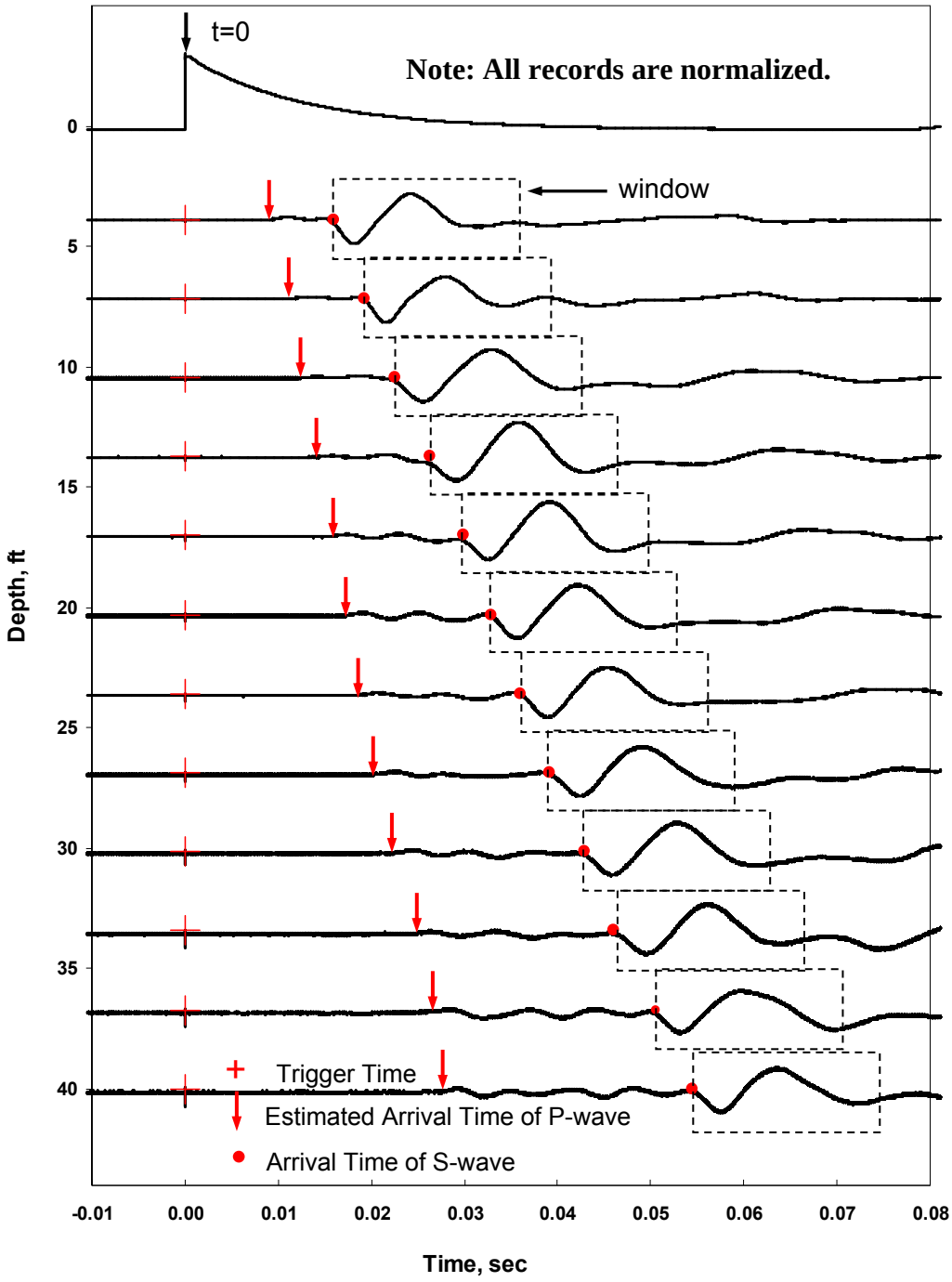

Figure A.12: Waterfall Plot of Signals Recorded by the Horizontal H-2 Geophone in the 3-D Receiver of the Seismic Cone in Figure A.11 and S_{vh} Waves Windowed by a Rectangular Window with the Time Period of 0.02 Seconds

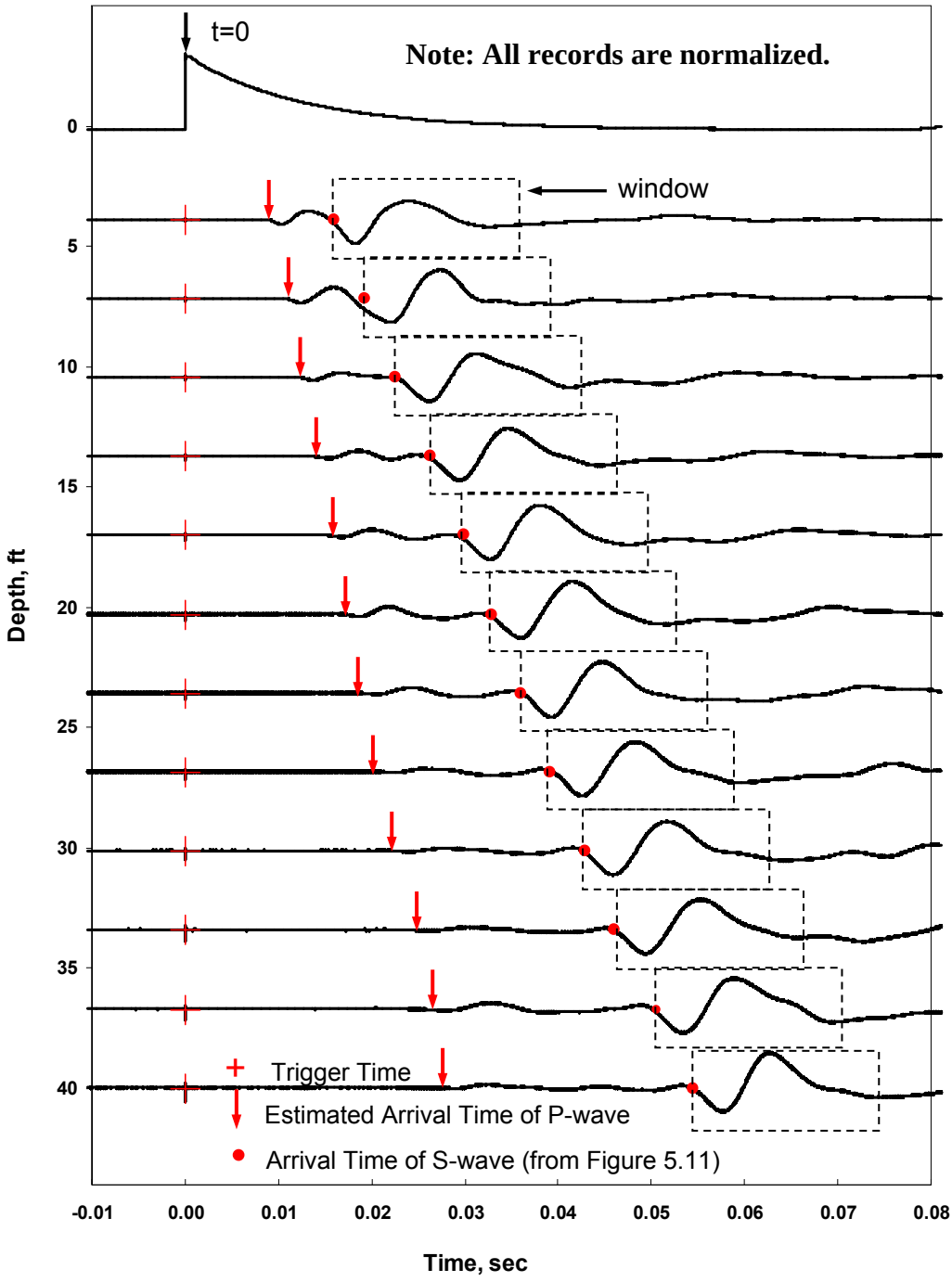

Figure A.13: Waterfall Plot of Signals Recorded by the Horizontal H-1 Geophone in the 3-D Receiver of the Seismic Cone and Windowed by a Rectangular Window with the Time Period of 0.02 Seconds at Exactly the Same Times Shown in Figure A.12

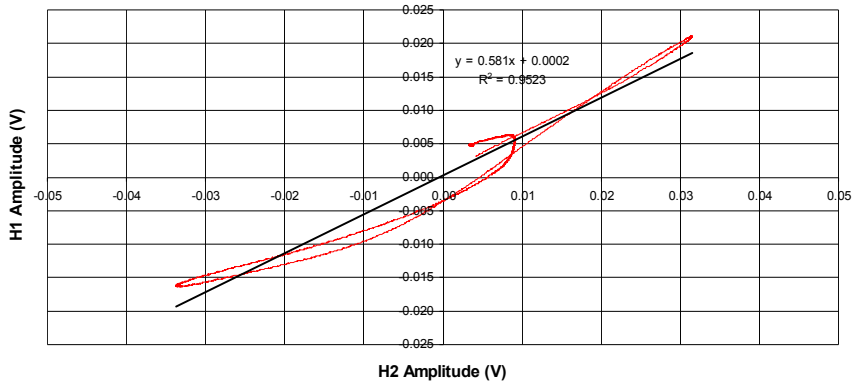

(a) Sensor Location_3.9 ft (θ=30.2˚)

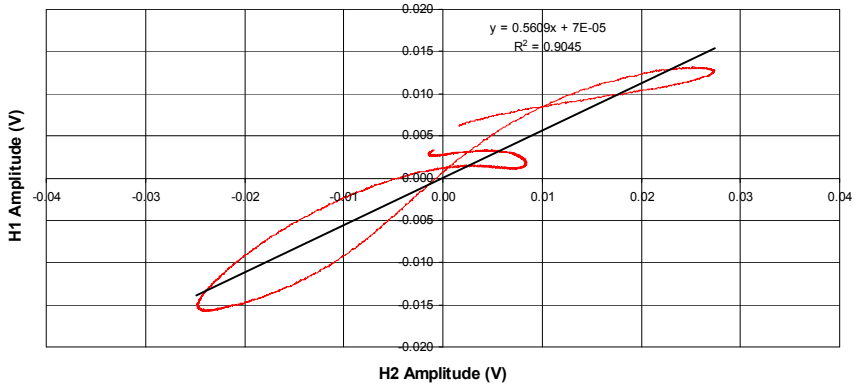

(b) Sensor Location_7.2 ft (θ=29.3˚)

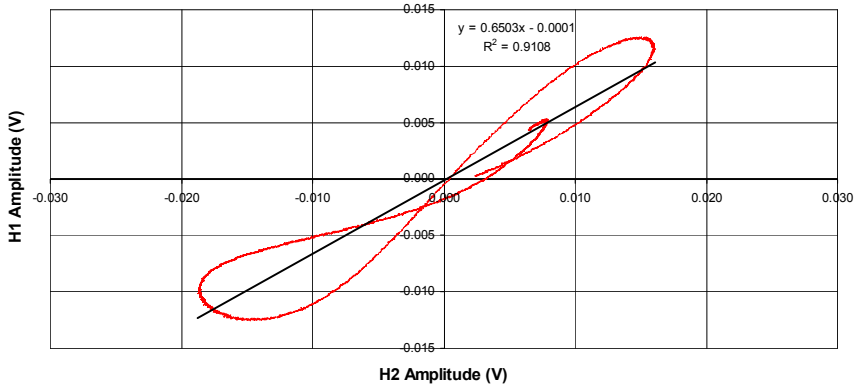

(c) Sensor Location_10.5 ft (θ=33.0˚)

Figure A.14: Relative Amplitudes of the Two Horizontal Geophones in the SCPT Showing that the Rotation of Seismic Cone Increases with the Increasing Depth; Depths = 3.9 to 10.5 ft

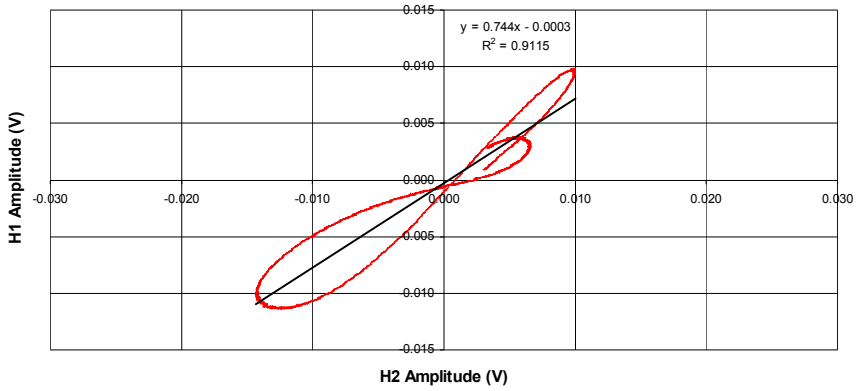

(d) Sensor Location_13.7 ft (θ=36.7˚)

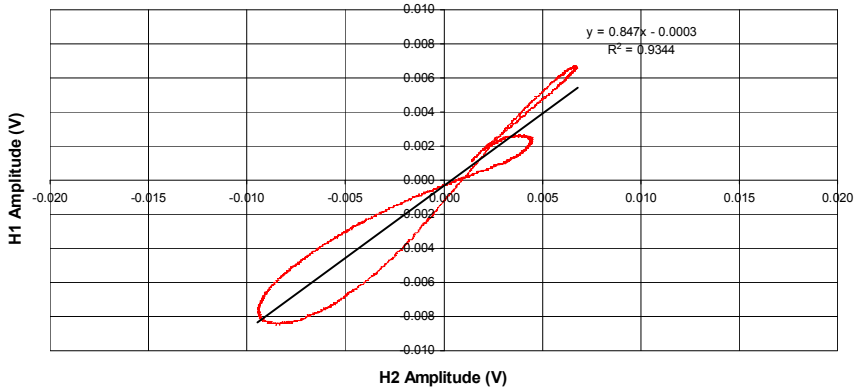

(e) Sensor Location_17.0 ft (θ=40.3˚)

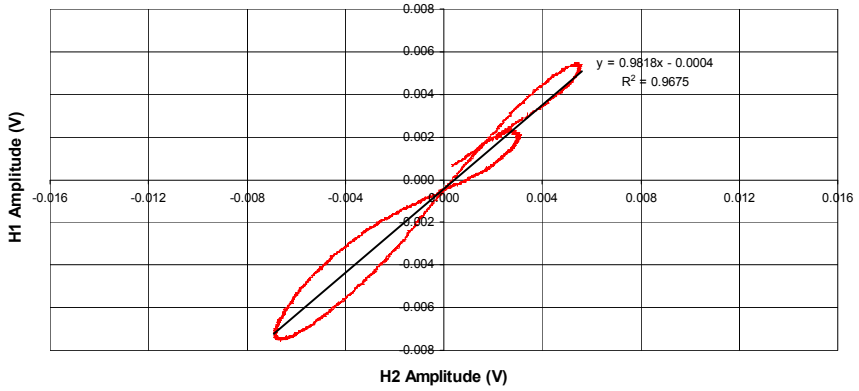

(f) Sensor Location_20.3 ft (θ=44.5˚)

Figure A.15: Relative Amplitudes of the Two Horizontal Geophones in the SCPT Showing that the Rotation of Seismic Cone Increases with the Increasing Depth; Depths = 13.7 to 20.3 ft

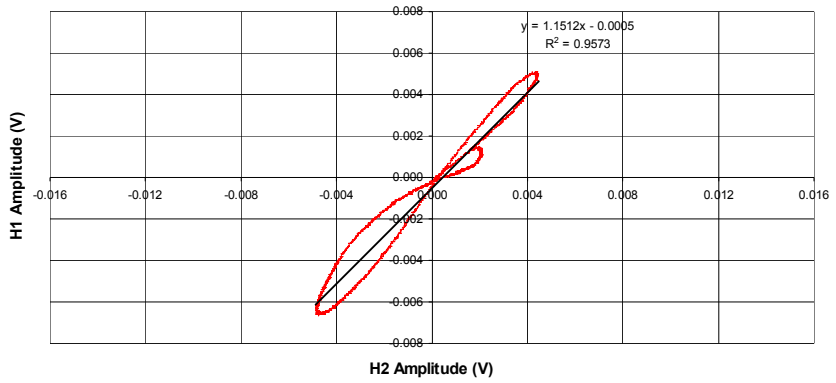

(g) Sensor Location_23.6 ft (θ=49.0˚)

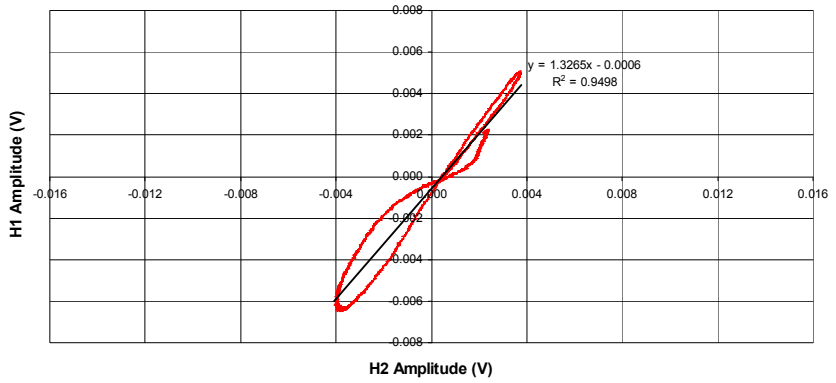

(h) Sensor Location_26.9 ft (θ=53.0˚)

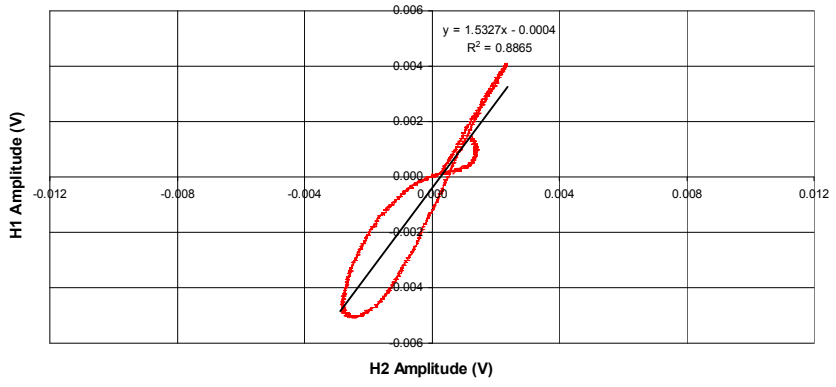

(i) Sensor Location_30.1 ft (θ=56.9˚)

Figure A.16: Relative Amplitudes of the Two Horizontal Geophones in the SCPT Showing that the Rotation of Seismic Cone Increases with the Increasing Depth; Depths = 23.6 to 30.1 ft

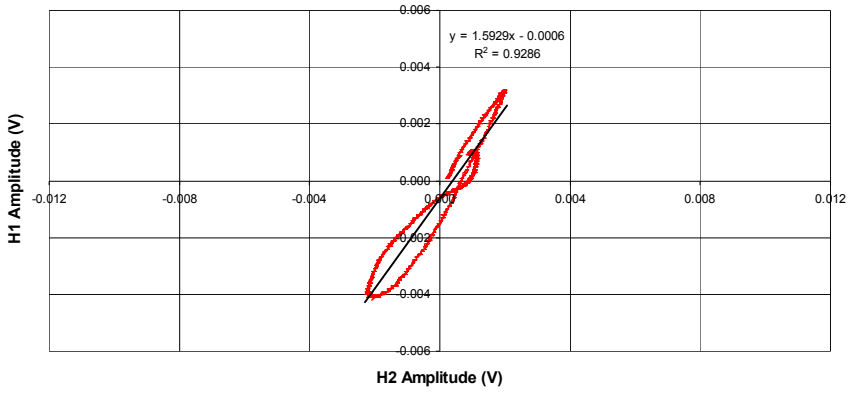

(j) Sensor Location_33.4 ft (θ=57.9˚)

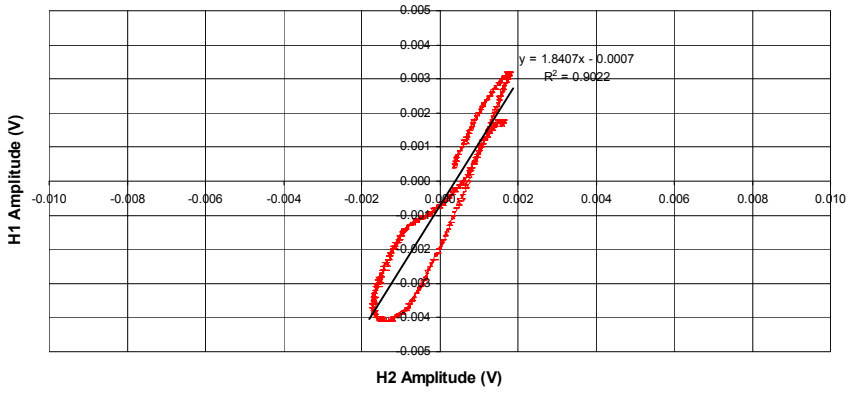

(k) Sensor Location_36.7 ft (θ=61.5˚)

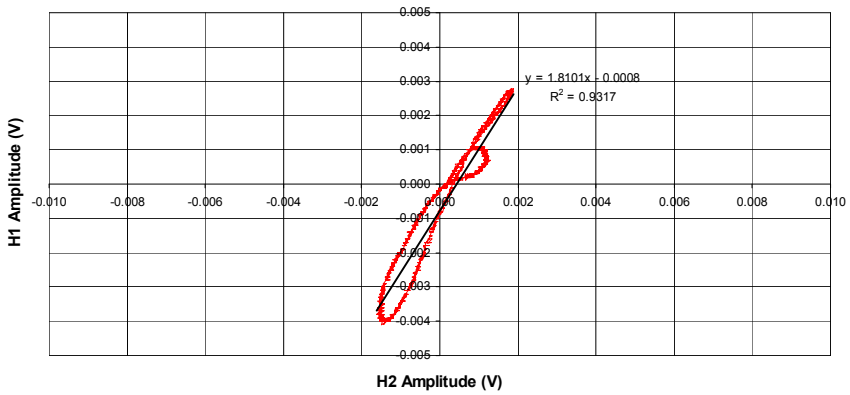

(l) Sensor Location_40.0 ft (θ=61.1˚)

Figure A.17: Relative Amplitudes of the Two Horizontal Geophones in the SCPT Showing that the Rotation of Seismic Cone Increases with the Increasing Depth; Depths = 33.4 to 40.0 ft

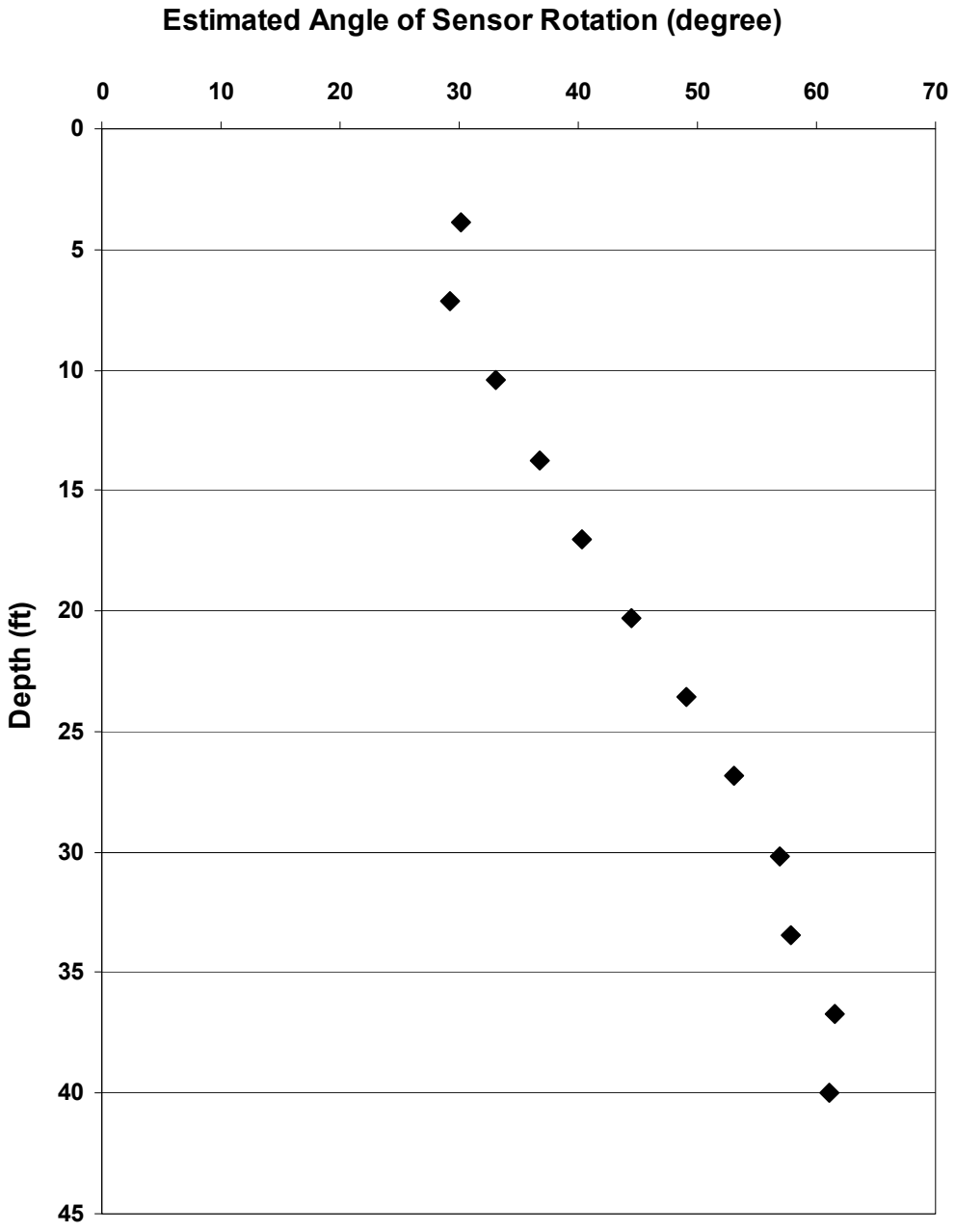

Figure A.18: Estimated Angle of Sensor Rotation versus Depth Showing that the Rotation of the Seismic Cone Increased with Increasing Depth during SCPT testing at Lower Tract B, Hornsby Bend

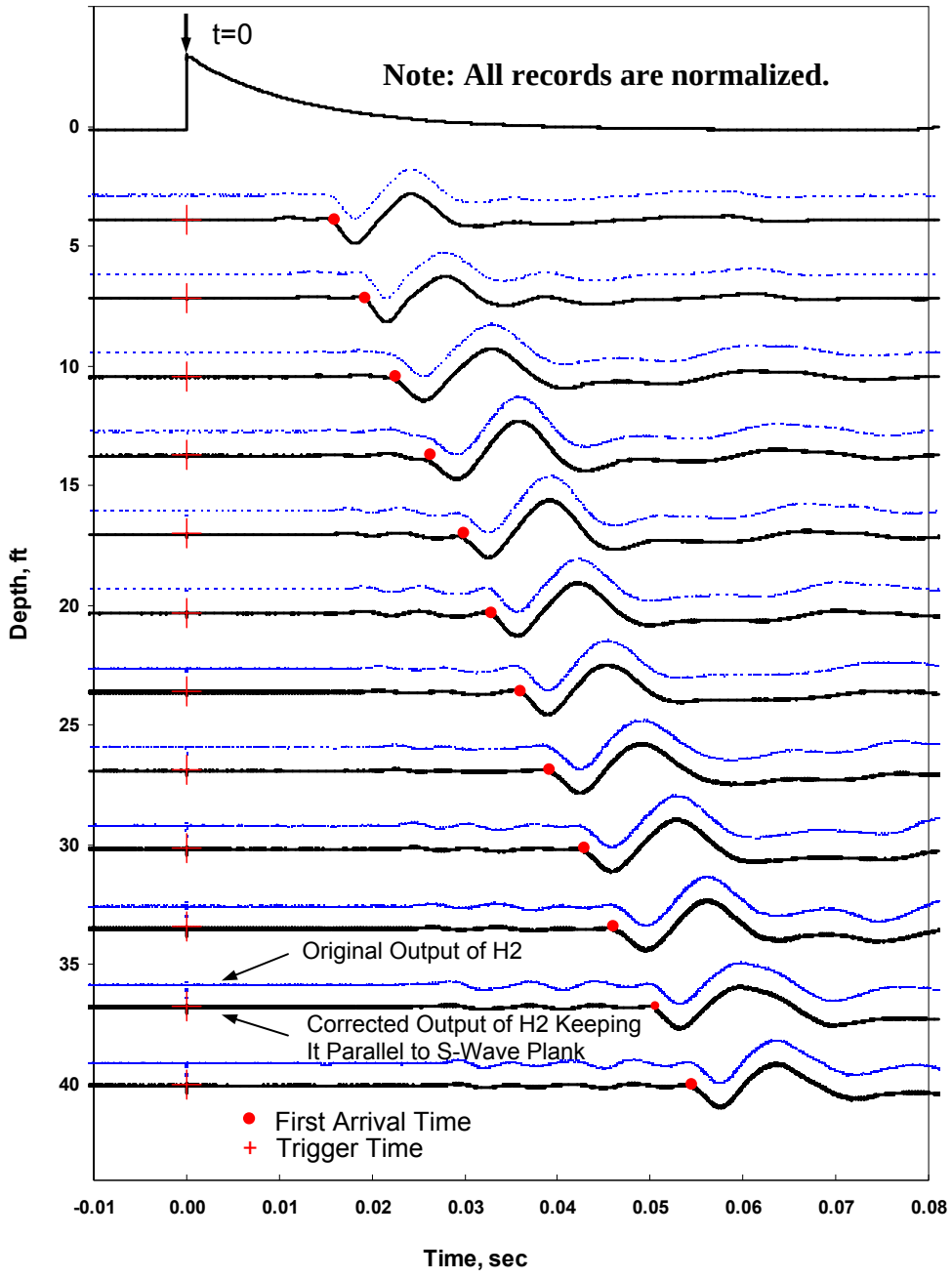

Figure A.19: Waterfall Plot Showing S_{vh} Waves Windowed by a Rectangular Window with the Time Period of 0.02 Seconds and the Amplitudes of the Other Waves Reduced by Considering the Sensor Rotation (Note: Waveform at Each Depth Normalized to Have Peak-to-Peak S-Wave Amplitude Equal to 1.0)

A.6 VERIFICATION OF SENSOR ROTATION FROM TWO HORIZONTAL GEOPHONE OUTPUTS

Because the seismic cone can rotate while it is pushed into the ground with the hydraulic cylinder as well as during the process of adding additional rods with two adjustable spanners, a program of evaluating the output from two horizontal geophones to estimate the rotation was conducted in the laboratory. In this section, rotational angles estimated by the amplitudes of the two horizontal geophones in the 3-D receiver of the seismic cone are compared with the actual angle that the cone was manually rotated. The procedure and results of laboratory testing are discussed below.

A.6.1 Laboratory Testing

In Figure A.20, a photograph of the laboratory setup is shown. A yellow tape with divisions marked by every 15˚ was attached to the surface of the seismic cone that was used in the field SCPT testing. The angle between the axial direction of horizontal geophone H-2 and the shaking direction (vertical with the shaker) were controlled simply by rotating the seismic cone using the known angles shown on the yellow tape. The two horizontal geophones are omni-directional because of their stiff springs and hence the horizontal H-2 can also operate in the vertical direction on the vertical shaker. The angle between the axial direction of the H-2 geophone and the vertical shaking direction was increased in 15˚ increment from 0˚ to 90˚. At each rotated angle, the seismic cone was excited with the electromagnetic shaker using frequencies ranging from 5 to 600 Hz in a swept mode. The seismic cone was fixed by a sensor-holding chamber which was connected to the electromagnetic shaker. The spectral amplitudes generated from the two horizontal geophones inside the seismic cone were recorded with the Quattro dynamic signal analyzer.

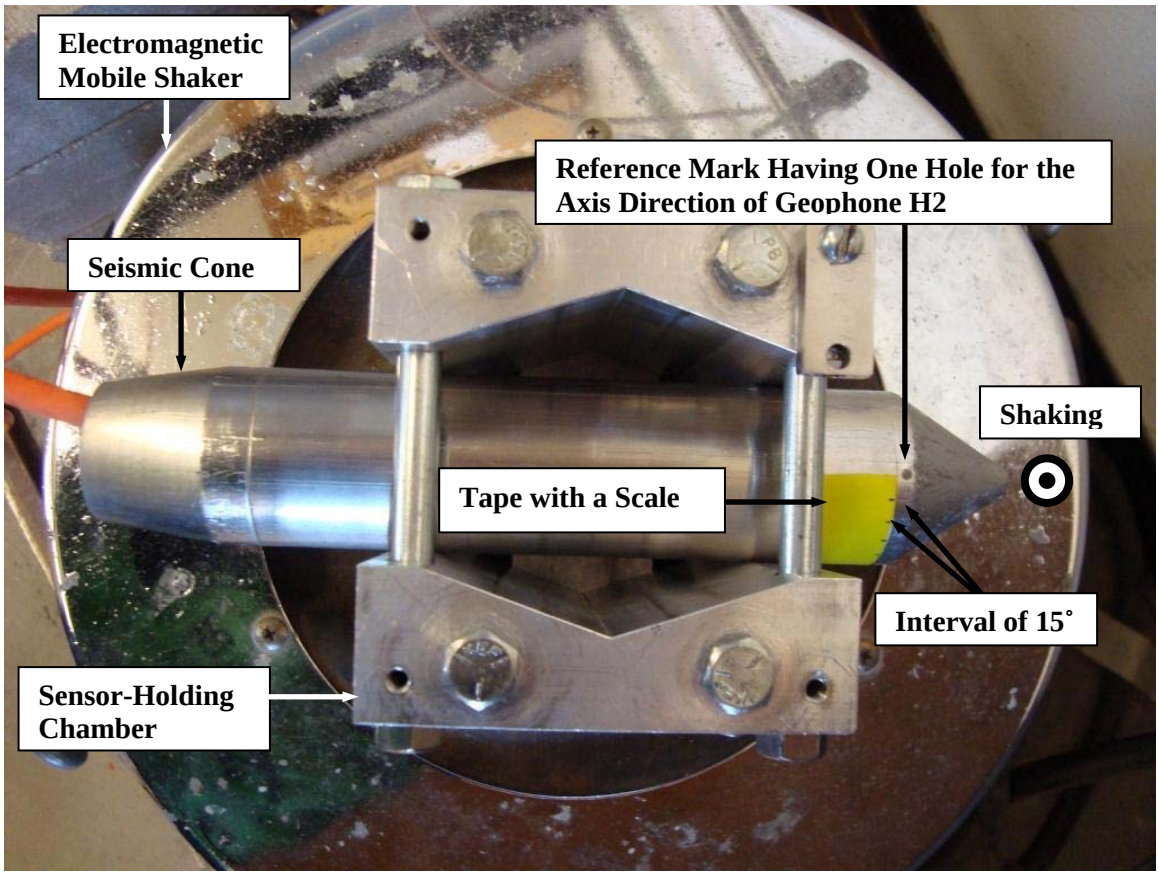

Figure A.20: Laboratory Testing to Measure Amplitude Changes of the Two Horizontal Geophones in the SCPT with Angle of Rotation from 0 to 90˚ between the Axial Direction of H-2 and the Shaking Direction

A.6.2 Discussion of Laboratory Testing Results

The spectral amplitudes from the two horizontal geophones at each rotated angle are plotted with red dots on the axes of H2 versus H1 in Figures A.21 and A.22. A best-fit straight line and associated R^2 was determined for each rotated angle (θ). These best-fit lines and equations are shown in Figures A.21 and A.22. The degrees of the estimated rotation (ϕ) were calculated from:

$$\phi = \tan^{-1}\left(\frac{H1}{H2}\right) \qquad \text{(A.1)}$$

where ϕ is the estimated degrees of rotation, $H1$ is the value of best-fit straight line on the vertical axis, and $H2$ is the value of best-fit straight line on the horizontal axis.

The angles of the estimated rotation (ϕ) are compared with the actual rotated angles in Figures A.23. The estimated rotation increases with the increasing rotation of the seismic cone, with R^2 ranging from 0.88 to 0.97 for the angles ranging from 15˚ to 75˚ (see Figures A.21b, c and d, and A.22e and f). When the physically rotated angles (θ) are 0˚ and 90˚, the estimated angles (ϕ) are 5.1˚ and -6.9˚, and these results show lower R^2 values of 0.64 and 0.44, respectively (see Figures A.21a and A.22g). The values of frequencies ranging from 15 to 60 Hz are included in the dashed ellipses in Figures A.21 and A.22. The values included in a dashed ellipse were eliminated because the values in the frequency range, 15 to 60 Hz are significantly affected by small phase shifts around the natural frequency of the 24-Hz geophones. The estimated rotations were calculated without the values in the dashed ellipses in Figures A.21 and A.22. Figure A.23 presents a comparison of the estimated angle versus the rotated angle for the two frequency ranges: (1) 5 – 600 Hz, and (2) 5 – 15 Hz and 60 – 600 Hz. The values in the two frequency ranges are tabulated in Table A.4. The comparison in Figure A.23 excluding the values of ϕs around the natural frequency range shows that the estimated angles are closer to the rotated angles. As a result, amplitudes of the output signals from the two horizontal geophones can be used to predict the rotated angle.

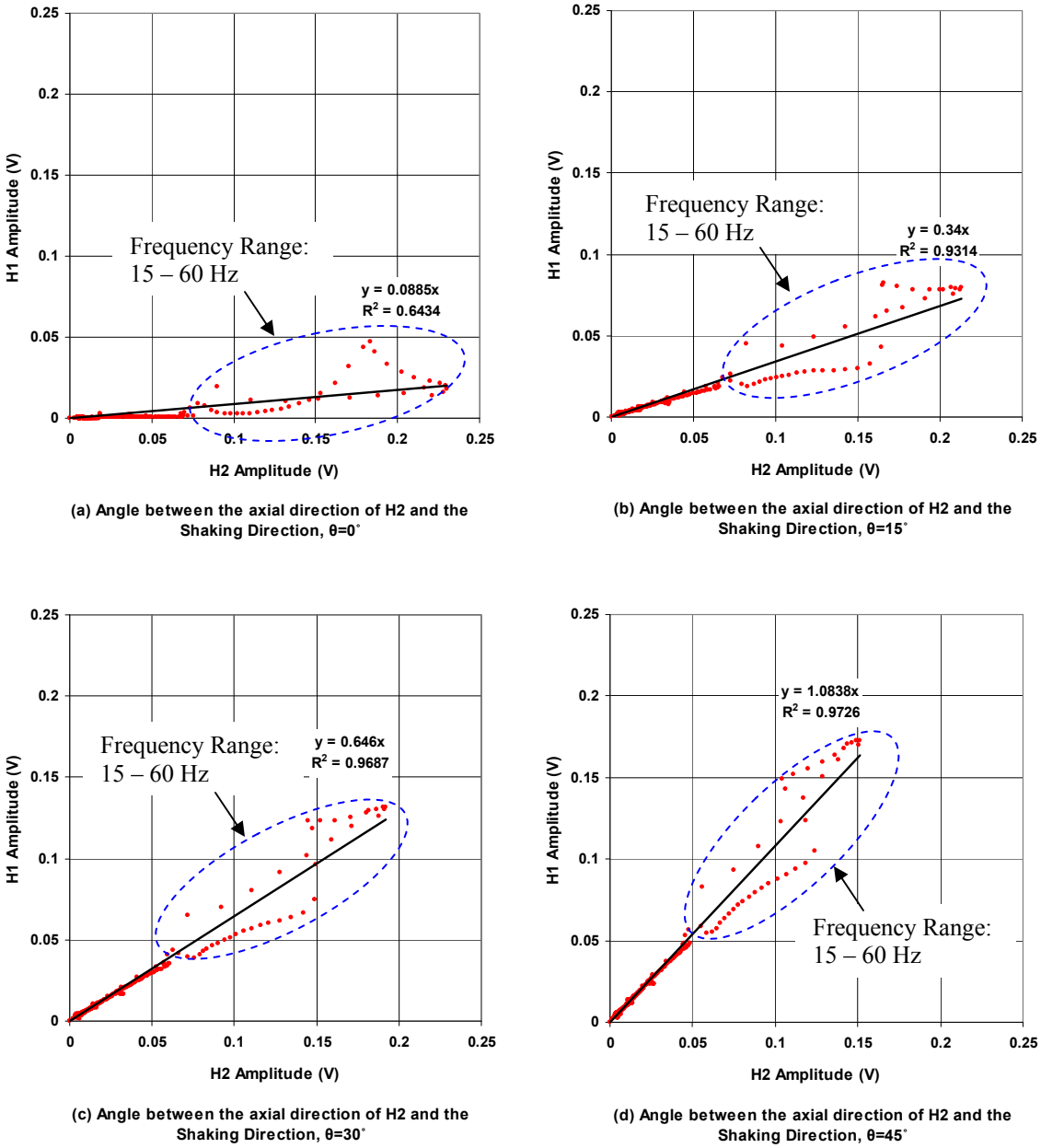

Figure A.21: Amplitude Changes in the Output from the Two Horizontal Geophones Showing that the Estimated Rotation of the Seismic Cone Linearly Increases with the Increasing Rotational Angle of the Seismic Cone

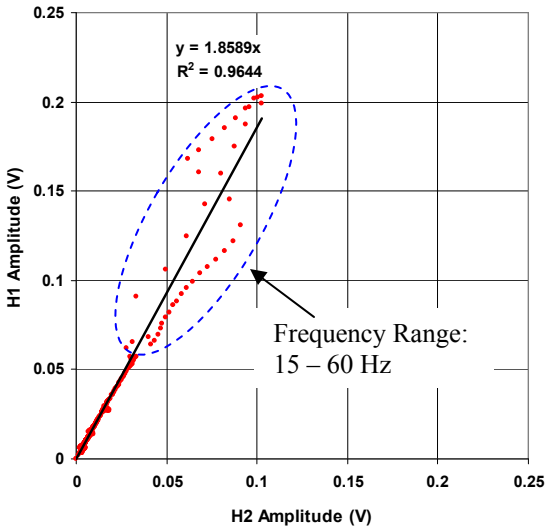

(e) Angle between the axial direction of H2 and the Shaking Direction, θ=60°

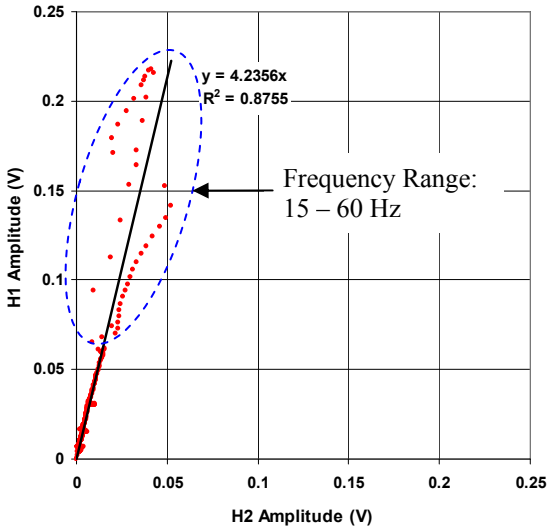

(f) Angle between the axial direction of H2 and the Shaking Direction, θ=75°

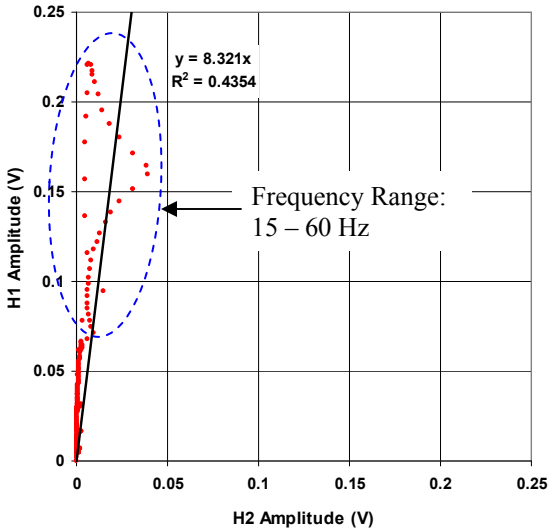

(g) Angle between the axial direction of H2 and the Shaking Direction, θ=90°

Figure A.22: Amplitude Changes in the Output from the Two Horizontal Geophones Showing that the Estimated Rotation of the Seismic Cone Linearly Increases with the Increasing Rotational Angle of the Seismic Cone

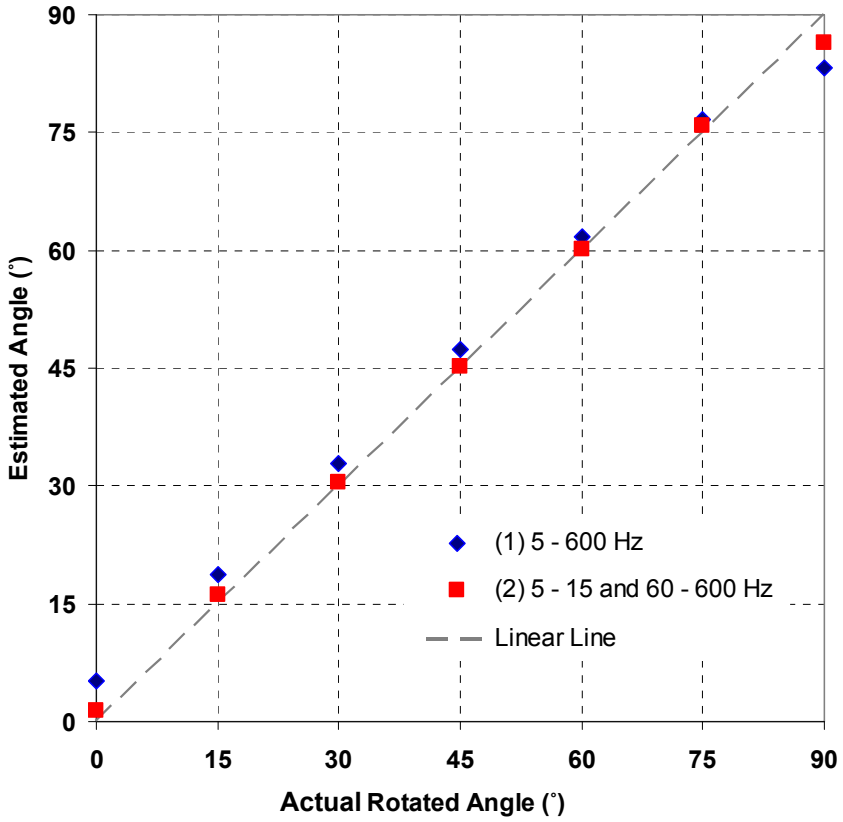

Figure A.23: Plots Showing the Estimated Angle Versus the Actual Rotated Angle in Two Frequency Ranges: (1) 5 – 600 Hz, and (2) only 5 – 15 Hz and 60 – 600 Hz

Table A.4: Tabulation of the Rotated Angle versus the Estimated Angle in the Two Frequency Ranges: (1) 5 – 600 Hz and (2) 5 – 15 Hz and 60 – 600 Hz

Rotated Angle	Estimated Angle for 5 – 600 Hz	Estimated Angle for 5 – 15 Hz and 60 – 600 Hz
0	5.1	1.3
15	18.8	16.14
30	32.9	30.56
45	47.3	45.28
60	61.7	60.05
75	76.7	75.83
90	83.2	86.35

A.7 SUMMARY

Seismic cone testing equivalent to SCPT testing was conducted. This testing consisted of a CPT test and a seismic cone test that were performed close to each other at Lower Tract B, Hornsby Bend, Austin, TX. The relative locations and times of the CPT and seismic tests were quite close. The seismic cone test was performed with the traditional downhole testing procedure. The collected field data were presented in a waterfall-type plot in the time domain. First arrival times of shear waves were carefully picked by eye from the waterfall plot. Travel times obtained from the first S-wave arrivals were converted to corrected travel times for pure vertical propagation. The converted travel-time versus depth data were best fit with linear equations that showed high R^2 (>0.999) and allowed V_S values to be determined for each layer.

The amplitudes of the travel-time records in the waterfall plots were normalized using the peak S-wave amplitude. The relative P-wave amplitudes in the normalized S-wave records increased with the increasing depth. Rotation of the seismic cone was a

possible reason for the relative increase in P-wave amplitude. Rotated angles of the seismic cone were estimated using the amplitudes of output signals that the two horizontal geophones generated. The angles of the estimated rotation were compared with actual rotated angles in a set of laboratory tests. The estimated angles obtained from linear, best-fit equations were close to actual rotated angles of a seismic cone. Estimated angles determined over frequencies ranging from 5 to 15 Hz and 60 to 600 Hz gave the best comparisons.

Appendix B: In-Situ Seismic Test Results

B.1 INTRODUCTION

Various in-situ seismic tests were performed at two testing areas of the Hornsby Bend site. The two sites are Platt 4 and Lower Tract B shown in Figure B.1. The in-situ seismic tests consist of SCPT, SASW tests and downhole tests, and these in-situ tests were performed at the two sites. The testing set up and procedure of the in-situ seismic tests performed in this chapter are introduced in Chapter 4. The data collected from the seismic tests were analyzed and interpreted as discussed in Chapters 5 and 6.

The in-situ test results obtained from Platt 4 are discussed for: (1) the comparison of analysis methods for the SCPT test at an example site, and (2) the 2-D V_S profile obtained with SCPT tests performed along the test array.

SCPT, downhole and SASW test results obtained at Lower Tract B are compared in this chapter. The SABW method is used and discussed to analyze the data collected from downhole tests.

B.2 TESTING SITES INFORMATION

Hornsby Bend has been used as a research area for a bird observatory in Austin, Texas. A small portion of the land has also been used as farmland or a seismic field testing site. As shown in Figure B.1, seismic field tests were performed at two locations which were Platt 4 and Lower Tract B. The soil stiffness in the depth range from the ground surface to 15 ft was changed by weather. The stiffness of soil in this shallow depth range was affected by water contents that change negative pore pressure. The effective stress of shallow soil layer significantly increased during the dry season (summer in Austin), unlike the rainy season (winter in Austin). The in-situ seismic tests

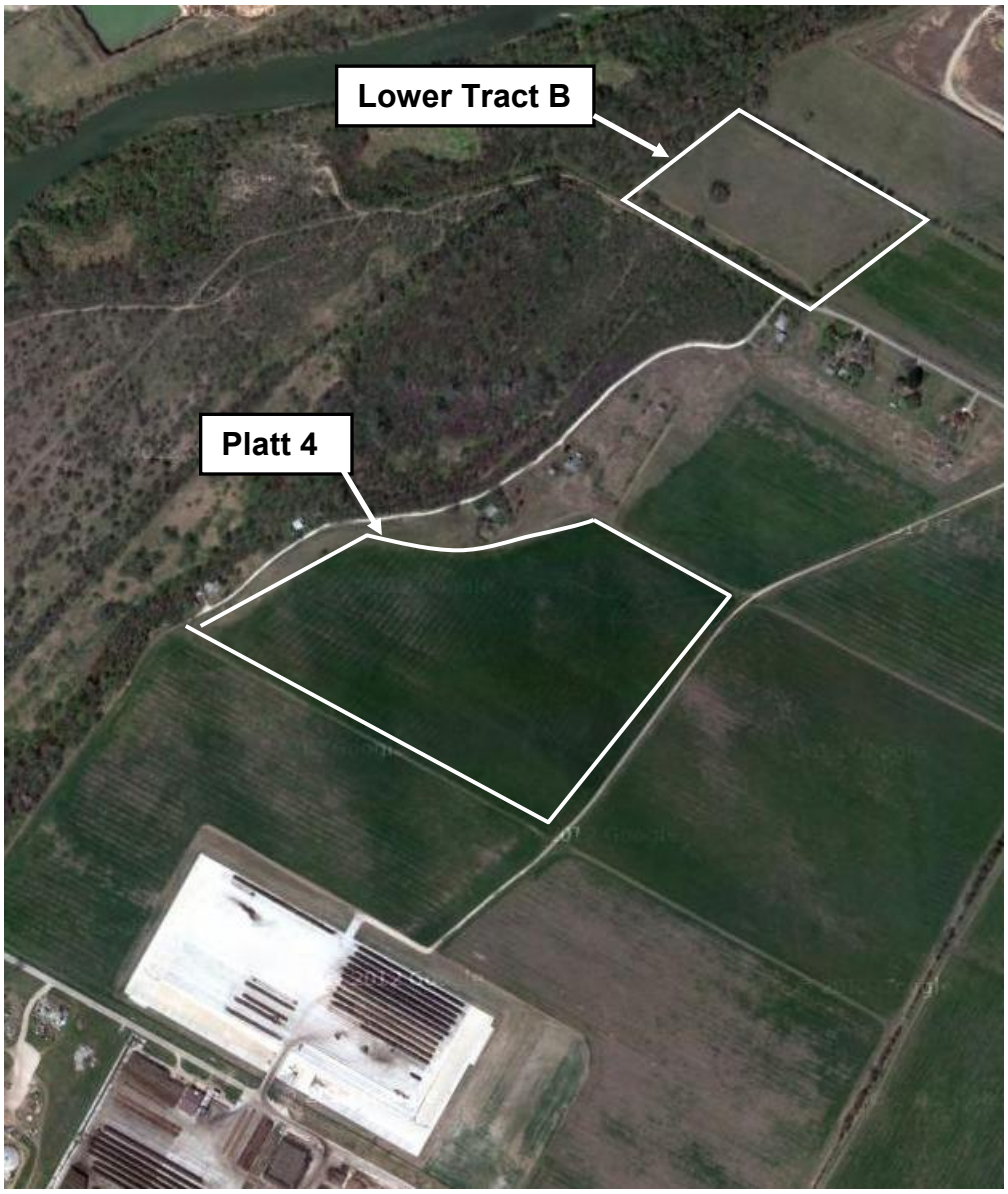

Figure B.1: Satellite Image of the Testing Sites at Hornsby Bend: Platt 4 and Lower Tract B (Courtesy of Google Map)

performed for three years showed the weather effects on the data analysis results. The specific locations for tests performed at Platt 4 and Lower Tract B are marked and discussed in the next section.

B.2.1 Platt 4 at Hornsby Bend site

Various in-situ seismic tests were performed at Platt 4 as a part of research for "Full-Waveform Inversion for Site Characterization" funded by National Science Foundation (NSF). As shown in Figure B.2, three spots were marked with flags with 330 ft (100 m) interval distance. The test array connecting three spots are shown in Figure B.2. To characterize the area including the test array, 13 Cone Penetration Tests (CPT) were performed at Platt 4, and the testing spots were marked with blue triangles on GPS coordinates in Figure B.3.

Cone resistance and friction ratio profiles are plotted for the CPT results. Similar profiles are plotted together into four groups as shown in Figures B.4 and B.5. While the cone resistance and friction ratio profiles of group 2 are similar for the entire depth in Figure B.4b, the cone resistance profiles of groups 3 and 4 (Figure B.5a and b) were not similar in shallow depths ranging from ground surface to 15 ft. It is because the CPT tests of groups 3 and 4 were not performed in the same season. While most CPT tests were performed in the rainy season, winter in Texas, C11 and C12 of group 3 and C13 of group 4 were performed in the dry season, summer in Texas. As shown in Figure B.5, the cone resistances are much larger than other profiles for the top 15 ft because the stiffness of soil in shallow depths significantly increased in summer.

For group 2, the interpreted soil profiles from the ground surface to a depth of around 48 ft consist of five layers. The five layers are: (1) thin, cohesive layer, (2) thick cohesionless soil layer, (3) cohesive soil layer, (4) cohesionless soil layer, and (5) cohesive and cohesionless soil interbed layer in order from top to bottom.

Figure B.2: Satellite Image of Test Array at Platt 4 (Courtesy of Google Map)

For the group 3, the interpreted soil profiles consist of three layers with the same thickness of 15 ft. The three layers are: (1) top sand layer in the depth range of ground surface to about 15 ft, (2) middle clay layer in the depth range of about 15 to 30 ft, and (3) clay and silty sand interbeds in the depth range of about 30 to 45 ft. The cone resistances of group 3 continuously decrease in the depth range of about 15 to 40 ft.

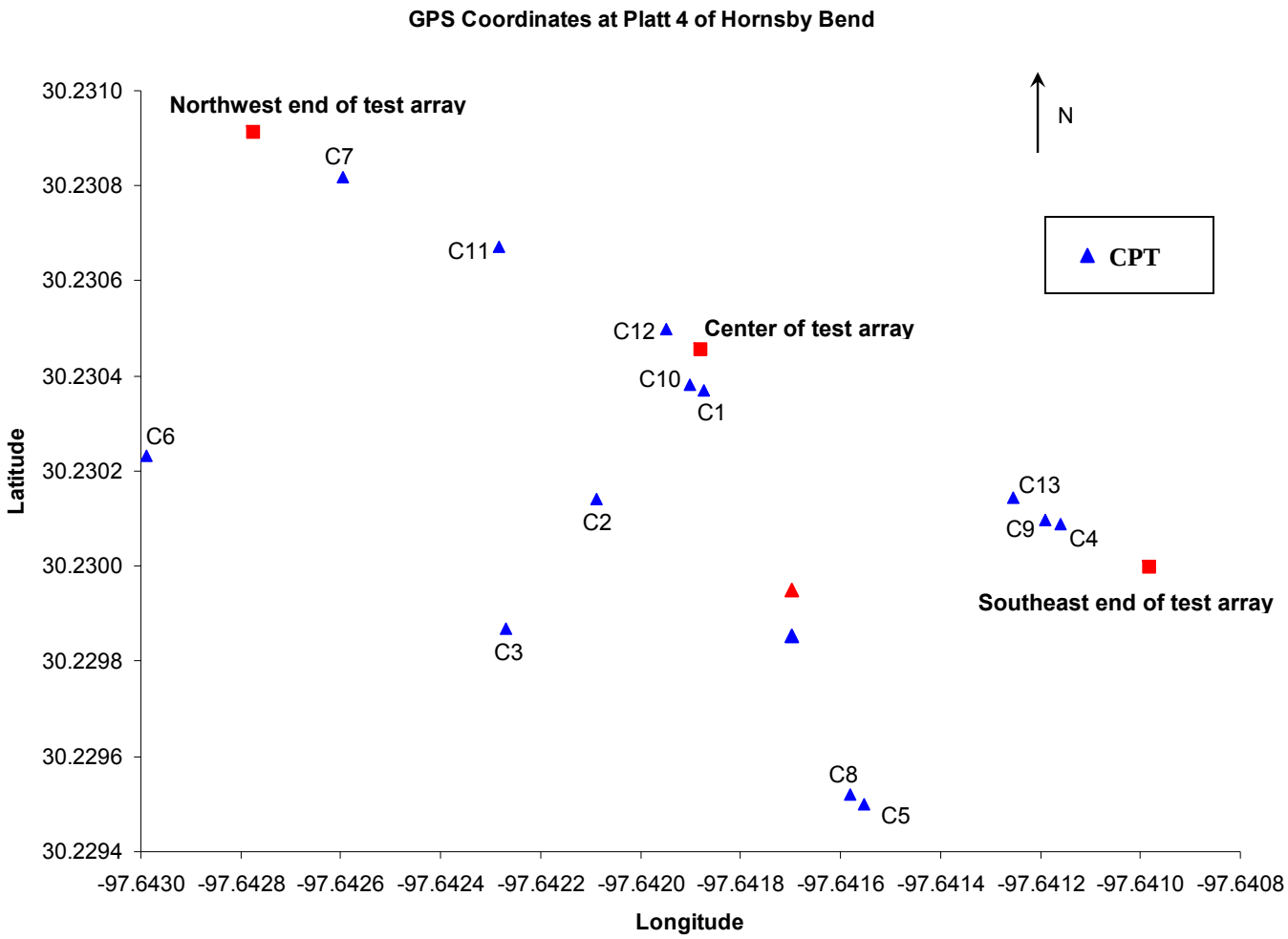

Figure B.3: CPT Testing Locations Displayed on GPS Coordinates at Platt 4

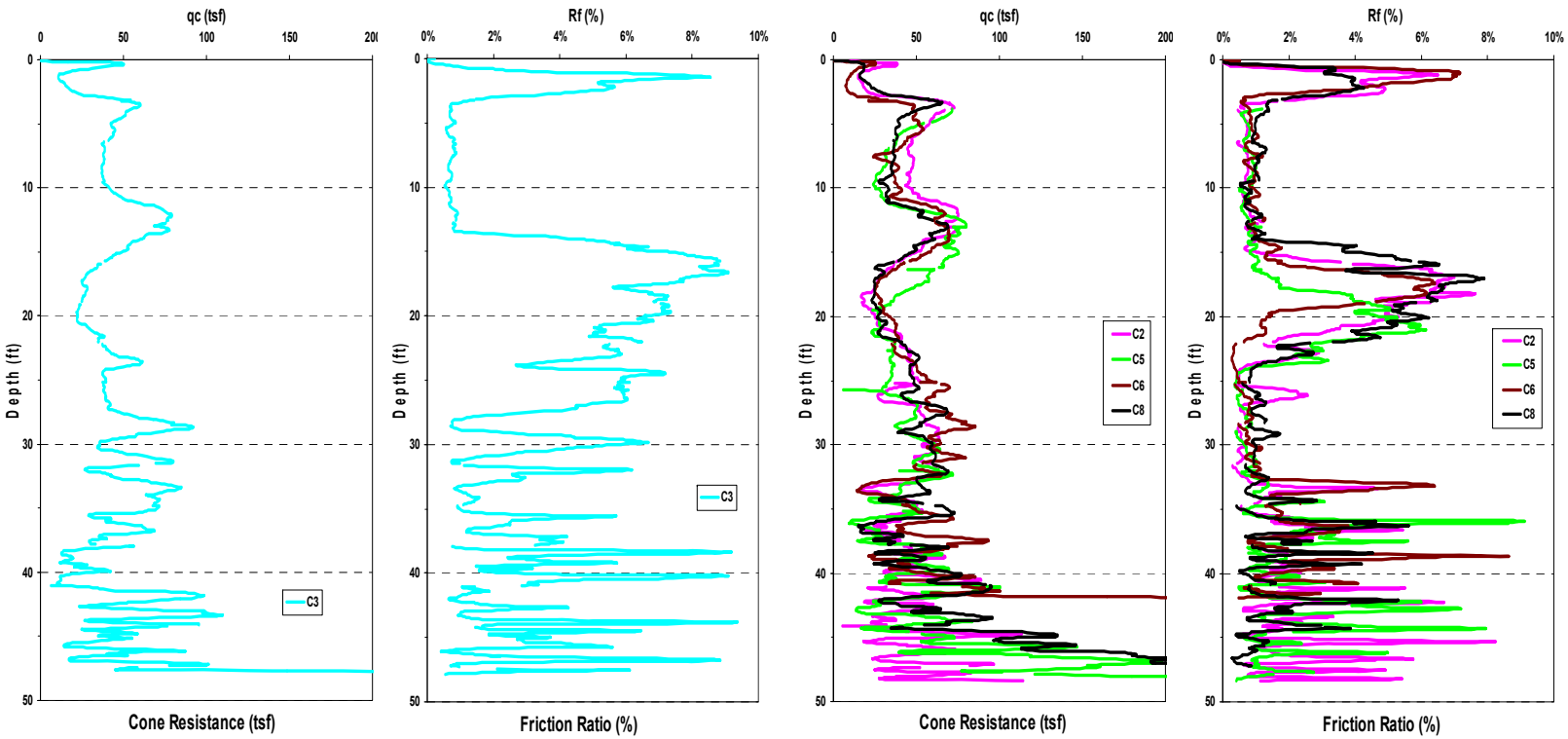

(a) CPT Profile of Group 1: C3

(b) CPT Profiles of Group 2: C2, C5, C6 and C8

Figure B.4: CPT Profiles Grouped for the Similar Soil Profiles at the Platt 4 Test Site ((a) Group 1 and (b) Group 2)

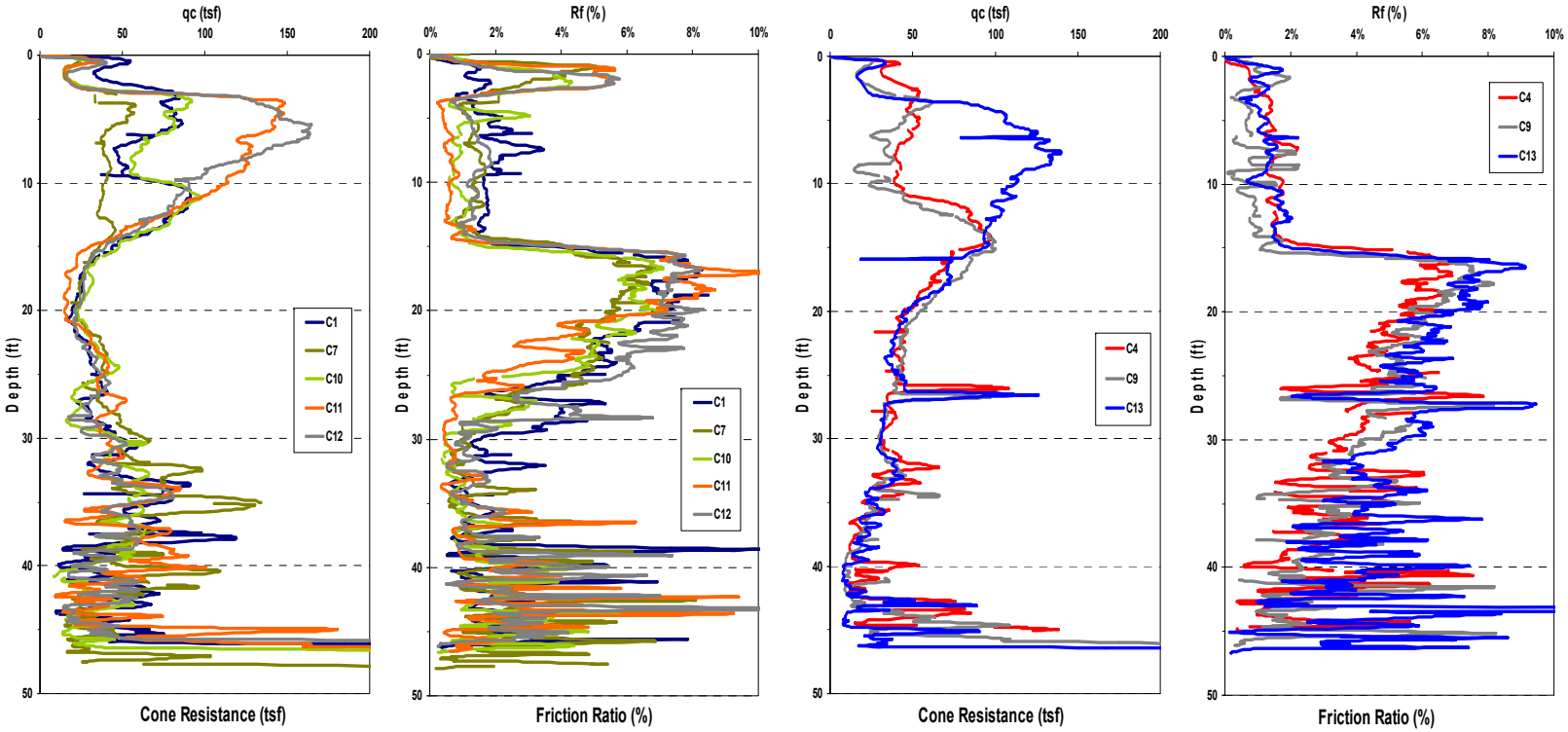

(a) CPT Profiles of Group 3: C1, C7, C10, C11 and C12

(b) CPT Profiles of Group 4: C4, C9, and C13

Figure B.5: CPT Profiles Grouped for the Similar Soil Profiles at the Platt 4 Test Site ((a) Group 3 and (b) Group 4)

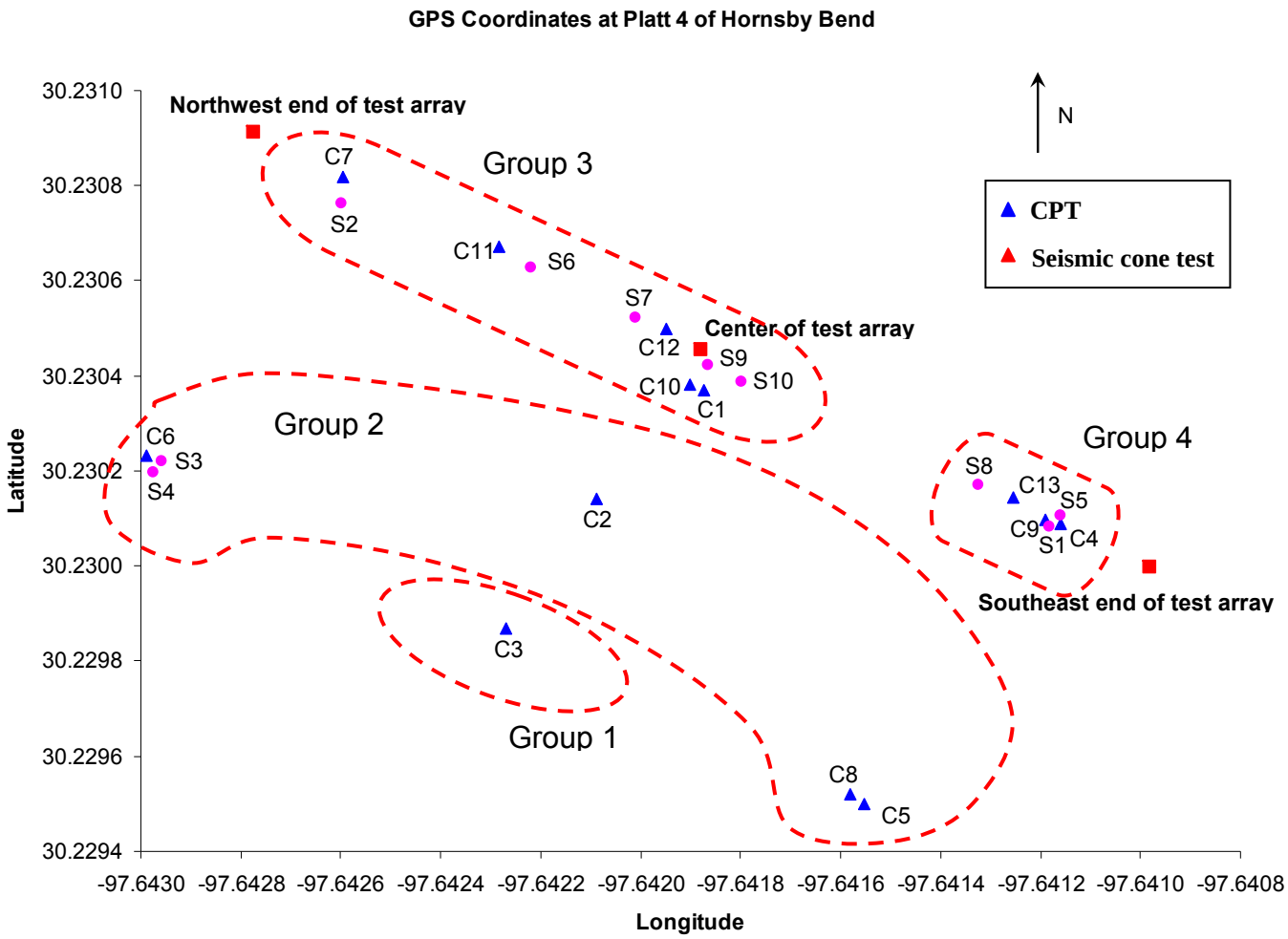

Figure B.6: Testing Locations Grouped for Similar CPT Soil Profiles to Perform the SCPT Tests

For group 3, the profiles are similar to the soil profiles of group 2 but the cohesive soil layer between two cohesionless soil layers is thicker than group 2. In addition, the two cohesionless soil layers include more cohesive soil. The cone resistance profiles of groups 2 and 3 have an inversion near 20 ft depth.

The areas of four groups are sectioned with red dashed line in Figure B.6. Seismic cone tests were performed at the areas of groups 2, 3 and 4. The locations of seismic cone test are marked with pink circles in Figure B.6. Most seismic cone tests were performed along the 660 ft (200 m) test array as a part of the research project.

B.2.2 Lower Tract B at Hornsby Bend site

The University of Texas (UT) and Los Alamos National Laboratory (LANL) performed a collaborative research project at Lower Tract B. Site characterization was performed at the site as a part of the research project. The soil and rock materials were sampled from a borehole shown in Figure B.7. A seismic cone, two CPT and SASW tests were performed at the locations shown in Figure B.7. Seismic cone testing was performed 40 ft away from the borehole for downhole testing. Then, two CPT tests were performed 15 ft away from the location of seismic cone testing. SASW testing was performed 50 ft away from the location of seismic cone testing. The locations of the three seismic tests were not able to be closer to each other due to the site condition. The relatively large difference of the locations caused the difference between the shear wave velocity profiles. The difference is discussed in the section B.4.1.

Soil profiles of CPT 1 and 2 are plotted in Figure B.8a and b, respectively. The location of CPT 2 is 30 ft away from the location of CPT 1. While cone resistance profiles are very similar for the entire depth range, the friction ratio of CPT 1 is larger than the friction ratio of CPT 2 in the depth range of about ground surface to 20 ft.

However, both CPT 1 and CPT2 consist of three layers in the depth range of about 0 to 40 ft. The location of each layer is very similar as shown in Figure B.8. Based on this similarity, it was assumed that the CPT profiles of CPT 1 and CPT 2 also represent the CPT profile at the location of the seismic cone test.

As described in Chapter 4, the soil materials were sampled using thin-wall Shelby tubes, standard penetration tests and a double-tube core barrel sampler before the borehole of 75 ft depth was drilled. The soil and rock profile obtained from the boring logs is shown in Figure B.9. The soil and rock profile consists of six layers. The profile above the depth of 40 ft is similar to the profiles of CPT 1 and 2. The top layer ranging from ground surface to 23 ft is brown silt. Two cohesive soil layers consisting of clayey brown silt layer and brown clay layer with the thickness of 12 ft is laid under a sandy brown silt layer. The water table was at 39 ft depth, and a soft brown clay layer was above the water table. Sand and gravel layer with SPT blow counts of 6, 11 and 26 exists in the depth range of about 39 to 47 ft. A shale layer was laid below the sand and gravel layer. The Rock-Quality-Designation (RQD) of shale samples is shown in Figure B.9.

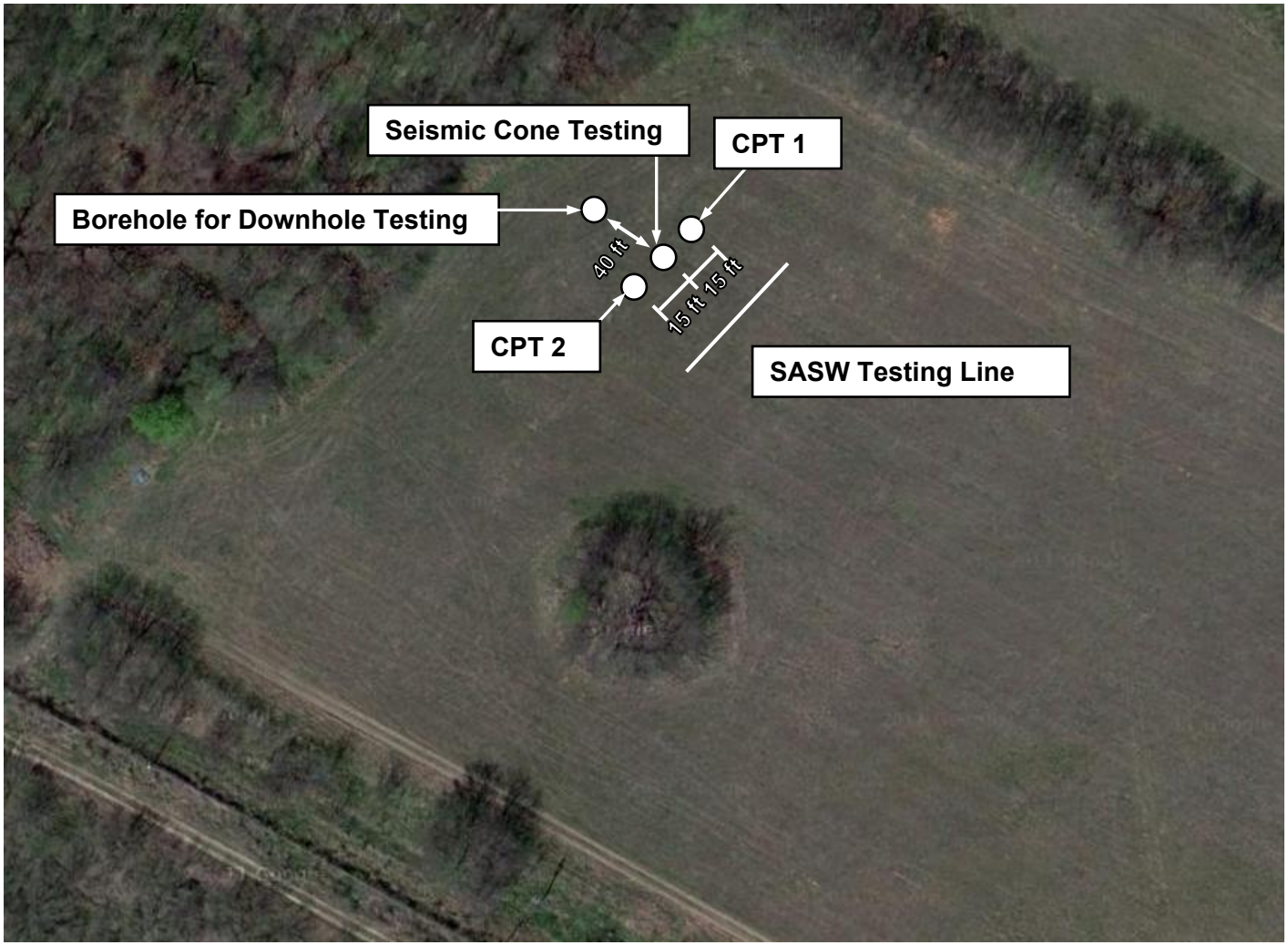

Figure B.7: Satellite Image of the Testing Locations at Lower Tract B (Courtesy of Google Map)

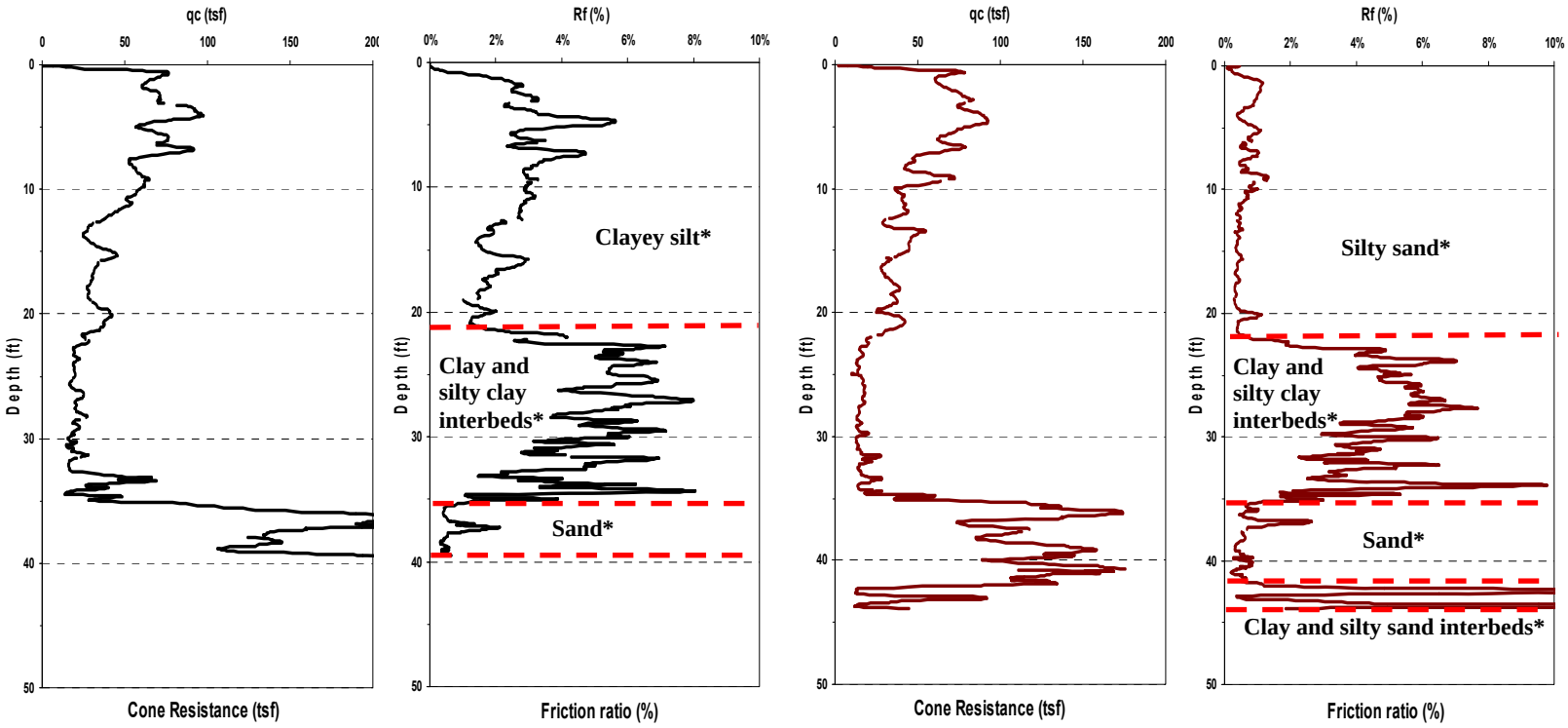

Figure B.8: Two CPT Profiles at the Lower Track B Test Site is Used in the Analysis of the Near-by SCPT, Downhole and SASW Testing Results: (a) Profiles of CPT 1 and (b) Profiles of CPT 2

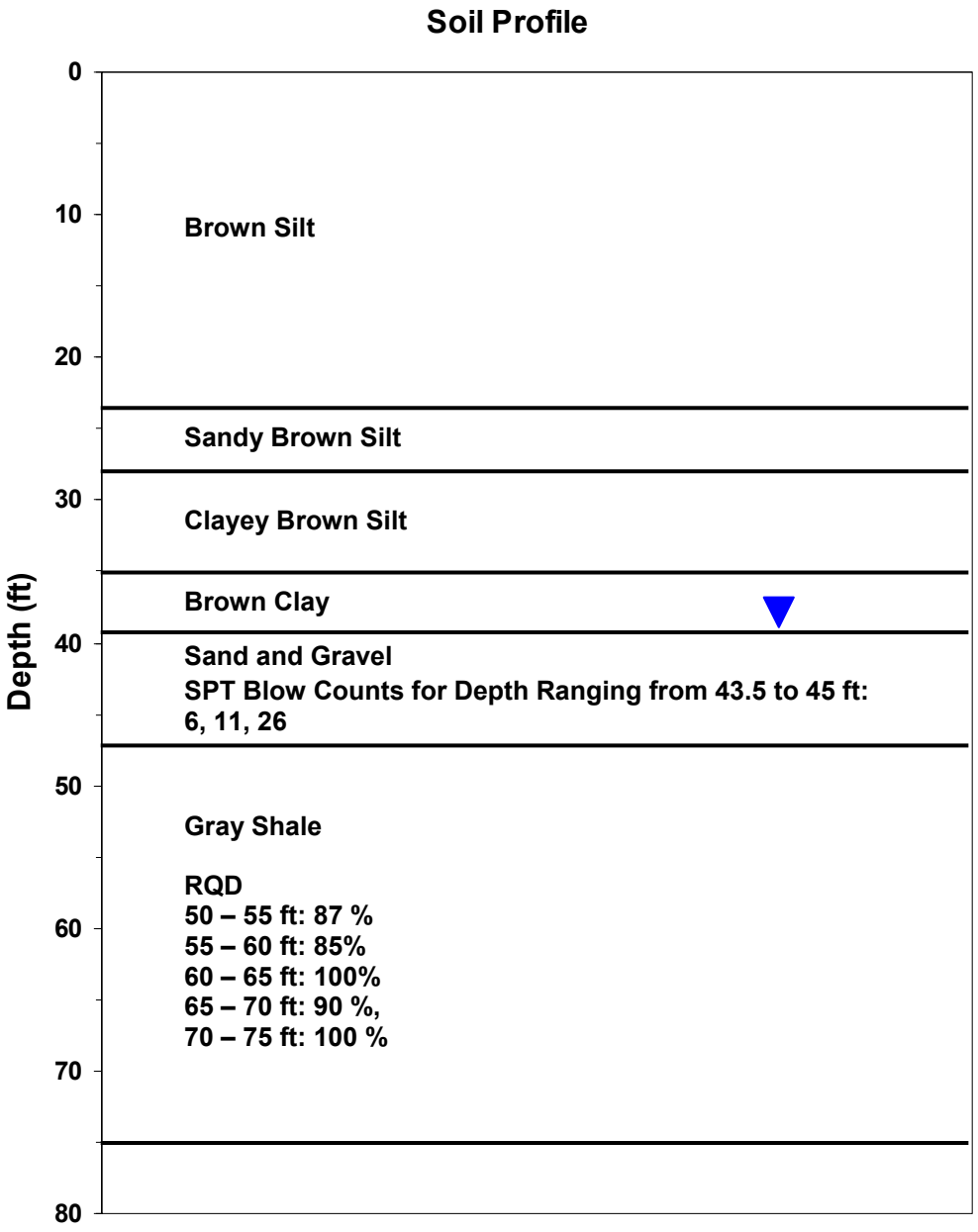

Figure B.9: Soil and Rock Profile at Lower Tract B from Boring Logs

B.3 TESTING RESULTS: PLATT 4

B.3.1 Comparison of analysis methods at example site (Group 2)

Two seismic cone tests were performed at S3 and S4 of group 2. S- and P-wave velocities obtained from S3 were calculated using the analysis methods described in Chapters 5 and 6.

The S-wave velocity at S3 is calculated using the frequency domain method described in Chapter 6. Phase velocities of S-waves that propagate through the soil layer in the depth range of 3.3 to 26.0 ft are shown in Figure B.10. The calculation procedure for phase velocities of S-waves in the depth range of 3.3 to 29.3 ft is shown in Figure B.11. The phases in the depth range of 26.0 to 29.3 ft are calculated and plotted in Figure B.12b. The phase was zoomed by wrapping the phase to delete the data in the frequency range that shows complex phase. The phase velocities in the depth range of 26.0 to 29.3 ft are calculated and plotted considering the wavelength shown in Figure B.12c. The S-wave velocity calculated by cross correlation was plotted with a blue dashed line and compared with phase velocities in Figure B.12d. The S-wave velocity of cross correlation and the phase velocity averaged above 100 Hz are 1167 and 1144 ft/s, respectively. The difference is less than 2.0 %. As shown in Figure B.12d, the phase velocities do not increase with increasing frequency so the layer ranging from 26.0 to 29.3 ft is assumed as a cohesionless soil layer. The friction ratio profile at C6 (see Figure B.4b) that is 10 ft away from S3 shows a cohesionless soil layer in the depth range of 26.0 to 29.3 ft.

V_S profiles that use the averaged first arrival times, cross correlation of two signals and phase differences are plotted for comparison as shown in Figure B.13. The three wave velocity profiles are similar. P-wave velocities at S3 were calculated using cross correlation, and the V_P profile is plotted with V_S profile in Figure B.14. P-wave velocity more rapidly increases than S-wave velocity below the depth of 32.5 ft. It is

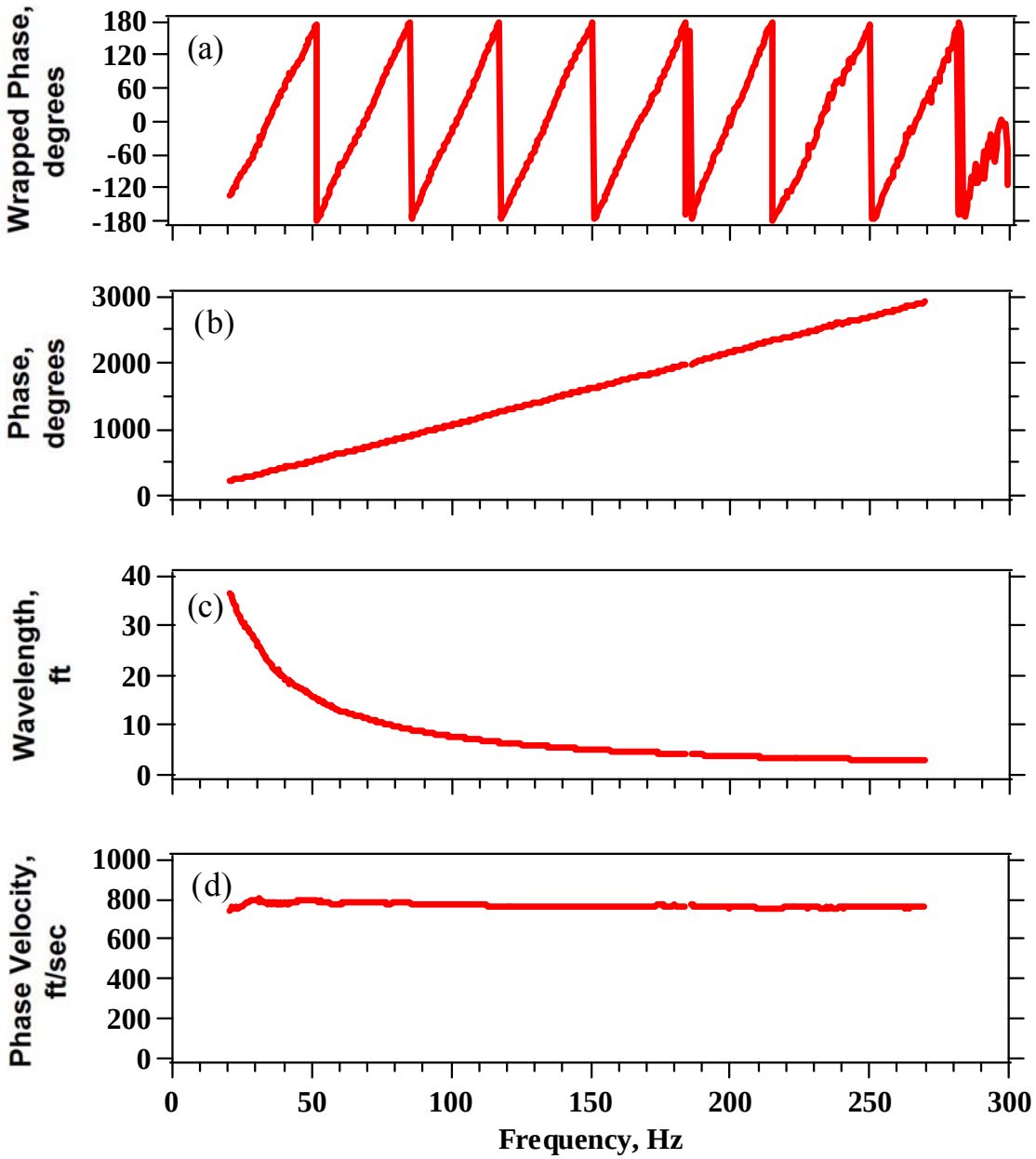

Figure B.10: Analysis of the Transfer Function between Embedded Reference Trigger at Depth of 3.3 ft and Seismic Cone at Depth of 26.0 ft (Location: S3)

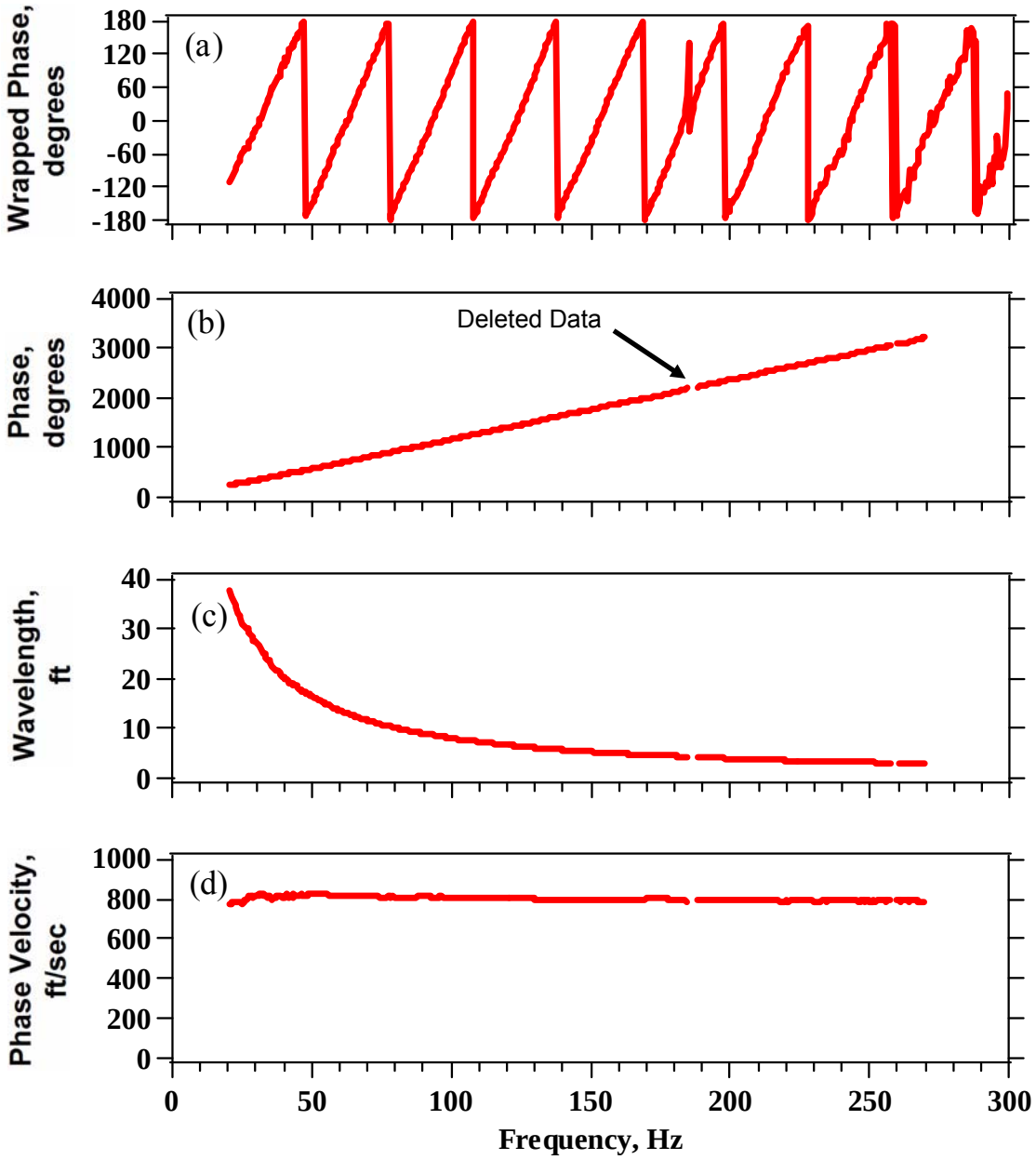

Figure B.11: Analysis of the Transfer Function between Embedded Reference Receiver at Depth of 3.3 ft and Seismic Cone at Depth of 29.3 ft (Location: S3)

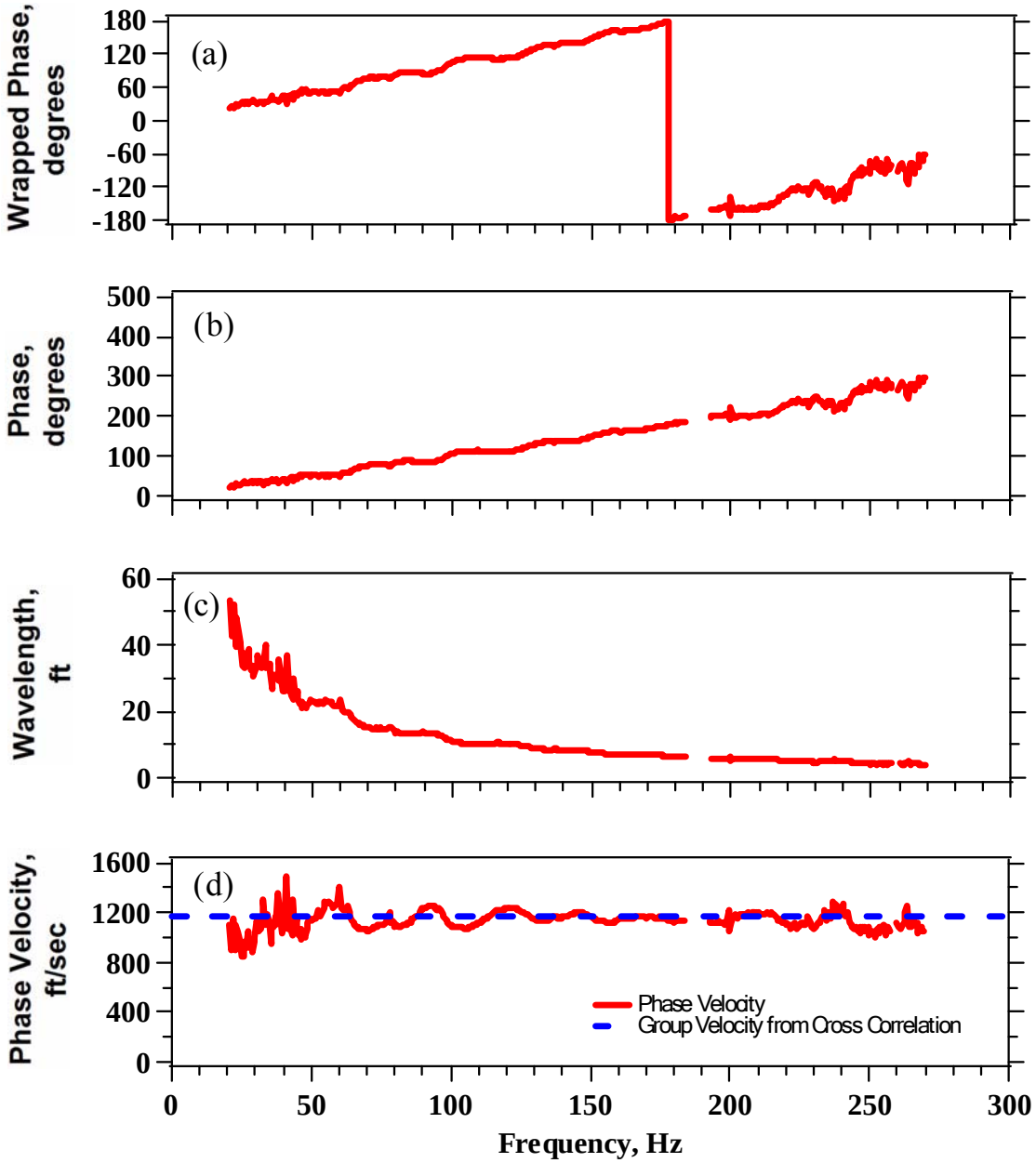

Figure B.12: Analysis of the Transfer Function between Seismic Cone at Depth of 26.0 ft and Seismic Cone at Depth of 29.3 ft (Location: S3)

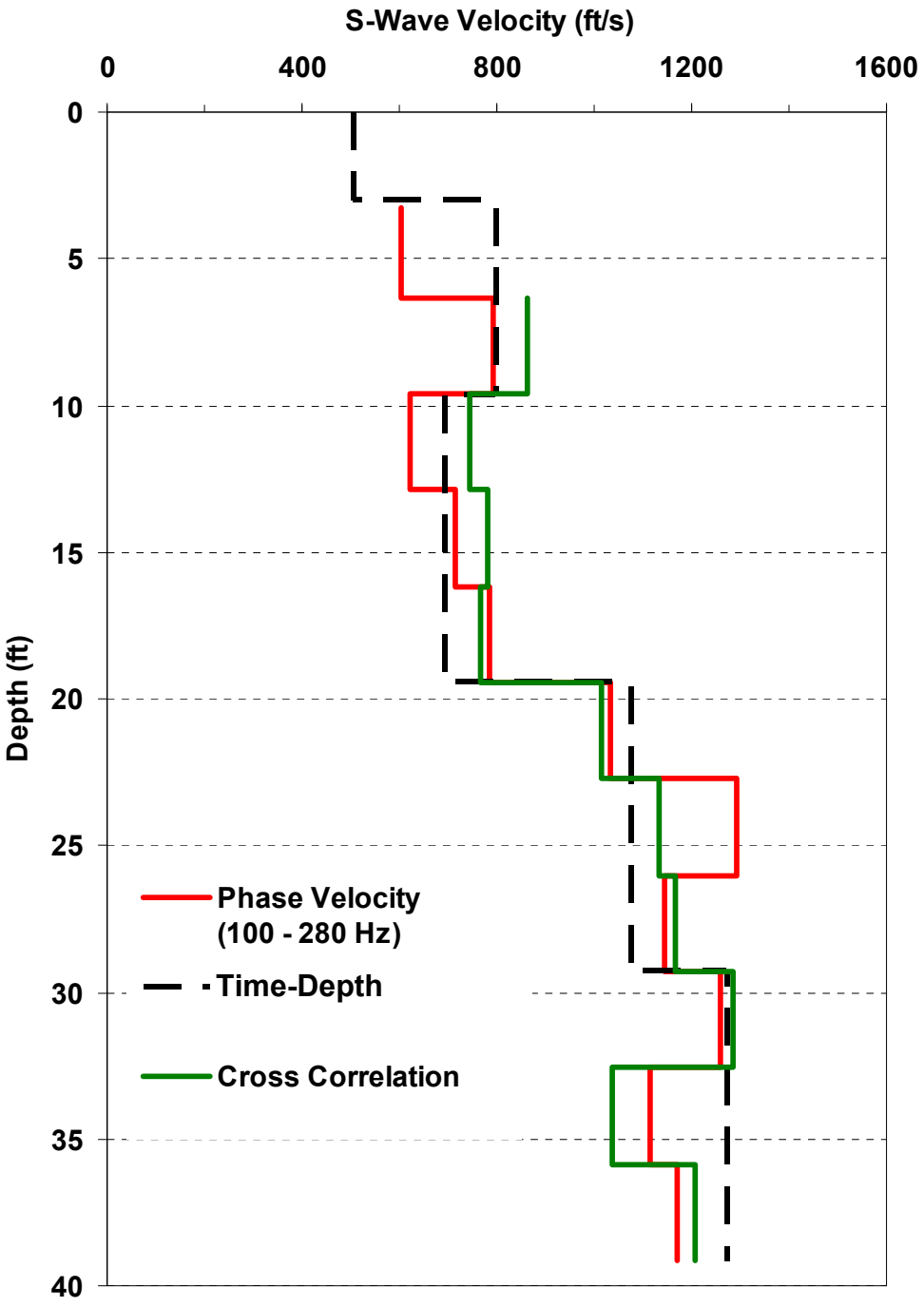

Figure B.13: V_S Profile Comparison of Analysis Methods (Location: S3)

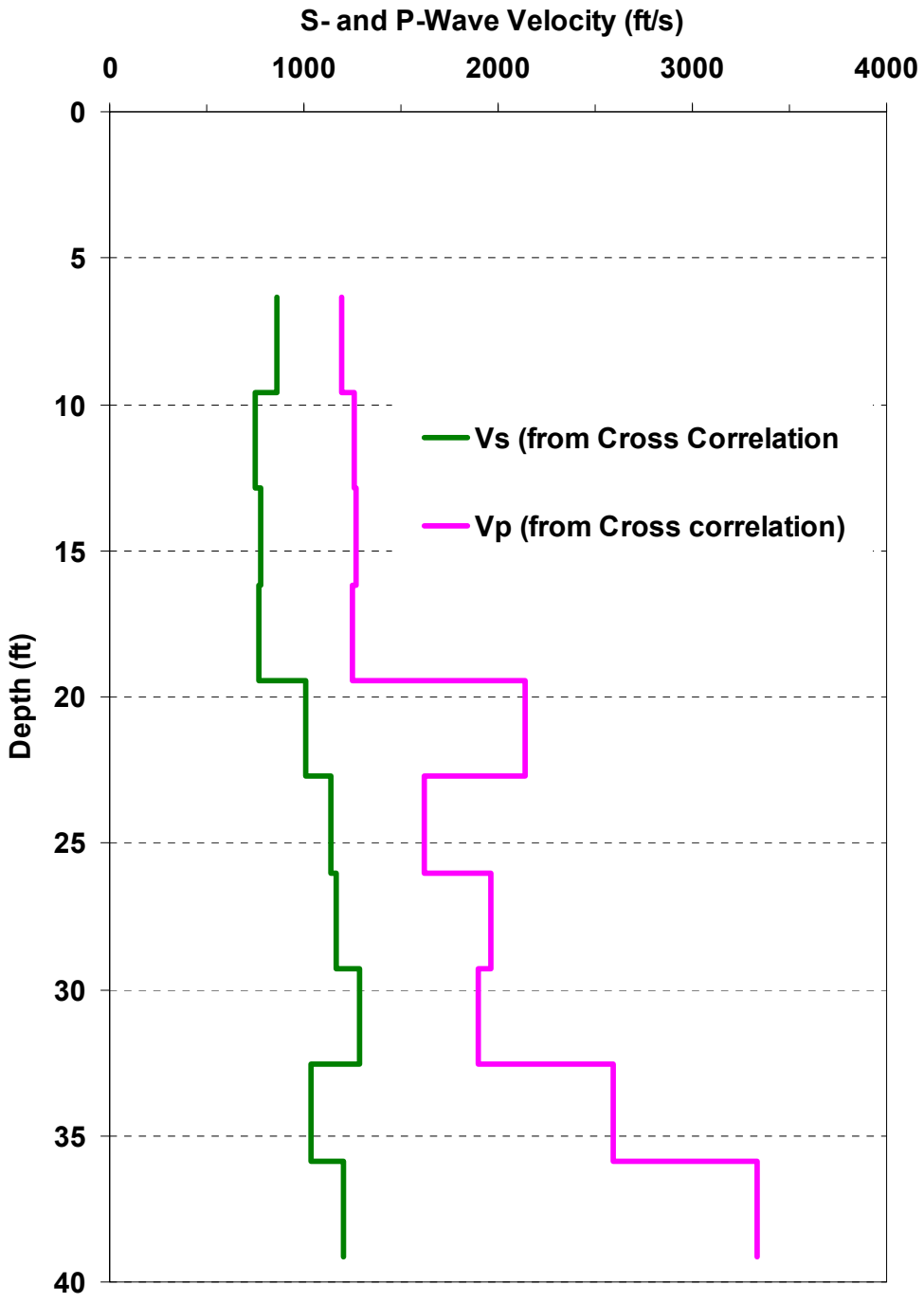

Figure B.14: V_S and V_P Profiles Obtained with Cross Correlation Method (Location: S3)

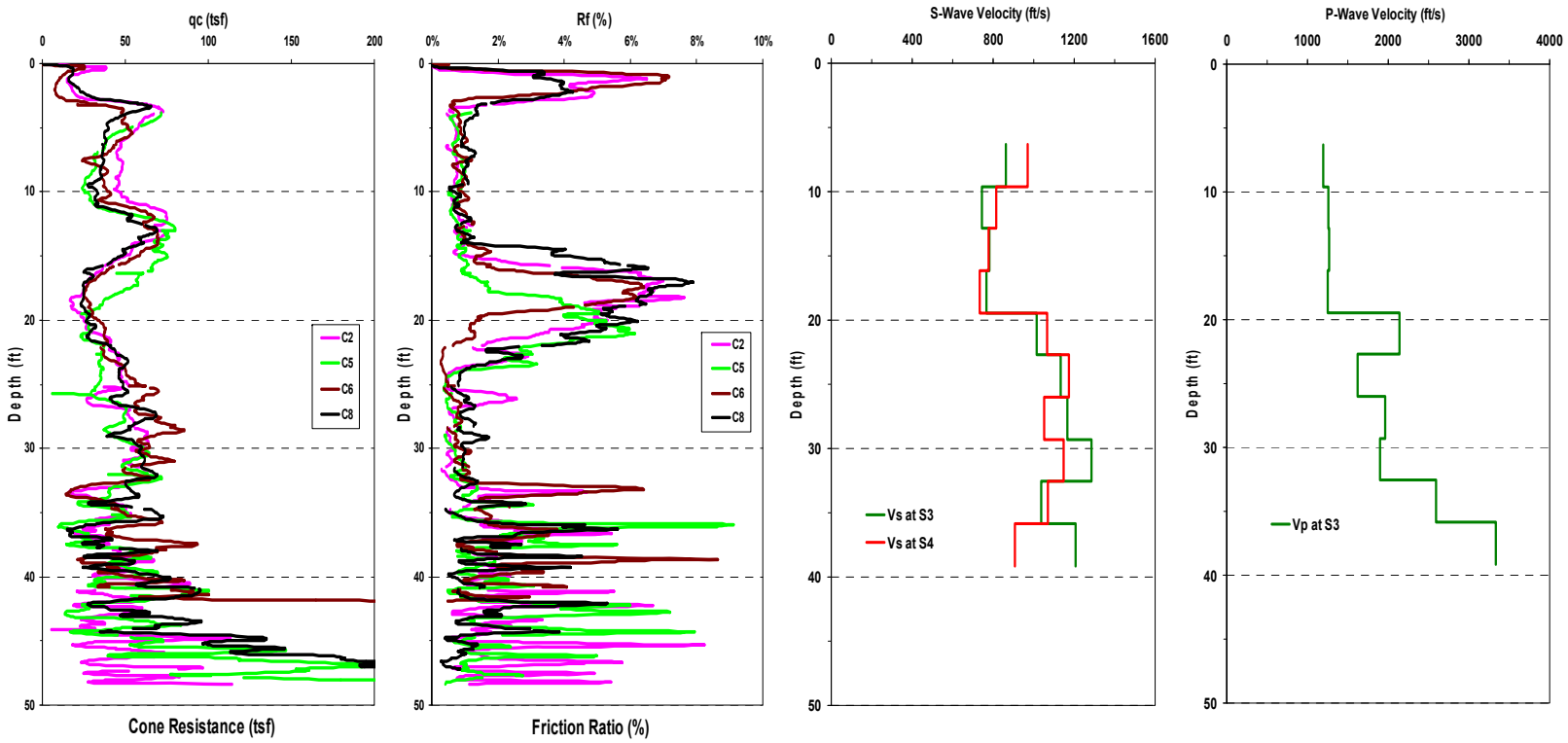

(a) CPT Profiles of Group 2: C2, C5, C6 and C8

(b) V_S and V_P Profiles of Group 2: S3 and S4

Figure B.15: CPT Soil Profiles and V_S and V_P Profiles Evaluated by Seismic Cone Testing at the Location Grouped for the Similar CPT Soil Profiles (Group 2)

assumed that the soil layer is close to water table.

The V_S profiles obtained at S3 and S4 are compared with CPT profiles of group 2 in Figure B.15. Both V_S profiles and cone resistance profiles show inversions near the depths of 20 and 35 ft. The overall shapes of both V_S profiles and cone resistance profiles are similar.

B.3.2 2-D V_S profile obtained with SCPT tests

SCPT tests consisting of five pairs of CPT and seismic cone tests were performed along the test array, and the test locations are bounded with a red dashed line in the area of group 3 as shown in Figure B.6. As discussed before, the cone resistance varies in the top soil layer ranging from ground surface to 15 ft due to the weather effect that changes the effective stress of the top soil layer. The CPT tests of C11 and C12 and seismic cone tests of S6 and S7 were performed in the dry season, summer, unlike other tests performed in the rainy season, winter, in group 3. The cone resistances and S-wave velocities obtained in shallow depth are relatively larger than the values obtained at other locations (see Figure B.16). The shapes of cone resistance profiles and V_S profiles are similar with the same inversion at the depth of 20 ft (see Figure B.16).

Three SCPT tests of group 4 were performed in the southeast area along the test array. Even though the relative distance of three CPT tests and three seismic cone tests is close to each other, the cone resistance of C13 and S-wave velocity of S8 are different from other profiles in the depth ranging from ground surface to 15 ft because C13 and S8 were performed in a dry season (see Figure B.17). Both the cone resistance profiles at C4 and C9 and V_S profiles at S1 and S5 show an inversion at the depth of 10 ft in Figure B.17. However, the inversions of S1 and S5 are not as clear as the inversion of C4 and C9 because V_S profiles are less sensitive than cone resistance profiles for soil stiffness.

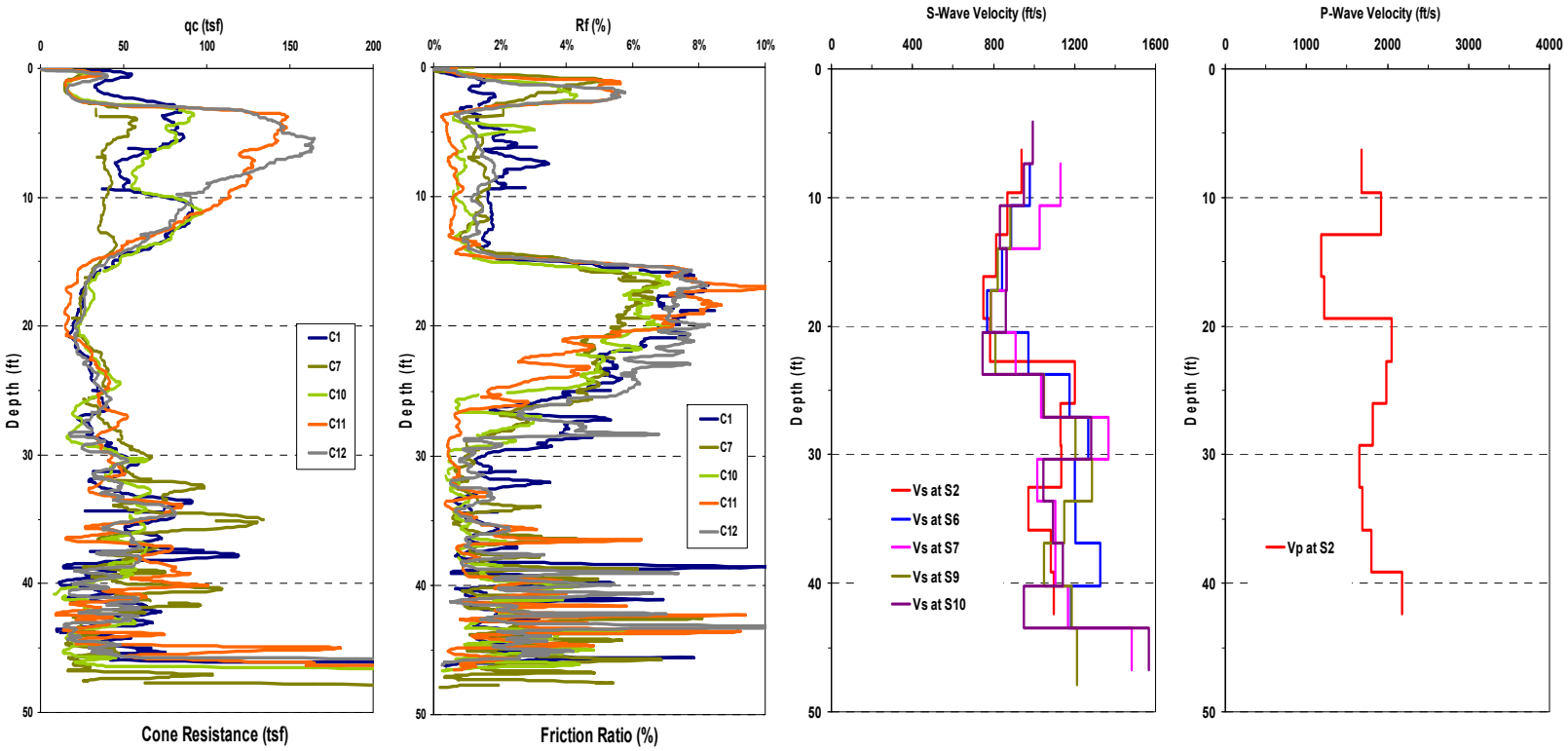

(a) CPT Profiles of Group 3: C1, C7, C10, C11 and C12

(b) V_S and V_P Profiles of Group 3: S2, S6, S7, S9 and S10

Figure B.16: CPT Soil Profiles and V_S and V_P Profiles Evaluated by Seismic Cone Testing at the Location Grouped for the Similar CPT Soil Profiles (Group 3)

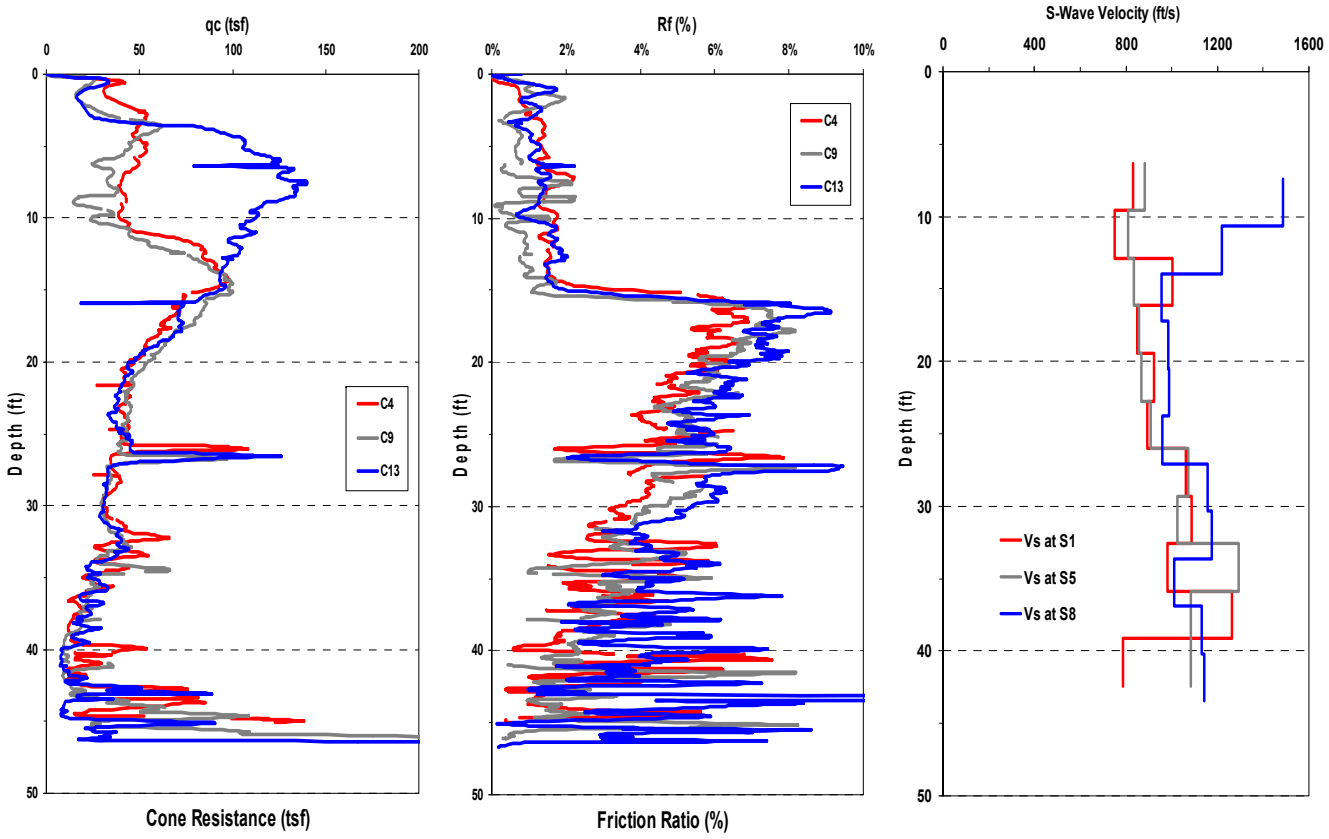

(a) CPT Profiles of Group 4: C4, C9 and C13

(b) V_S Profiles of Group 4: S1, S5 and S8

Figure B.17: CPT Soil Profiles and V_S Profiles Evaluated by Seismic Cone Testing at the Location Grouped for the Similar CPT Soil Profiles (Group 4)

while the cone resistances gradually decrease with the increasing depth, the S-wave velocities do not gradually decrease due to the less sensitive characteristic of S-wave velocity for soil stiffness.

The 2-D V_S profile obtained with the results of eight seismic cone tests performed along the 660 ft test array is plotted in Figure B.18. The northwest end and southeast end of test array are the coordinates of 0 and 660 ft in Figure B.18 ("0" is not included in this figure). Locations of seismic cone tests are marked with arrows on the horizontal axis of the 2-D profile. The 2-D V_S profile shows inversion at the depth of about 20 ft for the test array at the distances from 73 to 363 ft. However, the inversion gradually decreases approaching the southeast end of the test array. Even though the resolution of the 2-D V_S profile is not high due to the small number of tests, the V_S profile at the locations that tests were not performed can be interpolated using the contour of the V_S profile as shown in Figure B.18.

B.4 TESTING RESULTS: LOWER TRACT B

Various seismic tests were performed at Lower Tract B to characterize the soil profile as part of collaborative research project with LANL. Seismic cone, downhole and SASW tests were performed at the site as shown in Figure B.7. The testing results are compared and discussed in this section.

B.4.1 Comparison of SCPT, downhole and SASW test results

V_S profiles obtained from SCPT, downhole and SASW tests are plotted in Figure B.19. While the three profiles shows similar trend for the entire depth, V_S profiles in the shallow depth range from the ground surface to 10 ft are different. The S-wave velocity of SCPT in the shallow depth range is higher than other test results. CPT profiles

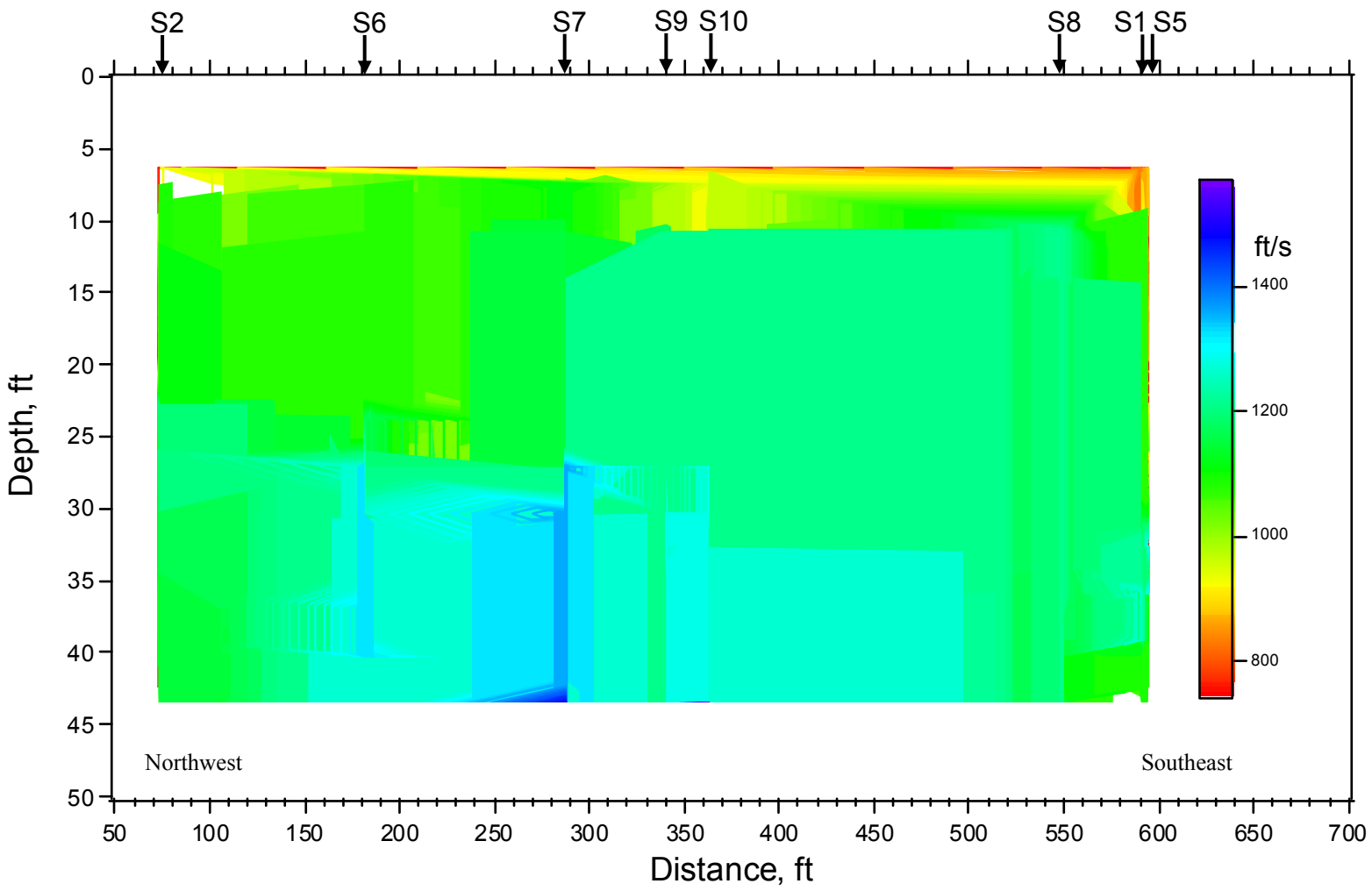

Figure B.18: 2-D V_S Profile Obtained with the Results of SCPT Performed Along a Straight Line of 660 ft

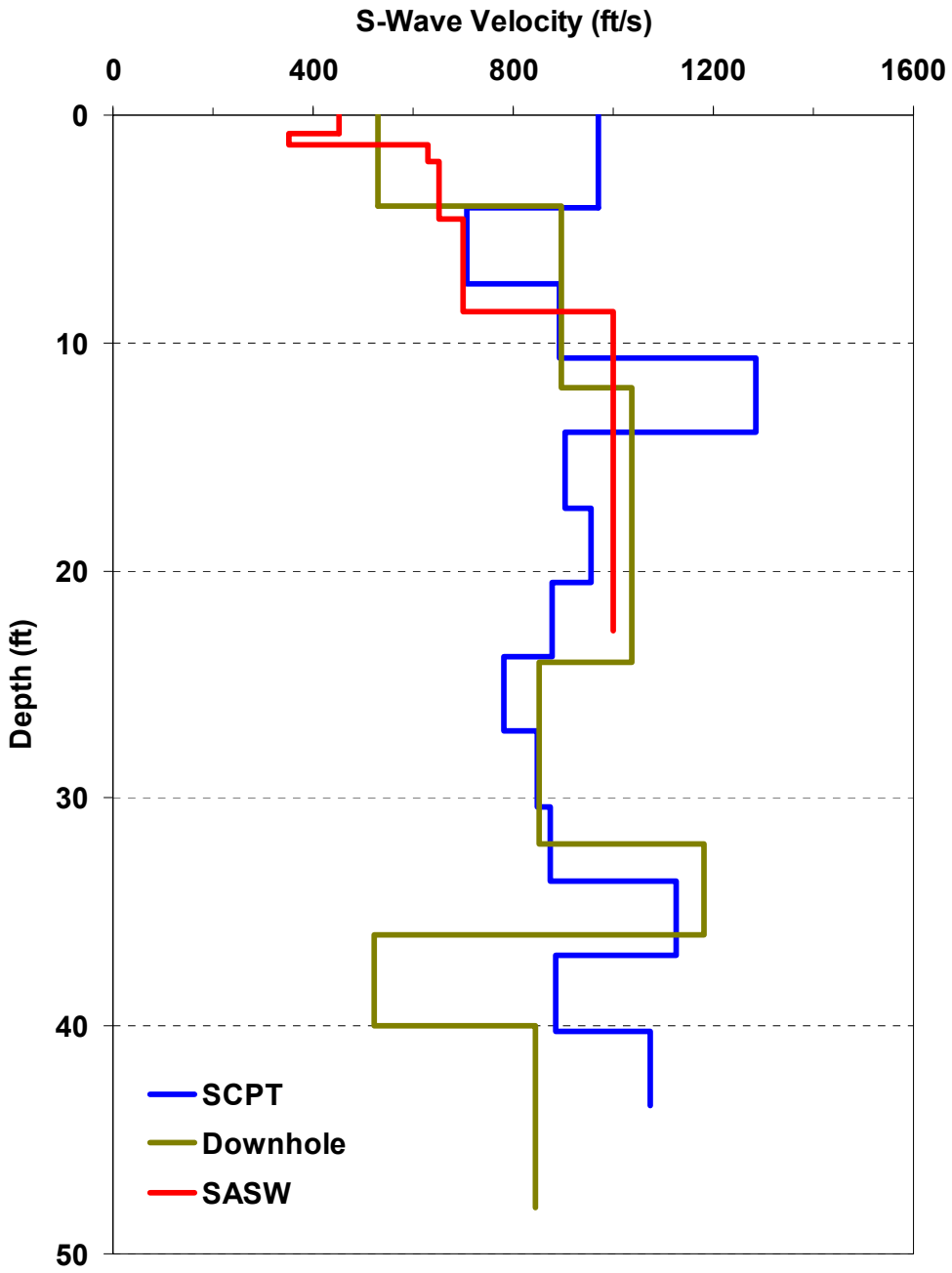

Figure B.19: Comparison V_S Profiles Evaluated by Near-by Seismic Cone, Downhole and SASW Tests Performed at Lower Tract B; Interpreted Soil Profiles Shown in Figure B.3

performed near the seismic cone test show that the cone resistance in the shallow depth range is largest in entire depth range as shown in Figure B.8. The locations of downhole test and SASW test are 40 ft and 50 ft away from the location of seismic cone test, respectively. In addition, each test was performed with a time difference of about two or three weeks that may change the effective stress for surface soil. Natural weakness of seismic cone and downhole tests in shallow depth range may be another reason for the difference.

P-wave velocities are obtained by downhole testing. The signals used for calculation are from a horizontal geophone, not a vertical geophone. First arrival times of P-waves that propagate through soil layers were not properly measured with the vertical geophone because P-waves propagate through the concrete grout of a borehole. The V_P profile is shown in Figure B.20.

B.4.2 Use of the SABW method for downhole tests

Downhole tests were performed using two, 3-dimensional sensors connected by an adapter rod. The orientation of the downhole sensor was controlled by connecting rods of 5 ft length. Phase of S_{vh} waves between two, 3-D sensors were not properly measured. It is attributed to the fact that P-waves may propagate through the concrete grouted borehole contaminating the phase values of S-waves. Use of the adapter rod of two, 3-D sensors may be another reason.

B.5 SUMMARY

Various seismic tests were performed at Platt 4 and Lower Tract B as a part of research projects. SCPT (consisting of CPT and seismic cone tests), SASW and downhole tests were performed at different locations and times, and the results were

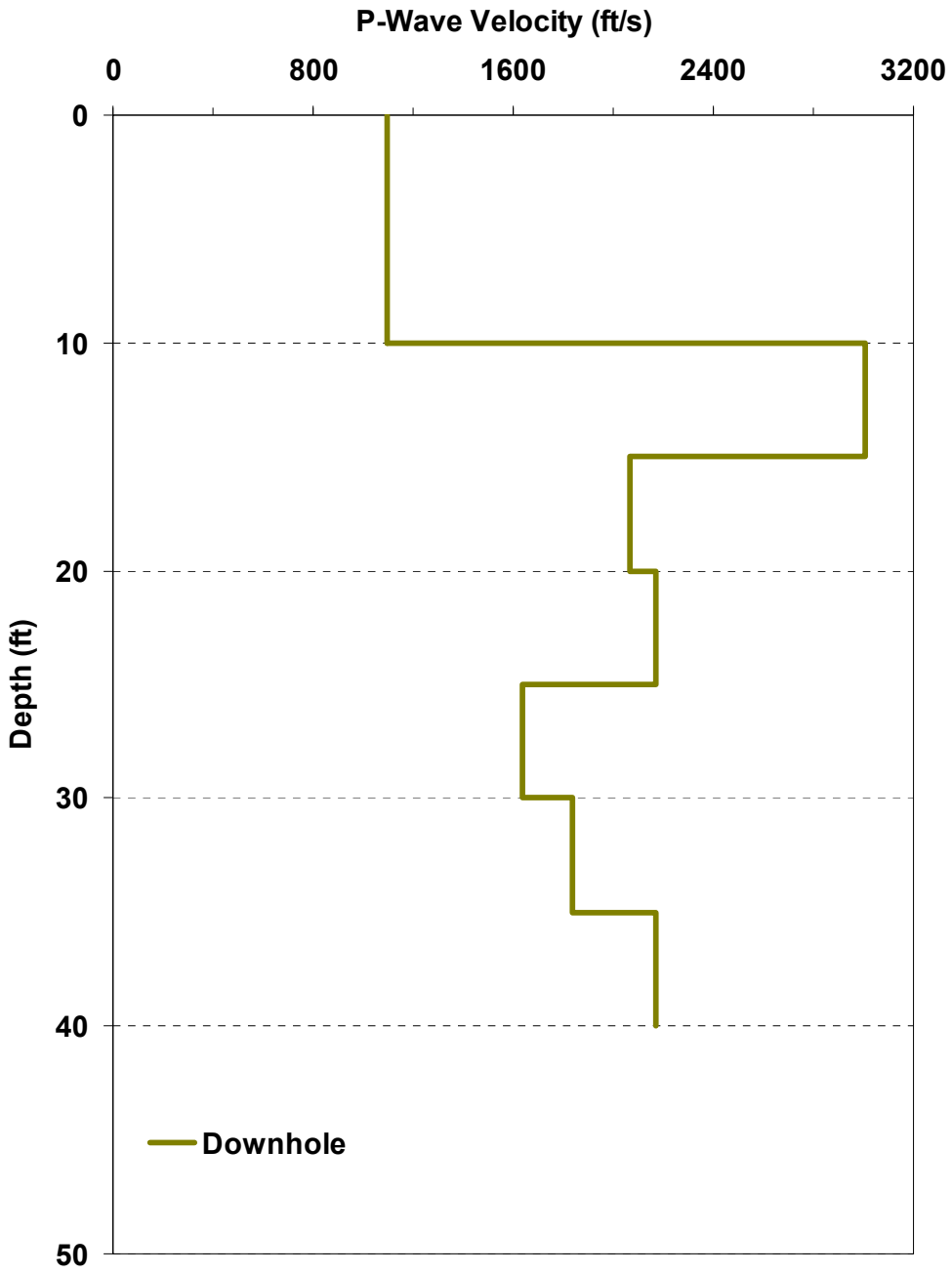

Figure B.20: V_P Profiles Evaluated by Downhole Testing

compared and discussed.

The test site of Platt 4 is divided into four areas by CPT profiles consisting of cone resistance profile and friction ratio profile. The CPT profiles were compared with the S- and P-wave velocity profiles in each group, and the results were discussed. Both cone resistance profile and V_S profile show similar trend and clear inversion location. Cone resistance profiles were more sensitive than V_S profiles because the stiffness of soil is more directly related to the cone resistance.

Eight S-wave velocity profiles obtained along the test array with seismic cone tests were plotted in a 2-D profile. Even though the tests were not performed at many locations, V_S profiles were efficiently interpolated at other locations where tests were not performed.

SCPT, downhole and SASW tests were performed at Lower Tract B. The V_S profiles results are similar.

References

Areias, L. and Van Impe, W. F. (2006), "Effect of Travel Path in the SCPT Test Method", Proceeding of Conference on ASCE Site and Geomaterial Characterization (GSP 149), pp. 236-242

ASTM D5778-07 (2007), "Standard Test Method for Electronic Friction Cone and Piezocone Penetration Testing of Soils", ASTM International. www.astm.org

Barzilai, A. (2000). Improving a geophone to produce an affordable broadband seismometer. Ph.D. Thesis, Stanford University, U.S.A.

Batsila, E. V. (1995), "Investigation of Ray Path Assumption on Downhole Velocity Profile", M.Sc. Thesis, The University of Texas at Austin, Austin, Texas.

Bendat, J. S. and Piersol, A. G., "RANDOM DATA (Second Edition)", A Wiley-Interscience Publication, pp. 118-120.

Bolt, B.A. (1976). Nuclear Explosions and Earthquakes, W.H. Freeman and Company.

Butcher, A. P., Campanella, R.G., Kaynia, A.M., and Massarch, K.R., (2005), "Seismic cone downhole procedure to measure shear wave velocity – a guidline", Report of Tech. Comm. TC10, Geophysical Testing, Int. Soc. of Soil Mech. & Geotech. Eng., (ISSMGE), 5 pgs.

Campanella, R. G., Robertson, P. K., and Gillespie, D. (1986), "Seismic Cone Penetration Test", ASCE Specialty Conference, In situ 86, Special Publication, No 6, Virginia Tech., Blacksurg, VA, pp. 116-131.

Campanella, R.G. and Stewart, W.P. (1991), "Downhole Seismic Cone Analysis Using Digital Signal Processing", 2nd International Conference on Recent Advances in Geotechnical Earthquake Engineering and Soil Dynamics, No. 1.32, Vol. 1, pp. 77-83.

Companella, R. G., and Stewart, W. P. (1992), "Seismic Cone Analysis Using Digital Signal Processing for Dynamic Site Characterization", Soil Mechanics Series, No.144, Civil Engineering Department, The University of British Columbia.

Cox, B. R. (2006). "Development of a Direct Test Method for Dynamically Assessing the Liquefaction Resistance of Soil In Situ," Ph. D. Dissertation, the University of Texas at Austin.

Darendeli, M.B. (2001). "Development of A New Family of Normalized Modulus Reduction and Material Damping," Ph. D. Dissertation, the University of Texas at Austin.

Darendeli, M.B., Stokoe, K.H., II, and Rathje, E.M. (2001). "Importance of confining pressure on nonlinear soil behavior and its impact on earthquake response predictions of deep sites," Fifteen Inernational Conference on Soil Mechanics and Geotechnical Engineering, August 27-31, 2001, Istabul, Turkey.

Drnevich, V.P., Hardin, B.O., and Shippy, D.J. (1978). "Modulus and damping of soils by the resonant-column method," Dynamic Geotechnical Testing, ASTM STP 654, American Society of Testing and Materials, pp. 91-125.

Hardin, B. O., and Drnevich, V. P. (1972a), "Shear Modulus and Damping in Soils: Measurements and Parameter Effects," Journal of the Soil Mechanics and Foundation Division, ASCE, Vol. 98, No. SM6, pp. 603-624

Hardin, B. O., and Drnevich, V. P. (1972b), "Shear Modulus and Damping in Soils: Design Equations and Curves," Journal of the Soil Mechanics and Foundation Division, ASCE, Vol. 98, No. SM7, pp. 667-692

Hardin, B.O. (1978). "The nature of stress-strain behavior for soils," Proceedings of the ASCE Geotechnical Engineering Division Specialty Conference, Earthquake Engineering and Soil Dynamics, Vol. 1, pp. 3-91.

Hoar, R.J. (1982), "Field Measurement of Seismic Wave Velocity and Attenuation", Ph.D. Dissertation, The University of Texas at Austin, Austin, Texas.

Idriss, I.M. (1990), "Response of Soft Soil Sites during Earthquakes," Proceedings, H. Bolton Seed Memorial Symposium, Vol. 2, pp. 273-289.

Ishihara, K. (1996), Soil Behaviour in Earthquake Geotechnics, Oxford Engineering Science Series, Vol. 46, Clarendon Press.

Joh, Sung-Ho, (1996). "Advances in interpretation and analysis techniques for spectral-analysis-of-surfacewaves (SASW) Measurements," Ph.D. Dissertation, Univeristy of Texas at Austin, December.

Johnston, D.H. and Toksoz, M.N. (1981), "Definitions and terminology in Seismic Wave Attenuation", Geophysics reprint series No.2. Soc. Exp. Geophy. pp.1-5.

Karl, L. (2005), "Dynamic Soil Properties out of SCPT and Bender Element Tests with Emphasis on Material Damping", Ph.D. Dissertation, Ghent University.

Kates, G. (1996), "Development and Implementation of a Seismic Flat Dilatometer Test for Small- and High- Strain Soil Properties," MS Thesis, Georgia Institute of Technology, Department of Civil and Environment Engineering

Kim, D. S., Bang, E. S., and Kim, W. C. (2004), "Evaluation of Various Downhole Data Reduction Methods for Obtaining Reliable Vs Profiles", Geotechnical Testing Journal, Vol. 27, No.6

Marchetti, S., Monaco, P., Totani, G. & Marchetti, D. 2008. In Situ Tests by Seismic Dilatometer (SDMT). In J.E. Laier, D.K. Crapps & M.H. Hussein (eds), From

Research to Practice in Geotechnical Engineering, ASCE Geotech. Spec. Publ. No. 180: 292-311.

Martin, G.K. and Mayne, P.W. (1997). "Seismic Flat Dilatometer Tests in Connecticut Valley Varved Clay", ASTM Geotechnical Testing Journal 20 (3), pp. 357-361.

Martin, G.K. and Mayne, P.W. (1998). Seismic Flat Dilatometer Tests in Piedmont Residual Soils", Geotechnical Site Characterization, Vol. 2, Balkema, Rotterdam, pp. 837-843.

Mayne, P.W., Schneider, J.A., and Martin, G.K. (1999). "Small- and Large-Strain Soil Properties from Seismic Flat Dilatometer Tests", Pre-Failure Deformation Characteristics of Geomaterials, Vol 1, (Proc. Torino Conference, Italy), A.A. Balkema, Rotterdam, 419-426.

Mok, Y.J. (1987), "Analytical and Experimental Studies of Borehole Seismic Methods", Ph.D. Dissertation, The University of Texas at Austin, Austin, Texas.

Mok, Y.J., Sanchez-Salinero, Stokoe, K.H., II, and Roesset, J.M. (1988). "In Situ Damping Measurements by Crosshole Seismic Method", Proceedings, American Society of Civil Engineers, Specialty Conference on Earthquake Engineering and Soil Dynamics II – Recent Advances in Ground Motion Evaluation, Park City, Utah, June 1988.

Nazarian, S. and Stokoe, K. H., II (1984), "Use of Surface Waves in Pavement Evaluation." *Transportation Research Record* 1070, pp.132-144

Patel, N.S. (1981), "Generation and attenuation of Seismic Waves in Downhole Testing", M.Sc. Thesis, The University of Texas at Austin, Austin, Texas.

Redpath, B.B., Edwards, R.B., Hale, R.J., and Kintzer, F.C. (1982), "Development of Field Techniques to Measure Damping Values for Near-surface Rocks and Soils", URS/John A. Blume & Associates, Engineers.

Redpath, B.B. and Lee, R.C. (1986), "In-situ Measurements of Shear-Wave Attenuation at a Strong-Motion Recording Site", URS/John A. Blume & Associates, Engineers.

Rice, A. H. (1984), "The Seismic Cone Penetrometer", M.Sc. Thesis, The University of British Columbia.

Richart, F. E., Jr., Hall J., R. Jr. and Woods, R. D. (1970), "Vibrations of Soils and Foundations", Prentice-Hall, Inc., New Jersey.

Robertson, P.K., Campanella, R.G., Gillespie, D. and Rice, A. (1986a), "Seismic CPT to Measure In-Situ Shear Wave Velocity", ASCE, Geotechnical Engineering, Vol. 112, No. 8, pp. 791-804.

Robertson, P.K., Campanella, R.G., Gillespie, D. and Greig, J. (1986b), "Use of piezometer cone data", Proceedings of the ASCE Specialty Conference In

Situ ’86: Use of In Situ Tests in Geotechnical Engineering, Blacksburg, 1263-80, American Society of Engineers (ASCE).

Sanchez-Salinero, I., Roesset, J.M. and Stokoe, K.H., II (1986). “Analytical Studies of Body Wave Propagation and Attenuation,” Geotechnical Engineering Report GR86-15, Department of Civil Engineering, The University of Texas at Austin.

Santamarina, J. C., Klein, K. A. and Fam, M. A. (2001). “Soils and Waves”, John Wiley & Sons Ltd.

Seed, H. B. and Idriss, I. M. (1970), “Soil Moduli and Damping Factors for Dynamic Response Analyses,” Report No. EERC 70-10, University of California, Berkley.

Seed, H. B., Wong, R. T., Idress, I. M., and Tokimatsu, K. (1984), “Moduli and Damping Factors for Dynamic Analyses of Cohesionless Soils,” Report No. UCB/EERC-84/14, University of California, Berkley.

Stokoe, K. H., II, Arnold, E. J., Hoar, R. J., Shirley, D. J., and Anderson, D. G. (1978), “Development of a Bottom-Hole Device for Offshore Shear Wave Velocity Measurement,” Proceedings of the Tenth Annual Offshore Technology Conference, Paper No. Otc 3210, pp. 1367-1380.

Stokoe, K. H., II, and Hoar, R. J. (1978a), “Field Measurement of Shear Wave Velocity by Crosshole and Downhole Seismic Methods”, Proceedings of the Conference on Dynamical Methods in Soil and Rock Mechanics, Karlsruhe, Germany, Vol. III, pp. 115-137.

Stokoe, K. H., II, and Hoar, R. J. (1978b), “Variables Affecting In Situ Seismic Measurements”, Proceedings of the Conference on Earthquake Engineering and Soil Dynamics, ASCE Geotechnical Engineering Division, Pasadena, California, Vol. II, pp. 919-939.

Stokoe, K.H., II, S.G. Wright, J.A. Bay, and J.M. Roesset (1994) “Characterization of geotechnical sites by SASW method”, in Technical Report - Geophysical Characterization of Sites, R.D. Woods (editor), ISSMFE Technical Committee 10, Oxford Publishers, 13th International Conference on Soil Mechanics and Foundation Engineering, New Delhi, India.

Stokoe, K.H., II, Cox, B., Jung, M.J. and Yuan, J. (2009a) “Field Seismic Crosshole and SASW Testing Data Summary Report”, Geotechnical Engineering Report GR09-01, University of Texas at Austin, January.

Stokoe, K.H., II, Yuan, J., Lin, Y.C., and Kim, C.Y. (2009b) “Seismic Testing with Surface Waves to Evaluate Vs Profiles at the Proposed Headworks Reservoir, Silver Lake Replacement Project, Los Angeles, CA.”, Geotechnical Engineering Report GR09-13, University of Texas at Austin, September, 100 pgs.

Stokoe, K.H. and Santamarina, J.C. (2000). "Seismic-Wave-Based Testing in Geotechnical Engineering," GeoEng 2000, Melbourne, Australia, November, pp. 1490-1536.

Stokoe, K. H., II, and Woods, R. D. (1972), "In Situ Shear Wave Velocity by Cross-hole Method", Journal of the Soil Mechanics and Foundations Division, ASCE, Vol. 98, No. SM5, pp. 443-460.

Stokoe, K.H., II, Wright, S.G., Bay,J.A. and J.M. Roesset (1994a), "Characterization of geotechnical sites by SASW method," Geophysical Characteristics of Sites, ISSMFE, Technical Committee 10 for XIII ICSMFE, International Science Publishers, New York, pp. 15-25.

Stokoe, K.H., II, Hwang, S.K. and Roesset, J.M. (1994b), "Laboratory Measurement of Small-Strain Material Damping of Soil Using a Free-Free Resonant Column", *Proceedings of the Second International Conference on Earthquake Resistant Construction and Design*, Berlin, Germany, June 15-17, 1994, pp. 195-202.

Stokoe, K.H., II and Jung, M.J. (2010), "Free-Free (Fr-Fr) Testing of Unconfined Concrete Samples, Internal Procedure Fr-Fr-1, Revision 0", Geotechnical Engineering Report GR10-03, University of Texas at Austin, August.

Stokoe, K.H., II, Umberg, D., Kaçar, O. and Kim, C.Y. (2011), "Dynamic Laboratory Tests of Seven Reconstituted Soil Specimens and One Intact Rock Core for the Cerro Verde", Geotechnical Engineering Report GR11-05, University of Texas at Austin, November.

Stewart, W.P. (1992), "Insitu Measurement of Dynamic Soil Properties with Emphasis on Damping", Ph.D. Dissertation, The University of British Columbia, Vancouver, B. C. Canada.

Sun, J.I., Golesorkhi, R., and Seed, H.B. (1988). "Dynamic Moduli and Damping Ratios for Cohesive Soils," Report, UCB/EERC-88/15, Univ. of California at Berkeley, 48 pp.

Totani G., Monaco P., Marchetti S, Marchetti D. (2009): "Vs measurements by Seismic Dilatometer (SDMT) in non penetrable soils". Proc. XVII International Conference on Soil Mechanics and Geotechnical Engineering, Alexandria, Egypt, 5-9 October 2009, Vol. 2, 977-980.

Woods, R. D. (1968), "Screening of Surface Waves in Soils", *J. Soil Mech. And Found. Div., Proc. ASCE*, Vol. 94, No. SM4, July, pp. 951-979.

Woods, R. D. (1978), "Measurement of Dynamic Soil Properties", Proceedings of the Conference on Earthquake Engineering and Soil Dynamics, ASCE, Vol. I, Pasadena, CA, pp. 91-178.

Vita

Changyoung Kim was born in Pohang, Korea in 1977 as the second son of Young Kwang Kim and Chun sik Kim. He graduated from Pusan National University, Busan, South Korea and earned Bachelor of Science degree in Civil Engineering in February 2004. Right after his graduation, he began graduated studies at Pusan National University, Busan, South Korea and specialized in Geotechnical Engineering. After earning his Master of Science degree in August 2006, he worked for Research Institute of Industrial Technology at Pusan National University as a geotechnical engineering researcher. He enrolled at the University of Texas at Austin in the fall of 2007 to begin work on his Ph.D. degree in Geotechnical Engineering.

Permanent address: 465-8, Guseo-dong, Geumjeong, Busan, 609-310, South Korea

This dissertation was typed by the author.